TECHNICAL REPORT NO. 65-112

SEMIANNUAL REPORT NO. 2, PROJECT VT/5051
DEEP-WELL RESEARCH

THE GEOTECHNICAL CORPORATION

3401 SHILOH ROAD   GARLAND, TEXAS

DISCLAIMER NOTICE

THIS DOCUMENT IS THE BEST
QUALITY AVAILABLE.

COPY FURNISHED CONTAINED
A SIGNIFICANT NUMBER OF
PAGES WHICH DO NOT
REPRODUCE LEGIBLY.

TECHNICAL REPORT NO. 65-112

SEMIANNUAL REPORT NO. 2, PROJECT VT/5051
DEEP-WELL RESEARCH

TELEDYNE INDUSTRIES, INC.
GEOTECH DIVISION
3401 Shiloh Road
Garland, Texas

24 August 1965

IDENTIFICATION

AFTAC Project No: VT/5051
Project Title: Deep Well Research
ARPA Order No: 104-60
ARPA Project Code No: 8100
Contractor: The Geotechnical Corporation
                                    Garland, Texas

Date of Contract: 16 July 1964
Amount of Contract: $470,150.00
CCN No. 1: $145,362.00
Contract No: AF 33(657)-13668
Contract Expiration Date: 30 September 1965
Program Manager   Richard M. Shappee, Garland, Texas
                                      BR 8-3102, Area Code 214

CONTENTS

CONTENTS, Continued

ILLUSTRATIONS

ABSTRACT

A deep-hole vertical array of six short-period seismometers was tested at Grapevine, Texas. The results indicated that the array performed satisfactorily. An array of four seismometers was then operated routinely in a deep hole near Apache, Oklahoma, to record noise and signals.

A deep-hole triaxial seismometer was constructed and tested. The results of the test program indicated that minor design modifications were required before the instrument would be ready for routine use.

A long-period response was obtained from a short-period deep-hole seismometer by the use of filters and amplifiers. The resultant system was capable of operation at a magnification greater than 50,000 at 0.04 Hz and did not appear to be limited by system noise at that magnification.

Routine measurements of noise and signals in deep holes were made at sites in Oklahoma, Texas, and West Virginia. The measurements were used in a theoretical study program designed to increase understanding of the nature of noise and signals. Effort was expended to define optimum processing techniques for signals recorded from both triaxial and vertical seismometers. The results of this effort will lead to an optimum on-line processor for routine field use.

BLANK PAGE

SEMIANNUAL REPORT NO. 2, PROJECT VT/5051
DEEP-WELL RESEARCH

1. INTRODUCTION

This report discusses a project of research in deep-hole seismology. The work reported herein covers tests of a vertical array of seismometers, evaluation of a deep-hole triaxial seismometer, results of operation of a deep-hole short-period seismograph with a filter system to obtain a long-period response, operation of deep-hole field measurement teams, and the results of detailed analysis of signals and noise. Also included in this report as appendices are two deep-hole site reports, a report of an offshore measurement program, and a preliminary evaluation of a vector-correlation process for a three-component set of orthogonal seismographs.

The purpose of this report is to present the technical findings and accomplishments of the project from 1 February 1965 to 31 July 1965. It is submitted in compliance with paragraph 2, Reports, of the Statement of Work to be Done, Project VT/5051. The project is under the technical direction of the Air Force Technical Applications Center (AFTAC) and under the overall direction of the Advanced Research Projects Agency (ARPA).

The main body of the report is presented in the same sequence as the tasks in the Statement of Work. A copy of the Statement of Work and of Contract Change Notification No. 1 are included as an appendix.

2. CONDUCT TESTS, VERTICAL ARRAY, TASK 1a

Routine operation of the vertical array at the site near Grapevine, Texas (GV-TX), showed that the vertical array of six seismometers operated satisfactorily. The seismometers were operated at depths of 2900, 2600, 2300, 2000, 1700, and 1400 m. The seismometers operated at depths of 2300 and 2600 m recorded frequent "spikes," with the instrument at 2600 m having many more spikes than the instrument at 2300 m. Since these instruments were locked to the casing with cam-type hole locks and the instrument at

2600 m was secured with an arm-type lock, it was thought that the cam locks were slipping. To test this possibility, an arm-type lock was installed at 2600 m, and cam-type hole locks were installed on the seismometers at 2300 and 2900 m. The spikes continued to be present at 2600 m. Thus, the noise was shown to be characteristic of this depth in the hole and not related to instrumentation. It is probable that the noise was caused by minute move-ments of the casing since the top of the cement around the casing is at 2660 m.

As a practical matter, the frequency of the noise spikes decreased as a func-tion of the length of time the seismometers were left in the hole. After a period of a week or so, the spikes occurred about 20 times a day.

After the array had operated routinely at GV-TX, one half the array was moved to AP-OK. There, the three array elements were operated in con-junction with a fourth instrument in the hole and a fifth instrument in a shallow hole nearby. The array performed satisfactorily. Results of the measurement program using the array are given in a later section of this report.

At the time of the last semiannual report, a summing amplifier had been constructed for use with the array and field tested. Subsequently, an adjustable-delay tape head was designed and constructed. This unit, shown in figure 1, allows a time delay of up to about 1-1/3 sec to be introduced into each of six channels on the tape when the head stack is installed on an Ampex 300 tape transport operated at 0.3 ips. The tape head is useful whenever delayed summations are required. Figure 2 shows a delayed, summed signal recorded at AP-OK. The summation was done off-line but represents the type of processing that would result from on-line processing.

3. EVALUATE DEEP-HOLE TRIAXIAL SEISMOMETER, TASK 1b (1)

A triaxial seismometer, figure 3, was constructed. It was tested both in the laboratory and at the GV-TX site. The laboratory tests demonstrated that the seismometer was stable, had the proper response, and was capable of being adjusted to desired free periods and damping. The response curves of the three modules comprising this instrument are shown in figure 4. Also shown are the theoretical response and a typical response made in the field using the electromagnetic calibrator in the seismometer. The responses are identical within experimental reading error.

(a) Magnetic head stack
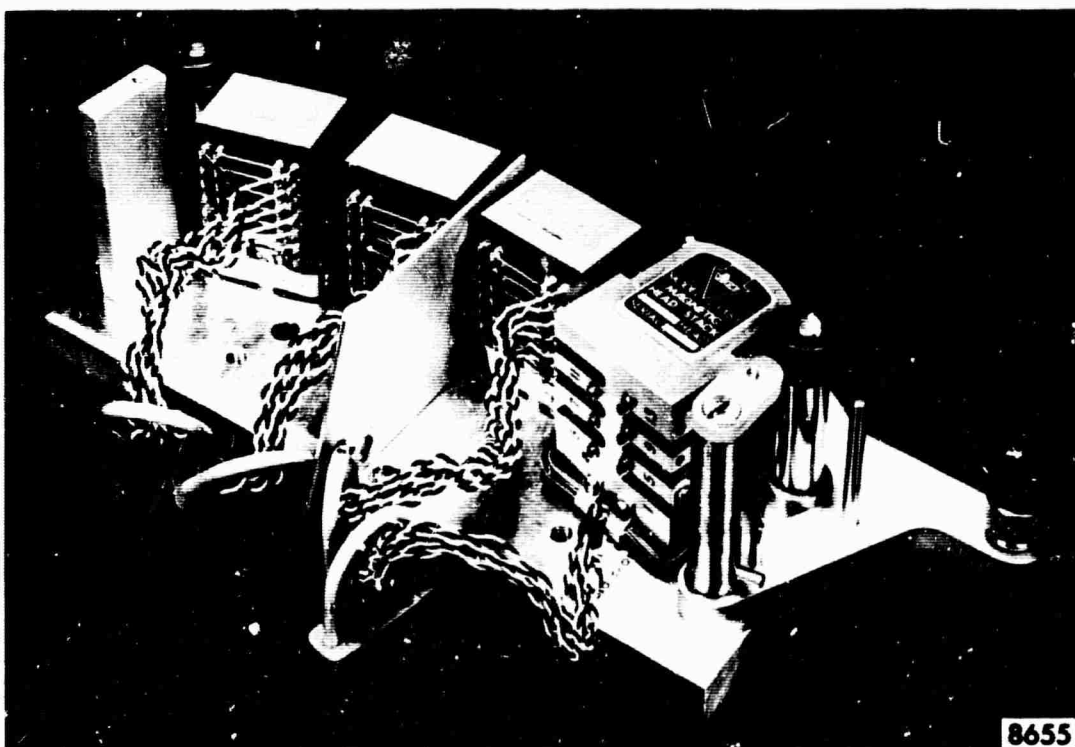
(b) Assembly for Ampex 300 reccrder

Figure 1. Adjustable delay tape head
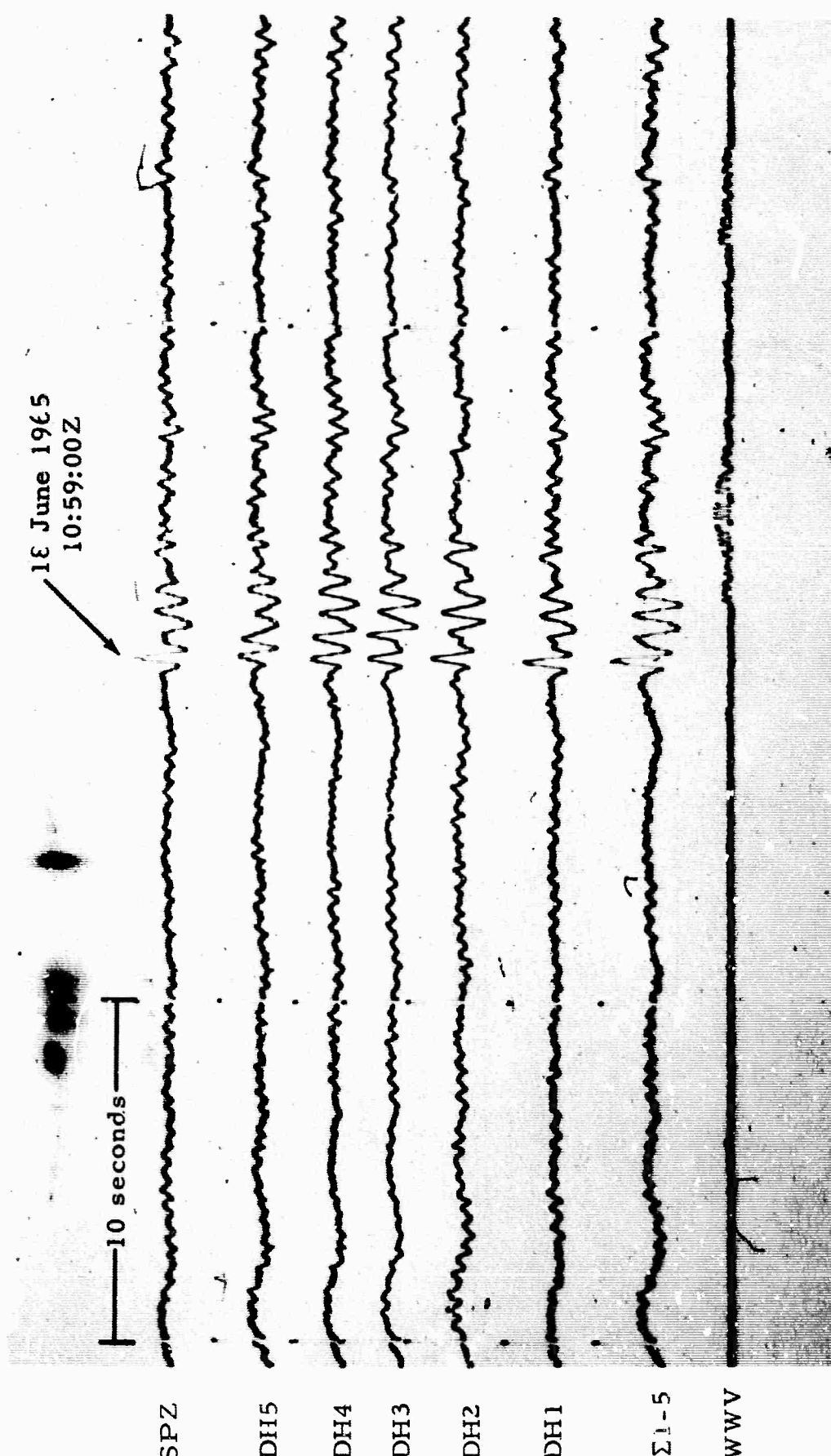
Figure 2. Time-delayed summation of a signal received at AP-OK. Summation made off-line from signals delayed on-line by Model 23361 adjustable-delay tape head. DH1 at 2281 m., DH2 at 2270 m, DH3 at 1970 m, DH4 at 1660 m, and DH5 at 15 m.
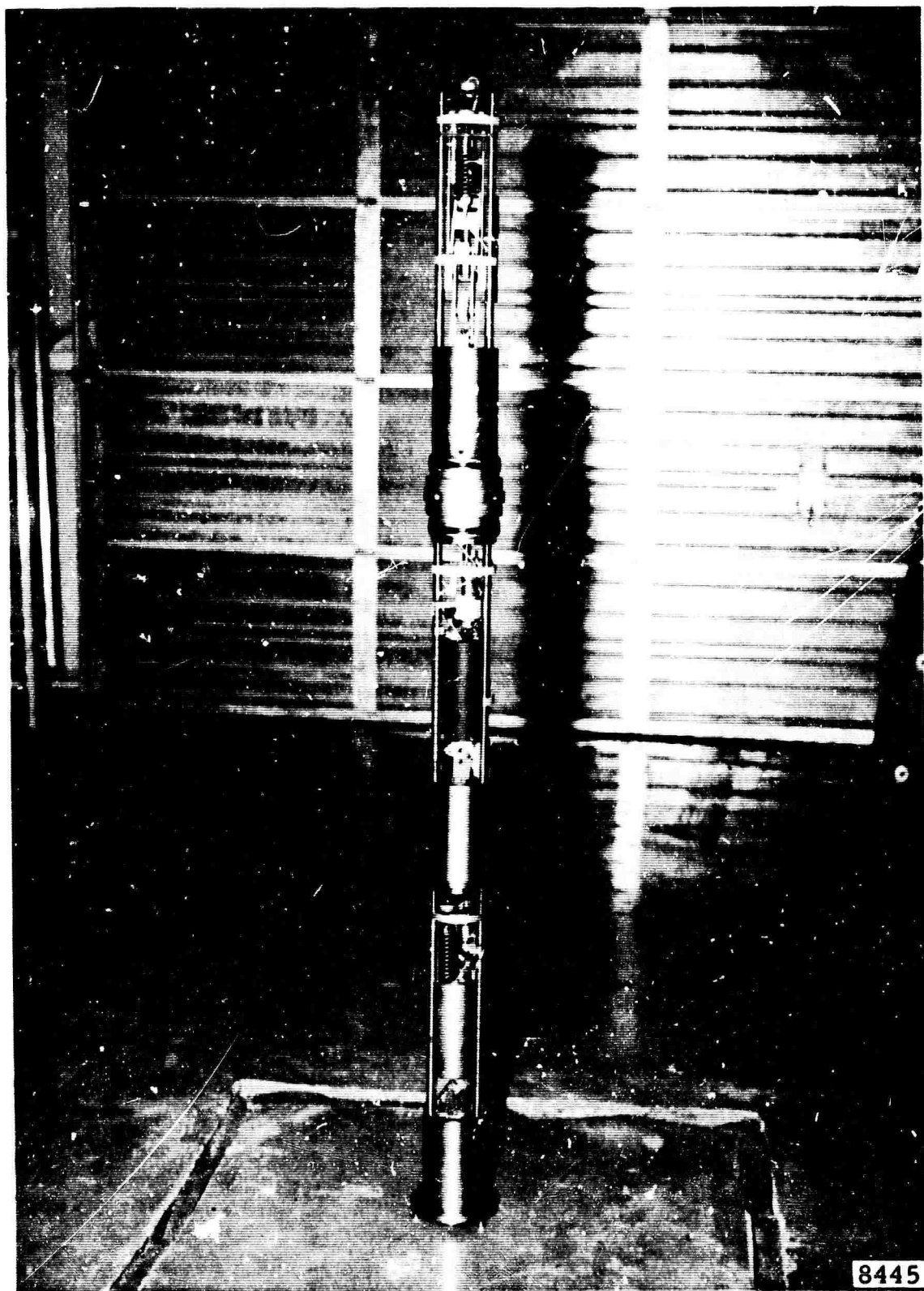
Figure 3.   Triaxial seismometer
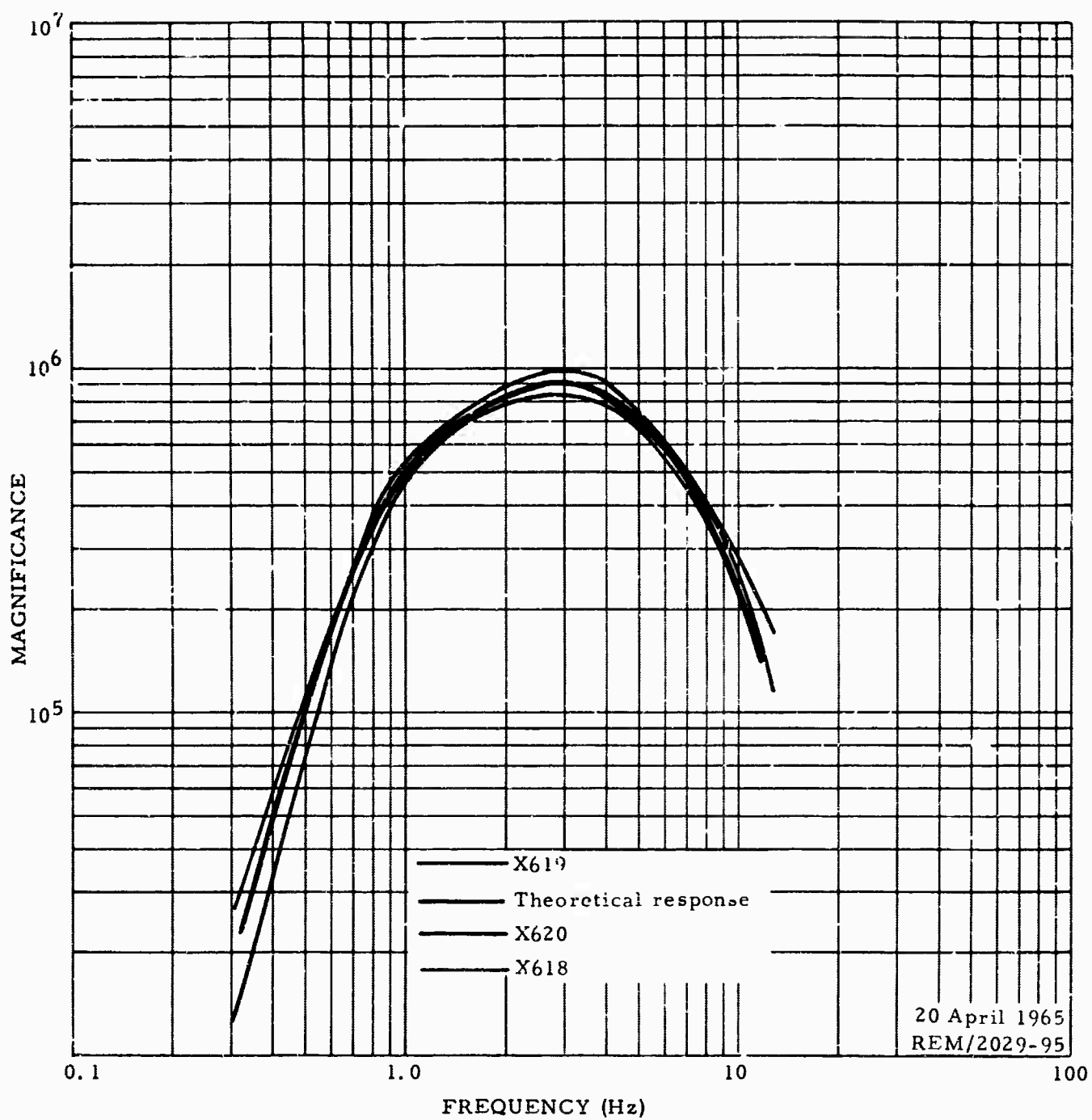
Figure 4. Theoretical and shake-table response, Model 22700 seismometer and Model 4300 PTA. $F_s = 0.8$ Hz, $\lambda_s = 0.51$; $F_g = 3.0$ Hz, $\lambda_g = 0.7$

Tests at GV-TX showed the seismometer was rugged enough for field use, stable under field conditions, and sensitive enough for routine operation. Figure 5 shows an event recorded with this instrument. The traces identified Triax Vertical, Triax North, and Triax East were made using a Coordinate Transformer, Model 16432. A comparison of the surface trace (SPZ) and Triax Vertical trace shows the similarity that would be expected. Figure 6 shows an event recorded with the triaxial seismometer at a depth of 2100 m.

The experience gained in these tests indicated that the seismometer was basically sound, although some changes in packaging and modifications of the linkage system are desirable to facilitate maintenance. In addition, a weight-lift calibrator will be added to improve calibration accuracy.

4. DESIGN AND OPERATE DEEP-HOLE LONG-PERIOD SYSTEM, TASK 1b (2)

The deep-hole long-period system designed and operated under this task consisted of a deep-hole seismometer, suitable long-period filters to shape the response, amplifiers, and normal calibration and recording provisions. The best performance of the system was obtained using a deep-hole seismometer that was specially constructed to eliminate, as far as possible, all sources of thermal electromotive potentials.

Previously, the long cable required in a deep-hole seismograph was thought to be the major source of long-period noise. However, it was found that with extreme care and attention to all electrical connections, an ordinary deep-hole system would perform quite well at long periods. The block diagram and response curve of such a system are shown in figure 7.

An event recorded by the system diagramed in figure 7 is shown in figure 8. Some drift is evident in this example. This very long period drift was never completely eliminated. The seismometer was at 1700 m in the deep, dry hole at GV-TX. A comparison of this drift with a microbarograph did not yield significant correlation.

Some work was done in an attempt to obtain both a long-period and a short-period response from one seismometer. The results, though inconclusive, indicated that such a dual system would be too complex and unstable for routine field operation.
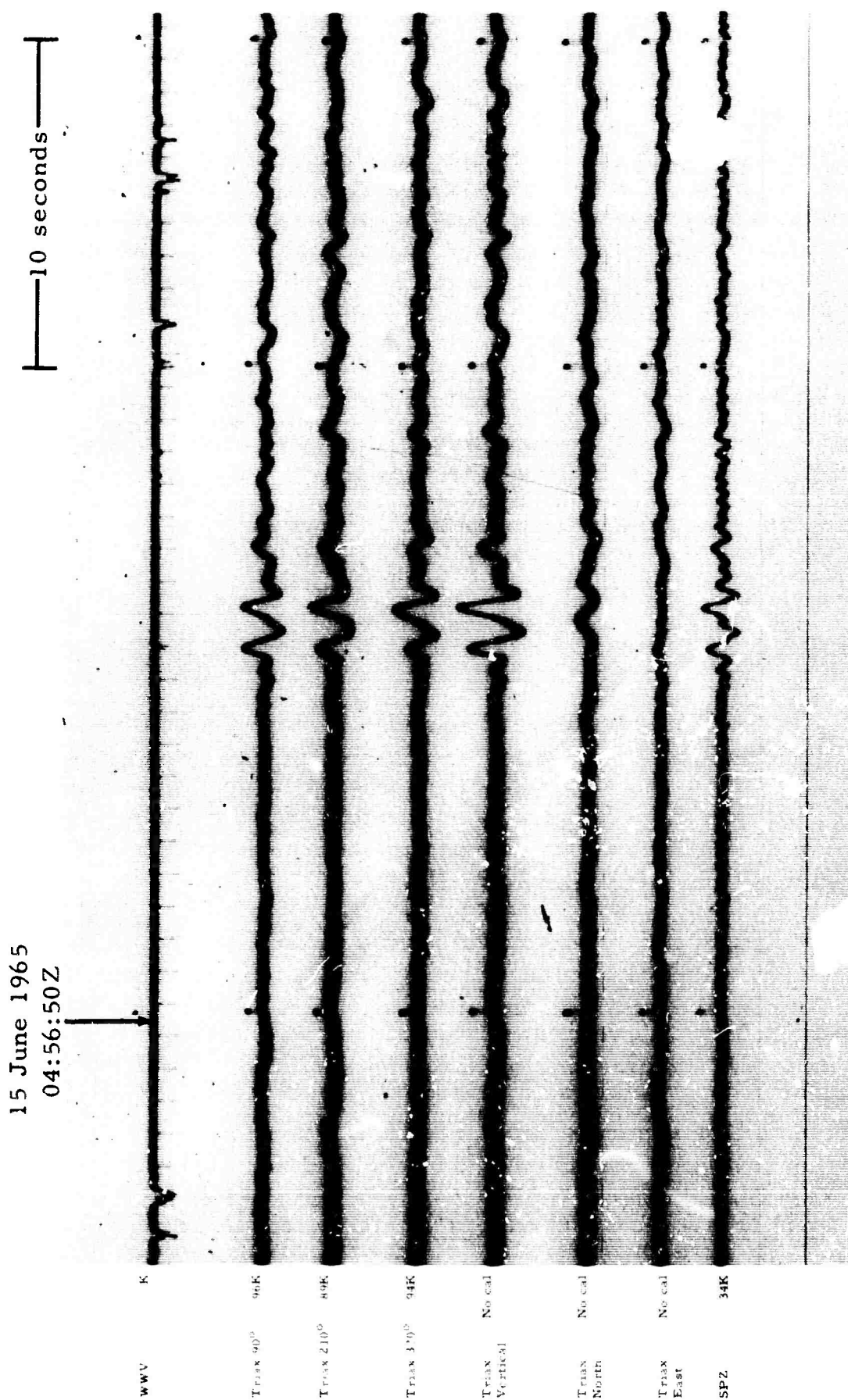
Figure 5. Recording of event by surface seismograph and triaxial seismograph with and without coordinate transformer, at GV-TX. Epicenter unknown. Magnification at 1 Hz (X10 enlargement of 16-mm film). Triaxial seismograph is at 150 m.

228
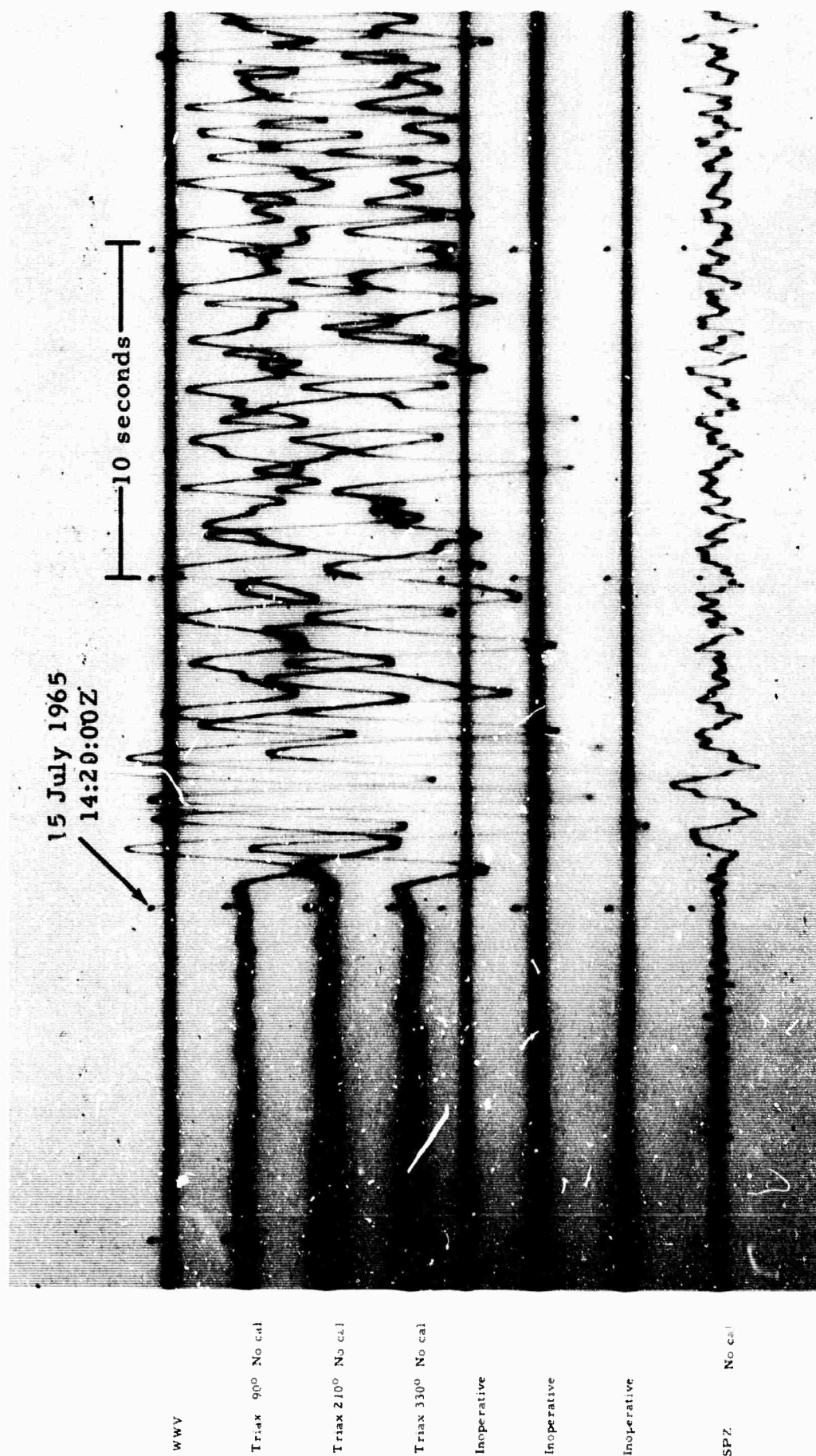
Figure 6. Recording of event by surface vertical seismograph and deep-hole triaxial seismograph at GV-TX. Epicenter 37.3 N, 74.25 W near coast of North Carolina (X10 enlargement of 16-mm film). Triaxial seismograph at 2134 m

232
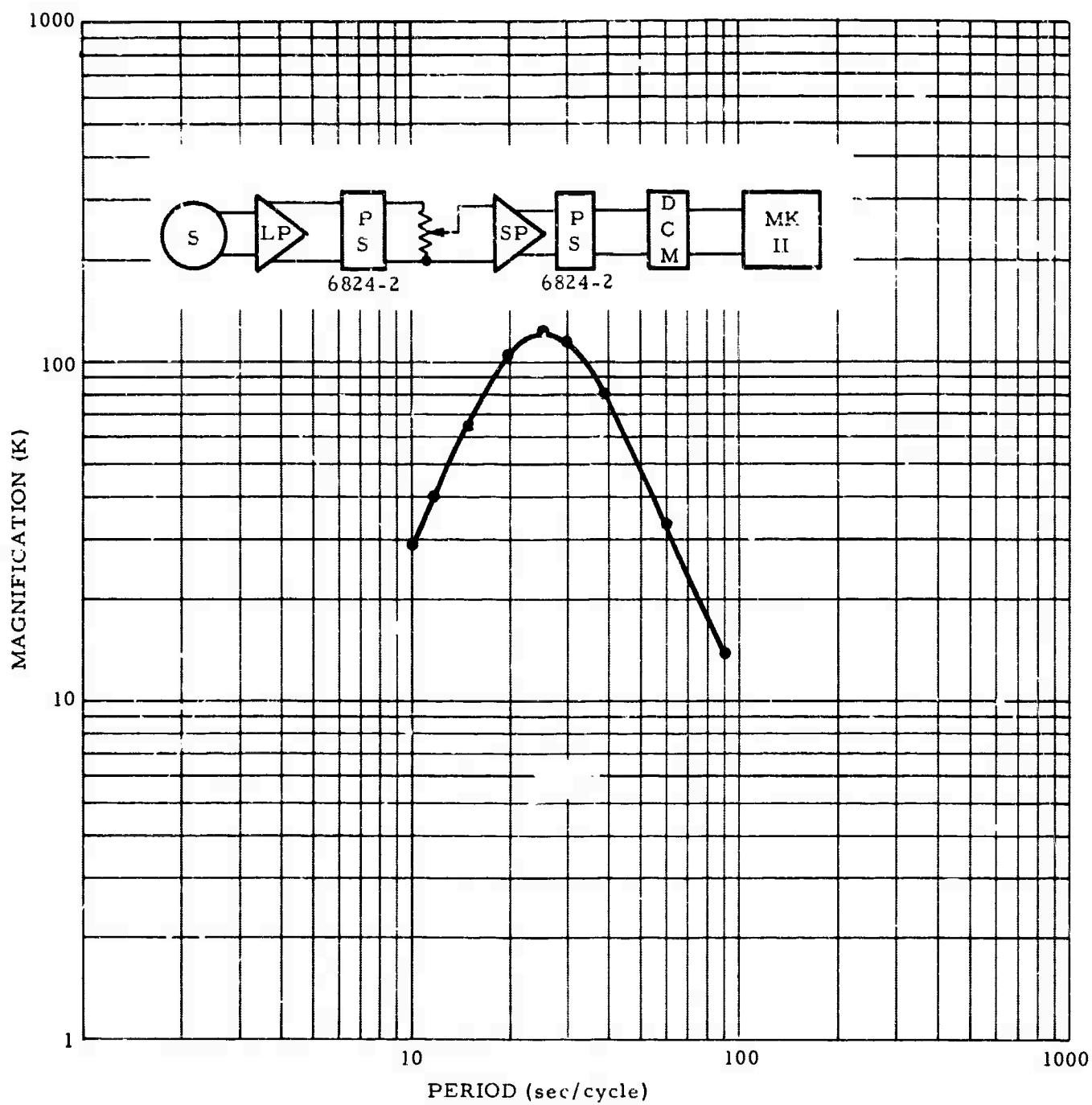
Figure 7. Block diagram and response curve of a deep-hole
long-period system

LPZ   108K

DH LP   127K

24 April 1965
03:25:00Z

←10 sec→
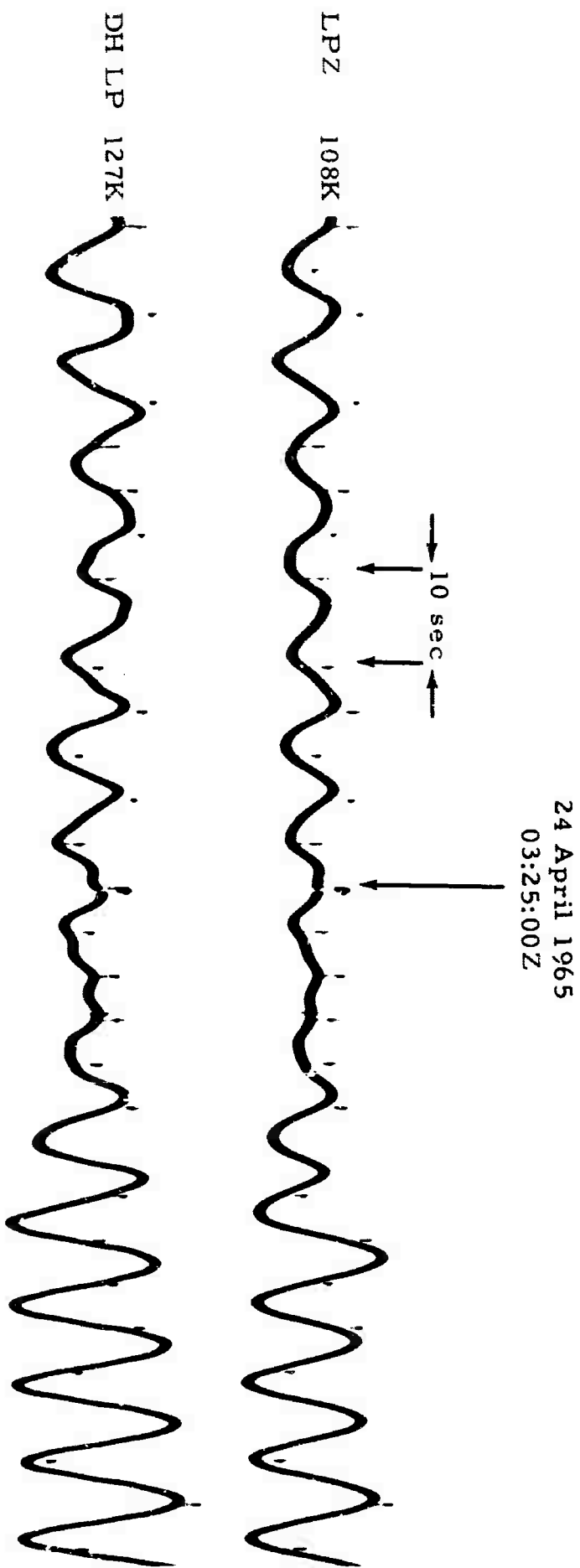
Figure 8.   Recording of event by long-period surface vertical seismograph and a deep-hole long-period system.   Deep hole at 152 m.   Epicenter 7.3 N, 126.6 E.   Phillippine Islands.

5. OPERATE DEEP-HOLE TEAMS, TASK 1c

Measurements were made at Apache, Oklahoma (AP-OK), Fort Stockton, Texas (FO-TX), and Franklin, West Virginia (FN-WV).

The measurements at FO-TX were started under Project VT/1139 in 1964 and concluded under the present project. This hole has a usable depth greater than 5500 m. This great depth, together with the gas present in the hole, made operations extremely difficult and time-consuming. An improved seal at the wellhead reduced the noise due to gas being produced in the well, although several days were required for equilibrium to be reached each time the hole was opened. The data obtained at this site are discussed in another section of this report and in appendix 1.

The site at AP-OK was reactivated in order to install an array of deep-hole seismometers. The measurements made with the array are discussed elsewhere in this report.

Measurements are presently underway at the FN-WV site with two seismometers at a time operating in the hole. An array of vertical seismometers will be operated in the hole during the next reporting period.

As specified in Contract Change Notification No. 1 to this project, measurements were made on the ccean bottom using a system specially designed for offshore use. This measurement program is described in appendix 3 of this report.

6. PROCESS DATA AND PERFORM DETAILED ANALYSIS, TASK 1d

6.1 SHORT-PERIOD SEISMIC NOISE

6.1.1 Introduction

Previous studies (Douze, 1964) of short-period seismic noise have often assumed that only surface waves were present in short-period noise. However, the experimental results obtained to date cannot, in general, be explained in this fashion. The presence of random body-wave noise must also be taken into account. Seismometers placed at depth below the surface

allow examination of the amplitude-depth relationships of the waves. If only surface waves, fundamental and higher modes, are present in the noise, the amplitude-depth relationships provide definite identification of the modes present. It is only necessary that the number of seismometers operating at depth be equal to the number of modes present (further explained in section 6.1.4.1). When body waves are present in the noise, the identification of wave types is no longer as simple, because all the angles of incidence of the random body waves must be taken into account.

In general, the amplitude-depth relationships obtained from deep-hole seismographs are not sufficient to differentiate between body waves and surface waves. As an example, the amplitude-depth relationships of the vertical component of the first higher mode and of P waves at close to vertical incidence are very similar for periods around 3.0 sec. Therefore, additional information must be obtained to differentiate between the possibilities. In this section of the report, the information was obtained by measuring phase velocities at the Wichita Mountains Seismological Observatory. In addition, the cross-correlation of surface and deep-hole noise was used to prove the presence of body-wave noise. Using all these data, a reasonably comprehensive understanding of the types of waves present was obtained. The results could only be interpreted qualitatively and not quantitatively. Despite the large amount of data available, the types of waves present could not always be proven conclusively. A possible explanation of the experimental results is given, while sufficient data are presented so that the reader can draw his own conclusion.

The results described were obtained with a deep-hole vertical-motion seismometer developed under Project VT/1139. The seismograph system has an amplitude and phase response similar to the short-period vertical Benioff seismograph (Benioff, 1932). The only surface waves considered are Rayleigh waves since all measurements were made with vertical seismometers. The period range discussed extends from the 6.0-sec microseisms to noise of 0.3-sec period.

The theoretical Rayleigh wave group velocities, phase velocities, and amplitude-depth relationships were obtained from the Seismic Data Laboratory in Alexandria, Virginia.

A brief description of the sites from which the experimental data discussed in this report were obtained is given in table 1. A complete description of the sites can be found elsewhere (Geotechnical Corporation, 1964).

Table 1. Site descriptions

Site	Location	Depth (m)	Geologic section
Apache, Oklahoma	34°49'59" N 98°02'09" W	2917	Consists of 1500 m of high-velocity limestones (6000 m/sec) overlying volcanics of somewhat lower velocities (5500 m/sec)
Eureka, Nevada	39°12'32" N 115°42'37" W	3130	The top 1100 m is made up of sandstones, shales, thinly bedded limestones, and dolomites overlying higher-velocity limestones and dolomites.
Fort Stockton, Texas	30°54'06" N 102°41'52" W	5792	Upper 3700 m consists of low-velocity shales, sand, and limestones overlying higher-velocity limestones and dolomites.
Franklin, W. Virginia	38°33'02" N 79°30'47" W	3815	The upper 3060 m consists of high-velocity limestones and dolomites; below a major thrust fault of 3060 m, the section has lower velocities although the formations are repeated.
Grapevine, Texas	32°53'09" N 96°59'54" W	3118	The top section consists of shales. The hole bottoms in a limestone; velocity increases steadily with depth.
Pinedale, Wyoming	42°27'24" N 109°33'04" W	3022	Consists entirely of sandy shales; velocity increases slowly with depth.
Wichi Mountains Seismological Observatory	34°43'05" N 98°35'21" W		Located on the same volcanics as encountered in the Apache deep hole. Measured surface velocities vary between 3000 and 4000 m/sec.

The following sites are of particular interest: (a) Fort Stockton, Texas, because of the great depth (5790 m) of the deep hole; (b) Eureka, Nevada, because of the very low noise level; (c) Apache, Oklahoma, because the velocity section is a close approximation of a half space and because it is close (20 km) to the Wichita Mountains Seismological Observatory (WMSO) where phase velocities were measured.

The site at Apache was of additional interest because the noise spectrum was similar to that at WMSO. Therefore, the phase velocities and amplitude-depth relationship can be used.

It must be noted that all the information presented was obtained from sites at some distance from the coast. Sites close to the coast typically exhibit large amplitudes at periods around 1.0 sec (Douze, 1964). There are not sufficient experimental results available to determine the waves responsible.

6.1.2 Rayleigh Waves

The theory of higher Rayleigh modes has been extensively discussed in the literature (Ewing, et al., 1957), and the presence of higher Rayleigh modes in earthquake surface waves has been established (Oliver and Ewing, 1958). It has previously been suggested that Rayleigh waves, both fundamental and higher modes, are responsible for seismic noise (Gutenberg, 1958).

The data used in calculating the theoretical change in amplitude with depth of the different Rayleigh modes were obtained as follows. The compressional-wave velocities were obtained from sonic logs; the shear-wave velocities were calculated from the compressional-wave velocities by assuming an appropriate Poisson's ratio (usually around 0.27); and densities were used appropriate to the lithologies encountered in the hole.

No attempt was made to model the layers below approximately 6000 m, except in the case of AP-OK. At AP-OK, a higher velocity was assumed at depth to increase the velocity above the velocity encountered at the surface in order to obtain the theoretical higher-mode Rayleigh wave amplitude-depth relationships.

By trial and error, it was found that for the shorter periods (less than 2.0 sec), the decrease of amplitude with depth is not greatly affected by the failure to model the deeper layers; however, for longer periods, the error may be considerable. The highest shear velocities assumed in the section limits the maximum period at which the higher modes exist; one consequence

of the failure to model the deeper layers is the limited period range in which the higher modes are theoretically present. The higher modes would be present up to longer periods if higher shear velocities were used in the model.

The oscillatory nature of the higher mode group velocities is a basic property of even simple structures, but is accentuated when a low-velocity channel, such as a sedimentary section, is present. The maxima and minima of the group velocity curves are of interest, because they produce large amplitude arrivals from earthquakes and may be associated with peaks in the noise spectra (Gutenberg, 1958).

An example of the results obtained for the change with depth of the displacements of the different Rayleigh modes (at FO-TX) is shown in figure 9. The fundamental mode displacement decreases monotonically with depth with only slight inflections at discontinuities. Large displacements are present at depth when a lobe of a higher mode occurs in a low-velocity zone which traps a large percentage of the total energy of the wave. Low-velocity zones are present at all the holes studied. At all the sites, except AP-OK, the low-velocity zone is caused by the sediments, and at AP-OK, by the volcanics below the high-velocity limestone.

6. 1. 3 Spectral Analysis

The principal tool used in the interpretation of the data consisted of obtaining spectra and cross spectra, and the associated auto- and cross-correlations of long noise samples. The techniques used to obtain spectra, and the accuracy and resolution that is obtained have been extensively discussed in the literature (for example, Blackman and Tukey, 1958) and need not be discussed here.

The length of the noise sample used varied between 180 and 450 sec. As a compromise between accuracy and resolution, a lag of 8 percent of the sample was usually used; however, either smaller or greater lags were sometimes employed to increase either the accuracy or the resolution of the results. In this section of the report, each figure will give the length of sample and the lag used, to allow the reader to determine the reliability of the results. The sampling rate used (usually 25 samples/sec) insured that the folding frequency was well outside of the frequency range of interest.

Theoretical studies on the accuracy of cross spectra have been published in the literature (for example, Amos, et al., 1963). The results indicate that the experimental coherences are a complex function of the actual coherence, the
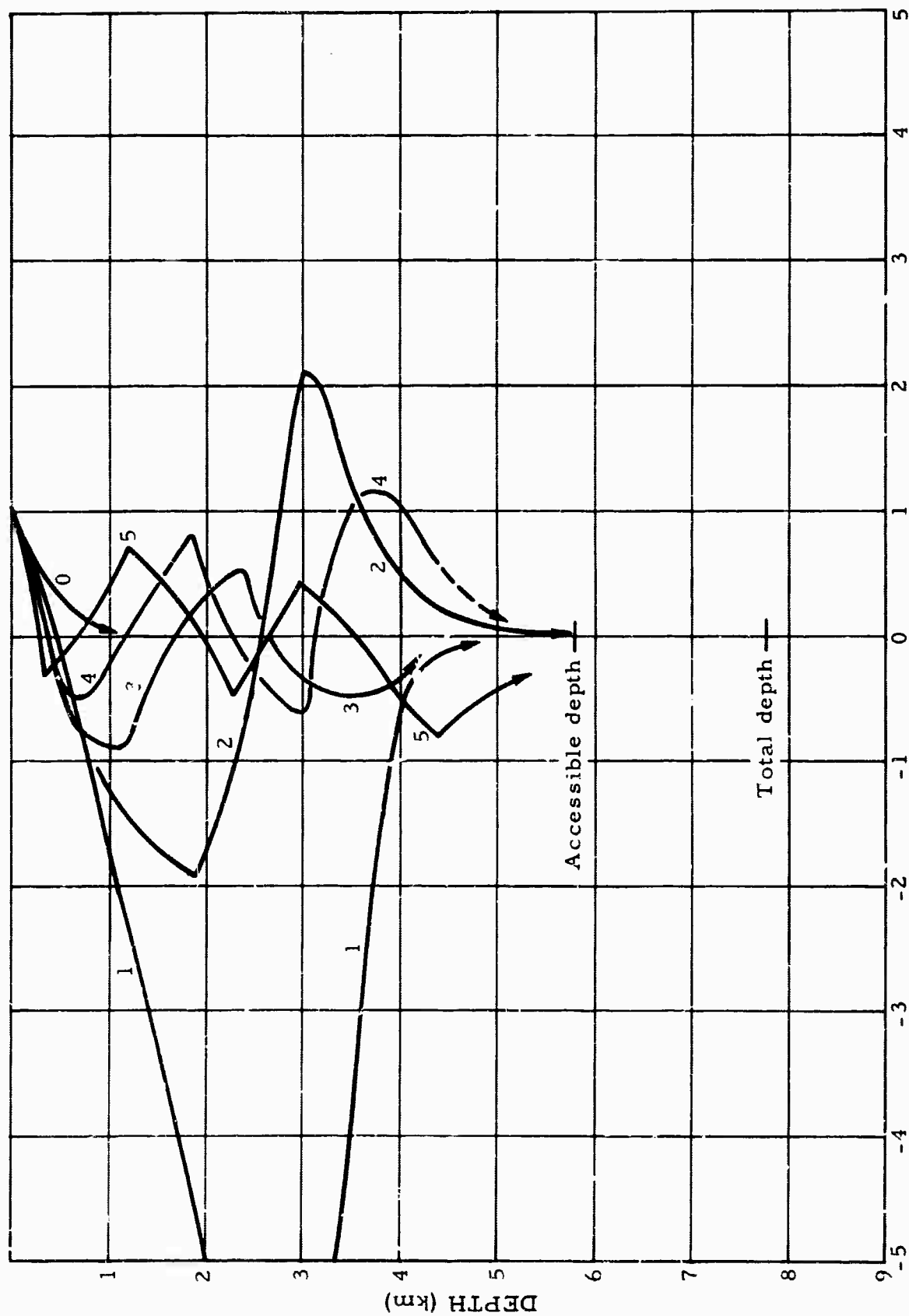
Figure 9. Rayleigh and higher-mode amplitude (normalized to amplitude at Earth's surface) as a function of depth at FO-TX. Period = 0.5 sec.

smoothing function, and the lag window. Figure 10 shows a graph of the confidence limits for different lag windows. A hanning smoothing function was used in all cases. Examination of the figure indicates that considerable errors are to be expected when the actual coherences are close to zero. It must be noted that figure 10 shows coherence for clearer presentation while all experimental plots are the square of coherence, as obtained from the computer program.

The magnifications at 1 Hz were used to calibrate the power spectrum; therefore, only the values at 1 Hz are correct ground motion values. Because of the identical responses of the seismographs used, the deep-hole-divided-by-surface ratios used in the interpretation are correct at all frequencies. The ratios are obtained by dividing the deep-hole noise spectrum by the surface spectrum, and will be called power ratios in the body of the report. The square root of the power ratio will be referred to as the amplitude ratio.

6.1.4 Theory

This section derives the theory necessary to interpret the experimental results. Both body waves and Rayleigh waves will be considered. For the deep-hole measurements, the amplitude-depth relationships need to be considered, while for the surface array measurements, the phase velocities are of interest. In both cases, the phase angles and coherences yield valuable information.

The main tool in the interpretation are the spectra and cross spectra of the noise of different seismometers placed in either a horizontal or vertical plane. Therefore, the theory will be concerned with the results obtained by spectral analysis techniques. The theory of the behavior of body waves in the deep hole and across arrays is, in general, confined to the results that would be obtained in a half space. For the case of a layered media, the amplitude-depth relationships for P waves at vertical incidence has been solved (Gupta, 1965). The reason for not extending the theory to the layered case is that convenient matrix method does not appear to be applicable when each term is an integral, as is the case when spectra are considered. In the case of fundamental and higher mode Rayleigh waves recorded by the deep-hole seismometer, the azimuth of approach is not important because the amplitude-depth relationships are the values measured. However, in the case of body waves, the angle of incidence must be considered.

First, the theoretical amplitude-depth relationships that will be obtained from a mixture of Rayleigh modes is discussed. Then, the theory of body-wave noise at random angles of incidence is discussed in relation to the results that

TR 65-112   -18-
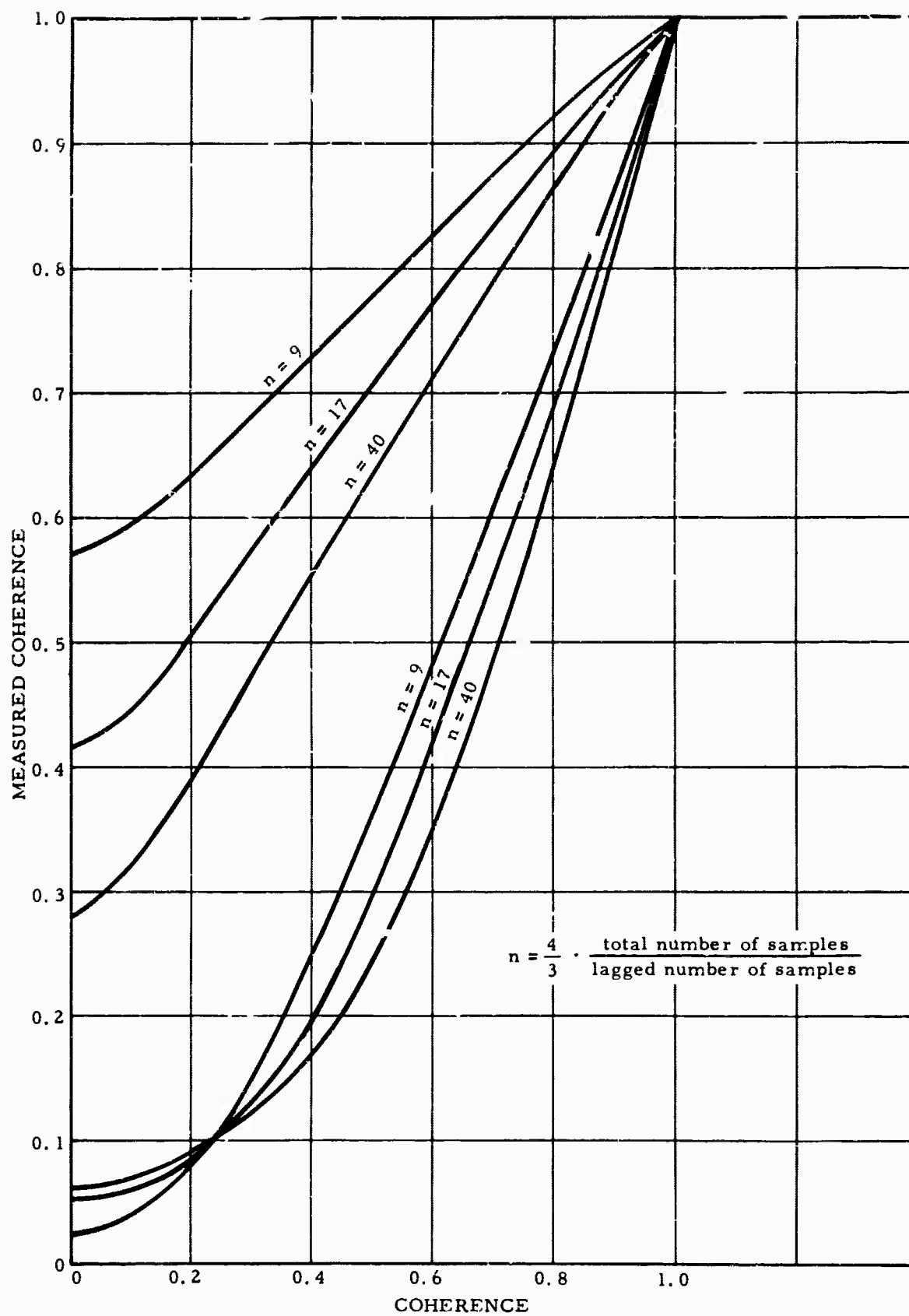
Figure 10. 90-percent confidence limits for spectral coherence

would be obtained from deep-hole measurements. The assumption of no P-to S-wave conversion at the free surface is made to show the mathematical procedure followed; the solution can, in this case, be obtained in closed form. Then, the formulas (not in closed form) that include P- to S-wave conversion at the free surface are derived. Next shown are the results that would be obtained in the deep hole if a mixture of Rayleigh waves were present.

The results obtained from cross spectra of the vertical seismometers of a surface array are discussed for the case of surface waves and body waves.

6.1.4.1 Deep-Hole Theory

If the noise is assumed to consist of a mixture of Rayleigh modes, the results of spectral analyses can be explained in the following manner.

$$X_1(t) = \sum_{n=1}^{N} X_n(t)$$

where N is the number of Rayleigh modes present in the noise. The spectrum is obtained by first autocorrelating and then taking the Fourier transform of the autocorrelation. The result is

$$\varphi_{11}(\omega) = \sum_{n=1}^{N} \varphi_n(\omega) \tag{1}$$

The spectrum of the noise recorded by the deep-hole seismograph is related to the surface noise by a transfer function $h_n(\omega) \exp(i\theta_n)$,

$$\varphi_{22}(\omega) = \sum_{n=1}^{N} \left| H_n(\omega) \right|^2 \varphi_n(\omega) \tag{2}$$

The transfer function is the theoretical change of the displacements of the Rayleigh modes with depth. According to theory, the angle δ is always 0 or 180 deg; therefore, the absolute value signs are not strictly necessary in the equation.

The cross spectrum between a surface and a deep-hole noise sample is given by

$$\varphi_{12}(\omega) = \sum_1^N H_n(\omega)\, e^{i\delta_n}\, \varphi_n(\omega) \tag{3}$$

Examination of equation 3 indicates that the cross spectrum will be a real quantity if only Rayleigh waves are present, because the angle δ_n is either 0 or 180 deg. A negative cross spectrum indicates that the "power" in the Rayleigh modes, 180 deg out-of-phase at depth, is larger than the power of the Rayleigh modes in phase at depth. The coherence is defined as

$$Coh = \frac{\left|\varphi_{12}\right|^2}{\varphi_{11} \cdot \varphi_{22}}$$

Examination of the equations indicates that the coherence is unity at all depths if only one Rayleigh mode is present, and will always be less than unity for a mixture of modes. The coherence will be zero when equal amounts of power are in phase and 180 deg out-of-phase.

The behavior of seismic noise in the frequency range between 0.5 and 5.0 Hz as a function of depth suggests the possibility of body-wave noise at random angles of incidence. First, the equations are solved under somewhat restrictive assumptions that allow a solution in closed form to be obtained. The more general solution can only be solved by numerical integration.

The following assumptions are made:

    a. P-wave noise arriving independently from all angles of incidence with equal energy content;

    b. No conversion from P to S waves at the free surface;

    c. An isotropic, homogeneous half space.

The equations are derived for the noise as it would be detected by a vertical-motion seismograph.

The solutions are derived in some detail to indicate the methods used. The particle displacement at the surface is taken to be

$$X_1(t) = \sum_{n=1}^{N} f_n(t) \cos \theta_n$$

where the subscript 1 denotes quantities measured at the surface and θ is the angle of incidence measured from the vertical. The autocorrelation of each independent time series $f_i(t)$ is denoted by $\frac{1}{N} \psi(\tau)$.

The autocorrelation of $X_1(t)$ then becomes

$$\psi_{11}(\tau) = \frac{1}{N} \sum_{n=1}^{N} \psi_n(\tau) \cos^2 \theta_n$$

By taking the Fourier transform, the power spectrum is obtained

$$\phi_{11}(\omega) = \frac{1}{N} \sum_{n=1}^{N} \phi_n(\omega) \cos^2 \theta_n$$

Now let $N \to \infty$, the power spectrum of the surface noise becomes

$$\phi_{11}(\omega) = \phi(\omega) \frac{1}{\pi} \int_{-\pi/2}^{\pi/2} \cos^2 \theta \, d\theta = \frac{\phi(\omega)}{2} \tag{4}$$

The spectrum of the noise at any depth (denoted by subscript 2) is obtained as follows:

$$X_2(t) = \sum_{n=1}^{N} \left\{ \left[\frac{1}{2} f_n(t - \frac{\alpha}{2} \cos \theta_n) \right] + \left[\frac{1}{2} f_n(t + \frac{\alpha}{2} \cos \theta_n) \right] \right\} \cos \theta_n$$

where $\frac{\alpha}{2}$ is the vertical uphole time.

Going through the same procedure as for the surface, we obtain the spectrum at depth

$$\phi_{22}(\omega) = \phi(\omega) \frac{1}{2\pi} \int_{-\pi/2}^{\pi/2} \left\{ \cos^2\theta + \cos(\omega a \cos\theta)\cos^2\theta \right\} d\theta$$

$$= \phi(\omega) \left\{ \frac{1}{4} + \frac{J_0(a\omega)}{2} - \frac{J_1(a\omega)}{2a\omega} \right\} \tag{5}$$

Note that the solution approaches $\frac{1}{2}$ as $\omega \to 0$ because $\frac{J_1(a\omega)}{a\omega} \to 0.5$. The ratio of the deep-hole spectrum divided by the surface spectrum often used in the interpretation then becomes

$$R = \frac{1}{2} + J_0(\omega a) - J_1(\omega a)/(a\omega)$$

which, as expected, approaches unity for very low frequencies.

The cross spectra between the surface and the deep-hole spectra are obtained in the same way

$$\phi_{12}(\omega) = \phi(\omega) \left\{ J_0\left(\frac{a\omega}{2}\right) - \frac{J_1\left(\frac{a\omega}{2}\right)}{\frac{a\omega}{2}} \right\} \tag{6}$$

Notice that the cross spectrum is either positive or negative, but does not have an imaginary component, indicating that the phase changes from 0 to 180 deg. The coherence between the surface and the deep-hole noise becomes

$$\text{Coh}^2 = \frac{\left| J_0\left(\frac{a\omega}{2}\right) - \frac{J_1\left(\frac{a\omega}{2}\right)}{a\omega/2} \right|^2}{\frac{1}{8} + \frac{J_0(a\omega)}{4} - \frac{J_1(a\omega)}{4 a\omega}}$$

which approaches unity as $\omega \to 0$.

The theory for S waves at random angles of incidence is similar. Define $\frac{3}{2}$ as the uphole time for S waves.

The equations become:

$$\phi_{11}(\omega) = \frac{1}{2} \cdot \phi(\omega)$$

$$\phi_{22}(\omega) = \phi(\omega) \left\{ \frac{1}{4} + \frac{J_1(\beta\omega)}{2\beta\omega} \right\}$$

$$\phi_{12}(\omega) = \phi(\omega) \frac{J_1(\frac{\beta\omega}{2})}{\frac{\beta\omega}{2}}$$

In the previous example, the conversion of P to S waves at the free surface was neglected. Taking the conversions into account and keeping the rest of the assumptions made before, a more realistic solution can be obtained; however, the solution could not be obtained in closed form and numerical integration of the integrals is necessary.

In this case, the time series at the surface and at depth become

$$X_1(t) = \sum_{n=1}^{N} f_n(t) \cos \theta_n + b(\theta) f_n(t) \cos \theta_n + c(\theta) f_n(t) \sin \xi_n$$

$$X_2(t) = \sum_{n=1}^{N} f_n(t - \alpha \cos \theta) \cos \theta + b(\theta) f_n(f + \alpha \cos \theta) \cos \theta + c(\theta) f_n(t + \beta \cos \xi) \sin \xi$$

where b and c are reflection coefficients for P and S waves from an incoming P wave. These coefficients are functions of the angle of incidence and can be found in the literature (Ewing, et al., 1957). S waves are reflected at an angle ξ, which is connected with θ by Snell's Law.

The procedure followed in obtaining the required integrals is the same as that employed previously. Because of the large number of terms involved in the derivation, only the resulting integrals will be given.

$$\phi_{11}(\omega) = \phi(\omega) \frac{1}{2\theta} \int_{-\theta}^{\theta} \left[\cos^2\theta + b^2 \cos^2\theta + c^2 \sin^2\xi \right. $$

$$\left. + 2b \cos^2\theta + 2c \cos\theta \sin\xi + 2bc \cos\theta \sin\xi \right] d\theta \tag{7}$$

$$\varphi_{22}(\omega) = \varphi(\omega)\frac{1}{2\theta}\int_{-\theta}^{\theta}\left[\cos^2\theta + b\cos^2\theta + c^2\sin^2\xi\right.$$

$$+ 2b\cos(\omega\alpha\cos\theta)\cos^2\theta$$

$$+ 2c\cos\omega(\frac{\alpha}{2}\cos\theta + \frac{\beta}{2}\cos\xi)\cos\theta\sin\xi$$

$$\left. + 2bc\cos\omega(\frac{\beta}{2}\cos\xi - \frac{\alpha}{2}\cos\theta)\cos\theta\sin\xi\right]d\theta \qquad (8)$$

$$\varphi_{12}(\omega) = \varphi(\omega)\frac{1}{2\theta}\int_{-\theta}^{\theta}\left[\cos(\omega\frac{\alpha}{2}\cos\theta)\cos^2\theta + b^2\cos(\omega\frac{\alpha}{2}\cos\theta)\cos^2\theta\right.$$

$$+ c^2\cos(\omega\frac{\beta}{2}\cos\xi)\sin^2\xi + 2b\cos(\omega\frac{\alpha}{2}\cos\theta)\cos^2\theta$$

$$+ ic\left\{\sin(\omega\frac{\alpha}{2}\cos\theta) - \sin(\omega\frac{\beta}{2}\cos\xi)\right\}\cos\theta\sin\xi \qquad (9)$$

$$\left. + ibc\left\{\sin(\omega\frac{\alpha}{2}\cos\theta) + \sin(\omega\frac{\beta}{2}\cos\xi)\right\}\cos\theta\sin\xi\right]d\theta$$

Examination of these formulas indicates that if the numerical integration is carried out between even limits, a number of the terms disappear because they are odd functions.

It will be noted that while the spectra are real quantities, as expected, the cross spectrum is a complex quantity, so that the phase is no longer either 0 or 180 deg but attains intermediate values. In cases of practical interest, the phase angles are so close to 0 or 180 that spectral analyses are not sufficiently accurate to detect the difference.

Numerical integration of the integrals was carried out on a CDC 160-A computer.

Rayleigh waves and body waves at vertical incidence result in standing wave patterns because of the interference effects of incident and surface-reflected waves. Consequently, the phase angle at depth can only be either 0 or 180 deg as compared with the surface. The cross spectra given in equation 9

indicates that this is no longer the case for body waves at angles of incidence other than the vertical. The cross spectrum has an imaginary component indicating that a standing wave pattern is not set up with depth. The same conclusion has been reached by Felix Nagel (unpublished manuscript) from the amplitude-depth relationship s obtained when plane waves arrive at the free surface at some arbitrary angle of incidence. The amplitude-depth relationships are a function of time and standing waves are not obtained. The position of the zero amplitude value changes only slightly with time; therefore, a low value resembling a nodal point will be obtained at depth (for a particular frequency) if the wave motion is averaged over some time.

In general, over a narrow band of frequencies, the amplitude-depth relationship of P waves at close to vertical incidence are ofter similar to one of the Rayleigh-mode amplitude-depth relationships. For example, the third higher Rayleigh mode and P waves at close to vertical incidence are almost identical for a frequency of 2 Hz at AP-OK.

Narrow band-pass filtering together with cross-correlation offers the possibility of distinguishing between surface waves and body waves.

If surface waves are present in the noise, the cross-correlation between surface and deep-hole noise samples will have a maximum at zero lag. The maximum will be positive or negative, depending on whether the surface waves at depth are in phase or 180 deg out-of-phase with the surface. In the case of body waves, the maximum in the cross-correlation will be at a lag time equal to the up-hole travel time of the body waves.

It must be recognized that if any one frequency acts like a plane wave, P waves at vertical incidence will set up a standing wave pattern and cross-correlation results will look as if surface waves are present. Therefore, some caution is necessary in interpreting the results. If very narrow-band filtering were employed, i.e., examining essentially one frequency, it would be possible to interpret the results quantitatively. However, the cross-correlations over a finite bandwidth used here can only be interpreted qualititatively to distinguish between surface waves and body waves.

6.1.4.2 Surface Arrays

In the case of surface waves arriving at the array from a given direction (or a given direction and angle of incidence in the case of body waves), the equations can be obtained easily. The spectrum of the noise at each seismometer will be the same (ignoring seismometer-to-ground coupling problems).

$$\omega_{11} = \omega_{22} = \sum_{n=1}^{N} \omega_n(\omega)$$

The cross spectra will be:

$$\omega_{12} = \sum_{n=1}^{N} \omega_n(\omega) \, e^{-i\omega(\frac{\Delta x}{v_n} \cos \xi)} \tag{10}$$

where

N = number of wave types present in the noise

Δx = distance between the seisometers

v = phase velocity of the waves

ξ = angle between the direction connecting the seismometers and the direction of arrival.

The cross spectra between two seismometers give only apparent phase velocities, and two cross spectra are necessary to obtain the real phase velocities and directions of arrival.

The theoretical results indicate that coherence will be unity if only one wave type is present, and less than unity in all other cases.

Experimental data from arrays usually indicates that the noise is essentially omnidirectional (isotropic), i.e., arriving with approximately equal energy content from all directions. For the case of surface waves, the solution that would be obtained has been solved by Backus, et al., (1964). The spectrum of each seismometer is the same, $\omega(\omega)$, and the cross spectra become

$$\omega_{12}(\omega) = \omega(\omega) \, J_o\left(\frac{\omega \Delta x}{v}\right) \tag{11}$$

where the Δx and v are, respectively, separation between seismometers and phase velocity.

This solution can easily be extended to more than one wave type and results in the sum of Bessel functions equal to the number of wave types present.

Because of the possible presence of body-wave noise, it is necessary to also consider the case of body waves from random directions and random angles of incidence.

For P waves arriving at the surface seismometers with equal energy content from random directions and all angles of incidence, the time series for a vertical-motion seismometer No. 1 is

$$X_1(t) = \sum_1^N f_n(t) \cos \theta_n$$

At seismometer No. 2, the time series becomes

$$X_2(t) = \sum_1^N f_n(t - \frac{\Delta x}{v} \sin \theta_n \cos \xi_n) \cos \theta_n$$

where θ refers to the angle of incidence and ξ to the direction of the waves. Proceeding in exactly the same fashion as described in section 6.1.4.1, the spectrum of each seismometer becomes

$$\omega_{11}(\omega) = \omega_{22}(\omega) = \frac{1}{2} \omega(\omega)$$

and the cross spectrum becomes

$$\omega_{12}(\omega) = \omega(\omega) \cdot \frac{1}{2\pi} \cdot \frac{1}{\pi} \int_0^{2\pi} \int_{-\pi/2}^{\pi/2} e^{-i\omega(\frac{\Delta x}{v} \sin \theta \cos \xi)} \cos^2 \theta \cdot d\xi d\theta$$

By performing the last integration, the expression reduces to

$$\omega_{12}(\omega) = \omega(\omega) \frac{1}{2\pi} \int_0^{2\pi} \frac{J_1(\frac{\omega \Delta x}{v} \cos \xi)}{\frac{\omega \Delta x}{v} \cos \xi} \cdot d\xi \tag{12}$$

This equation must be solved by numerical methods of integration.

Notice that under the assumptions made, both formulas 11 and 12 have no imaginary parts and the phase angle is either 0 or 180 deg. Therefore, velocities can only be obtained from the coherence values.

6.1.5 Experimental Results

In order to facilitate discussion of the experimental results, the passband of the short-period Benioff was divided somewhat arbitrarily into three period ranges: 5.0 to 2.0 sec, 2.0 to 0.8 sec, and 0.8 to 0.3 sec. These divisions were chosen partly for convenience, and partly because somewhat different wave types appear to predominate in the different period ranges.

The 6.0-sec microseisms are not discussed here, because the analyses indicated clearly that, as measured by a vertical-motion seismometer, the fundamental mode Rayleigh wave is the only wave type present. This conclusion has been previously reached by a number of authors (see for example, Gutenberg, 1958).

6.1.5.1 Microseisms, 5.0 to 2.0 Sec

The ratio of deep-hole divided by surface noise spectra at all sites investigated indicates that fundamental mode Rayleigh waves do not usually predominate in the period range between 5.0 and 2.0 sec.

Figure 11 shows the experimental power ratio, and figure 12, the phase angle and coherence obtained from noise samples when the deep-hole seismometer was located at a depth of 5200 m at FO-TX. The theoretical curves for the first three Rayleigh modes and for P waves at vertical incidence are also shown. These analyses were made at a time when a storm in the Atlantic was the cause of large microseisms in the period range of 2.0 to 6.0 sec. The lowest value of the power ratio occurs at a period of 4.0 sec; however, the coherence is not zero until a period of 3.4 sec is reached. This behavior indicates that between 3.4 and 4.0 sec most of the power was in phase; therefore, the fundamental mode, which is the only wave in phase, predominated at these periods. To explain the power ratio, the rest of the energy must be in the first higher mode. Examination of the figures indicates that for periods less than 3.4 sec, only a small amount of fundamental mode Rayleigh waves can be present in the noise. The experimental values lie between the theoretical first higher Rayleigh mode and P-wave curves. The experimental data can be explained by either mixtures of fundamental and first higher mode Rayleigh waves, or P waves and first higher mode Rayleigh waves.
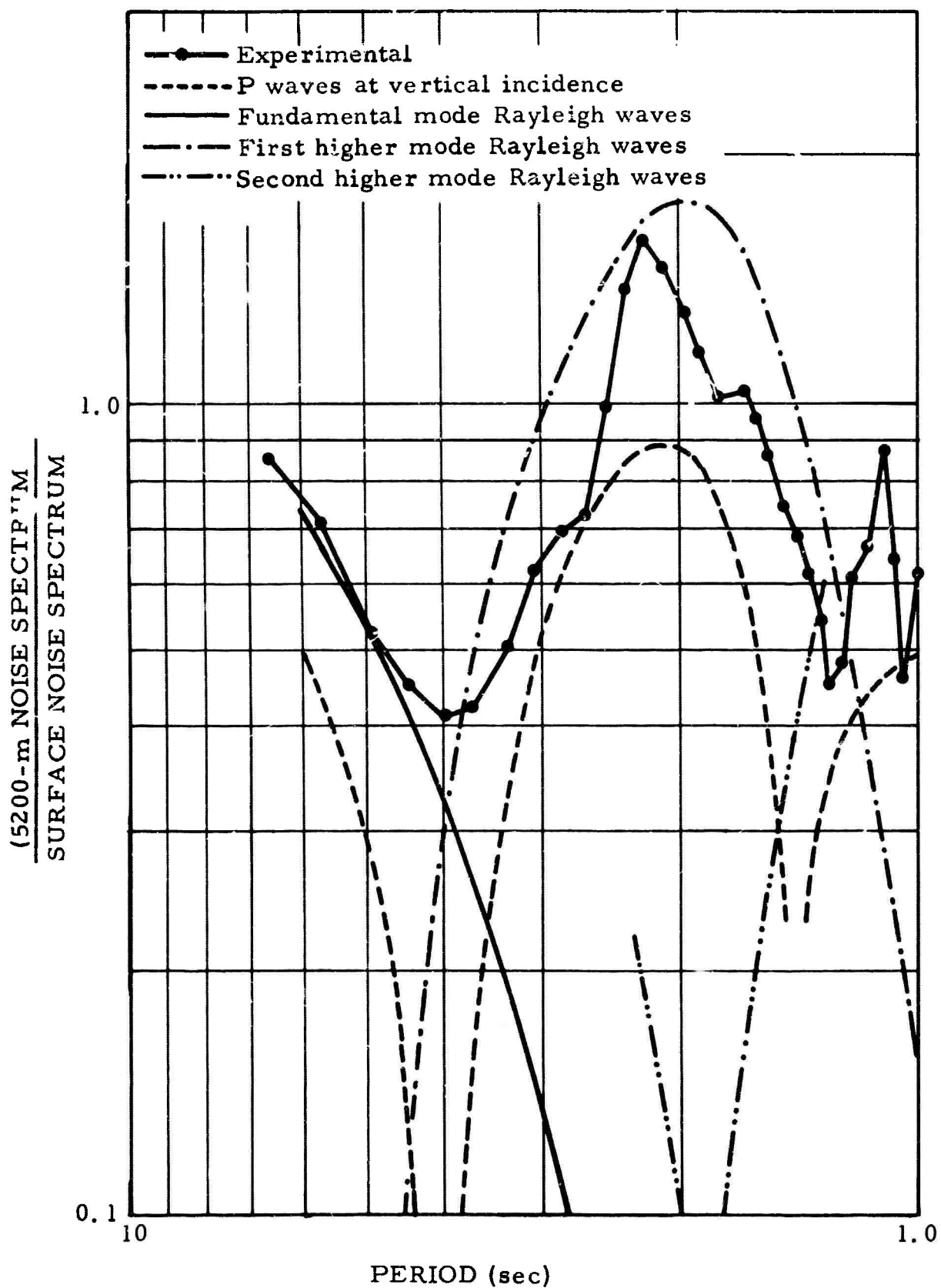
Figure 11. Deep-hole (5200-m) vertical noise spectrum divided by surface noise spectrum. Theoretical amplitudes are included. FO TX. 300-sec sample, 10 samples/sec, 5-percent lags.
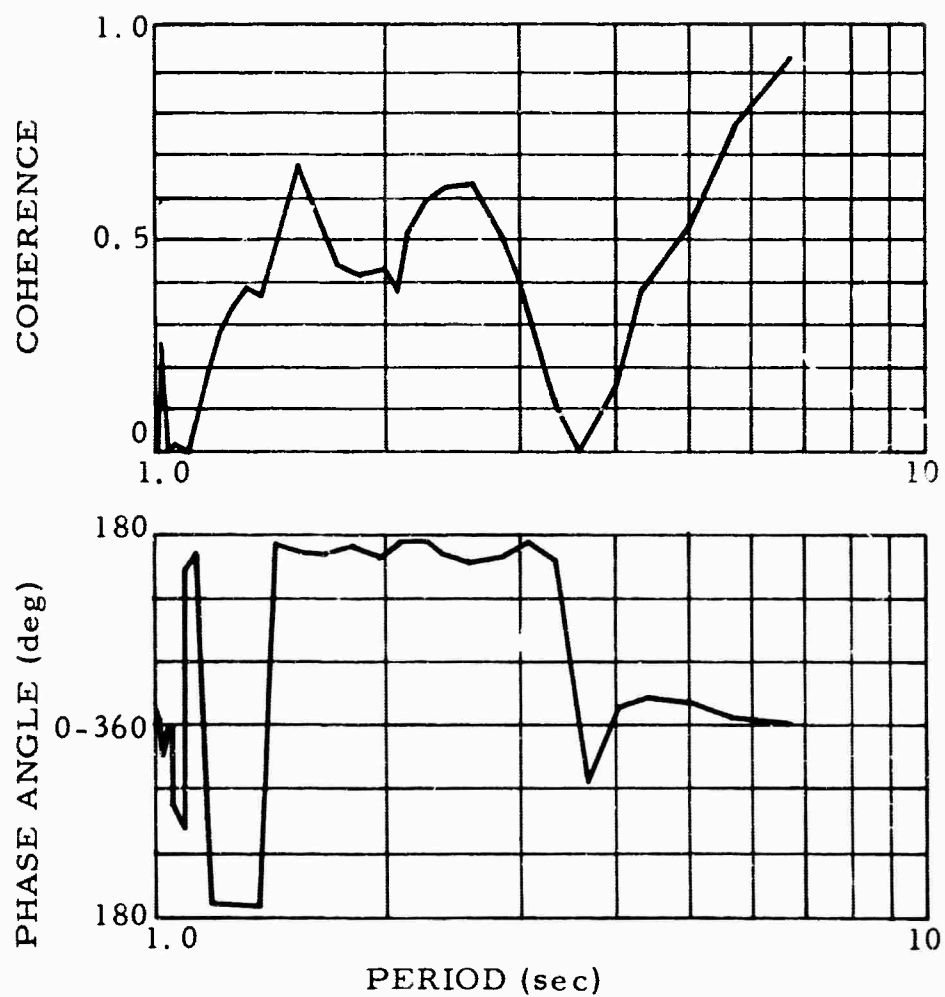
Figure 12. Phase angle and coherence of the noise between the surface and 5200 m, FO-TX. 300-sec sample, 10 samples/sec, 5-percent lags

Considering the accuracy of the spectral analyses and the possibility of some error in the Rayleigh-wave amplitude-depth relationships caused by the lack of information about the velocity section below the hole, no attempt was made to calculate the power in each type of wave.

The deep-hole results at FO-TX indicated that either P waves or first higher mode Rayleigh waves predominated in the noise but the results could not be used to conclusively distinguish between the two waves. In an attempt to distinguish between these two possibilities, information from WMSO was used. Cross spectra between noise samples from three seismometers located in a 3-km tripartite were obtained. The cross spectra of the noise from two seismometers are sufficient to specify an apparent velocity. Two pairs of seismometers are sufficient to specify phase velocity and angle of arrival. The cross spectra between the noise samples from all three noise samples were used to check if consistent results were obtained from all combinations of pairs. The results obtained are given in table 2.

Table 2. Phase velocity measurements from cross spectra, WMSO

Period (sec)	Freq. (Hz)	Azimuth (deg)	Velocity (km/sec)	Average (coherence)^2	Spectral amplitude (mμ^2/Hz)
6.667	.1499	213	2.85	.88	51.0
5.714	.1750	215	3.16	.88	91.1
5.000	.2000	219	3.49	.86	92.2
4.444	.2250	226	3.68	.83	67.0
4.000	.2500	229	3.63	.76	39.8
3.636	.2750	228	3.83	.70	26.3
3.333	.3000	228	4.26	.69	22.4
3.077	.3249	229	4.33	.64	23.6
2.857	.3500	226	4.41	.54	21.8
2.667	.3749	226	4.24	.46	18.5
2.500	.4000	228	4.51	.46	1
2.353	.4249	229	4.87	.41	15.1
2.222	.4500	231	4.23	.22	13.2
2.105	.4750	237	4.69	.23	10.6
2.000	.5000	235	5.70	.25	9.12

As indicated in the theoretical results, if the noise field is isotropic, the phase angle is 0 or 180 deg. The phase angles obtained from the experimental results indicated clearly that part of the noise at periods greater than 2.0 sec was directional. The directions obtained indicated that the storm in the Atlantic was responsible for the directional part of the noise.

Examination of combinations of directional and nondirectional noise (from equations 10, 11, and 12) indicates that the phase velocity obtained for periods greater than approximately 2.0 sec by these measurements is too large. This behavior is caused by the isotropic noise staying either in phase or 180-deg out-of-phase. In the period range under examination here, this causes the phase angle from the cross spectra to be intermediate between the actual value for the directional noise and the 0 deg value of the omnidirectional noise. As an example, assume 50-percent isotropic 3.0-sec period waves at 4 km/sec and 50-percent directional waves at 4 km/sec arriving along the line connecting two seismometers 3 km apart; in the case, the phase angle will be 64 deg. If only the unidirectional waves were present, the phase angle would be 88 deg. The above presented argument indicates that the real phase velocities of the directional noise are less than those obtained from the cross spectra. Therefore, the phase velocities in table 2 indicate that body waves are excluded for anything except every shallow angles of emergence.

The choice, therefore, lies between fundamental and first higher mode Rayleigh waves; however, results from FO-TX during the same time indicate that only small amounts of fundamental mode Rayleigh waves were present in the noise at these periods. Therefore, the first higher mode Rayleigh waves must predominate.

The arguments given above are meant to show the existence of the first higher Rayleigh mode, and are not intended to prove that this mode pre-minates at all times and at all locations. However, phase angles from all deep-hole measurements always show the same behavior; the phase angle changes from 0 to 180 deg at a period that can be explained by P waves or higher modes. The fundamental mode never predominates at periods less than approximately 4.0 sec. It is of interest that when the first higher mode can be shown to predominate, a small high in the spectra usually appears at 3.0 sec (see table 2).

Particle motion diagrams of the 3.0-sec microseisms produced ambiguous results; almost all sizes and shapes of ellipses were obtained. This failure was possibly caused by the presence of different wave types in closely adjacent period ranges. The possible presence of Love waves in the noise could also contribute to the failure to obtain reproducible results.

At the sites where thick sections of low-velocity rock are present (usually shales), the results obtained are more difficult to interpret than at the sites where predominantly high-velocity rocks are present. Figure 13 shows an example of the results obtained at the Pinedale, Wyoming, site. The section at this location is composed entirely of shales. The results can probably be best explained by a combination of P waves and fundamental Rayleigh waves if the location of the nodal point is taken as the main crite.ia for interpretation. However, there is some doubt as to the validity of this interpretation. Figure 13 also shows the results obtained from spectral analysis of a surface wave of an earthquake from Baja California. The group velocity of these waves was about 3.2 km/sec, indicating that they are surface waves, probably higher mode Rayleigh waves as recorded by the vertical-motion seismographs. It is noticeable from the figure that the behavior of the amplitude-depth relationships of the noise and these surface waves is very similar, especially in regard to the location of the nodal point. This behavior suggests that the theoretical Rayleigh wave curves may be in error. The theoretical Rayleigh wave computer program used does not take into account the well-known velocity anisotropy of shales. Preliminary results from an anisotropic Rayleigh wave program suggest that the discrepancies between theoretical and experimental results can be explained in this way.

It is, of course, entirely possible that the noise does consist of fundamental mode Rayleigh waves and P waves, and that the first higher mode was not present at the time of the experiments. With the limited depth of the hole and with no surface array information, the problem cannot be solved. With holes of the u nal depth of approximately 3000 m, it is not possible to distinguish between the two possibilities of P waves or first higher mode Rayleigh waves. Figure 14 shows the amplitude-depth relationship of the 2.0-sec noise at AP-OK. Either theoretical curve will explain the experimental data.

6.1.5.2 Noise of Periods between 2.0 and 0.8 Sec

The noise in this period range predominates in the spectra at sites close to the coast; at quiet sites distant from the coast, the noise at these periods has usually been attenuated to very small values.

Considerable difficulty has been encountered in interpreting the data at these periods. The amplitude-depth relationships agree quite well with the theoretically predicted P-wave amplitude-depth relationships. As an example, figure 15 shows the power ratio obtained at AP-OK from the noise at the surface and 2917 m. The theoretically predicted amplitude-depth relationship for P wave at random angles of incidence between -45 and +45 deg from the
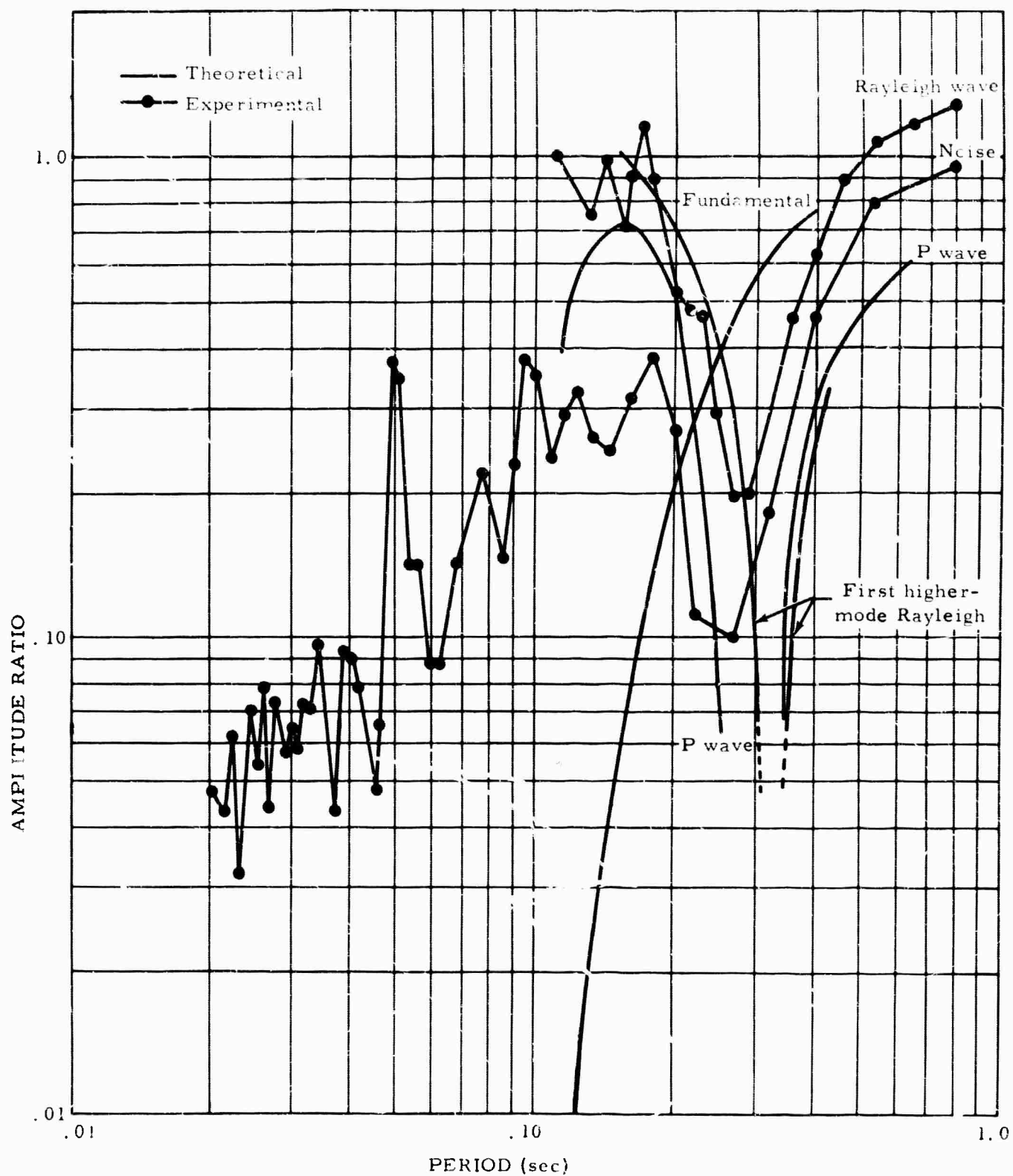
Figure 13. Amplitude ratio of the noise and a Rayleigh mode from Baja
California as recorded at 3060 m at Pinedale, Wyoming. Theoretical
curves for P waves and Rayleigh waves are included.

Figure 14. Observed and theoretical amplitude ratio with depth for periods of 0.5, 1.0, and 2.0 sec. 180-sec sample, 25 samples/sec, 5-percent lags

Figure 15. Theoretical and experimental power ratios, phase angles, and coherences theory for P waves arriving randomly -45 to +45 deg from the vertical. Uphole 0.5 sec. 180-sec sample, 25 sample/sec, 8-percent lags

vertical, and the experimental and theoretical phase angles and coherences
for the same noise sample are also shown in the same figure. The agree-
ment between theory and experiment is quite good, and could be improved
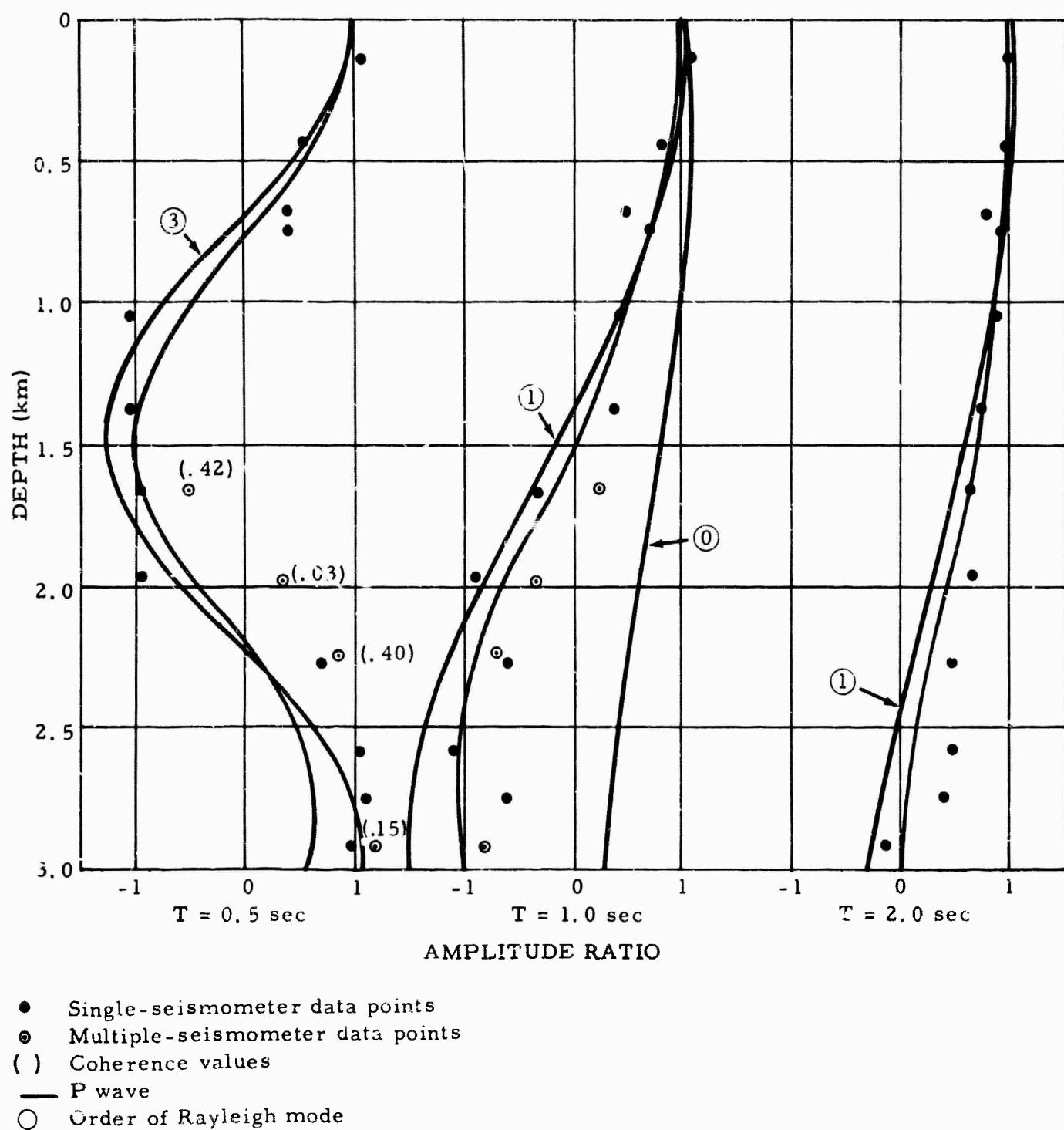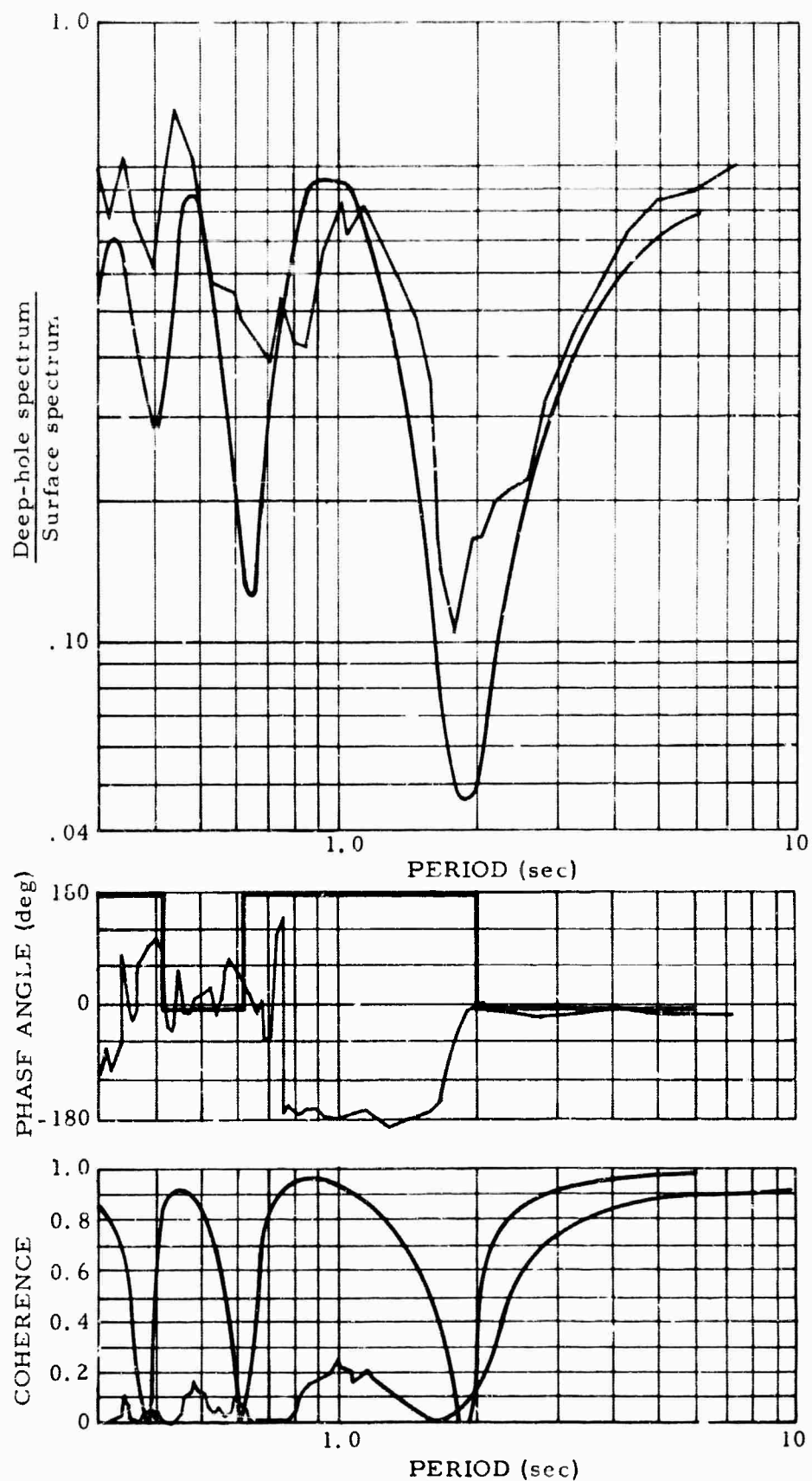even further by assuming the presence of some S-wave noise. Figure 14
shows the amplitude-depth relationships for the 1.0-sec noise as measured
at AP-OK; the theoretical curve for P waves at vertical incidence fits the
experimental data quite well. However, the first higher mode theory is also
quite close to the experimental data. There exists considerable doubt that
P waves are the correct explanation of the noise at these periods. In an
attempt to distinguish between the two possibilities (surface or body waves),
cross-correlations were obtained after digital filtering. The digital filters
had extremely sharp cut-offs, and only the noise in the period range of
interest passed through. Figure 16 shows the results obtained in the period
ranges of 2.5 to 1.5 sec and 1.5 to 0.8 sec.

The experimental evidence shown in figure 16 indicates that surface waves
are responsible for the noise in these two period ranges. As mentioned in
the section on deep-hole theory, P waves at close to vertical incidence can
set up a standing wave pattern that will result in cross-correlations of the
type shown in figure 16. However, it appears unlikely that noise, the statis-
tics of which indicate that it is a completely random phenomenon, will act in
this fashion. It must be noted at this time that the cross-correlation of
signals will result in the highest value at a lag equal to the uphole time.
Furthermore, as will be shown in the next section, random P waves, when
present, will give a maximum in the cross-correlation at a lag other than
zero.

Figure 17 shows the coherence between noise samples from seismometers
3 km apart at WMSO. The high coherences at periods greater than 2.0 sec
were caused by directional noise. For periods between 1.0 and 2.0 sec, the
phase angles indicated the presence of essentially isotropic noise. The
experimental results can best be explained by waves traveling at velocities
of 3.0 to 4.0 km/sec.

The most probable solution is that the noise consists of a mixture of Rayleigh
modes, possibly on the basis of equipartition of energy as proposed by Sax
and Hartenburger (1964). Some evidence for the presence of the second
higher mode is obtained from figure 11, where at a period of 1.1 sec, the
experimental data can only be explained by the presence of the second higher
mode. However, this peak in the power ratio did not appear at all times;
therefore, while it may be present, the second higher mode does not always
predominate. It is apparent from the results that the fundamental mode
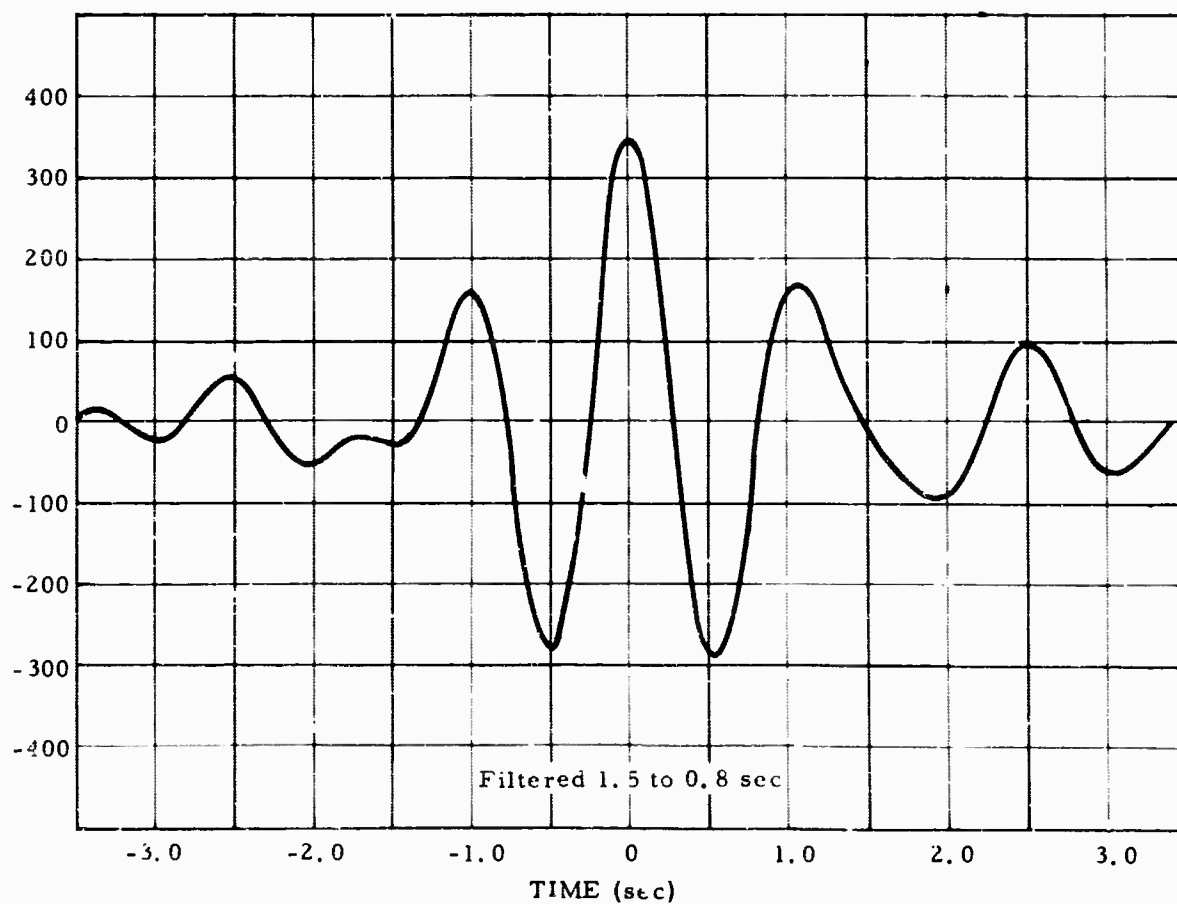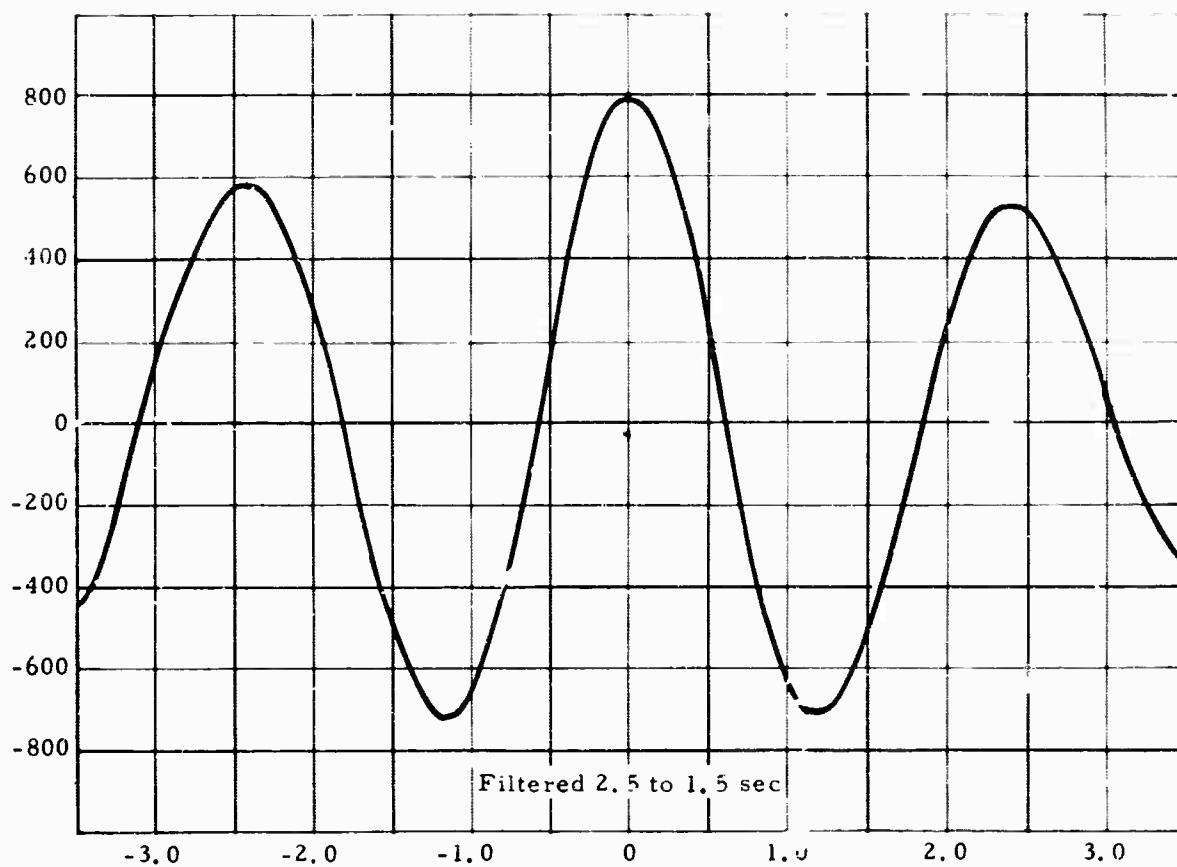
Figure 16. Cross-correlations of noise from seismometers at depths of 1970 and 2880 m, AP-OK
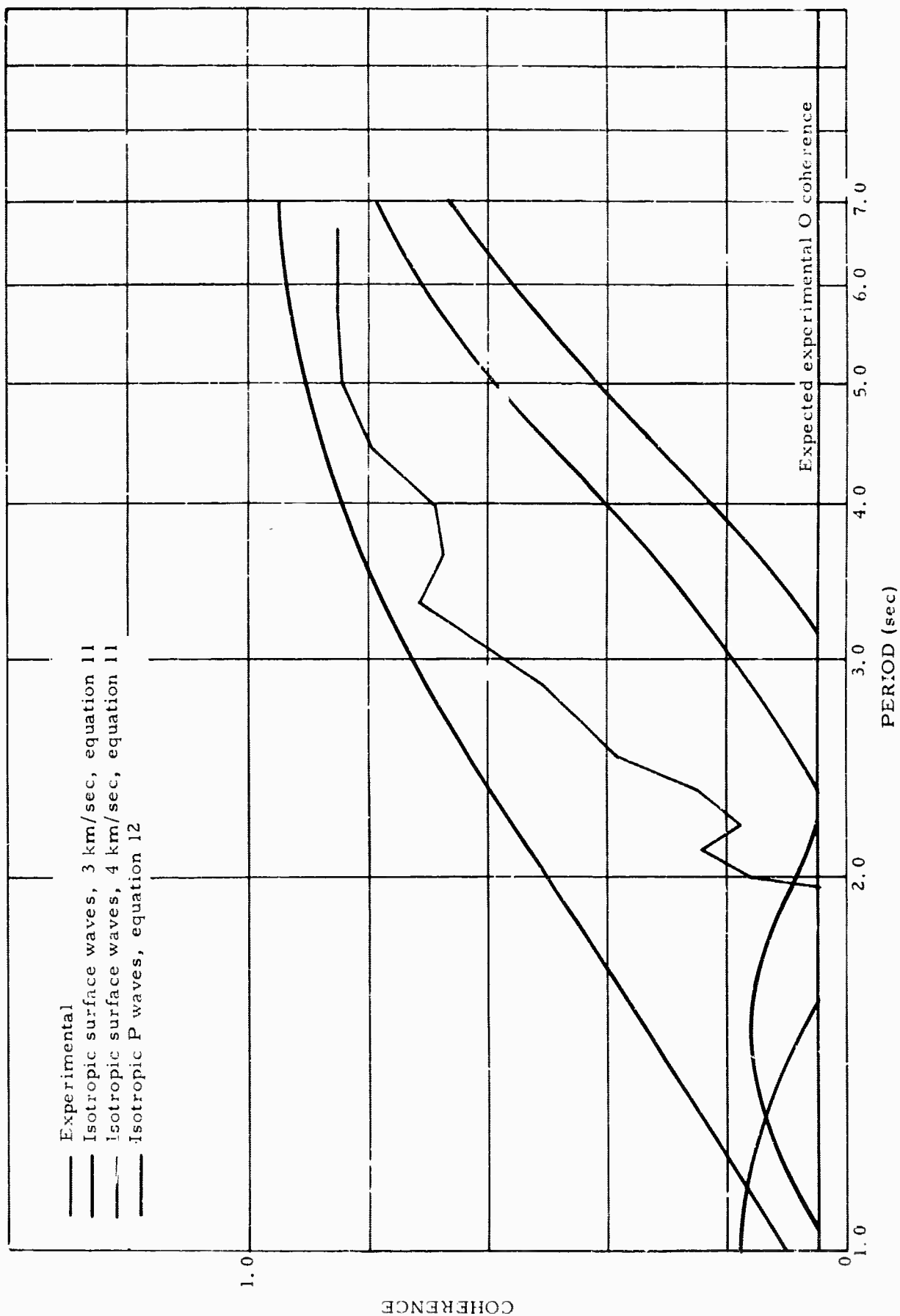
Figure 17. Experimental and theoretical coherences of noise from seismometers 3 km apart, WMSO. 180-sec sample, 25 samples/sec, 8-percent lags

Legend:
- Experimental
- Isotropic surface waves, 3 km/sec, equation 11
- Isotropic surface waves, 4 km/sec, equation 11
- Isotropic P waves, equation 12

PERIOD (sec)

COHERENCE

Expected experimental 0 coherence

Rayleigh wave does not exist with appreciable energy content at the quiet sites. Close to the coast, however, a considerable percentage of the noise must consist of the fundamental mode to explain results obtained during previously reported experiments (Douze, 1964).

6. 1. 5. 3 Noise in the Period Range of 0. 8 to 0. 3 Sec

The noise amplitudes in the period range between 0. 8 and 0. 3 sec varies considerably from site to site. The sites with large noise amplitudes are close to centers of population, and the noise is usually connected with cultural activity.

The noise at this period range can logically be divided into three parts: the cultural noise, the sharp spectral peaks, and the residual noise when the other two noise types are not present. Each of the three parts is characterized by different wave types.

Figure 18 shows the spectra of the noise at the surface, at 1370 and 2890 m at GV-TX. Because of the close proximity of the site to Dallas, Texas, the cultural noise background is extremely large at the surface. The spectra in figure 18 indicate clearly that the amplitude (on the average) of the noise decreased very rapidly from the surface down to 1200 m and that the level only decreased slowly below this depth.

The only wave type that decreases in amplitude with depth sufficiently rapidly to account for experimental results is the fundamental mode Rayleigh wave. Figure 19 shows the experimental power ratio between the 668-m depth and the surface, together with the theoretical fundamental mode, first higher mode, and P waves. The results clearly indicate, with minor discrepancies, that the fundamental mode accounts for the rapid decrease in noise amplitudes in the first 668 m. The coherences are close to zero within the accuracy of the spectral analyses. Zero coherence implies approximately equal power in phase and 180 deg out-of-phase; zero coherence indicates that the noise that did not consist of fundamental mode Rayleigh waves (which remain in phase) was out of phase with the surface.

In general, the amplitude-depth relationships can be explained by either a combination of higher-mode Rayleigh waves, by body waves, or by a mixture of both. The power ratio in figure 19 shows lows at both the nodal points of the first higher mode and the P waves indicating the possible presence of these waves. In an attempt to distinguish between the possibilities, the noise from seismometers at depths of 2570 and 2890 m were cross-correlated after

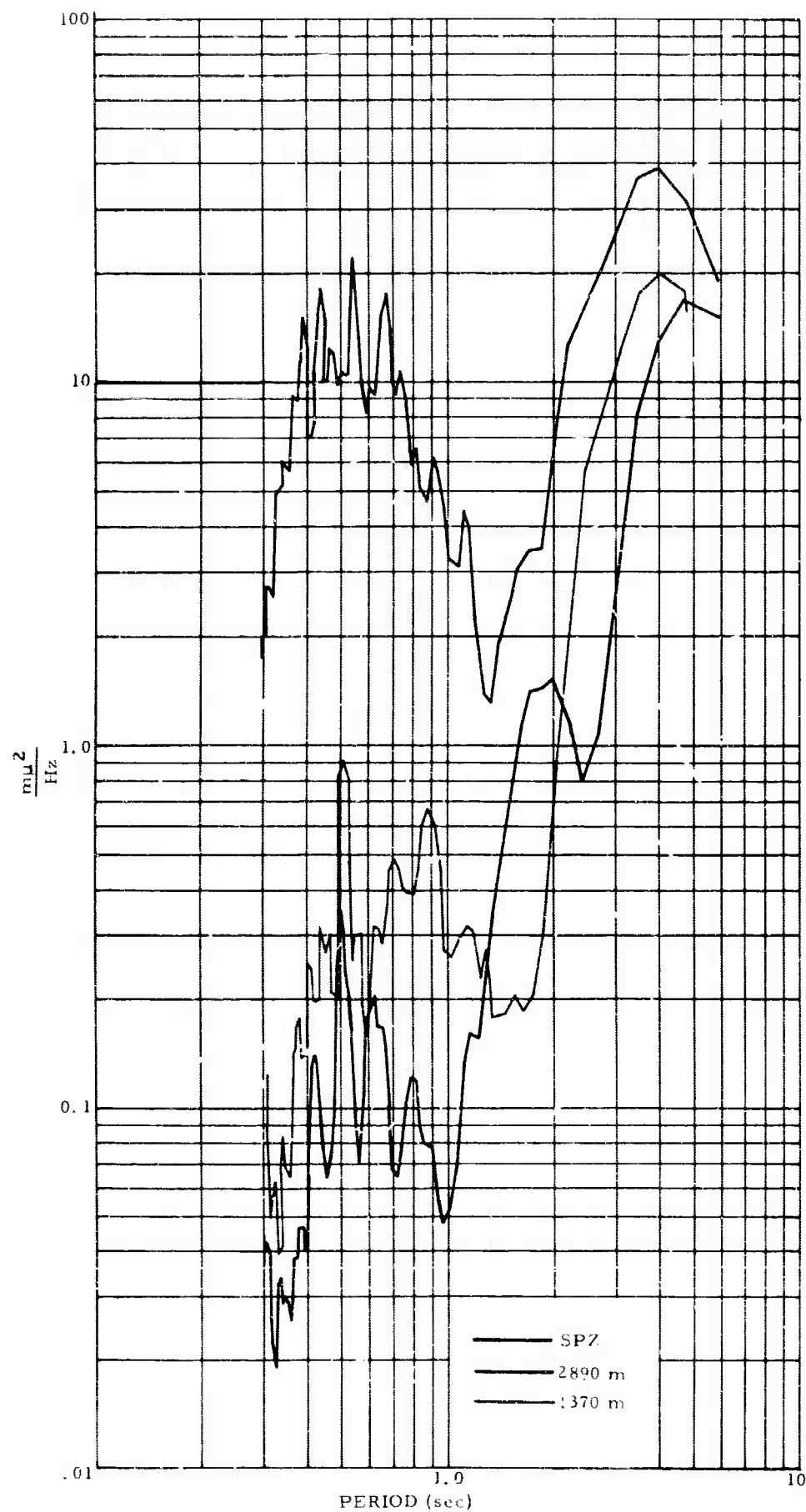Figure 18. Spectra of the noise at the surface, nd at 1370 and 2890 m, GV-TX. 180-sec sample, 25 samples/sec, 8-percent lags.
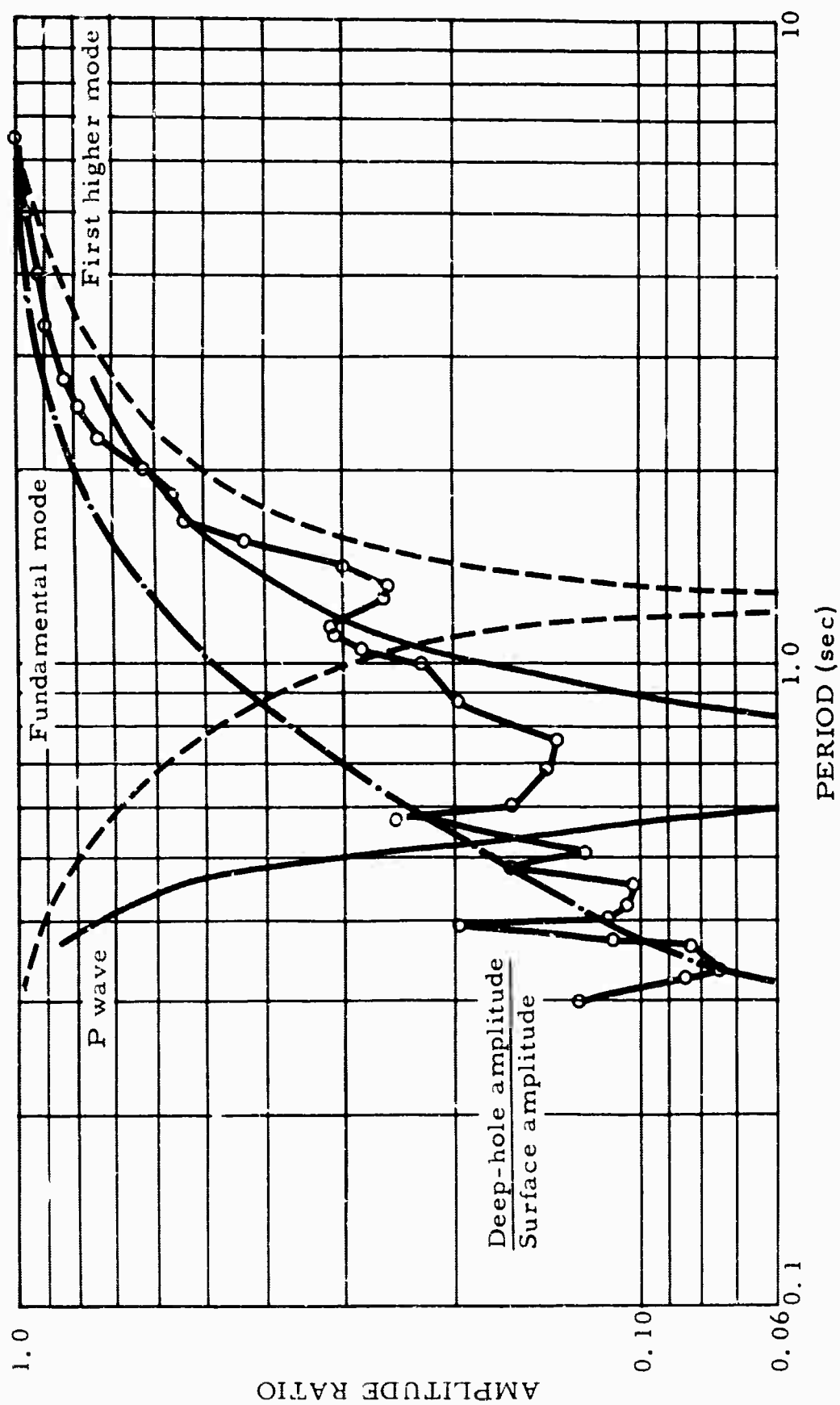
Figure 19. Amplitude ratio of deep-hole noise amplitude to surface noise amplitude as a function of period. Also shown are the theoretical fundamental and first higher Rayleigh modes and the theoretical P-wave amplitudes. Depth 668 m, GV-TX

narrow-band analog filtering (low pass and high pass at 3 Hz, 24 dB/oct). The result (figure 20) shows that the cross-correlation peaks at 0.1 sec, indicating that the noise consists of body waves and not of surface waves. If only P waves were present, the measured uphole time would indicate that the average angle of incidence is 45 deg from the vertical. However, it is likely that S waves also contributed to the average uphole time measured.

The coherences were typically high at all sites where multiple seismometers were placed in close proximity (<600 m). The coherence was a complex function of the distance between seismometers. Figure 21 shows the coherence and phase angle of the noise from seismometers at depths of 1370 and 1980 m. Notice that the phase angle departs from 0 deg at 0.5-sec period; as will be discussed later, the peak at this period probably consists of another wave type.

All sites investigated, with the exception of Eureka, Nevada, showed the presence of a sharp peak at 0.49-sec period. Often it was hidden by cultural noise at the surface; however, at depth it was always clearly visible in the spectra.

In discussing the 0.49-sec peak, the data will be used from AP-OK, FO-TX, and WMSO, where the peak is very prominent.

In a previous publication (Douze, 1964), the 0.49-sec noise was attributed to the presence of the third higher Rayleigh mode. Figure 22 shows the spectra of the noise at the surface, 3048, and 5486 m at FO-TX. The sharp peak at 0.49 sec was still present at the bottom of the hole; comparison with the theoretical amplitude-depth relationships (figure 9) indicates that the third higher mode cannot be the cause of the peak at this period unless the theoretical results are greatly in error. Theoretical investigations indicated that the amplitude-depth relationships can also be explained by P waves arriving at close to vertical incidence. Figure 14 shows the results obtained with a single seismometer in the deep hole and an array of four deep-hole seismometers at AP-OK. The data from the array does not fit either of the theoretical curves very well. The experimental second nodal point appears to occur at a shallower depth than indicated by either theory suggesting the presence of an even higher Rayleigh mode. However, the amplitude-depth relationships of the Rayleigh modes depend on the assumptions made on the velocity section below the hole, and the third mode could probably be made to fit by changing the velocities. It must be noted that the P-wave theory does not depend on the velocity section below the hole.
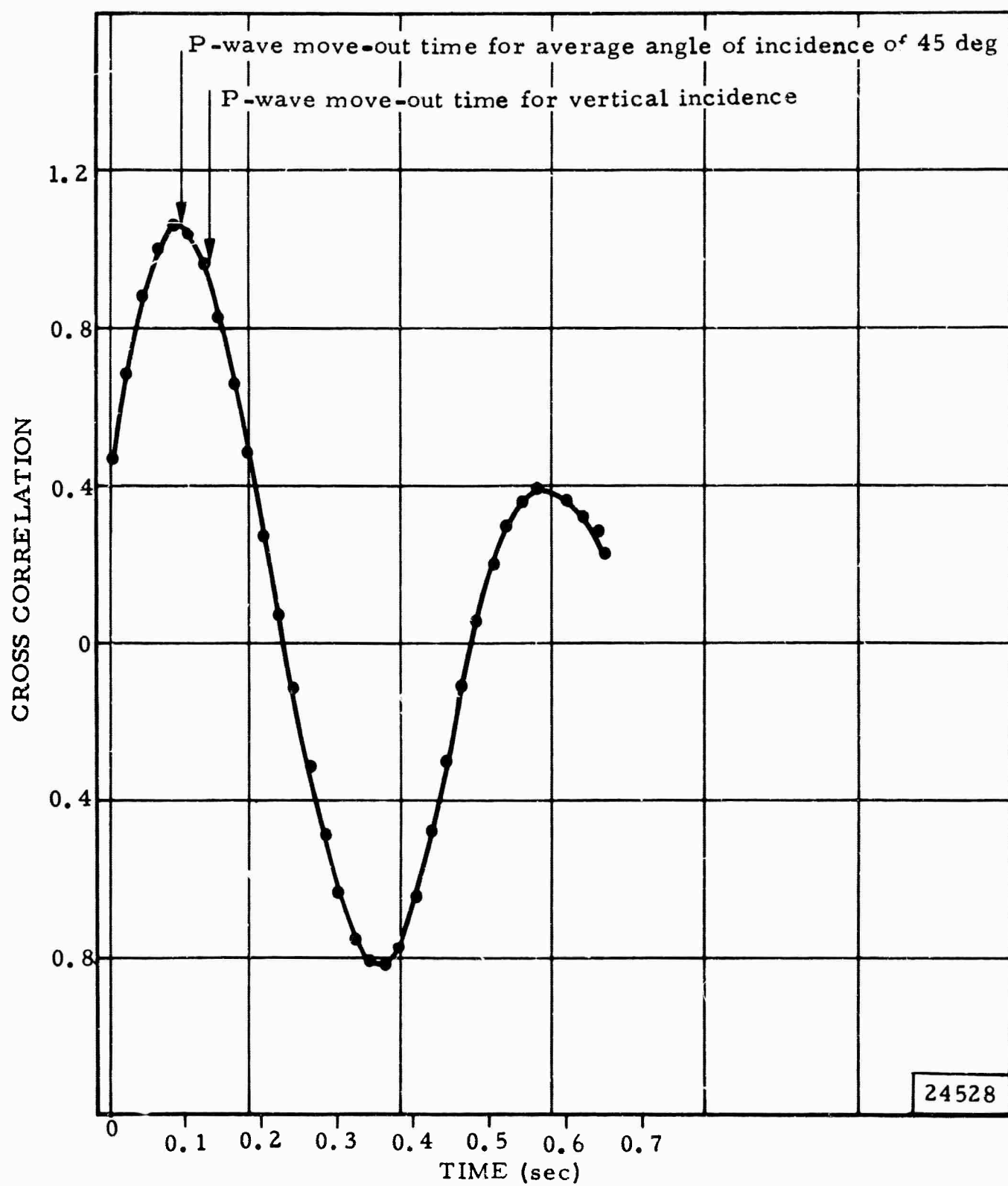
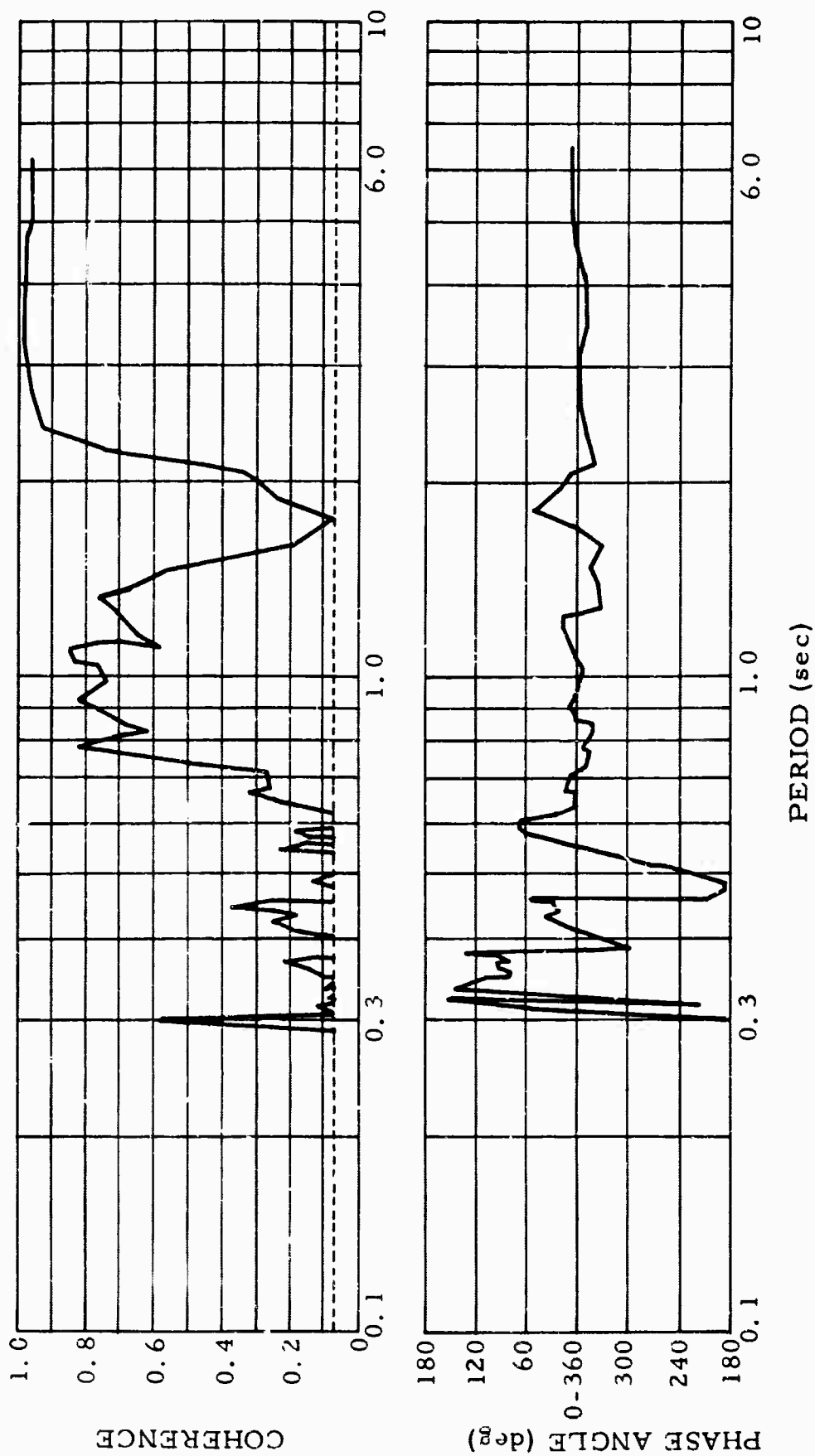Figure 20. Cross-correlation between seismometers at depths of 2890 and 2570 m at GV-TX

Figure 21. Coherence and phase angle of noise samples from seismometers at depths of 1980 and 1370 m, GV-TX. 180-sec sample, 25 samples/sec, 8-percent lags
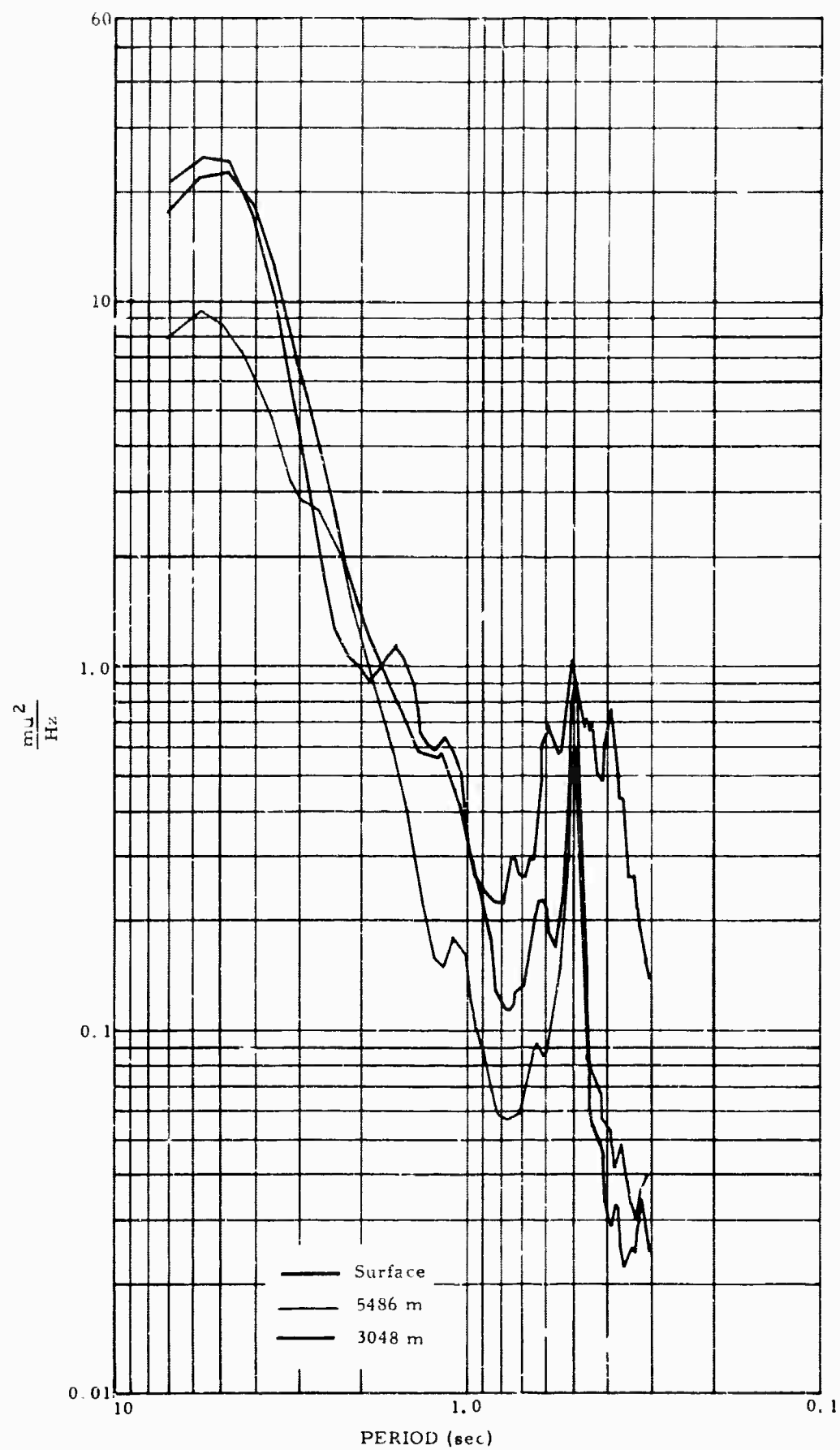
Figure 22. Spectra of the noise at the surface, and at 3048 and 5486 m, FO-TX. 180-sec sample, 10 samples/sec, 8-percent lags.

Surface and body waves can, in theory, be identified by their phase velocities. The phase velocity of the 0.49-sec noise is approximately 3.0 km/sec as measured by WMSO personnel (personal communication, George Gray). Figure 23 shows the cross spectrum between seismometers 1 km apart at the observatory. In general, the noise is isotropic as indicated by the tendency of the phase angle to remain at either 0 or 180 deg. If the 0.49-sec noise is assumed to be isotropic, the coherence (0.29) and the theoretical results (formulas 11 and 12) i᠎ ᠎te that the phase velocity can only be 3.2 km/sec. This velocity indicate᠎ ᠎ the noise consists of surface waves.

However, several features of the experimental data are difficult to explain by the presence of one higher Rayleigh mode alone. Despite numerous attempts to locate a seismometer at a nodal point, no such depth could be found. The presence of mixture of wave types could explain this behavior. High resolution spectra often indicate the presence of another peak at approximately 0.51-sec period. If these two adjacent peaks were caused by different wave types, the results from spectral analysis can be expected to be inconclusive because of lack of resolution.

The coherences (see figure 14) gave values that would be expected if the 0.49-sec peak had very high coherence and the noise at the same period apart from the peak was incoherent like the noise at adjacent periods. The low coherence at 1950 m is typical of results close to theoretical nodal points, indicating the presence of approximately equal power in and out of phase. In conclusion, the experimental results do not indicate which type of wave is responsible for the 0.49-sec noise.

A discussion of the 0.49-sec noise is incomplete without a discussion of the reason for the existence of the sharp peak. Either there exists a very widespread source of this peak, or the earth in some fashion acts as a filter. Despite considerable effort, no common surface source has been found that can explain the sharp peak at this period. If the waves are body waves, some subsurface source must be hypothesized; earthquake records show that the earth does not act as a filter which preferentially passes 0.49-sec noise for body waves. If the waves are surface waves, some filtering mechanism presently not understood must exist. It is quite possible that further investigation of this phenomenon will result in some fundamental discovery on wave transmission.

6.1.6 Conclusions

Some of the waves present in the noise have been identified. The evidence presented shows that apart from the fundamental mode, the first higher mode
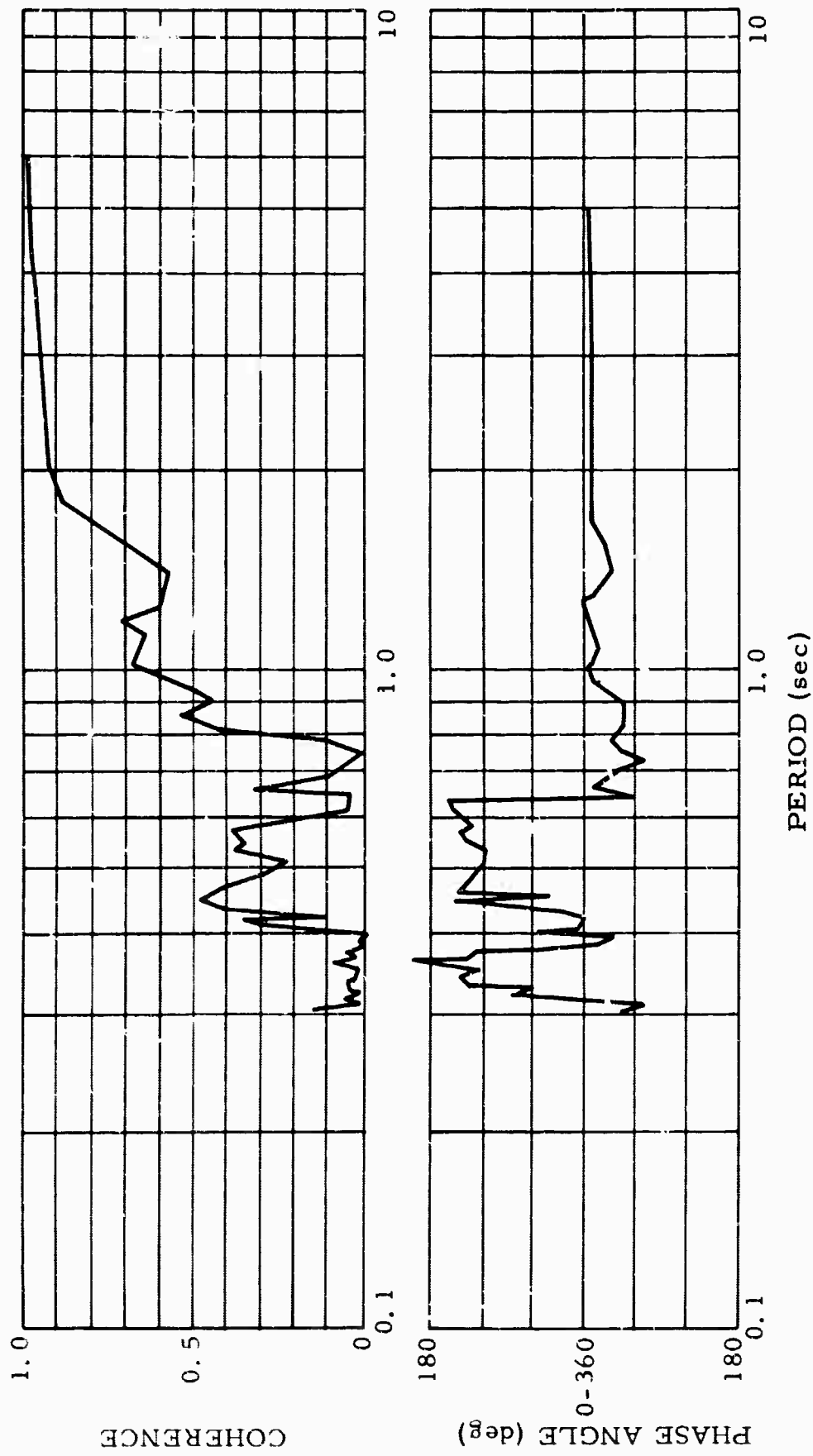
Figure 23. Phase angle and coherence of noise from seismometers 1 km apart, WMSO. 180-sec sample, 25 samples/sec, 8-percent lags

is present in the noise at periods around 3.0 sec. Because of the similarity between body waves and surface waves, it could not be established that the first higher Rayleigh mode always predominates at periods between 4.0 and 2.0 sec. However, it has been established that, at sites some distance from the coast, the fundamental Rayleigh mode is not present with appreciable amplitudes. In the period range of 2.0 to 0.8 sec, the experimental data were not conclusive. The amplitude-depth relationships can be explained by either a mixture of higher modes or by a predominance of P waves. Both cross-correlations and coherences across surface arrays indicated that surface waves are the preferred interpretation. In the period range of 0.8 to 0.3 sec, the cultural noise has been shown to consist principally of fundamental mode Rayleigh waves. At depths where the fundamental mode has decreased to negligible values, the remainder of the noise consists of random body waves. The sharp peak commonly present at 0.49 sec consists of Rayleigh mode or modes of order higher than third, or of body waves.

6.1.7 Acknowledgements

6.2 DATA PROCESSING

Deep-hole seismograms are more complex than seismograms recorded at the surface, principally because the surface-reflected P wave and the surface-generated SV wave interfere with the initial waveform. In a layered medium, reflections and conversions are generated at each interface and these will also interfere to a greater or lesser extent, depending upon the nature of the layering. In array processing techniques, it is usually desirable to remove these effects from the seismogram. This can be done by inverse filtering. If the layered medium between the seismometer and the surface is considered to be a filter, operation on the deep-hole seismogram with the inverse of this filter produces an estimate of what the signal would have looked like had the superimposed layers not been there. Several methods are being studied in an attempt to determine how these filters can best be realized.

In the following discussion, the term "filter" means a set of discrete weighting coefficients in the time domain; these filters have been specified for the arrays at GV-TX and AP-OK. The filter obtained for AP-OK will be discussed in some details.

6.3 SPECIFICATION OF THE FILTER FUNCTIONS

The steady-state response function of the layered medium to vertically-arriving P waves was calculated using the method derived in the last semi-annual report. The inverse function was then taken and transformed into the time domain. Computer programs were written to perform these calculations on the CDC 160-A computer. The function must be smoothed before transformation, otherwise spurious peaks occur in the time domain due to the convolution of the ideal transform with the transform of the bandwidth-limiting function. In this case, the usual "hanning" function was used over a 14-Hz bandwidth. The resulting time domain responses were stable due to the limiting and smoothing in the time domain, but this same operation imposed a somewhat arbitrary amplitude decrement on the weighting coefficients, making them unsatisfactory. Also, calculations were only performed for the case of vertical incidence and this was not considered adequate.

A more satisfactory method was developed directly in the time domain.

Consider the following layer configuration:
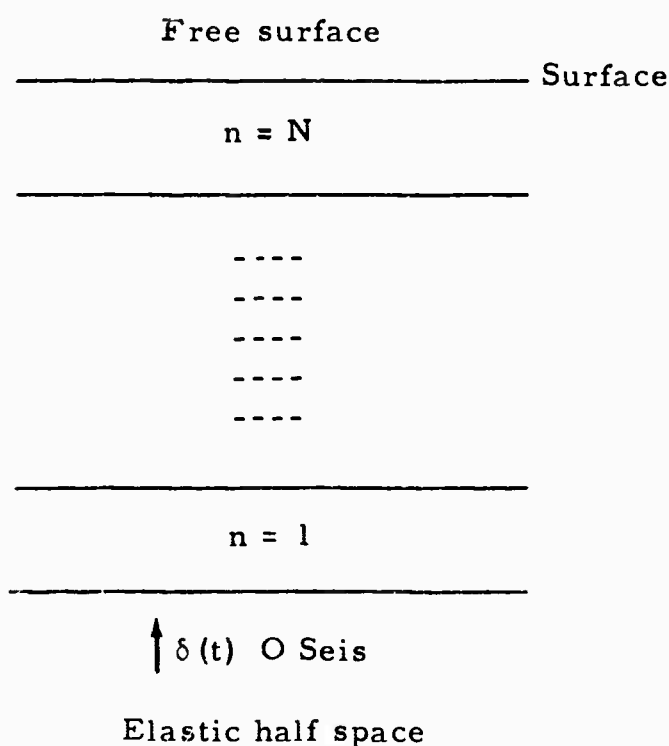
where, for the nth interface.

R_n = reflection coefficient of P waves

P_n = transmission coefficient of upward-travelling P waves

P'_n = transmission coefficient of downward-travelling P waves

S_n = conversion coefficient of P to reflected SV waves

Q_n = transmission coefficient for upward-travelling SV waves

Q'_n = transmission coefficient for downward-travelling SV waves

p_n = conversion coefficient of upward-travelling P to transmitted SV

p'_n = conversion coefficient of downward-travelling P to transmitted SV

S'_n = conversion coefficient of downward-travelling SV to transmitted P

S'_{N+1} = SV – P conversion coefficient at free surface

S_o = SV reflection coefficient at free surface.

To a first approximation, for a dilatational impulse function $\delta(t)$ incident in the underlying half space, the resulting seismogram will be of the form

$$f(t) = \delta(t) + \sum_{n=0}^{N} \prod_{i=1}^{n} \prod_{j=1}^{n} P_i P'_j R_{n+1} \delta(t - \tau'_{n+1}) \quad - \text{ incident \& reflected P}$$

$$+ \sum_{n=0}^{N} \prod_{i=1}^{n} \prod_{j=1}^{n} P_i Q'_j \delta(t - \tau''_{n+1}) \quad - \text{ reflected SV}$$

$$+ \sum_{n=1}^{N} \prod_{i=1}^{N} \prod_{j=N}^{n} \prod_{k=1}^{n-1} P_i P'_j Q'_k R_{N+1} p'_n \delta(t - \tau'''_n) - \text{ SV from surface-reflected P}$$

$$+ \sum_{n=1}^{N} \prod_{i=1}^{N} \prod_{j=N}^{n} \prod_{k=1}^{n-1} P_i Q'_j P'_k S_{N+1} S'_n \delta(t - \tau^{iv}_n) - \text{ P from surface-reflected SV}$$

$$+ \sum_{n=i}^{N} \prod_{i=1}^{n} \prod_{j=n+1}^{N} \prod_{k=1}^{N} P_i Q_j Q'_k p_n S_o \, \delta(t - \tau^v_n) \quad \text{- transmitted SV}$$
reflected from
free surface

$$+ \sum_{n=1}^{N} \prod_{i=1}^{n} \prod_{j=n+1}^{N} \prod_{k=1}^{N} P_i Q_j P'_k p_n S'_{N+1} \, \delta(t - \tau^{vi}_n) \quad \text{- upward trans-}$$
mitted SV
converted to P
at free surface

Multiple reflections and coversions have been ignored except where the free surface is involved. The above expression can be written more simply as:

$$\left. \begin{aligned} f(t) = \delta(t) &+ \sum_{n=0}^{N} a_n \delta(t - \tau'_{n+1}) + \sum_{n=0}^{N} b_n \delta(t - \tau''_{n+1}) \\ &+ \sum_{n=1}^{N} c_n \delta(t - \tau'''_n) + \sum_{n=1}^{N} d_n \delta(t - \tau^{iv}_n) \\ &+ \sum_{n=1}^{N} e_n \delta(t - \tau^v_n) + \sum_{n=1}^{N} f_n \delta(t - \tau^{vi}_n) \end{aligned} \right\} \quad (13)$$

where the coefficients a_n, b_n, c_n, d, , e_n, and f_n are dependent upon the elastic constants of the different layers and the angles of incidence. They can, of course, be negative or positive.

The coefficients that apply to SV waves take into account the vertical component only.

The inverse filter is required to remove all terms in equation (13) except the original impulse function. Hence, to remove a typical coefficient, Z_n, for example, the desired inverse filter has a time-domain response

$$h_n(t) = \sum_{k=0}^{\infty} (-1)^k Z_n^k \, \delta(t - k\tau_n)$$

This is a linear operator so the response of the filter required to reduce all coefficients of the series Z_n is:

$$H(t) = \sum_{k=0}^{\infty} \sum_{n=0}^{N} (-1)^k (Z_n)^k \delta(t - k\tau_n) \tag{14}$$

The final filter consists of up to six terms of the above form corresponding to the six coefficients in equation (13)

The frequency response $G(\omega)$ of the filter is readily derived.

$$\text{Let } G(\omega) = \int_{-\infty}^{\infty} H(t) e^{-i\omega t} \, dt$$

$$\therefore G(\omega) = \sum_{n=0}^{N} \sum_{k=0}^{\infty} (-1)^k (Z_n)^k e^{-i\omega k \tau_n} \tag{15}$$

$$= \sum_{n=0}^{N} \frac{1}{(1 + Z_n e^{-i\omega \tau_n})}$$

Again, the final filter function will be a sum of such terms.

In actual practice, most of the coefficients would be too small for consideration and useable filters can be specified for a particular site much more easily than the equations might suggest.

To date, the number of point operators used in the time domain filter has been somewhat arbitrary; the cutoff was taken where the coefficient of the last impulse operator was approximately one-tenth the first. The error that results from an N-point filter can be minimized in the least mean square sense by calculating the weighting coefficients from the matrix equation

$$[R] \{Z\} = \{U\}$$

where R is an $N \times N$ Toeplitz matrix whose elements are the values of N lags in the autocorrelation of expression (13), Z is the column matrix of weighting coefficients, and U is the column vector whose first element is unity and the rest zeros.

An example of inverse filtering is shown in figures 24 and 25. Figure 24 shows an event from the Aleutian Islands recorded at three different depths by the vertical array at AP-OK. The differences in waveform are quite noticeable. Digital filters were specified for the channels recorded at 1660 and 2881 m. respectively. Only two coefficients in expression (13), a_n and b_n, were calculated and used. The angle of incidence of the upward-traveling signal was obtained from tables. The filtered signals are shown in figure 25. These should be similar to the signal recorded at 15-m and it can be seen that the reproduction is quite good. The 15-m recording should be filtered to compensate for the filtering action of the layers between the lower seismometers and the surface, but this was not done because the effect is quite small.

7. REFERENCES

Amos, D. E., and Koopmans, L. H., 1963, Tables of the distribution of the coefficient of coherence for stationary bivariate Guassian processes: Sandia Corporation Monograph SCR 483.

Backus, M., and others, 1964, Wide-band extraction of mantle P waves from ambient noise: Geophysics, vol. 29, p. 672-292.

Benioff, H., 1932, A new vertical seismograph: Bull. Seism. Soc. Am., vol. 22, p. 155-169.

Blackman, R. B., and Tukey, J. W., 1958, The measurement of power spectra: Dover Publications, Inc., New York.

Douze, E. J., 1964, Rayleigh waves in short-period seismic noise: Bull. Seism. Soc. Am., vol. 54, p. 1197-1212.

Ewing, W. M., and others, 19__, Elastic waves in layered media: McGraw-Hill Book Company, Inc., New York.

Geotechnical Corporation, 1964, Deep-hole site report, Meridian unit No. 1 well, White Pine County, Nevada: TR 64-68, Project VT/1139, Contract AF 33(600)-43369.
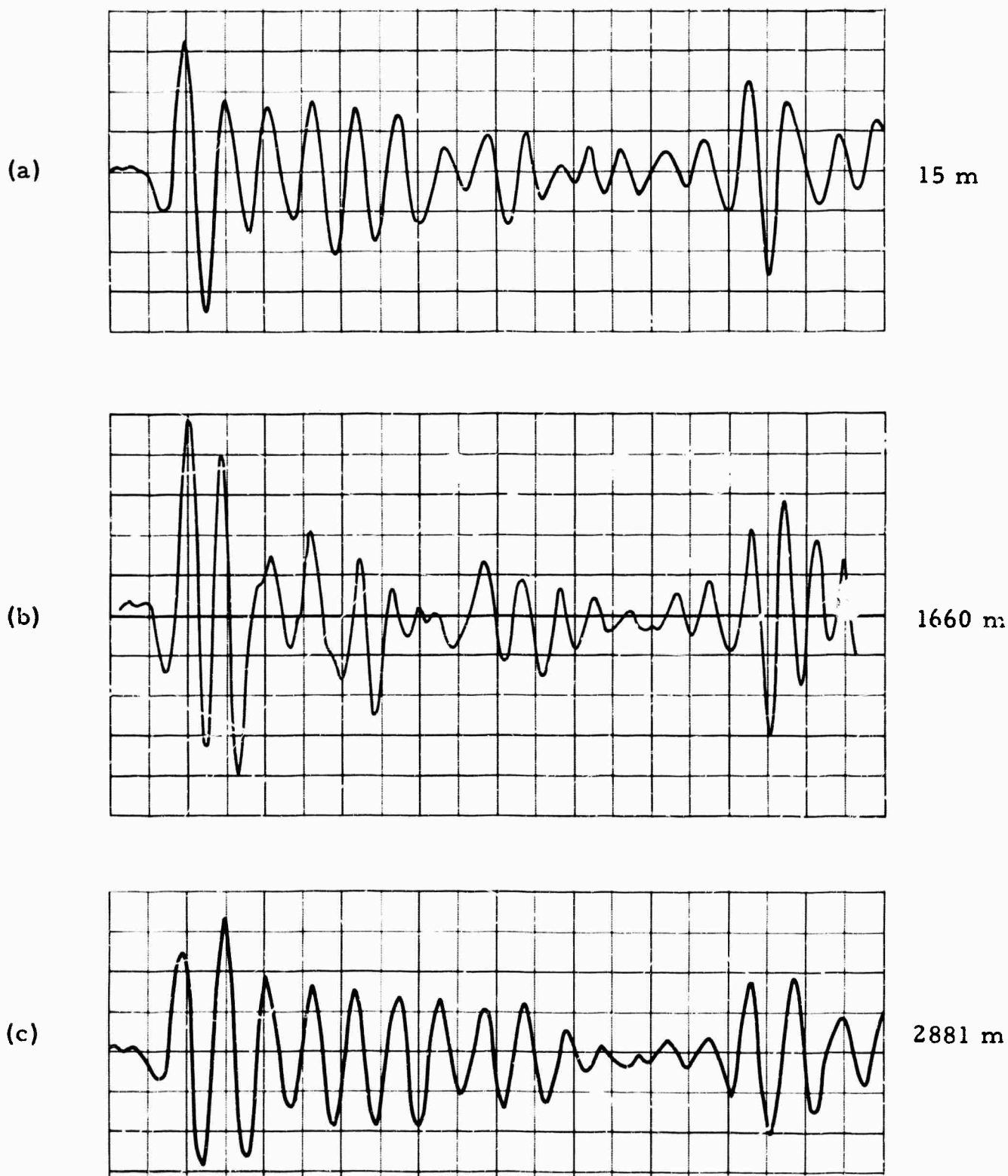
Figure 24. Event from the Aleutian Islands recorded at AP-OK at depths
of (a) 15 m, (b) 1660 m, and (c) 2881 m

(a)   1660 m
                                                       (filtered)

(b)   2881 m
                                                       (filtered)
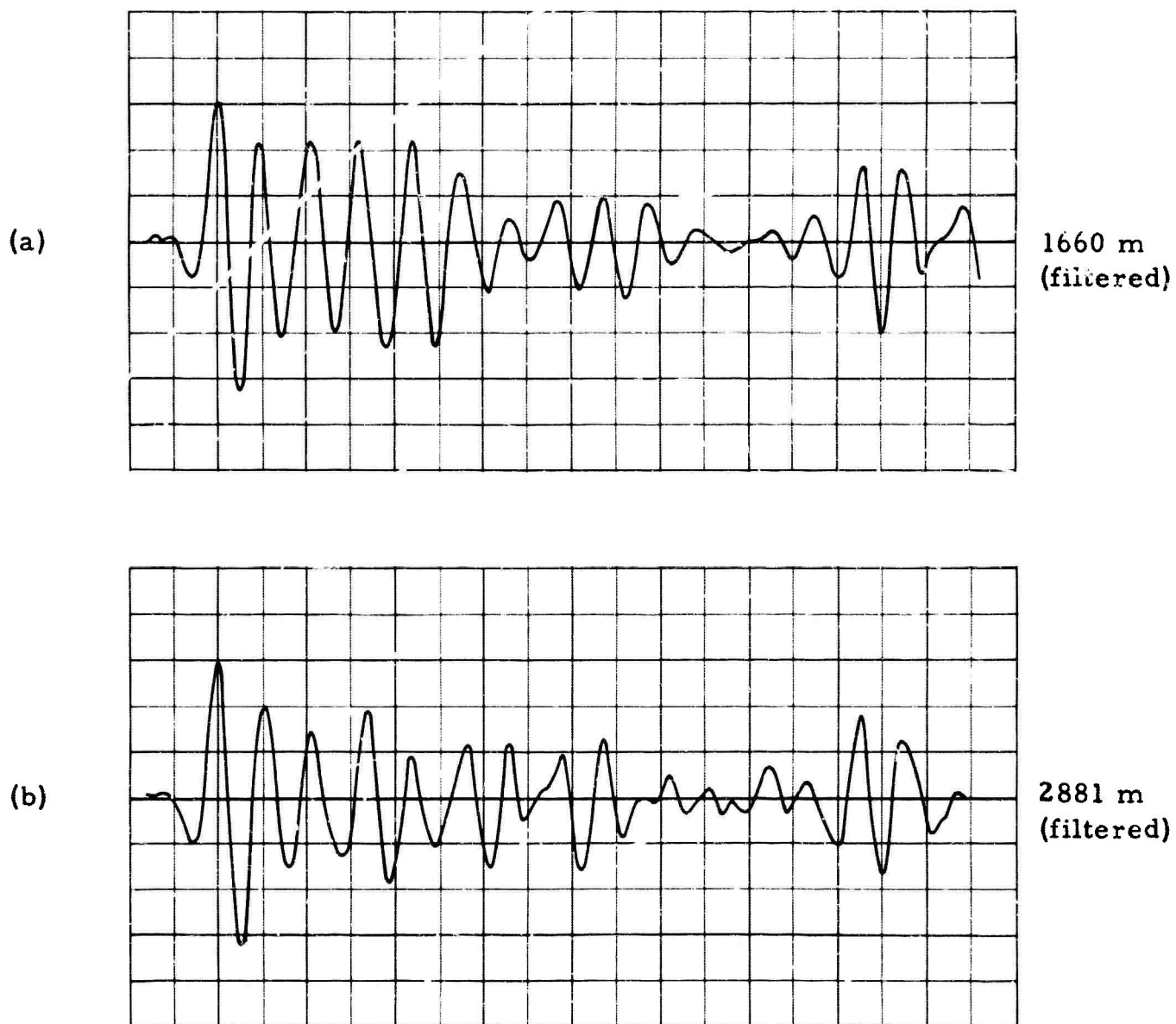
Figure 25. Results of inverse filtering applied to the signals shown in
figure 24 (b) and (c). Notice the good reproduction of the waveform
recorded at 15 m (figure 24 (a)

Gupta, I., 1965, Standing-wave phenomena in short-period seismic noise: submitted to Geophysics.

Gutenberg, E., 1958, Advances in geophysics: Academic Press, New York.

Oliver, J., and Ewing, M., 1958, Normal modes of continental surface waves: Bull. Seism. Soc. Am., vol. 48, p. 33-49.

Sax. R. L., and Hartenberger, R. A., 1964, Theoretical prediction of seismic noise in a deep borehole: Geophysics, vol. 29, p. 714-720.

APPENDIX 1 to TECHNICAL REPORT NO. 65-112

DEEP-HOLE SITE REPORT
UNIVERSITY OF TEXAS "EE" NO. 1, PECOS COUNTY, TEXAS

TECHNICAL REPORT NO. 65-104

DEEP-HOLE SITE REPORT
UNIVERSITY OF TEXAS "EE" NO. 1, PECOS COUNTY, TEXAS

THE GEOTECHNICAL CORPORATION
3401 Shiloh Road
Garland, Texas

15 July 1965

CONTENTS

ILLUSTRATIONS

ILLUSTRATIONS, Continued

ABSTRACT

The University of Texas "EE" No. 1 was prepared for use in a deep-hole
measurement program. It was originally drilled by Phillips Petroleum
Company, to a world's record total depth of 7724 m. Deep-hole and surface
seismographs were used to record both seismic signals and noise. Results
of the measurements show that only a small improvement in the signal-to-
noise ratio was obtained at depth.

DEEP-HOLE SITE REPORT
UNIVERSITY OF TEXAS "EE" NO. 1, PECOS COUNTY, TEXAS

1. INTRODUCTION

This report details the history and geology of the University of Texas "EE" No. 1, and its preparation for use in a deep-hole measurement program. It also includes a description of the measurement program conducted in the deep hole and the methods used in analyzing the records produced. The report covers all aspects of the work performed, including spectrum analysis of the noise samples.

This report was prepared to document the characteristics of this deep hole and the results of measurements therein using the deep-hole seismograph. This was done to provide a basis for future selection of holes and to provide this information for others who may wish to make measurements at this site.

The work described in this report was performed as part of Tasks 1h and 1k of the Statement of Work of Contract AF 33(600)-43369, Project VT/1139, and of Task 1c (2) and 1d of the Statement of Work of Contract AF 33(657)-13668, Project VT/5051.

2. HISTORY AND GEOLOGY OF THE UNIVERSITY OF TEXAS "EE" NO. 1

2.1 HISTORY

The University of Texas "EE" No. 1, is located in Pecos County, Texas, about 16 km east of the town of Fort Stockton (see map, figure 1). It was originally drilled by Phillips Petroleum Company as an exploratory test for oil and gas and was plugged and abandoned as a dry hole in February 1959. At its total depth, 7724 m, this hole set a new world's record for drilling depth.

University "EE" No. 1
Deep Hole Site
Pecos County, Texas
30° 54' 06" N
102° 41' 52" W
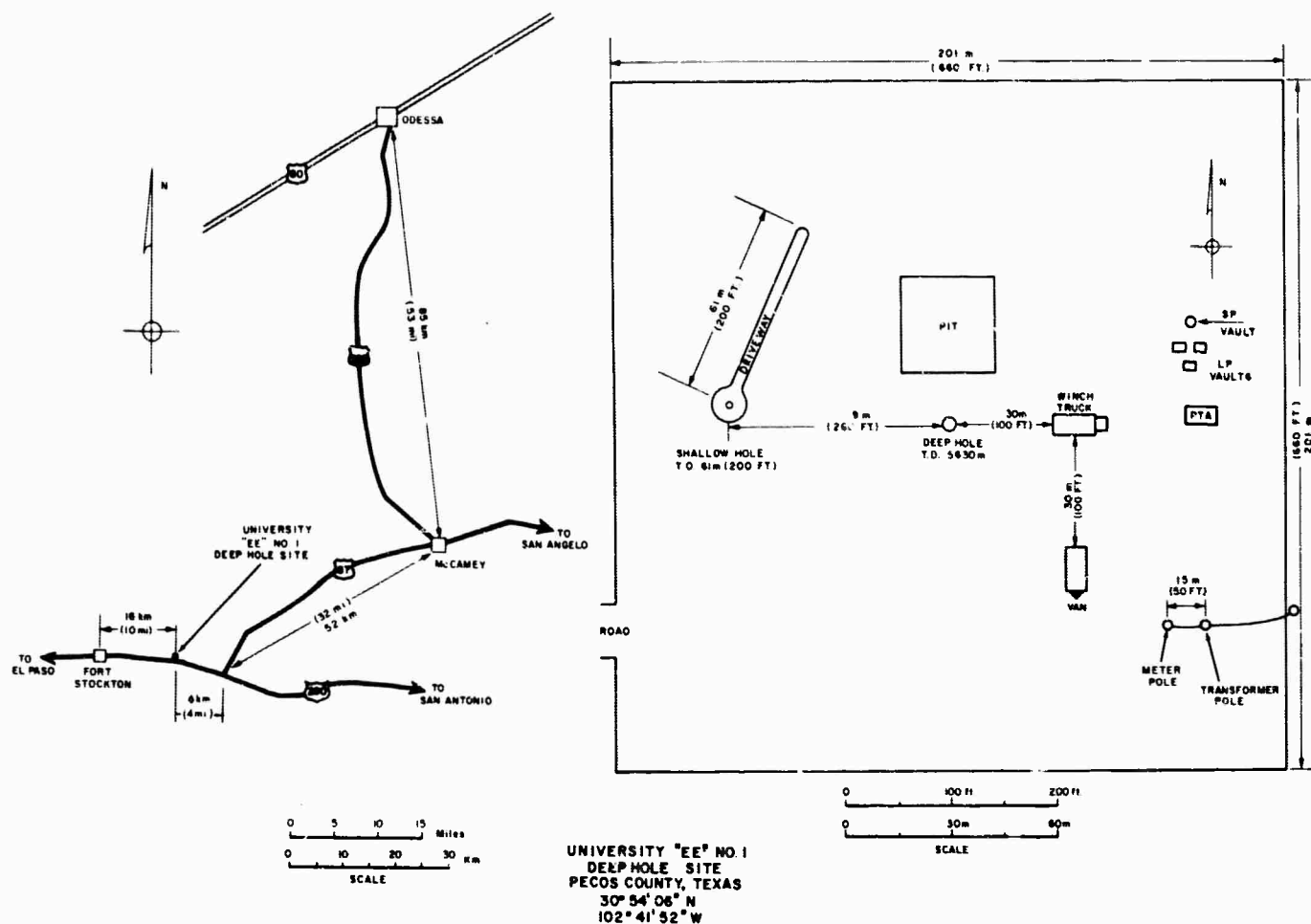
Figure 1. Site, University of Texas "EE" No. 1

2.2 GEOLOGY

The geology of the University of Texas "EE" No. 1, was described by Young, (1960):

(The University of Texas "EE" No. 1 is) the deepest test ever drilled into the earth's crust. Beyond this phenomenal depth, the well is also of very great interest because of unusual structural conditions which it encountered. The well penetrated a normal sequence of Cretaceous, Permian (including 4,800 feet of Wolfcamp), Strawn, and older Paleozoic formations to a depth of 13,765 feet, at which level a reverse fault was encountered, with Simpson overlying Devonian rocks. From that depth to 21,810 feet a whole series of structural abnormalities was met, and some units were repeated as many as four times. At the heart of this zone was a section of Ellenburger strata overlain and underlain by Simpson beds, the Ellenburger having an apparent thickness of 3,800 feet, although its true thickness is probably about 1,500 feet. The dip-meter recorded high-angle dips up to a maximum of 67 degrees. Below 21,800 feet no faults or other structural abnormalities were found; a normal sequence of lower Paleozoic strata was drilled, and the bottom of the hole is at a stratigraphic level 370 feet below the top of the Ellenburger group. The writer's interpretation, which is illustrated schematically in figure 65A (figure 2), is that the well is located in a structurally complex zone of multiple faulting, including high-angle reverse faults and possibly some overturning, which separates the Fort Stockton high from the Val Verde geosyncline. A relative uplift of the Fort Stockton high of about 20,000 feet is shown. It appears that the well completely penetrated the disturbed zone, and the bottom 3,500 feet is in the relatively undisturbed segment of the crust which forms the deeper portion of the Val Verde geosyncline.

This hole is designated as C in the cross section illustrated by figure 2. Figure 3 shows the University of Texas "EE" No. 1 in its tectonic setting. The stratigraphic section penetrated with related interval velocities, is illustrated in figure 4.

2.3 PREPARATION

This hole was recompleted as The Geotechnical Corporation's University of Texas "EE" No. 1 on 4 June 1964. Casing, 194 mm diameter, was installed in the hole to a depth of 427 m where a connection was made with the existing 194 mm casing. The hole was then re-entered to a depth of 5,830 m where
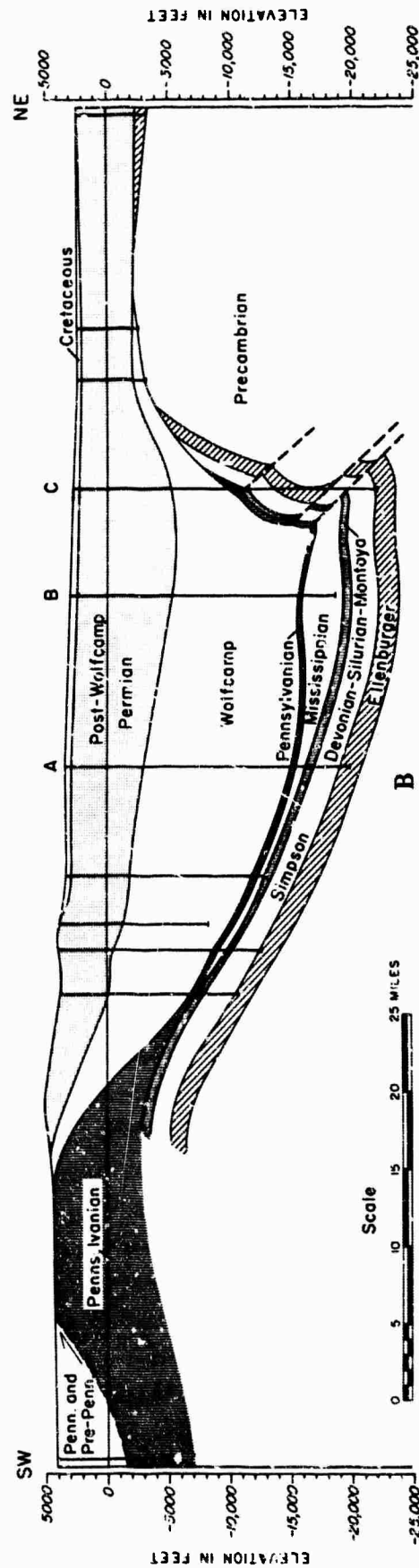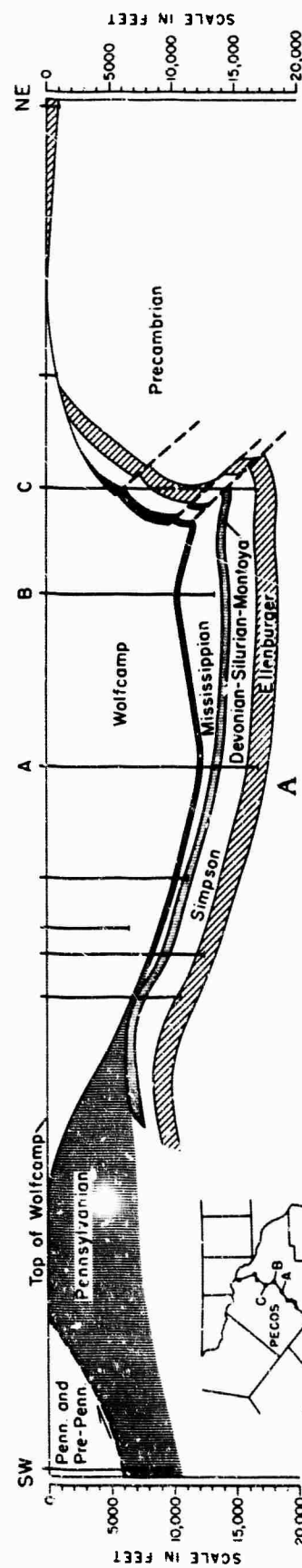
Fig. 65. Sections across central Val Verde geosyncline. A, Attitude of formations prior to Leonard time. B, Present attitude of formations.

(YOUNG, 1960)

Figure 2. Cross section through University of Texas "EE" No. 1
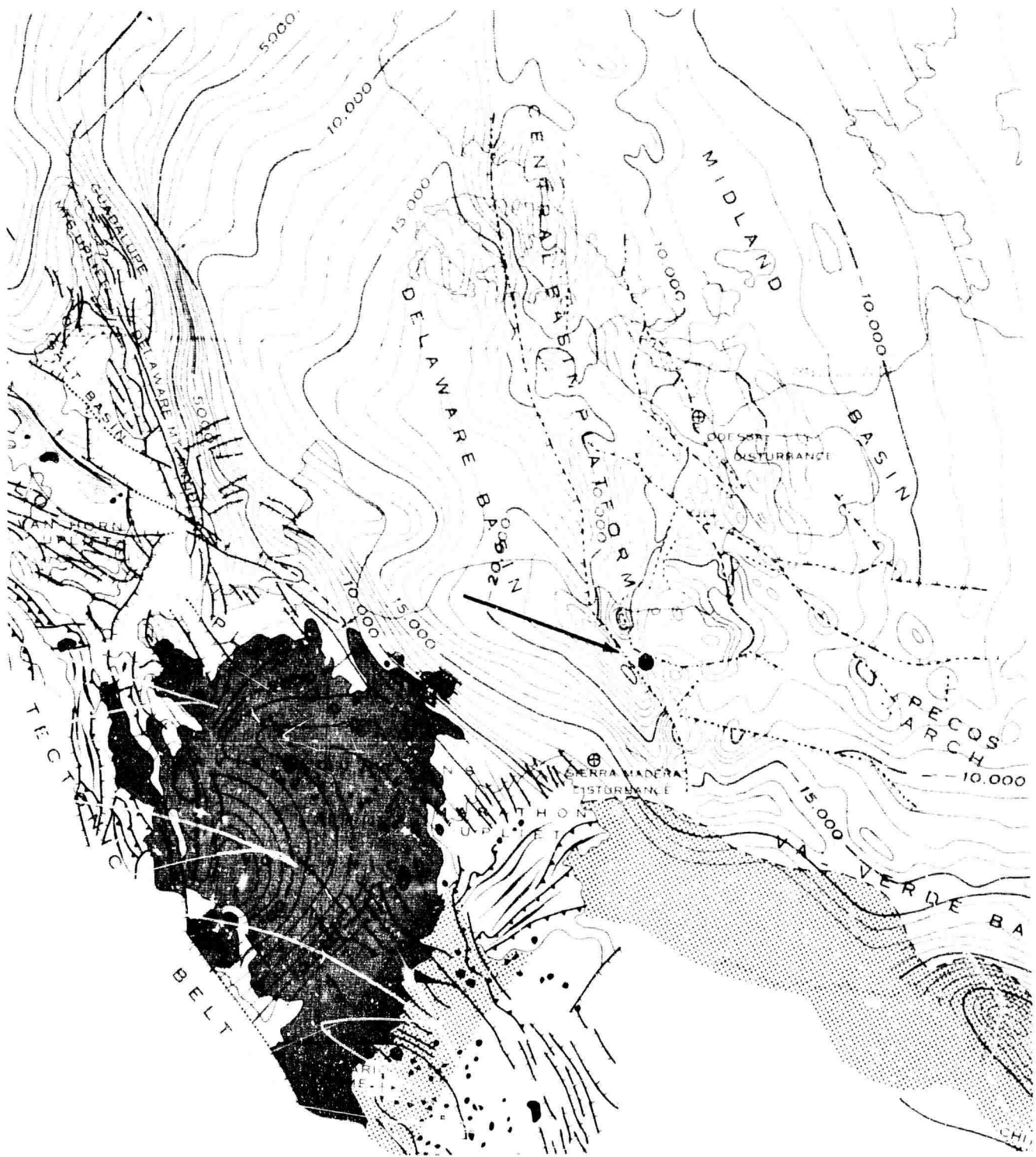
Source: Tectonic map of the United States (1961) USGS and AAPG

Figure 3. Tectonic setting, University of Texas "EE" No. 1
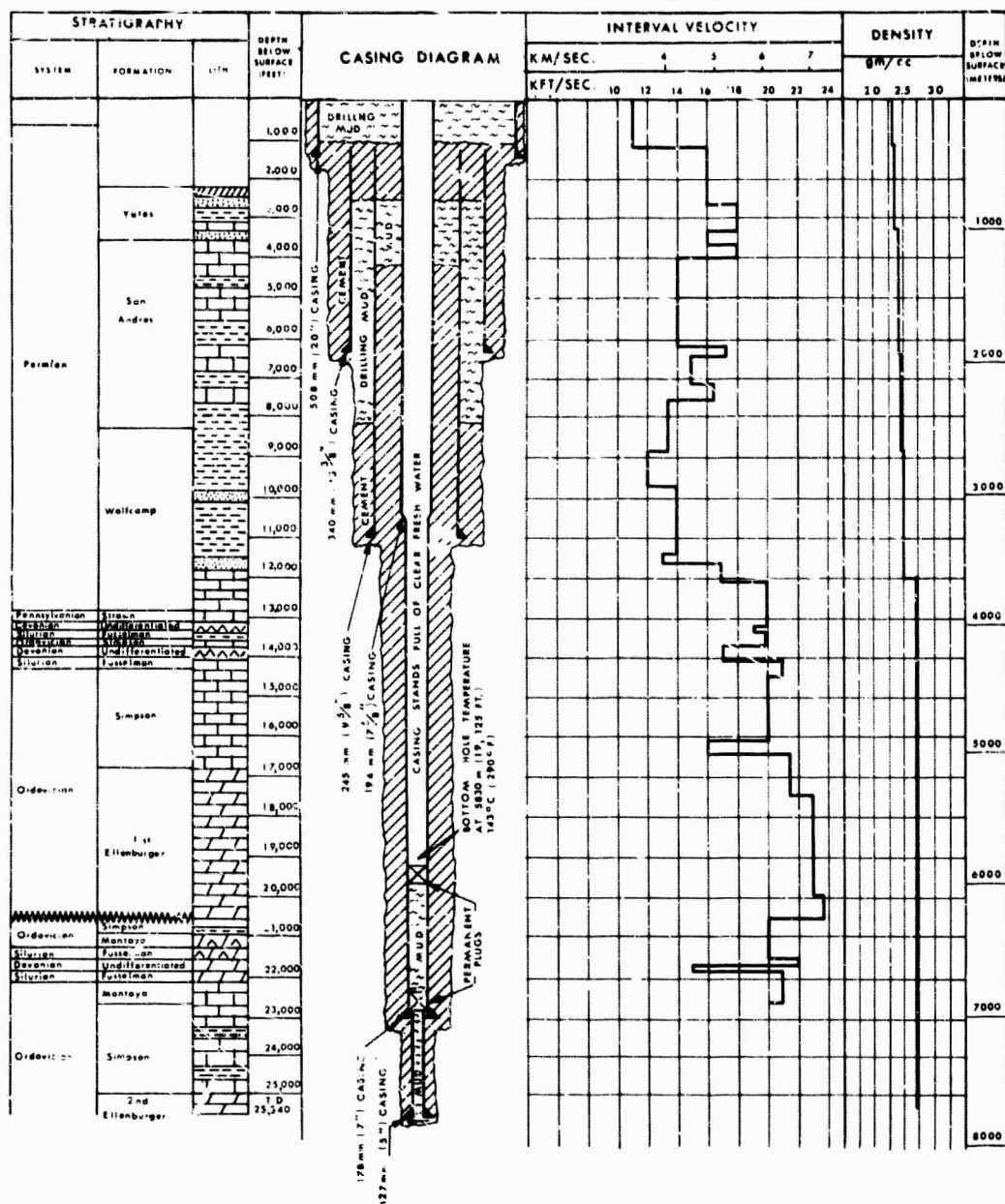
Figure 4. Subsurface diagram, University of Texas "EE" No. 1

the existing 178 m casing is permanently plugged, providing a fully cased operating environment (see figure 4).

During re-entry operations, small amounts of natural gas were observed entering the well casing under high pressure, but at low volume, at the following depths:

Casing coupling	427 m
Casing perforations	2640 m
Casing perforations	4050 m
Casing perforations	4275 m

The formation was cement squeezed at these depths and a substantial amount of the gas was shut off. A master control valve was installed on the casing at the surface to provide internal pressure control.

A seismometer may be operated locked in casing collars at approximately 12 m intervals from 5,800 m upward to the surface.

All depth measurements are from 6 m above the casing flange which is permanent datum, at about 1.5 m below the surface. Maximum deviation of the hole to 5,830 m is 5-1/4 deg and bottom hole temperature at that depth was $143^{\circ}C$.

An existing water well at the site is 70 m deep, contains 178 mm casing, and has a usable cased depth of 61 m. A seismometer may be operated in the well.

2.4 GENERAL

Detailed information on this site is given in appendix 1.

3. MEASUREMENT PROGRAM AT THE UNIVERSITY OF TEXAS "EE" NO. 1

Measurements were made with:

    a. Surface instruments;
    b. Two deep-hole seismometers simultaneously in the deep hole;
    c. Two deep-hole seismometers in the deep hole at the same time that a deep-hole seismometer was in a shallow hole.

The surface instrumentation consisted of the recording van and associated equipment, short-period and long-period seismometers, and phototube amplifiers. The recording van and surface instruments were provided by Contract AF 33(600)-41694, and are identical with the equipment used in the Long-Range Seismic

Measurements Program (LRSM), except that a film recorder was added to the van to provide additional recording capability.

3. 1 INSTRUMENTATION

Figure 5 shows the basic components of a deep-hole seismograph. Three systems were operated during the measurement work. Figure 6 shows a block diagram of the LRSM system, including long-period instrumentation. The deep-hole and short-period surface systems had similar response characteristics. Each system used a seismometer with an undamped natural frequency of 1 Hz and a phototube amplifier with a 5-Hz galvanometer. The surface and deep-hole seismometers included provisions for remote calibration, thus allowing their response characteristics to be verified. The calibration was accomplished by applying measured currents at various frequencies to the internal calibrators and recording the resultant output of the system. The outputs of the phototube amplifiers were connected to the recorders through attentuators, so that the amplitudes of the records could be adjusted as desired.

A 16-channel automatic processing camera was added to the van to make visual records on 16-mm film. Eleven channels of seismic data were recorded on the magnetic-tape recorder, and four channels were recorded on each of the 35-mm film recorders. The film recorders also recorded station time and radio station WWV was recorded on one channel of the magnetic-tape recorder. A control device was used to permit control of the various functions of each of the deep-hole seismometers. These functions included the calibration mentioned above, locking, unlocking, centering of the mass, and operation of a hole lock to secure the seismometer to the casing at any selected casing collar.

3. 2 SYSTEM RESPONSE

Figures 7 and 8 show the steady-state response of the seismographs to various frequencies.

3. 3 OPERATION IN UNIVERSITY OF TEXAS "EE" NO. 1

Gas that was produced in this hole resulted in noise that was detected by the seismographs. Although special seals were designed for use around the cables where they left the top of the hole, they did not bring the well to a complete pressure equilibrium. Each time the well was opened, as when instruments were moved, the noise background increased. After the well was resealed, the noise would decrease as a function of time and would be at a minimum after about 3 days. It is likely that as the pressure increased, and an equilibrium was reached, gas no longer entered the well.
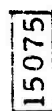
Figure 5. Deep-hole seismograph system , model 15075
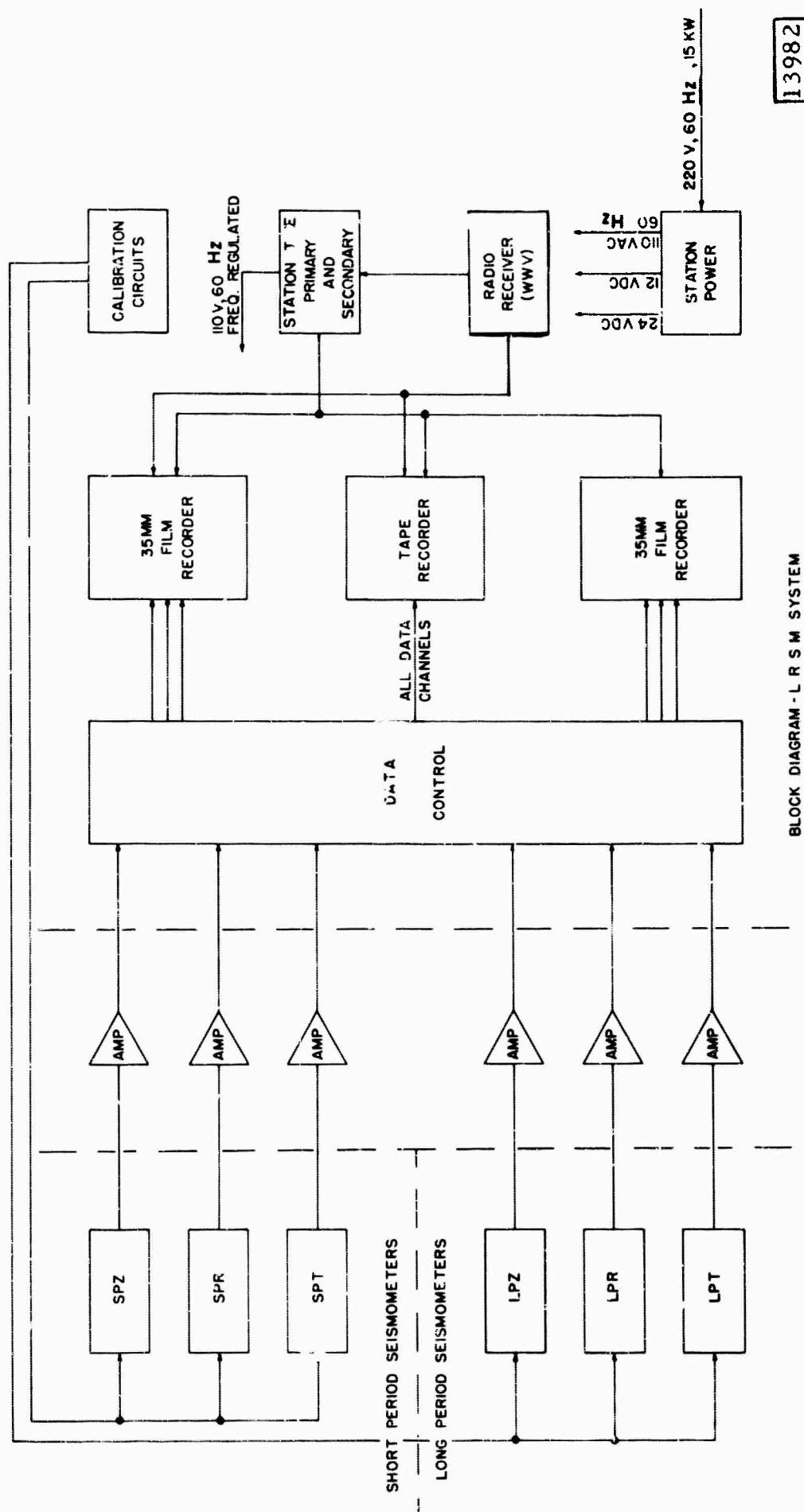
Figure 6. Simplified block diagram of the LRSM seismograph system
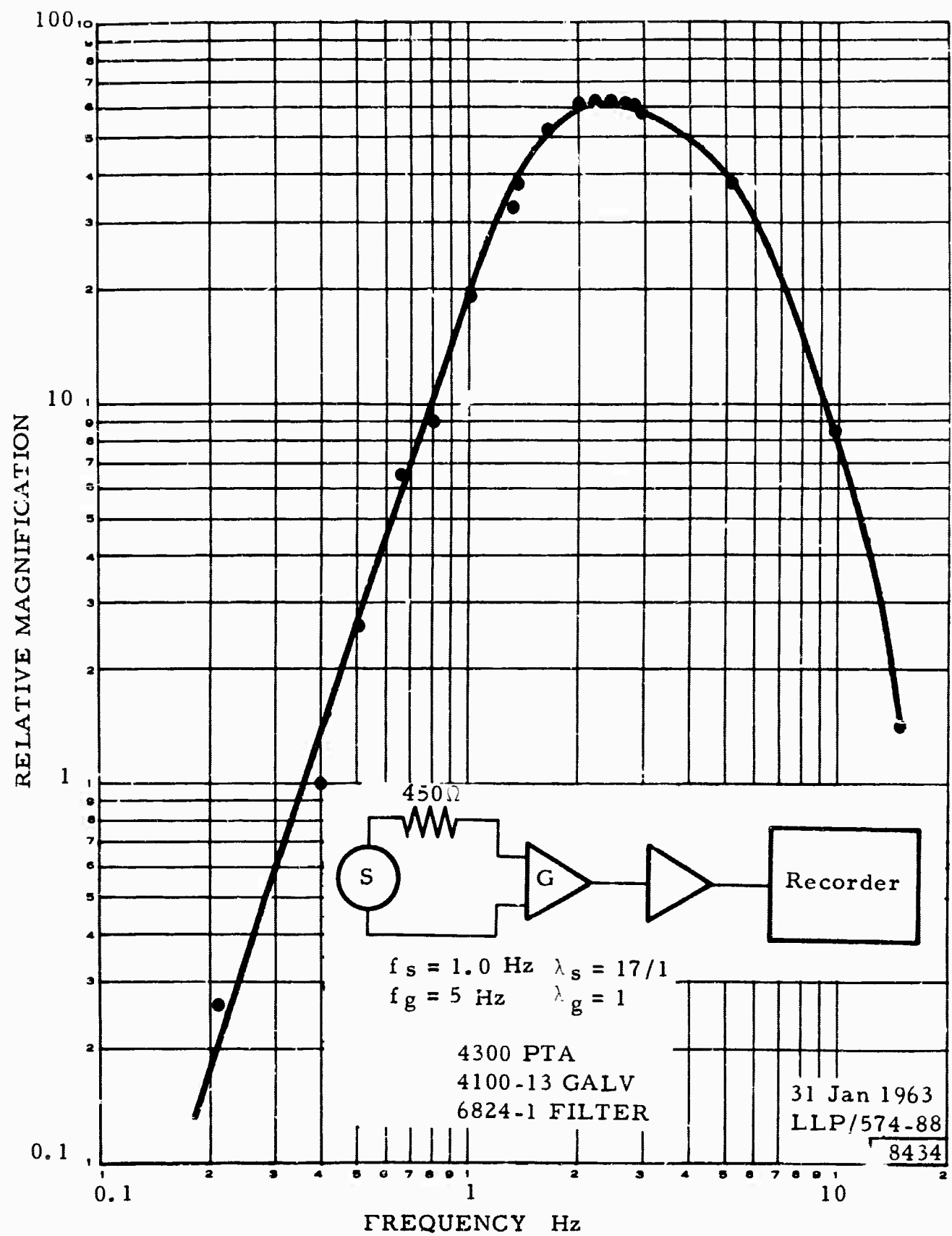
Figure 7. Frequency response of deep-hole seismographs
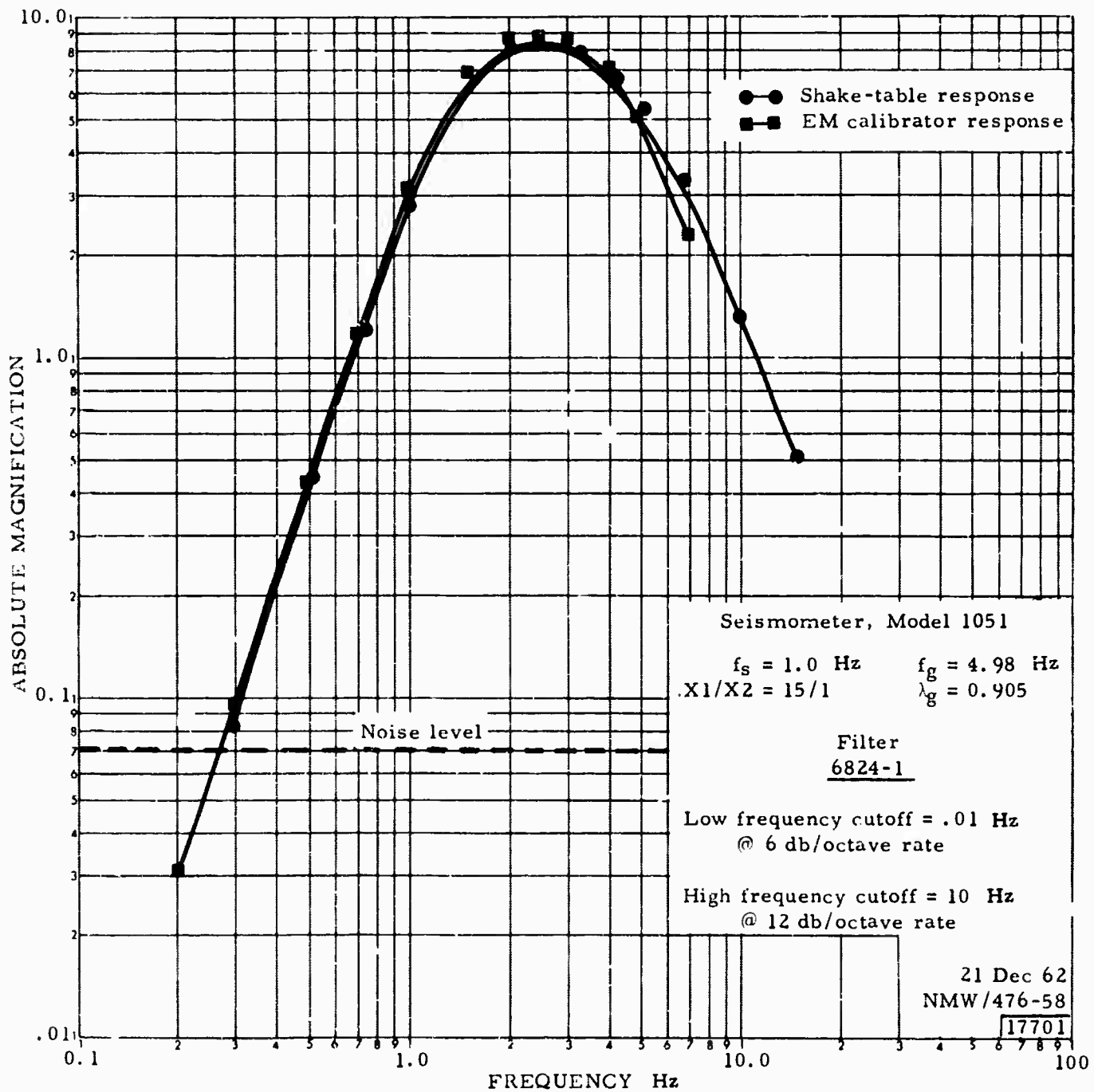
Figure 8. Frequency response of the short-period seismograph
from shake-table and electromagnetic calibrator tests

4. DATA ANALYSIS

The hole at Fort Stockton, Texas , is of interest mainly because of the great
depth that allows examination of the noise at depth below those investigated to
date. The great depth also allows examination of the behavior with depth of
the 2.0 to 4.0 sec microseisms by operating below the nodal points of these
waves. The hole has a total usable depth of 5,830 m.

P-wave velocities of the sediments in the hole were obtained from a sonic log
(courtesy of Phillips Petroleum Company). S-wave velocities were calculated
using Poisson ratios appropriate for the sediments encountered. The densities
used were averages for the types of rocks encountered in the hole. The P-wave
velocities in the hole are shown in figure 4. The velocity section, that starts
with low velocities close to the surface and increases to quite high velocities
at depth, resulted in a large number of theoretical Rayleigh modes.

Figure 9 shows the theoretical amplitude-depth relationships at a period of
1.0 sec. The theoretical Rayleigh wave program was run on the computer at
the Seismic Data Laboratory in Alexandria, Virginia. The theory indicates
that modes can be increased even further by increasing the assured velocities
below the hole. However, without knowledge of the velocities below the hole
there is no assurance that the amplitude depth relationships obtained will be
correct. Any mode that exists with appreciable amplitude below the depth for
which the velocity is accurately known (6,800 m) can be somewhat in error
because it is affected by these unknown velocities.

One of the main problems encountered in the analysis was the presence of
noise from gas entering the casing. Visual analysis of the data (see section
4.4) indicated that when the pressure increased above 3.3×10^6 newtons/m^2
the noise level no longer decreased with increasing pressure. This behavior
indicated that the gas was no longer entering the casing. However, there was
no assurance that minor amounts of gas noise were not contaminating the earth
noise. This possibility means that the results, especially of the spectral analy-
sis for the higher frequencies, must be interpreted with some caution. The
gas-induced noise appears to concentrate at the periods less than 1.0 sec, and
the longer periods can interpreted with some assurance that they are not
contaminated by this noise.
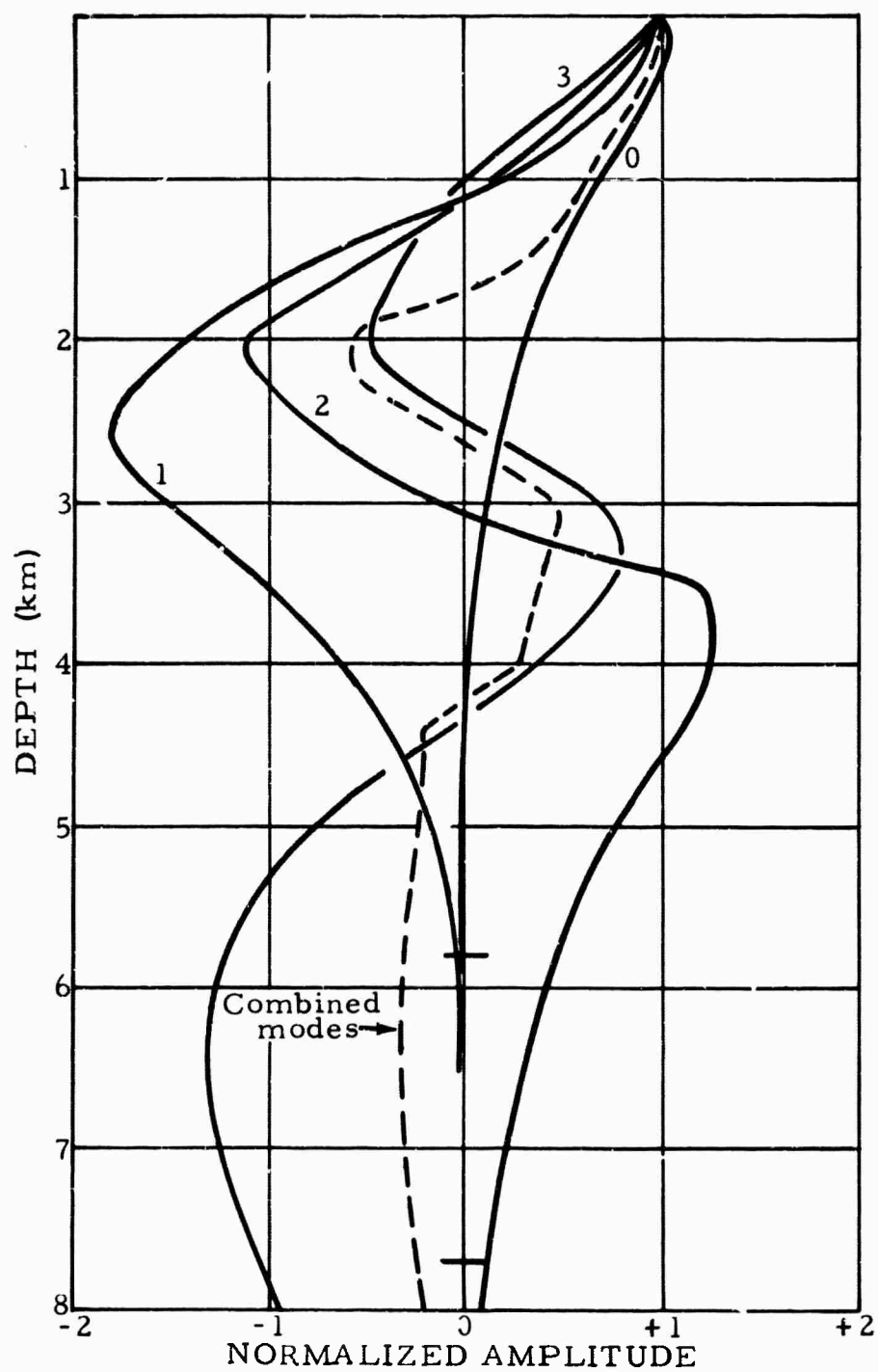
Figure 9. Theoretical amplitude-depth relationships of the first four Rayleigh modes. Number on curves indicates order of mode. FO-TX

4.1 METHOD OF MEASURING NOISE

The noise-distribution curves given in this report were obtained by measuring the largest noise amplitude present in the 10-sec interval immediately following a 5-min mark.

The amplitudes were not corrected for instrument response, and the magnifications at 1 Hz were used to obtain the millimicron (mμ) values given. Samples were taken during times when the cultural activity in the vicinity was minimum; 100 samples were taken at each depth. All measurements of amplitude were peak-to-peak.

This method of measuring the noise essentially defines the detection capability of the site. The results are given as "probability-of-occurrence" curves which determine the probability that a noise pulse of the same amplitude as a signal will occur at approximately the same time. The slopes of the curves give a measure of the variability of the noise amplitudes.

The periods of the pulses measured are also plotted to allow a comparison of the periods predominant at each depth.

The method has the advantage of ease of measurement and gives consistent, reproducible results by visual analysis; however, it should not be taken as a substitute for spectral analysis of the noise.

The probability-of-occurrence curves give a good picture of the decrease in noise level in the deep hole without making any attempt to distinguish between the decay of the different frequencies which occur in the noise.

4.2 NOISE ANALYSIS

Figures 10 through 12 show representative examples of the results obtained from noise surveys. The depths illustrated by the figures are 1520 m, 2140 m, 4570 m, and 58 m.

Examination the periods (figures 10 and 11) present in the noise indicate that the short-period (<0.8 sec) noise predominates. Close to the surface the high-frequency noise is at least partly caused by cultural sources. At depth,

Figure 10. Probability of occurrence and percentage of occurrence at the 0.3 - 1.4 sec noise in the shallow hole at 58 m and in the deep hole at 1520 m. Gas pressure in the deep hole 3.3 x 10⁶ newtons/m². FO-TX

Probability of occurrence of the 0.3 - to 1.4-second noise
at or above a given amplitude

Percentage of occurrence of noise at different periods

Figure 11. Probability of occurrence and percentage of occurrence of the 0.3 - 1.4
sec noise at the surface and in the deep hole at 2140 m and 4570 m. Gas pressure
9.0×10^5 newton/meters^2. FO-TX

Figure 12. Probability of occurrence and percentage of occurrence of the 0.3 - 1.4 sec noise at the surface and in the shallow hole at 58 m. Wind velocity 28 km/hr. FO-TX

the 2 Hz noise commonly found throughout the central United States is the pre-dominate, high-frequency noise.

The noise level, measured from the 50% probability of occurrence levels, decreased from approximately 3.5 mμ at 58 m to a minimum of 1.0 mμ at 1520 m. Below the 1520 m, the noise level increased, reaching a level of about 2.0 mμ at the bottom of the hole. The reason for the low noise level at 1520 m has not been established; spectral analysis appear to indicate that the 2 Hz noise was smaller than at other depths. Figure 13 shows the noise levels in the deep-hole when normalized to the 58 m depth. There is no obvious connection between the velocity section and the noise levels.

Figure 13. Plot of change with depth of the signal amplitude, noise amplitude and signal-to-noise ratio.   FO-TX

The noise surveys were conducted during times when traffic noise from a nearby road was at a minimum. The increase of the noise below 1,500 m could be caused by gas-induced noise because examination of the direction of propagation of gas-induced noise indicated that the source was below 3,000 m.

Figure 12 shows a typical example of noise surveys made from the surface and shallow-hole (58 m) seismograms. A small, but appreciable, decrease in the noise level was obtained at shallow depth. This behavior is typical of shallow holes at sites in low-velocity material. The exact reason for the decrease is not understood; however, it appears likely that some of the wave energy is trapped in the low-velocity weathered zone.

4.3 SIGNAL AND SIGNAL-TO-NOISE RATIO

Figure 13 shows the decrease of P-wave amplitudes with depth. The data points were obtained by measuring the amplitude at the surface and at depth of the first half cycle of large teleseisms (signal-to-noise ratio >5) to avoid the complexities caused by surface reflected waves.

The amplitude obtained at depth is somewhat larger than would be expected if the velocities and densities of the rocks are considered. Neglecting the internal reflections and refractions, the theoretical impedance indicates that the amplitude at depths below 3,500 m should be about 0.35 of the surface amplitude instead of 0.5. This behavior has been encountered before in similar velocity sections (see Technical Report 64-68, Deep-Hole Site Report, Meridian Unit No. 1, White Pine County, Nevada). No adequate explanation for this behavior has been determined.

Figure 13 also shows the change with depth of the signal-to-noise ratio. Only a small improvement was obtained at the bottom of the hole and at a depth of approximately 1,500 m. The behavior of the signal-to-noise ratio with depth was controlled by the behavior of the noise that is discussed in section 4.2.

4.4 GAS-INDUCED NOISE

Because the holes in the casing were not completely sealed during cementing operations, gas continued to enter the casing. Noise levels were measured to determine the pressures necessary to effectively prevent gas from entering the casing. Noise surveys were made using the standard method of visual analysis.

Figures 10 and 14 show the results obtained from noise surveys made on two consecutive days, first with the casing open, and later when the casing had been sealed and the gas pressure had increased to 3.3×10^6 newtons/m^2.

From the 50% probability of occurrence levels the noise level decreased from 11 mμ to 2.0 mμ when the pressure reached 2.8×10^5 newtons/m^2. For even greater pressures the noise level decreases only slowly, reaching a minimum of 1.0 mμ with pressures above approximately 6.9×10^5 newtons/m^2 and remaining constant thereafter to pressure as great as 3.5×10^6 newtons/m^2. These noise levels were all obtained while the deep-hole instrument was at 1520 m. Thus, gas-induced noise could not be detected visually in the noise at pressures above 6.9×10^5 newtons/m^2.

4.5 SPECTRAL ANALYSIS

The principal tool used in the interpretation of the data consisted of obtaining spectra and cross spectra, and associated auto and cross correlations, of long noise samples. The techniques used to obtain spectra, and the accuracy and resolution that is obtained have been extensively discussed in the literature and need not be discussed here.

The noise samples used were 300 sec long. As a compromise between accuracy and resolution, a lag of 8% of the sample was used; however, either small or greater lags were sometimes employed to increase either the accuracy or the resolution of the results. The sampling rate used (10 samples/sec) insured that the folding frequency was well outside of the frequency range of interest.

Theoretical studies on the accuracy of cross spectra have been published in the literature. The results indicate that the experimental coherences are a complex function of the actual coherence, the smoothing function, and the lag window. A Daniel smoothing function was used in all cases. Considerable errors are to be expected when the actual coherences are close to zero.

The magnifications at 1 Hz were used to calibrate the power spectra; therefore, only the values at 1 Hz are correct ground motion values. Because of the identical responses of the seismographs used, the deep-hole divided-by-surface ratios used in the interpretation are correct at all frequencies. The ratios are obtained by dividing the deep-hole noise spectrum by the surface spectrum, and will be called power ratios in the body of the report.
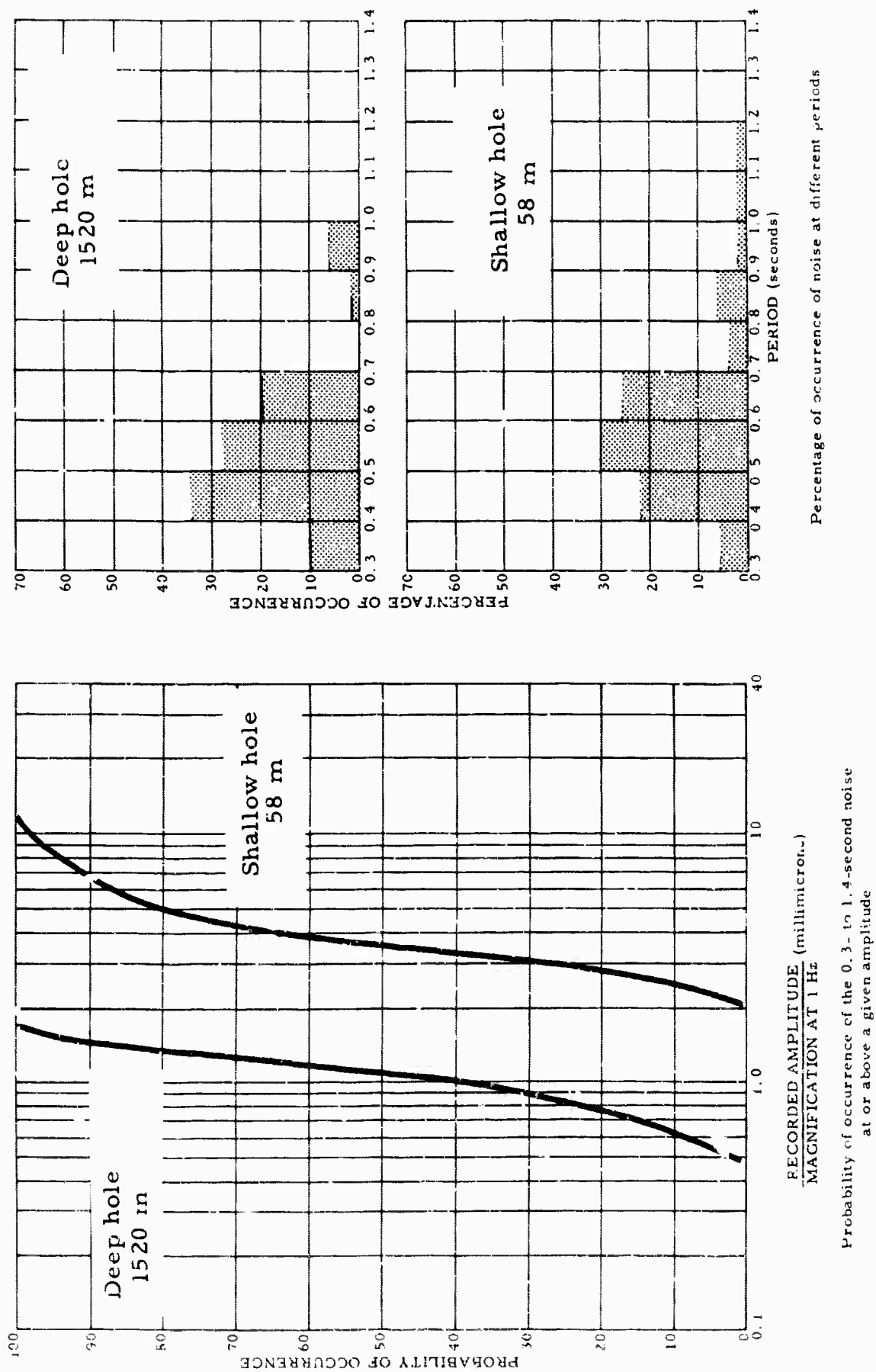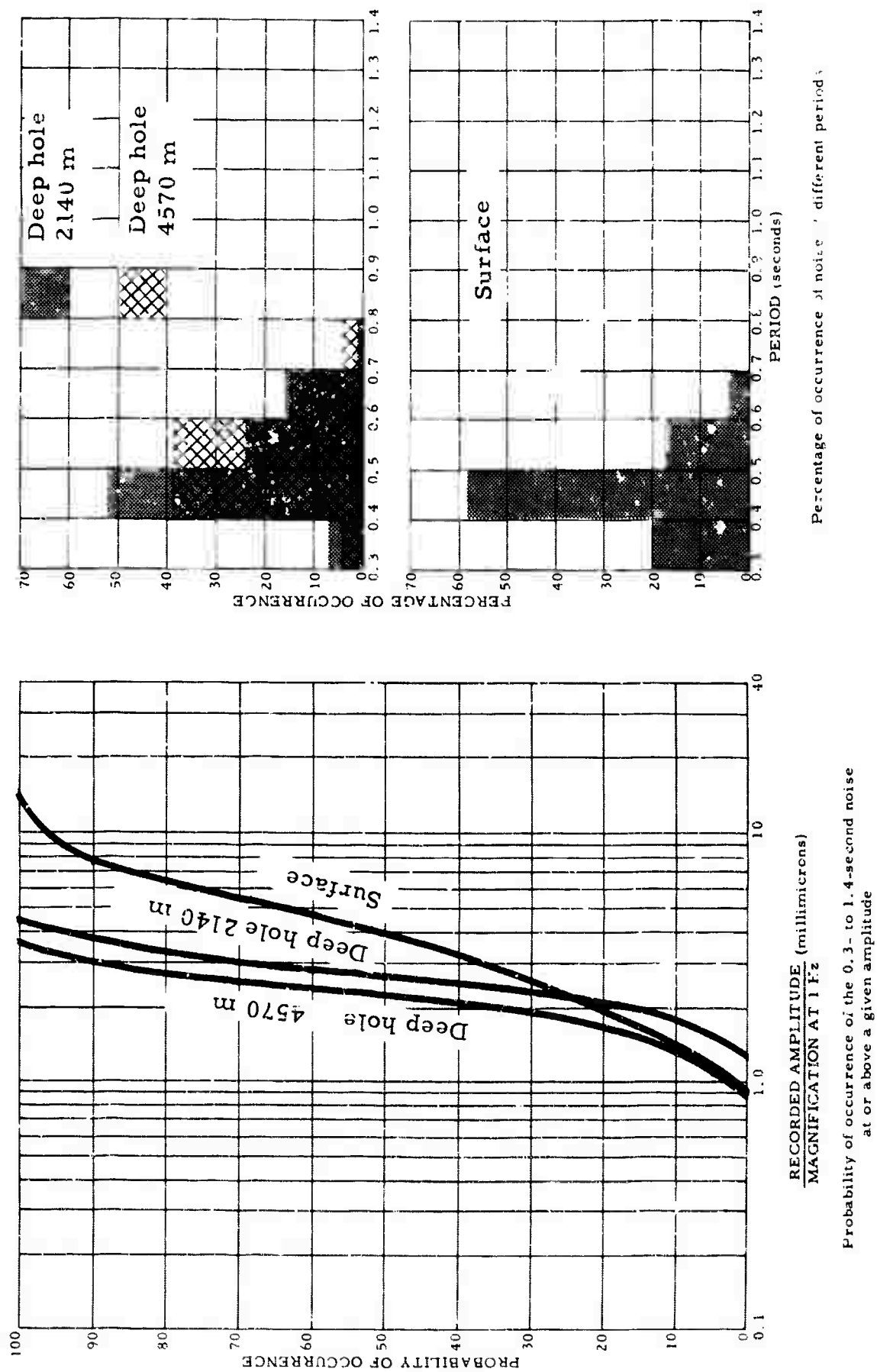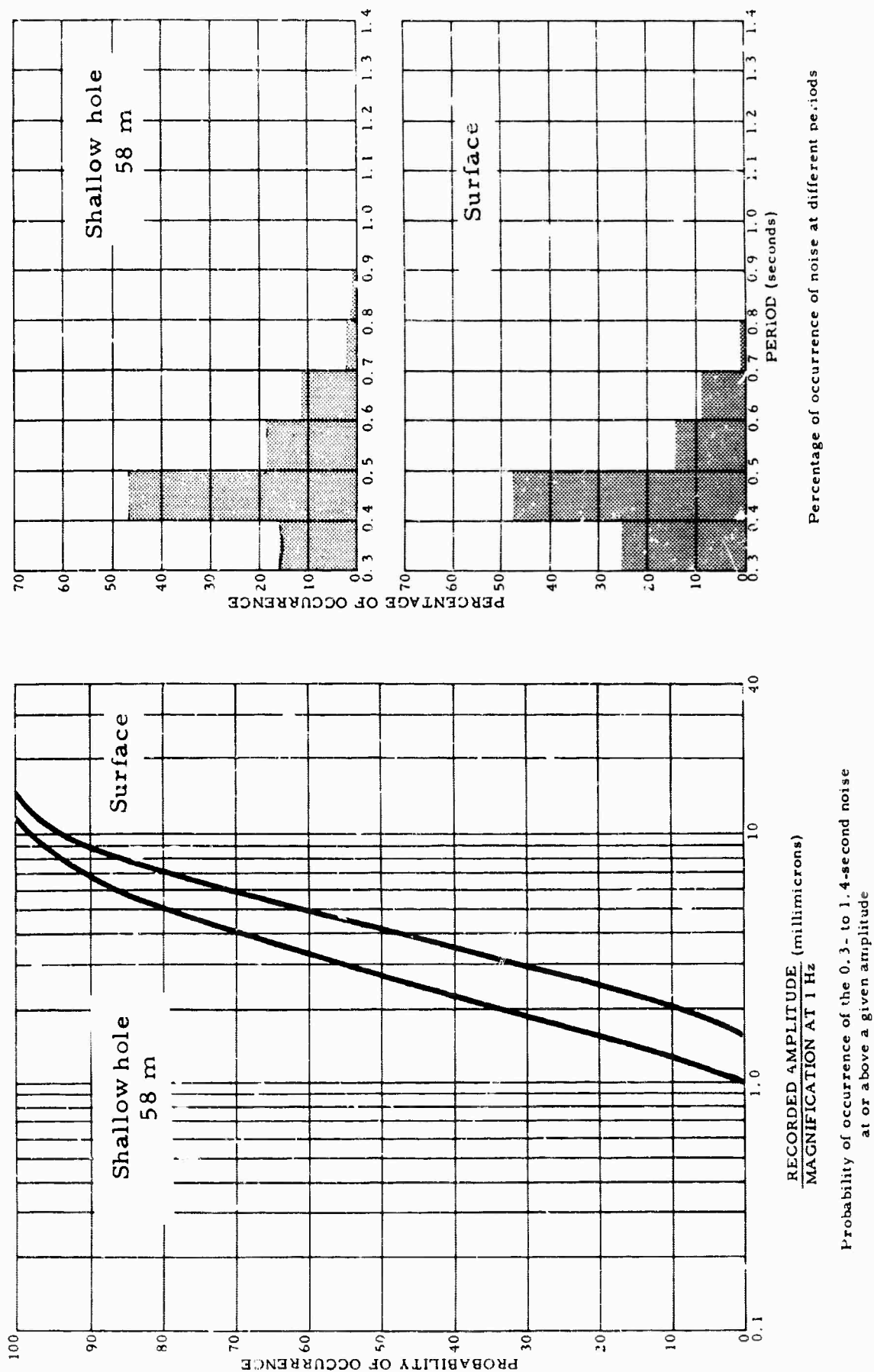
Figure 14. Probability of occurrence and percentage of occurrence of the 0.3 - 1.4 sec noise in the shallow hole at 58 m and in the deep hole at 1520 m. Gas pressure valve open. FO-TX

4.5.1 Noise at Periods Greater Than 1.0 Sec

Figure 15 shows the power spectra of the noise at a depth of 5,200 m and at the surface, and the ratio of deep-hole spectrum divided by surface spectrum. Figure 15 also shows the theoretical curves for the first three Rayleigh modes and for P waves at vertical incidence. These analyses were made at a time when a storm in the Atlantic was the cause of large microseisms in the period range of 6.0 to 2.0 sec. The ratio reached its lowest value at 4.0 sec; however, the coherence is not zero (figure 16) until a period of 3.4 is reached. This behavior indicates that between 3.4 and 4.0 sec period most of the power at depth was still in phase with the surface; therefore, the fundamental mode Rayleigh, which is the only wave in phase, predominated at these periods.

Examination of figure 15 shows that for periods less than 3.4 sec, only a small amount of fundamental mode Rayleigh waves can be present in the noise. The experimental values lie between the theoretical first higher mode Rayleigh and P-wave curves. To explain the ratio, the first higher mode must be present in the noise because the experimental ratio is larger than the theory for any other wave. The theory for P waves is not dependent on the velocities below the hole and therefore cannot be changed to agree with the experimental data. P waves at random angles of incidence will result in a lower ratio than for vertical incidence.

The small peak at 1.1 sec period was not always present in the ratios; however, it did appear on several occasions. It can only be explained by the presence of a second or even higher order Rayleigh mode. The phase angle (figure 16) changes back from 180 to 0 deg at 1.1 sec period indicating that first higher mode, which is still 180 deg out of phase, does not predominate. The phase angle does not change at 1.4 sec where the P wave should go back in phase indicating that a higher Rayleigh mode still predominates.

In conclusion, although it can not be proven conclusively, the evidence indicates that higher mode Rayleigh waves and not P waves predominate in the noise at periods greater than 1.0 sec.

4.5.2 Noise at Periods Less Than 1.0 Sec

Figure 17 shows the spectra of the noise at the surface and at depths of 3,048 m and 5,486 m. Figure 18 gives the phase angle and coherences between the same
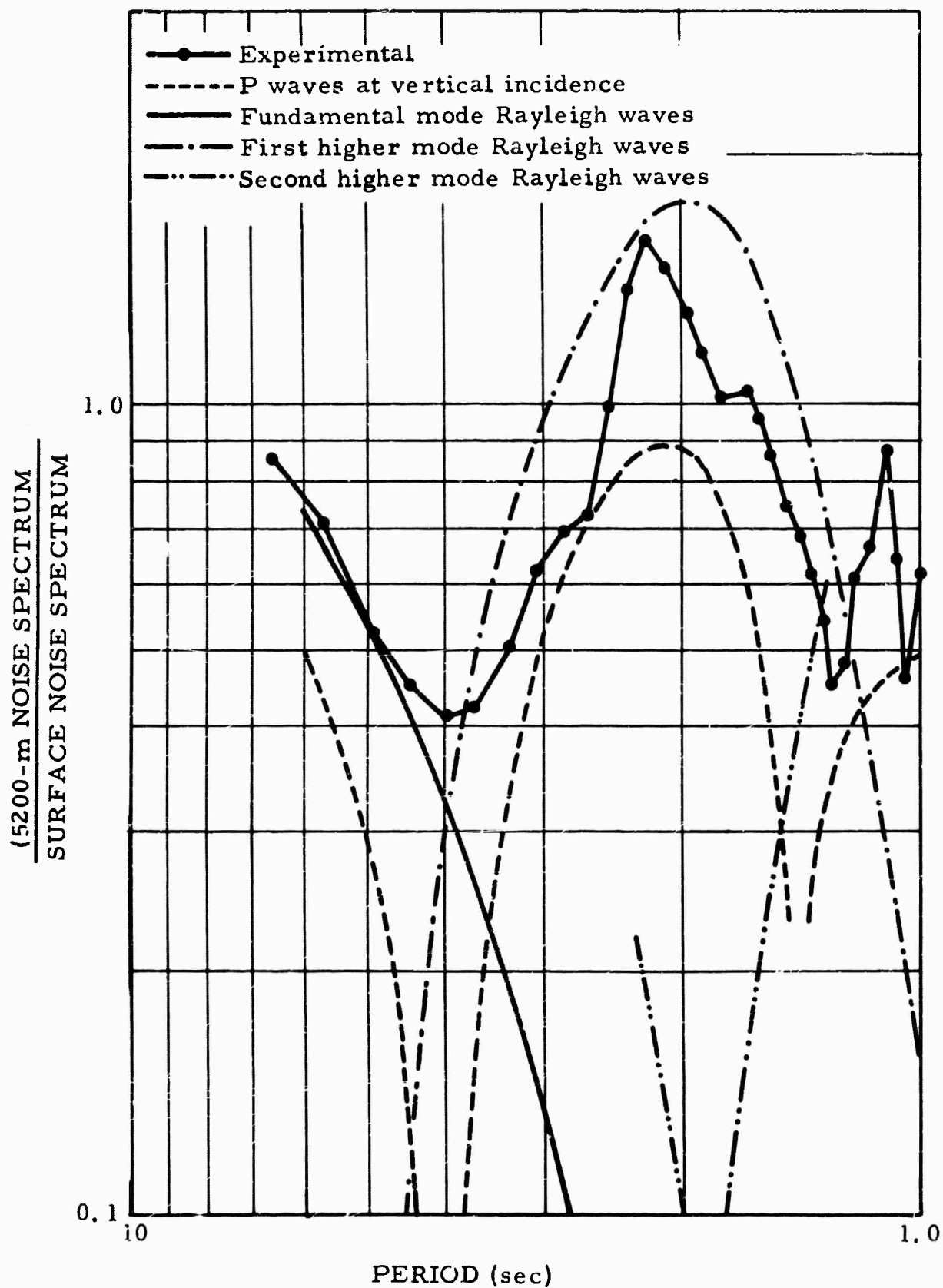
Figure 15. Deep-hole (5200-m) vertical noise spectrum divided by surface noise spectrum. Theoretical amplitudes are included. FO-TX. 300-sec sample, 10 samples/sec, 5-percent lags.
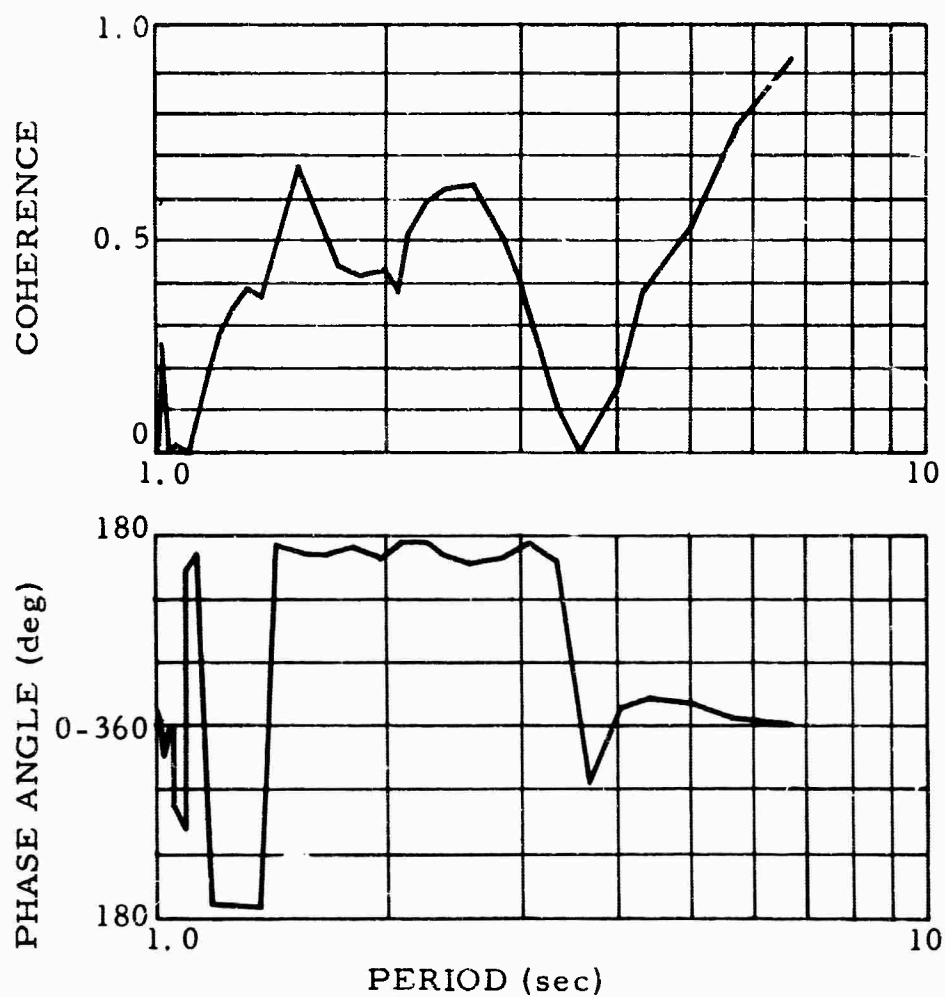
Figure 16. Phase angle and coherence of the noise between the surface and 5200 m, FO-TX. 300-sec sample, 10 samples/sec, 5-percent lags
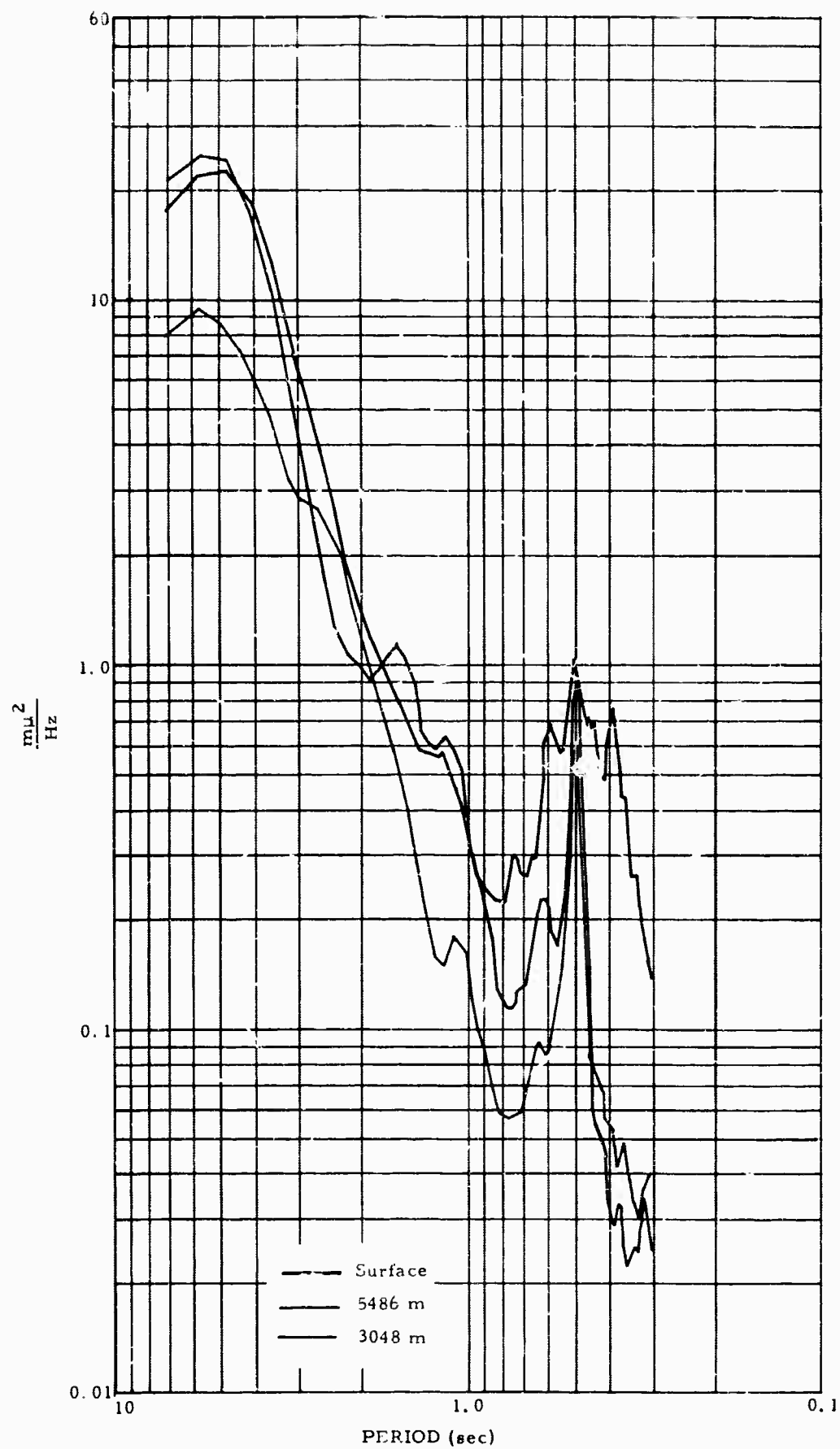
Figure 17. Spectra of the noise at the surface, and at 3048 and 5486 m, FO-TX. 180-sec sample, 10 samples/sec, 8-percent lags.
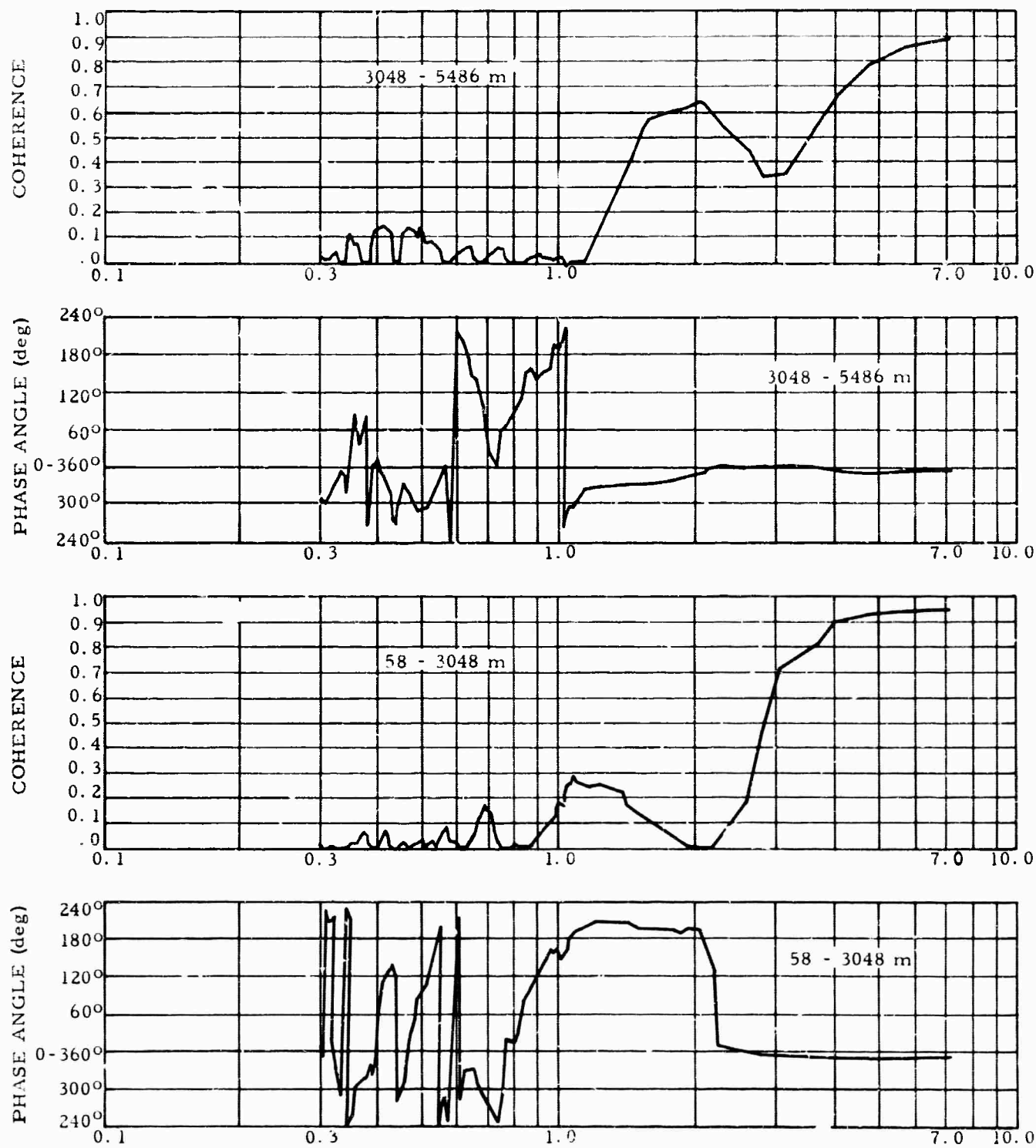
Figure 18. Phase angles and coherences of noise samples from seismometers at depths of 58 m, 3048 m, and 5486 m. FO-TX

noise samples. Examination of the spectra shows that a large decrease in noise amplitudes was obtained at all periods except 0.49 sec. This peak was not very prominent at the surface but large values were obtained at both depths; this behavior indicates that the 0.49 sec noise was the reason for the lack of decrease in noise amplitudes as measured by visual means.

The peak ot 0.49 sec period has been previously explained as consisting of the third higher mode Rayleigh wave. The large amplitude obtained at 5,486 m invalidates this explanation unless the theoretical amplitude-depth relationships are in error. The theory indicates that the third higher mode has decreased to negligible amplitudes at this depth. Coherences are low at this period and the coherences do not indicate clearly what the phase relationships are. The type of wave responsible for the peak cannot be determined.

Examination of figure 17 shows large decreases in noise amplitude at periods between 0.3 and 0.4 sec. Noise in this period range has been shown to be largely composed of fundamental mode Rayleigh waves and origin is usually from nearby cultural sources.

5. REFERENCE

Young, Addison, 1960, Paleozoic history of the Fort Stockton - Del Rio region, west Texas: The University of Texas pub. no. 6017 September 1, 1960, p 87-109

APPENDIX 1 to TECHNICAL REPORT NO. 65-104

UNIVERSITY OF TEXAS "EE" NO. 1 SITE DATA

UNIVERSITY OF TEXAS "EE" NO. 1 SITE DATA

LOCATION: Block 24, University Lands, Pecos County, Texas

LATITUDE: 30°54'06"N

LONGITUDE: 102°41'52"W

TOPO SHEET: Fort Stockton, HN13-6

ELEVATION: 885 m K.B.
                      880 m G.L.

LEASE: Special use lease dated 1 October 1963 for a period
                      of 5 years, $500.00 annual rental, from Board of
                      Regents of the University of Texas to the Geotechnical
                      Corporation

ACCESS: All-weather roads to site

POWER: At site

TELEPHONE: No service near site

SITE FACILITIES: Shallow reference hole 70 m with 178 mm casing
                      set at 61 m

APPENDIX 2 to TECHNICAL REPORT NO. 65-112

DEEP-HOLE SITE REPORT
LONG NO. 1, CENTRE COUNTY, PENNSYLVANIA

TECHNICAL REPORT NO. 65-105

DEEP-HOLE SITE REPORT
LONG NO. 1, CENTRE COUNTY, PENNSYLVANIA

THE GEOTECHNICAL CORPORATION
3401 Shiloh Road
Garland, Texas

15 July 1965

CONTENTS

ILLUSTRATIONS

ABSTRACT

The Long No. 1 was used in a deep-hole measurement program by special arrangement with Mobil Oil Company who drilled the hole to a depth of 4774 m in a highly folded and thrust-faulted section of Ordovician and Cambrian sediments. Deep-hole and surface seismographs were used to record both seismic signals and noise. Results of the measurements show that an improvement of 2.4 was obtained in the signal-to-noise ratio.

BLANK PAGE

DEEP-HOLE SITE REPORT
LONG NO. 1, CENTRE COUNTY, PENNSYLVANIA

1. INTRODUCTION

This report details the history and geology of the Long No. 1 and its preparation for use in a deep-hole measurement program. It also includes a description of the measurement program conducted in the deep hole and the methods used in analyzing the records produced. The report covers all aspects of the work performed including spectrum analyses of noise samples.

The report was prepared to document the characteristics of this deep hole and the results of measurements therein using the deep-hole seismograph.

The work described in this report was performed as part of Tasks 1c (2) and 1d of the Statement of Work of Contract AF 33(657)-13668, Project VT/5u51.

2. HISTORY AND GEOLOGY OF THE LONG NO. 1

2.1 HISTORY

The Long No. 1 is located in the northeastern part of Centre County, Pennsylvania, about 5 km east of the town of Howard (see map, figure 1). It was drilled by Mobil Oil Company as an exploratory test for oil and gas.

The hole was cased to 3036 m with 244 mm casing and drilled to a total depth of 4774 m, where Mobil decided to plug and abandon it in July 1964.

2.2 GEOLOGY

The Long No. 1 is located at the northwestern extremity of the Valley and Ridge physiographic province in central Pennsylvania. It was spudded in the Gatesburg formation of Cambrian age, crossed a thrust fault at 290 m and entered the Beekmantown dolomite (lower Ordovician). This formation was
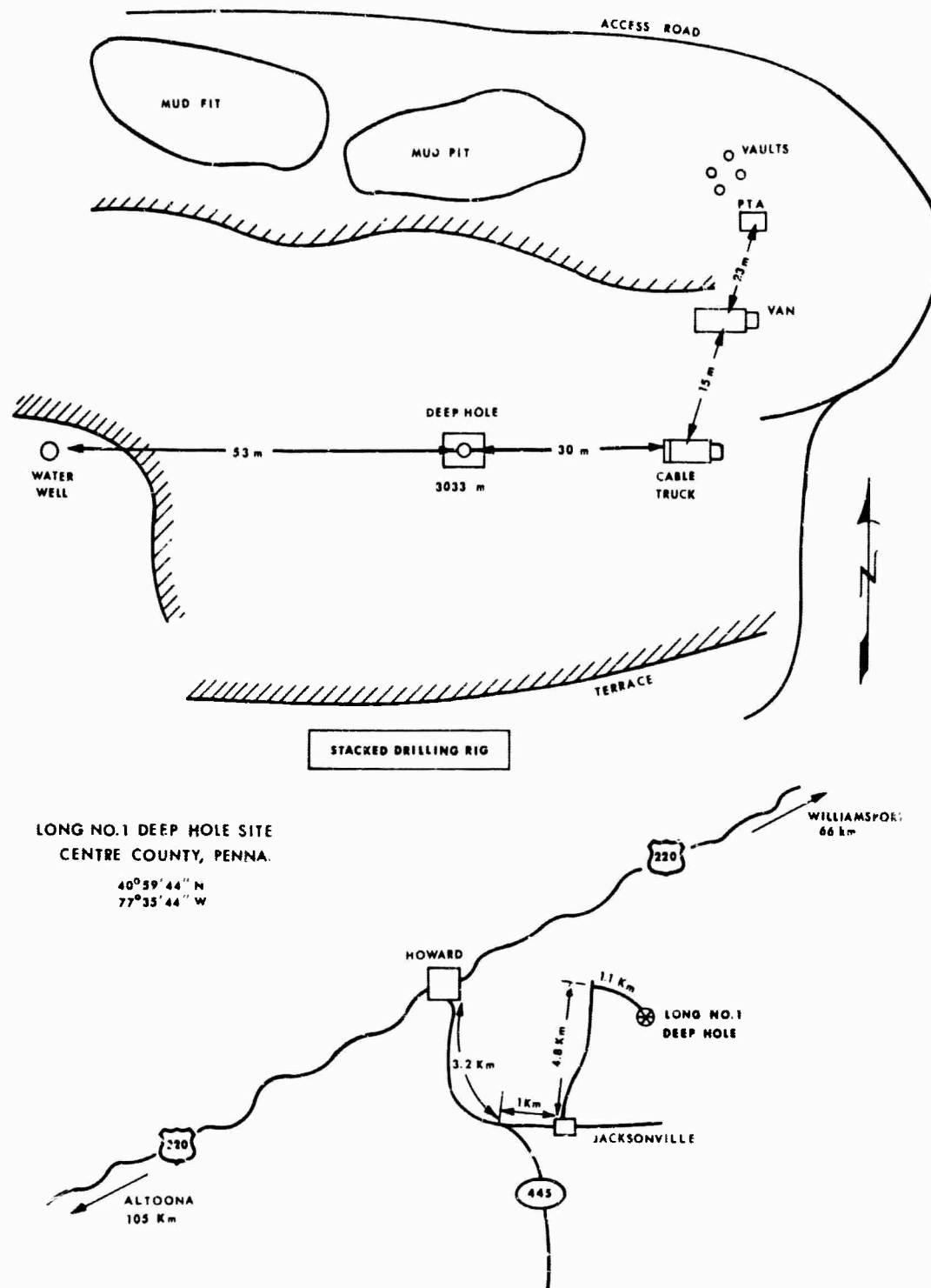
Figure 1. Deep-hole site map, Long No. 1

d. illed to a depth of 2637 m and was cored for dip determination near its base. Dips of 75 deg to 90 deg were observed. At 2637 m, the hole crossed a second thrust fault into the McKenzie shale (Silurian). Below this discontinuity, a normal sequence of Silurian and Ordovician was drilled to total depth at 4774 m in the Black River limestone.

Figure 2 shows the tectonic setting of the Long No. 1. Figures 3a and 3b illustrate the surface attitude of the Ordovician sediments near the Long No. 1 and figure 3c is a hypothetical cross section. The stratigraphic section penetrated is shown in figure 4.

2.3 PREPARATION

In July 1964, when Mobil was ready to plug and abandon the Long No. 1, an agreement was entered into with them providing for our temporary use of the cased hole for seismic measurements. Mobil's contract rig plugged the uncased portion of the hole and left the cased portion plugged at a depth of 3033 m, suitable for use by Project VT/5051. Maximum deviation of the cased hole was approximately 6 deg from the vertical and maximum bottom hole temperature at 3033 m was 47°C. All depth measurements are from the drilling rotary kelly bushing, 6 m above ground level. Figure 4 is a subsurface diagram. A water well at the site, cased with 152 · 'r~ to a depth of 173 m, was left intact for shallow reference measur.ments. The well and site were restored to their original condition when the measurement program was completed in February 1965.

2.4 GENERAL

Detailed information on the site location and facilities is given in appendix 1.

3. MEASUREMENT PROGRAM AT THE LONG NO. 1

Measurements were made with surface instruments, with a deep-hole seismometer operated at various depths in the deep hole, and with a deep-hole seismometer operated in the shallow hole. The surface instrumentation consisted of a recording van and associated equipmdnt, short-period and long-period

Source: Tectonic map of the United States, USGS, AAPG, 1961

Figure 2. Tectonic setting, Long No. 1
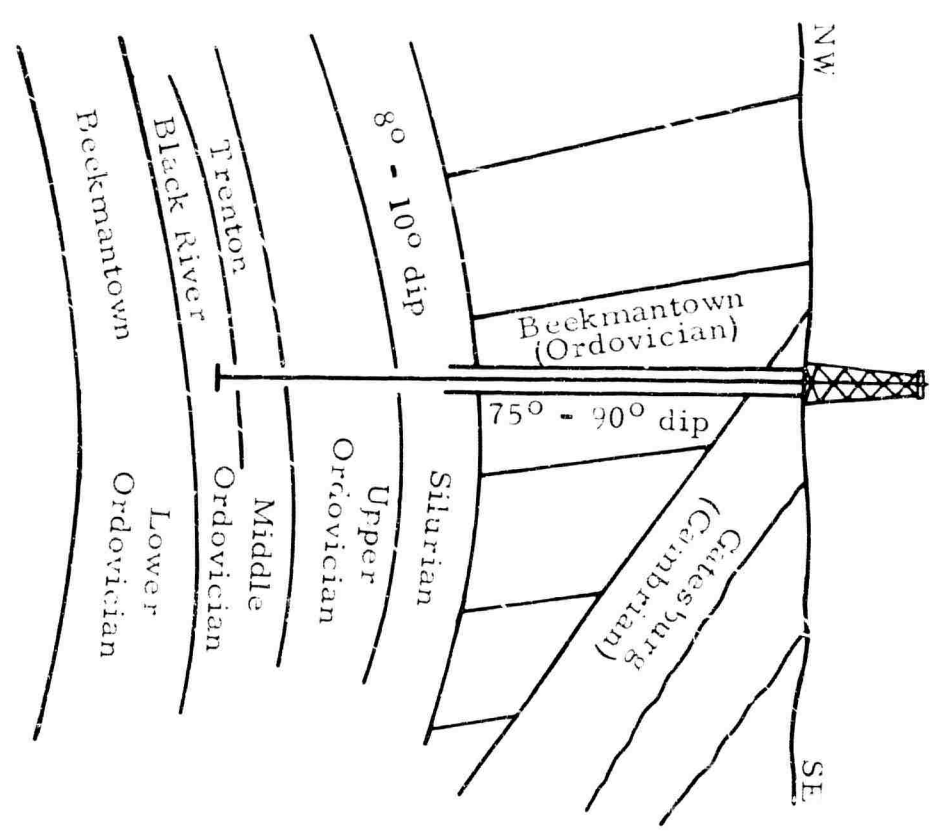
Figure 3. Surface and subsurface formation attitudes, Long No. 1
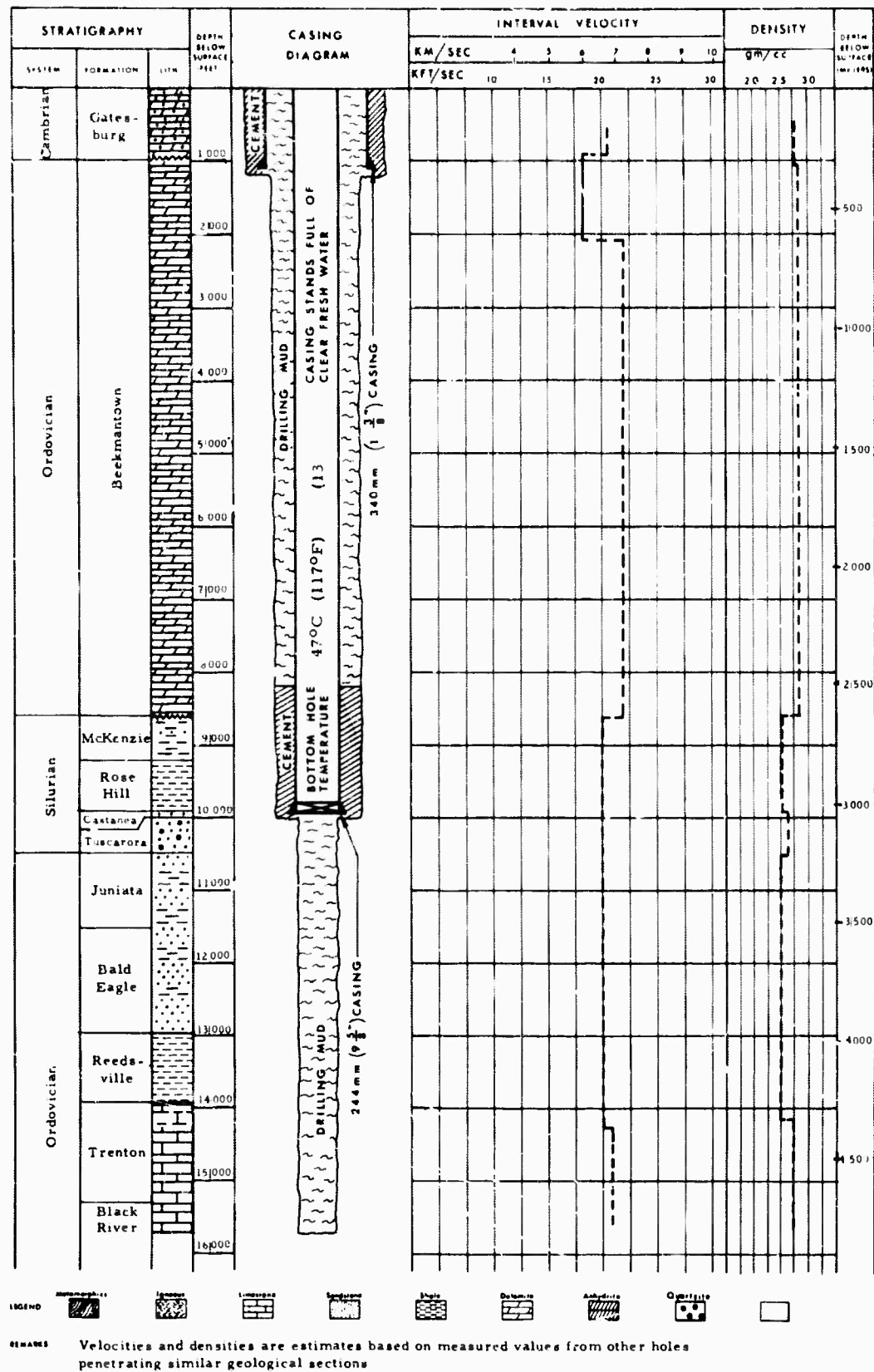
Figure 4. Subsurface diagram, Long No. 1

seismometers, and phototube amplifiers. The recording van and surface instruments were provided by Contract AF 33(600)-41694 and are identical with the equipment used in the Long-Range Seismics Measurements Program (LRSM), except that a film recorder was added to the van to provide additional recording capability.

3.1 INSTRUMENTATION

Figure 5 shows the basic components of the deep-hole seismograph. Figure 6 shows a block diagram of the LRSM system, including a long-period instrumentation. The deep-hole, shallow-hole and short-period surface systems had similar response characteristics. Each system used a seismometer with an undamped natural frequency of 1 Hz and a phototube amplifier with a 5 Hz galvanometer. The seismographs included provisions for remote calibration, thus allowing their response characteristics to be verified. The systems were calibrated by applying measured currents at various frequencies to the internal calibrators and recording the resultant output of the systems. The outputs of the phototube amplifiers were connected to the recorders through attentuators so that the amplitudes of the records could be adjusted as desired.

The film recorder that was added to the van is a 16-channel automatic processing camera that makes visual records of seismic data on 16 mm film. Eleven channels of seismic data were recorded on the magnetic-tape recorders, and four channels were recorded on each of the 35 mm film recorders. The film recorders also recorded station time, and radio station WWV was recorded on one channel of the magnetic-tape recorder

A control device was used to permit control of the various functions of the deep-hole seismometer. These functions included calibration, locking, unlocking, and centering of the mass, and operation of a hole lock to secure the seismometer to the casing at any selected casing collars.

3.2 SYSTEM RESPONSE

Figures 7 and 8 show the response of the seismographs to steady-state calibration frequencies.
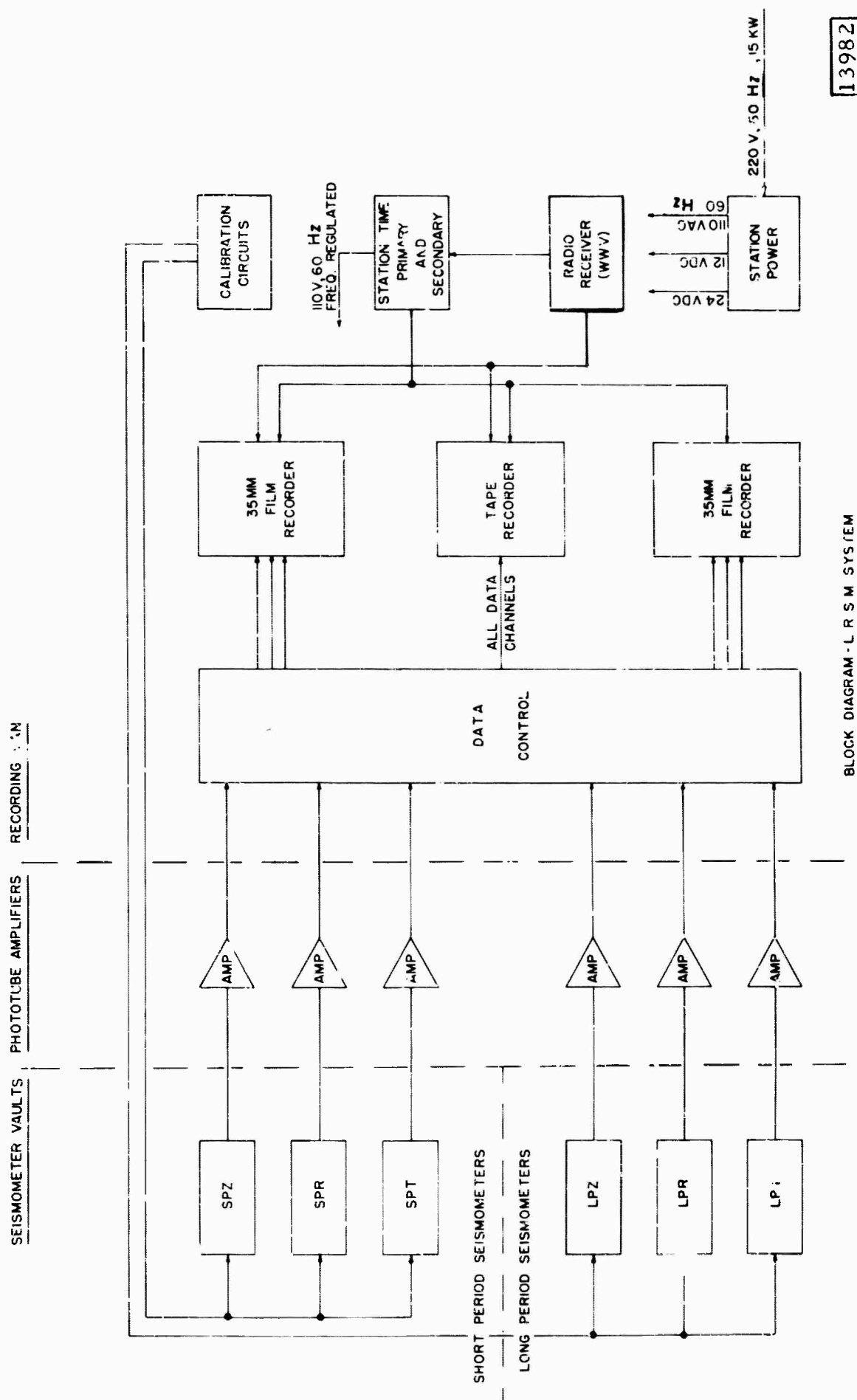
Figure 5. Deep-hole seismograph system, Model 15075

Figure 6. Simplified block diagram of the LRSM seismograph system
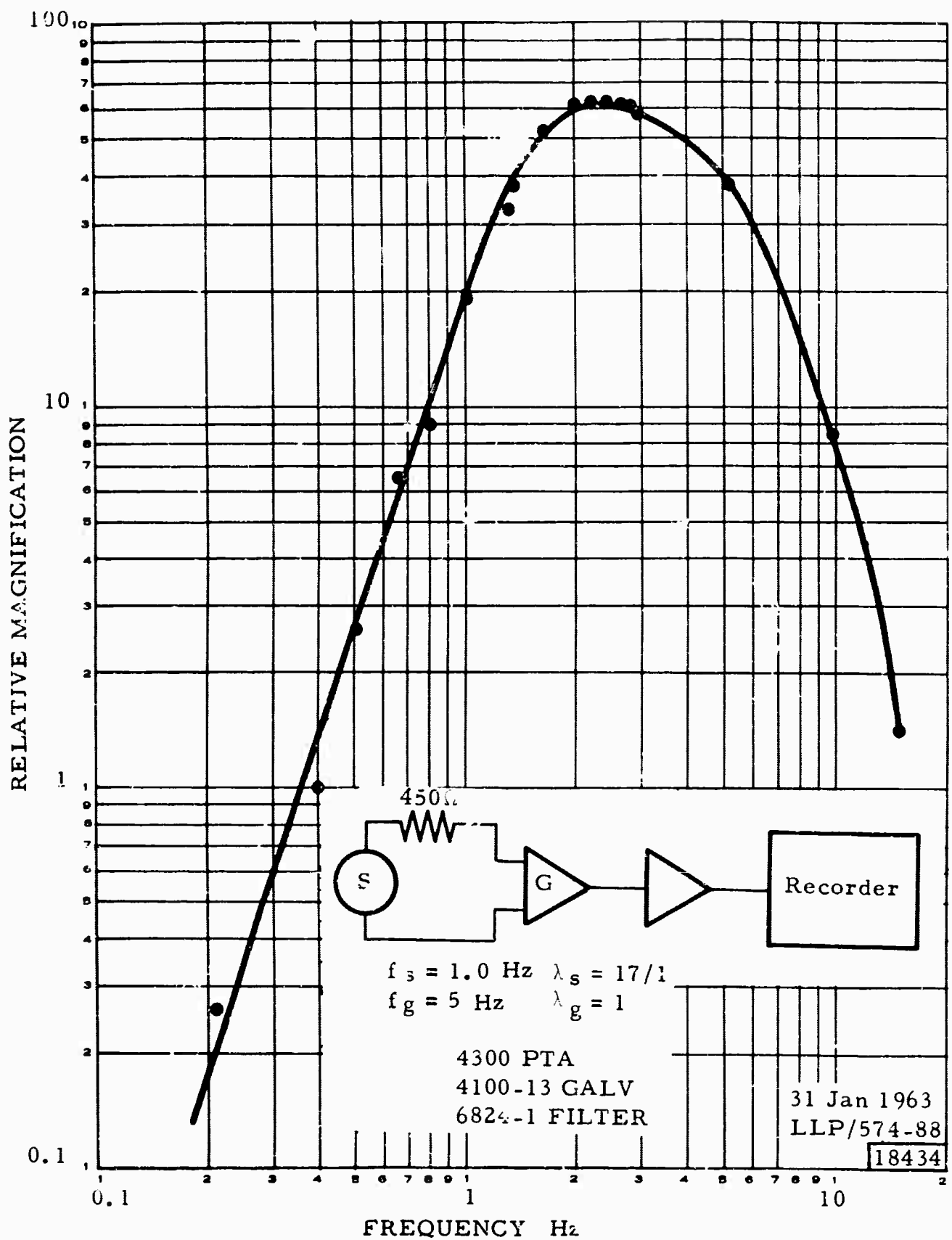
Figure 7. Frequency response of deep-hole and shallow-hole seismographs.
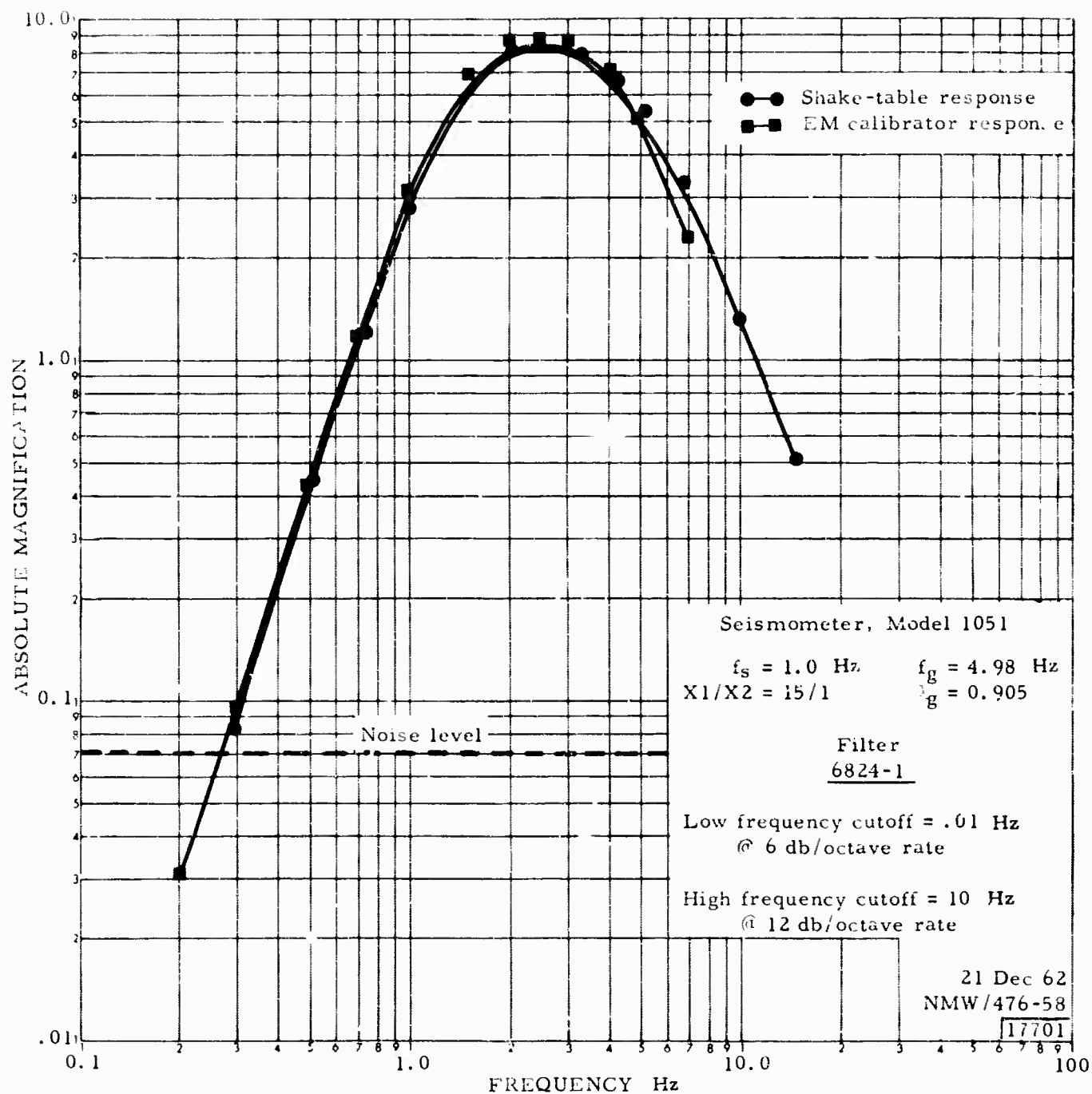
Figure 8. Frequency response of the short-period seismograph from shake-table and electromagnetic calibrator tests

4. DATA ANALYSES AT HOWARD, PENNSYLVANIA

The deep-hole at Howard, Pennsylvania has a usable depth of 3033 m in extremely high-velocity limestones (see figure 4). The velocities close to the surface are not known; however, as further described under the section on visual analyses, it appears that a weathered zone of appreciable thickness is present.

The geology of the general area is very complex, and the limestone beds dip almost vertically at the well site. Therefore, while there are no large vertical changes in velocity, lateral changes are probably quite large. The theoretical Rayleigh wave program, which assumes horizontal layering, was not run because the results would not be applicable to the actual behavior of Rayleigh waves in such a section. Most of the analyses of signal and noise were done by visual means.

4.1 METHOD OF MEASURING NOISE

The noise-distribution curves given in this report were obtained by measuring the largest noise amplitude present in the 10-sec interval immediately following a 5-min mark.

The amplitudes were not corrected for instrument response, and the magnifications at 1 Hz were used to obtain the millimicron (mμ) values given. Samples were taken during times when the cultural activity in the vicinity was minimum; 100 samples were taken at each depth. All measurements of amplitude were peak-to-peak.

This method of measuring the noise essentially defines the detection capability of the site. The results are given in "probability-of-occurrence" curves which determine the probability that a noise pulse of the same amplitude as a signal will occur at approximately the same time. The slopes of the curves give a measure of the variability of the noise amplitudes.

The periods of the pulses measured are also plotted to allow a comparison of the periods predominate at each depth.

The method has the advantage of ease of measurement and gives consistent, reproducible results by visual analysis; however, it should not be taken as a substitute for spectral analysis of the noise.

The probability-of-occurrence curves give a good picture of the decrease in noise level in the deep hole without making any attempt to distinguish between the decay of the different frequencies which occur in the noise.

4.2 VISUAL ANALYSES

Figure 9 shows the decrease with depth of the noise levels as measured from the 50% probability-of-occurrence levels. The surface Benioff was used as the surface reference. Figure 10 shows an example of the results of noise studies that were made at the different depths at which the instrument was operated.

A rapid decrease in the noise level was found between the surface and the bottom of the shallow hole at a depth of 136 m. This behavior is typical of sites with low-velocity weathered zones. Below this depth the noise level decreased only slowly with depth. A noise level decrease of a factor of 6.0 was obtained at the bottom of the hole.

Figure 11 shows the change in signal levels and the signal-to-noise ratio with depth using recordings from both the shallow and deep hole. An appreciable decrease in signal level was noted in the shallow hole; this behavior was a result of the low-velocity weathered zone. The slight increase in signal level at the bottom of the hole was probably caused by the somewhat lower velocities of the rocks below approximately 2600 m.

The signal-to-noise ratio shows an improvement over the surface in the shallow hole. At intermediate depths the ratio was lower than the surface because of destructive interference between incoming and surface reflected waves. Below the depths of interference the signal-to-noise ratio increased reaching a maximum of 2.4 at the bottom of the hole.

4.3 SPECTRAL ANALYSES

The principal tool used in the interpretation of the data consisted of obtaining spectra and cross spectra, and associated auto and cross correlations, of long-noise samples. The techniques used to obtain spectra, and the accuracy and resolution that is obtained have been extersively discussed in the literature and need not be discussed here.

Velocities are estimates based on measured values from other holes penetrating similar geological sections.
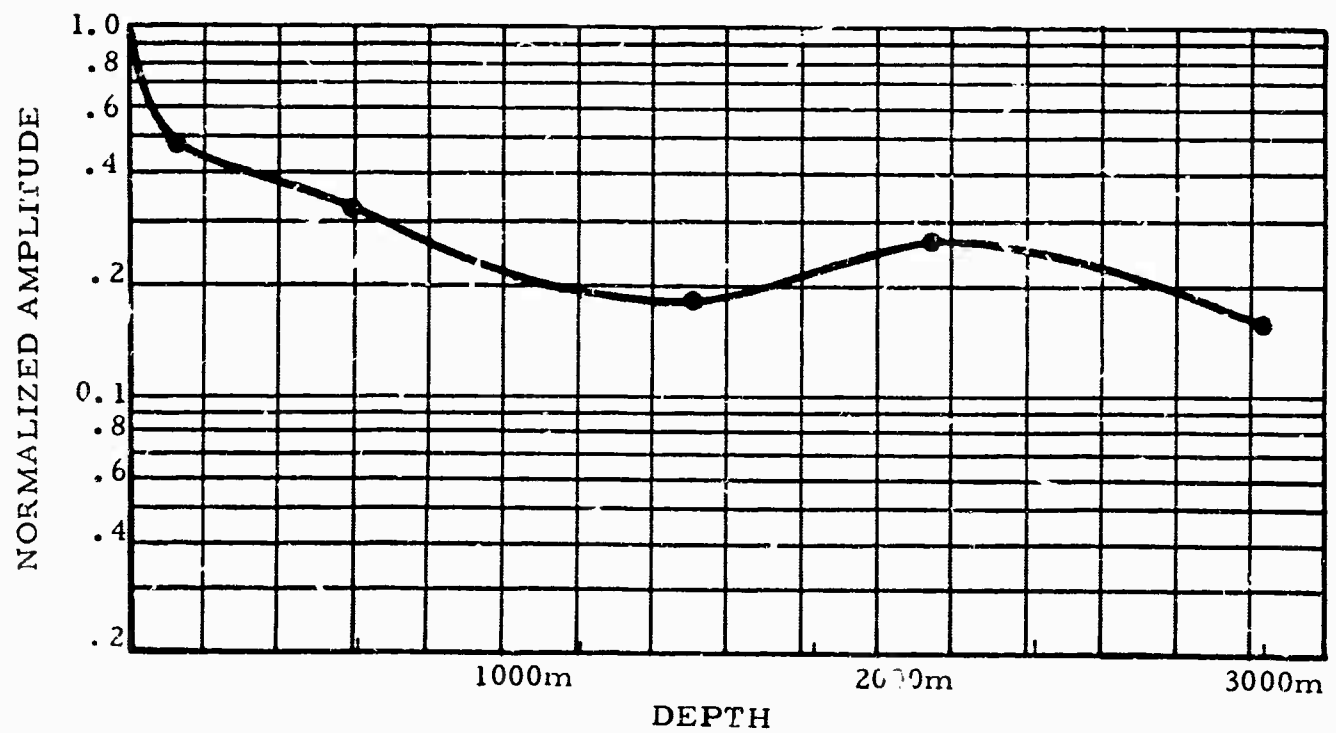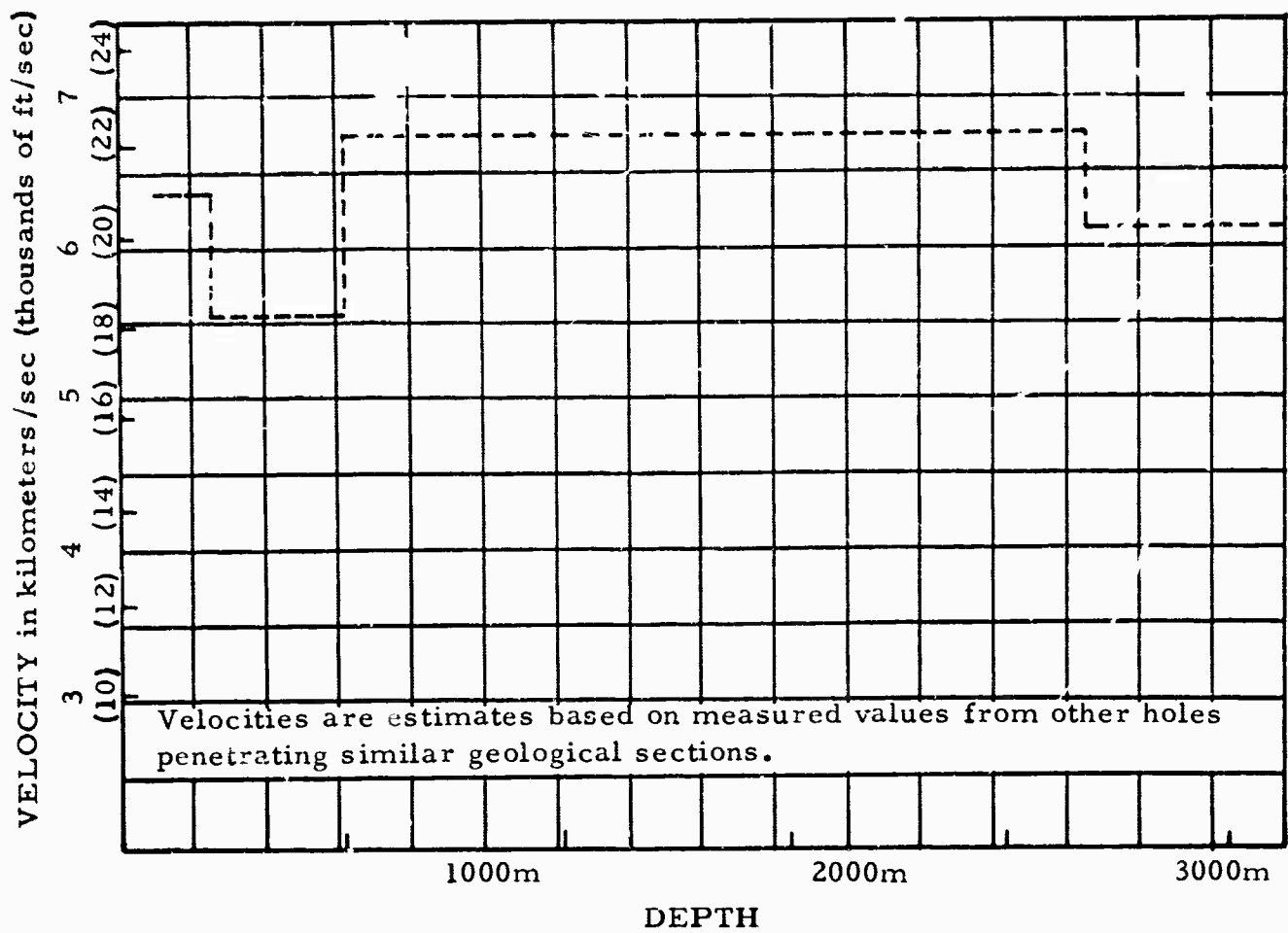
Figure 9. Depth versus P-wave velocity and depth versus noise amplitude.
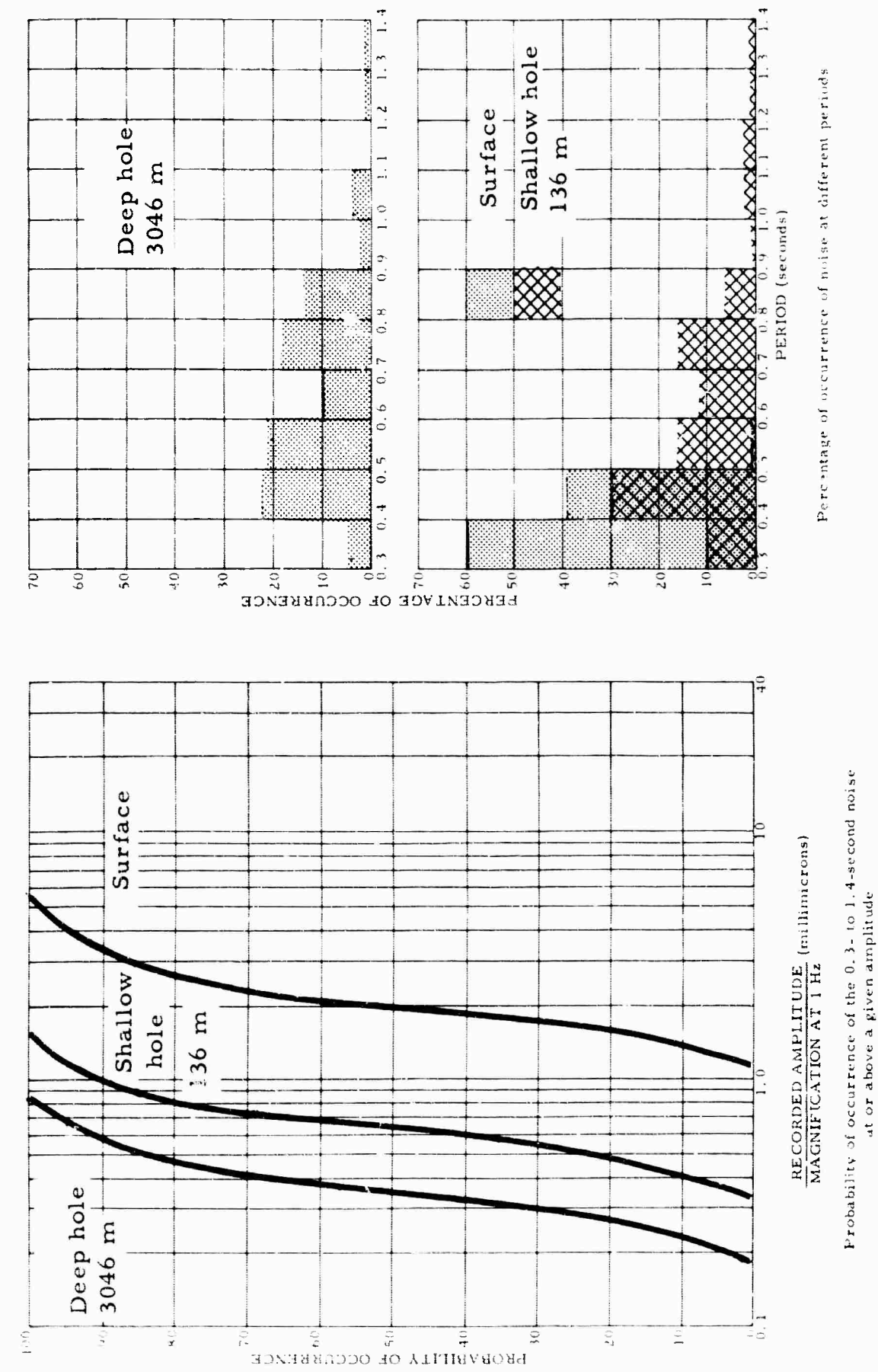
Figure 10. Probability of occurrence and percentage of occurrence of the 0.3 - 1.4 sec noise at the surface, in the shallow hole at 136 m, and in the deep-hole at 3046 m. HD PA   29 September 1964
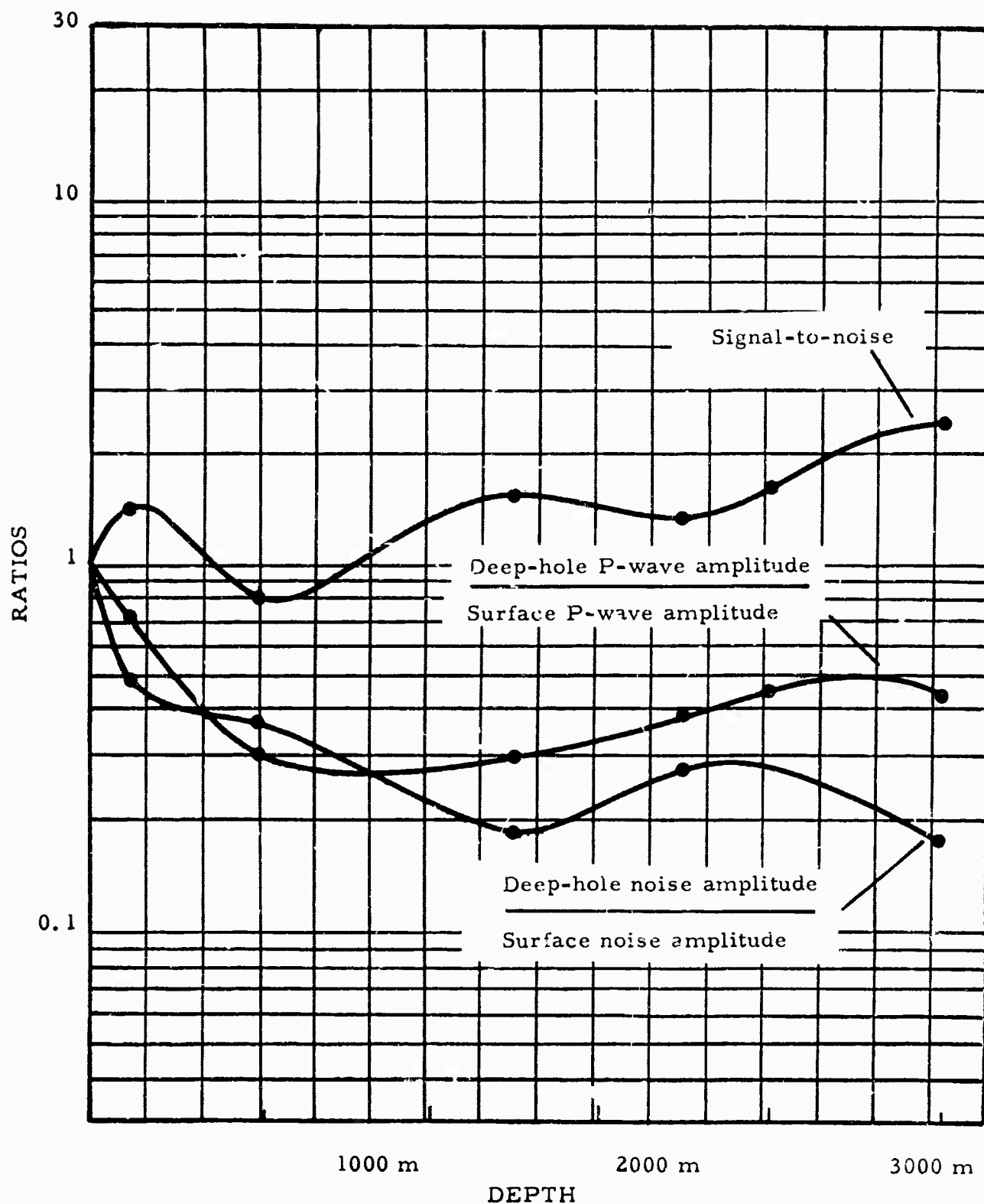
Figure 11.   Plot of change with depth of the signal amplitude,
noise amplitude and signal-to-noise ratio, HD PA.

The noise samples used were 180 sec long. As a compromise between accuracy and resolution, a lag of 8% of the sample was used; however, either small or greater lags were sometimes employed to increase either the accuracy or the resolution of the results. The sampling rate used (25 samples/sec) insured that the folding frequency was well outside of the frequency range of interest.

Theoretical studies on the accuracy of cross spectra have been published in the literature. The results indicate that the experimental coherences are a complex function of the actual coherence, the smoothing function, and the lag window. A Daniel smoothing function was used in all cases. Considerable errors are to be expected when the actual coherences are close to zero.

The magnifications at 1 Hz were used to calibrate the power spectra; therefore, only the values at 1 Hz are correct ground motion values. Because of the identical responses of the seismographs used, the deep-hole divided-by-surface ratios used in the interpretation are correct at all frequencies. The ratios are obtained by dividing the deep-hole noise spectrum by the surface spectrum, and will be called power ratios in the body of the report.

4.4 NOISE ANALYSES

Because of the lack of dependable theoretical amplitude-depth relationship, no attempt was made to compare experimental and theoretical results.

Figure 12 shows the spectra of the noise at the surface and at depths of 136 m (shallow hole), and 3046 m. The very sharp peaks at 0.3 and 0.5 sec period that were found at Franklin, West Virginia, are not present at this site. Possibly the extremely complex geology and the consequent rapid lateral changes of velocity have attentuated these waves. It is of interest to note that the spectra peak is at a period of 3.3 sec. Sites further removed from the coast usually have the largest spectral peak at a period of 6.0 sec. The phase angle and coherence (figure 13) show that the energy remained in phase with high coherences down to a period of 1.1 sec, indicating that the fundamental mode Rayleigh wave predominates. For periods less than 1.0 sec, the ratio in figure 13 shows large rapid changes indicating the presence of different wave types in closely adjacent period ranges. The coherences are, in general, quite large considering the separation of the seismometers. An array processor that operates on coherent noise might result in appreciable improvements in the signal-to-noise ratio.
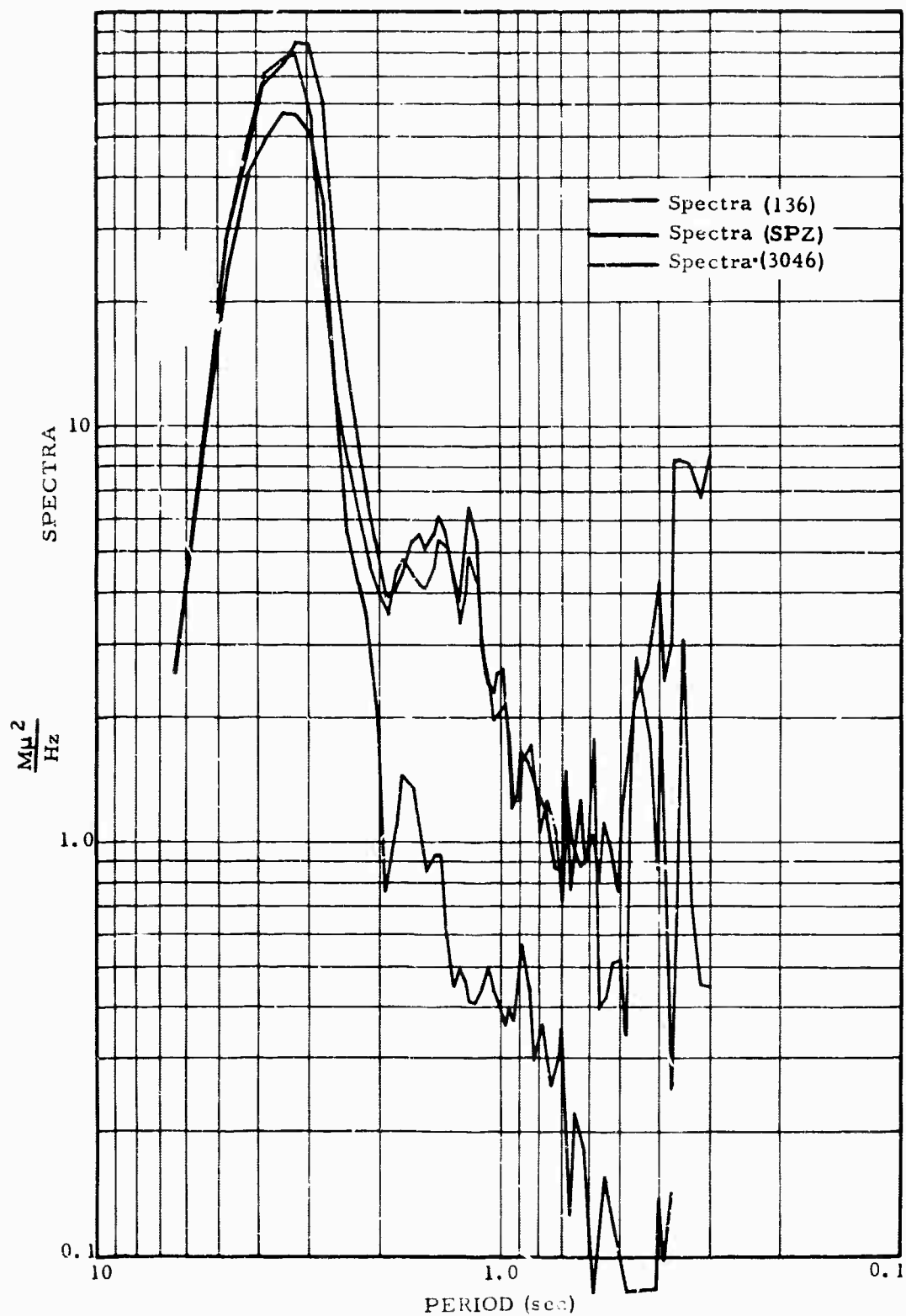
Figure 12.   Spectra of the noise at the surface and at depths
of 136 m and 3046 m.   HD PA
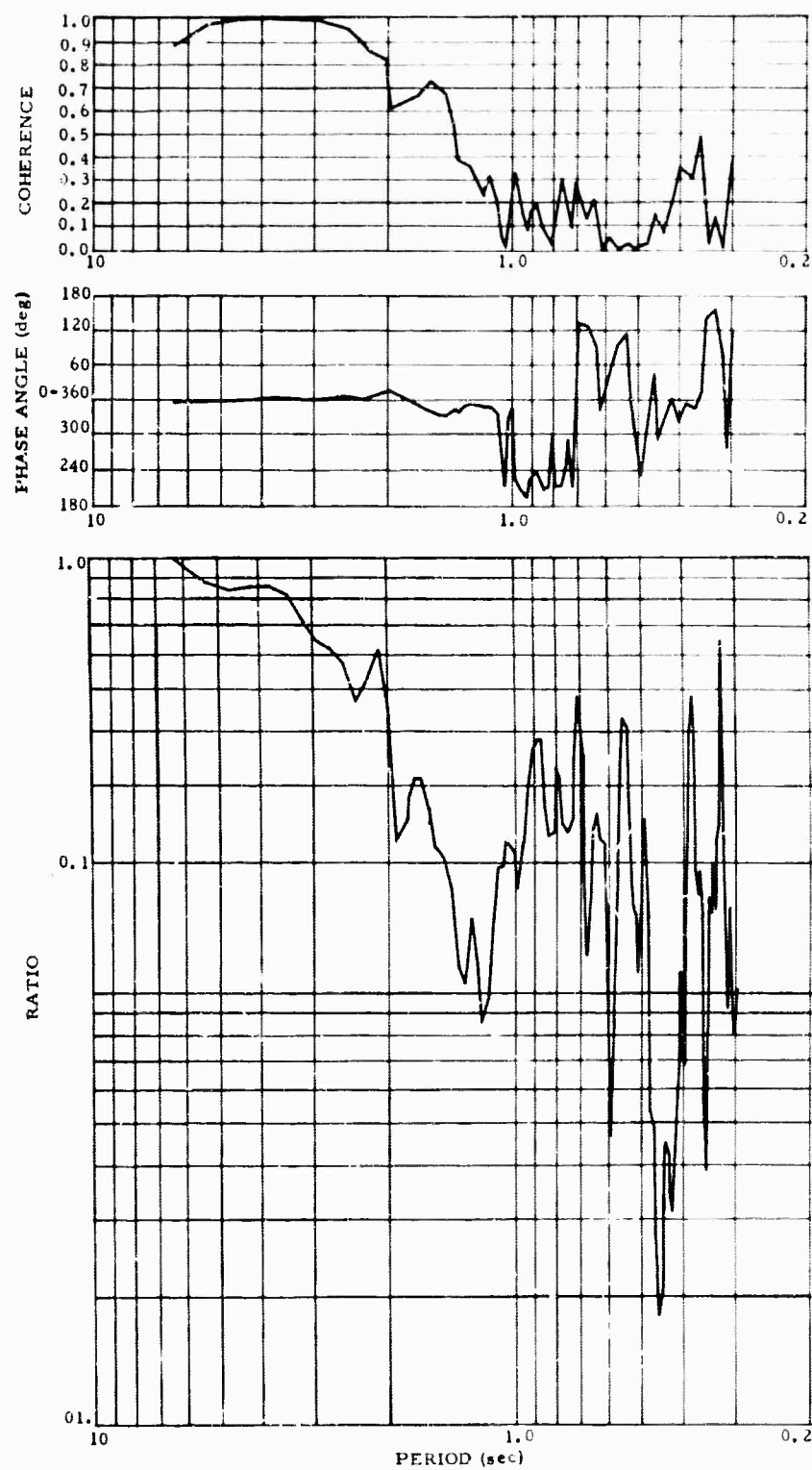
Figure 13.   Ratio of noise at 3048 m divided by
noise at 136 m, and the coherence and phase
angle between the noise samples, HD PA

APPENDIX 1 to TECHNICAL REPORT NO. 65-105

LONG NO. 1 SITE DATA

LONG NO. 1 SITE DATA

OPERATOR: Mobil Oil Company

WELL: No. 1 J. F. Long

COUNTY: Centre
STATE: Pennsylvania

LOCATION: Marion Township, 655 m south of $41°00'00''N$,
                            1433 m west of $77°35'00''W$, about 32 km
                            southwest of Lockhaven

COMPLETED: 23 July 1964

ELEVATION: 375 m K. B.
                            369 m G. R.

TOTAL DEPTH: 4774 m

CASINGS: 340 mm at 370 m
                            244 mm at 3036 m

PLUGS: Cement plug in casing at 3033 m

LAND OWNERSHIP: J. Franklin Long and Esther M. Long

EXISTING LEASES: Oil & Gas Lease - Mobil Oil Company
                            Surface Lease - The Geotechnical Corporation

AVAILABLE LOGS: Laterolog GRN
                            Continuous Velocity
                            Sonic
                            Density

REMARKS: All measurements from kelly bushing, 6 m
                            above ground level

APPENDIX 3 to TECHNICAL REPORT NO. 65-112

OFF-SHORE MEASUREMENTS PROGRAM

28 July 1965

TO: MEMORANDUM

FROM: Richard M. Shappee

SUBJECT: Off-Shore Measurements Program,
           Ref. P-436, Project VT/5051

ABSTRACT

A deep-ocean seismograph was installed in the ocean approximately 200 nautical
miles[1] off Cape Hatteras in water with a depth of approximately 2000 fathoms[2].
The seismograph consisted of: a Model 20171 seismometer modified to withstand
high pressure and further modified to permit remote mass locking, unlocking,
and centering; a Texas Instruments RA-3 amplifier; a voltage controlled oscil-
lator; a telemetry transmitter; a programmed calibrator; and seven-conductor,
deep-hole cable. Other portions of the seismograph included a telemetry receiver,
a discriminator, a Helicorder and a tape recorder. Four attempts were made
to install the seismograph, and the last attempt was partially successful.

INTRODUCTION

The Statement of Work to be Done of Project VT/5051 was amended on
26 May 1965 to include "....operational testing of the deep-well seismometer
on the ocean bottom in approximately 15,000 feet of water at locations to be
designated by the AFTAC Project Officer." In accordance with the Project
Officer's recommendation, a simple system was designed and made ready for
measurements at sea on 19 June. This date was chosen so that measurements
might be made of explosions scheduled as part of the East Coast On-Shore Off-
Shore Experiment (ECOOE). The appendix shows the planned locations of ex-
plosions and the locations at which we planned to install our equipment.

INSTALLATION OF EQUIPMENT

The design of the original system taken to sea is shown in figure 1. Figures 2
and 3 show block diagrams of the electronic equipment used throughout the work.

A vessel (R. V. Prospector) was leased and set out from Newport News with
equipment and personnel on 17 June. The ship was on station on 18 June but
the inital installation was delayed by severe weather until 20 June 1965.
Difficulty was experienced in putting the system into the ocean. It was found

---

[1] 1 nautical mile = 1.853 kilometers
[2] 1 fathom = 1.828804 meters

that the sub-surface buoys, chain, and anchor caused severe kinking of the
cable with resultant electrical shorts in the cable. The kinking was thought
to be caused by rotation of the subsurface buoys and tetrahedron and by
non-torque balance in the cable. Figure 4 illustrates the type of kinking. A
second attempt was made to put the system into the sea, replacing the chain
weight with zinc coring weights. The cable kinked again and the ship and equip-
ment returned to port, arriving at Newport News on 24 June 1965.

Modifications to the design were made. These included changing the cable
from 9.5 mm to 11 mm in diameter, construction of an ocean bottom "sled"
(figure 5) that was designed to stream into the ocean current, revision in
the surface buoy so that sub-surface buoys were not required, and revisions
to the anchor weights to increase their symmetry. The revisions were all
intended to minimize cable rotation. This system is shown in figure 6.

After the modifications were completed, the ship set out for sea on 3 July 1965.
The ocean bottom system was installed with a minimum of difficulty but it was
found impossible to unlock the seismometer mass because of a motor failure.
Later examination of the motor revealed that the failure was caused by mechani-
cal binding in the gear box. The system was raised to the surface without
having installed the surface buoy and all equipment was recovered except the
sled and anchor. In order that the system might be at sea for the resumption
of the ECOOE shot program on 6 July, a duplicate sled had not been constructed.
It seemed reasonable to assume that if the system was not adequate, redesign
would be required and a duplicate sled would be of little value. The ship re-
turned to port and a new sled was constructed. The loss of time that resulted
from the return to Newport News to construct a new sled did not greatly affect
the recording schedule, as shots were not detonated during most of this time.

The new design was similar to the original design but included runners on the
bottom of the sled in the belief that the sled might more readily be installed
and retrieved. Additionally, a smaller anchor (39 kg) was used rather than the
230 kg anchor used previously. As before, weak links were provided between
the cable and the seismometer, the seismometer and the sled, the sled and the
cable, and between the anchor and the cable. Figure 7 illustrates some of the
weak links.

Adverse weather prevented installation of the system until 12 July. When
weather permitted, the system was lowered to bottom, the mass unlocked,
and preparations started to connect the cable to the buoy. With approximately
8-1/2 turns of cable remaining on the winch drum and 3290 fathoms of cable

in the water, the T clamp was attached to the cable and secured with a doubled
length of 16-mm polypropylene line. When the load of the cable was partially
transferred to the 16-mm line, it appeared unsafe to continue to transfer
the load. Then a 25.4-mm nylon line with a breaking strength of 11,800 kg
was attached. With approximately 1/2 the load transferred to the nylon line,
it was observed that the line was stretching excessively. Therefore, the
load of the cable at the T clamp was taken by a 13-mm steel rope attached
to the winch boom while a 16-mm steel line and swivel from the winch was
prepared to take the load. The 16-mm line appeared safe and the signal
line was disconnected at deck level by breaking apart the connectors in the
line. A manila "tag line" was used to hold the clamp and signal line to the
side of the ship while the work proceeded. A tendency for the signal line to
kink was noted when it was slacked. The connector was made up to the buoy
and the system operated with the buoy on the ship's deck. A calibration was
performed and all appeared satisfactory. Next the manila tag line was
released, prior to lowering with the 16-mm line. Upon doing so, the signal
line revolved approximately 15 times at a high velocity. In doing so, the
signal line was severely wrapped about the T clamp (figure 8), damaging
the line. Since it then appeared impossible to respool the cable, it was
decided to provide a strain relief between the T clamp and the buoy so the
signal line would not be stressed and further damaged. The system was
still electrically operational at this time. Four strands of 16-mm polypropy-
lene line were used and the T clamp was lowered into the water while the buoy
was lowered into the water using a cargo boom. When the weight of the cable
was supported from the buoy, the 16-mm wire rope was cut. A line supporting
the buoy from the cargo boom was cut and the system was then free of the
vessel. Simultaneously, the data line failed electrically, undoubtedly from
damage at the T clamp.

The installation of the system began at 1300 EDST and was finished the
following morning at 0300 EDST. Work was concluded at that time, with the
telemetry transmitter and the f¹   her on the buoy operational. The buoy was
kept in sight throughout the night.

At daylight, the ship was brought near the buoy and it was observed that the
ocean current was about 4 kt[3] rather than 0.8 kt expected and shown on charts.
This greater current probably increased the cable load from about 450 kg to
about 1820 kg. Figure 9 shows the buoy in the water. Note that both floats
are below water.

---

[3]   1 kt = 1 nautical mile per hour

Because the signal cable was severely kinked and believed likely to break
at any time, no attempt was made to retrieve the buoy, cable, or subsurface
equipment. If the cable had broken during recovery operations it was possible
the buoyant force of the buoy would propel it upwards with a resultant injury
to personnel nearby. We were advised by the Captain of the Prospector that
no liability would result from leaving the equipment in the ocean.

RESULTS

The system operated from the time the cable was connected to the buoy until
the buoy was put in the water. The programmed calibrator was cycled sev-
eral times during this interval and operated satisfactorily. Although some
noise appears on the recordings that may be the result of movement of the
buoy while on the ship's deck, approximately 30 minutes of data were recorded
with the seismometer on the ocean bottom. Figure 10 shows a portion of
recorded noise which is believed to be representative of the noise at the ocean
bottom.

CONCLUSIONS AND RECOMMENDATIONS

1. The techniques developed during this work were, for the most part,
satisfactory.

2. Improvement must be made in the method by which the weight of the
cable is transferred from the ship and winch to the buoy.

3. Future installations will have a greater likelihood of success if they are
made at a location where the ocean currents have lower velocity.

APPENDIX

The East Coast On-Shore Off-Shore Experiment was planned as a part of the Transcontinental Geophysical Survey. Figures 1 and 2 show scheduled shot points and positions where the ocean bottom installations were attempted.

Figure 2. Data transmission and calibration
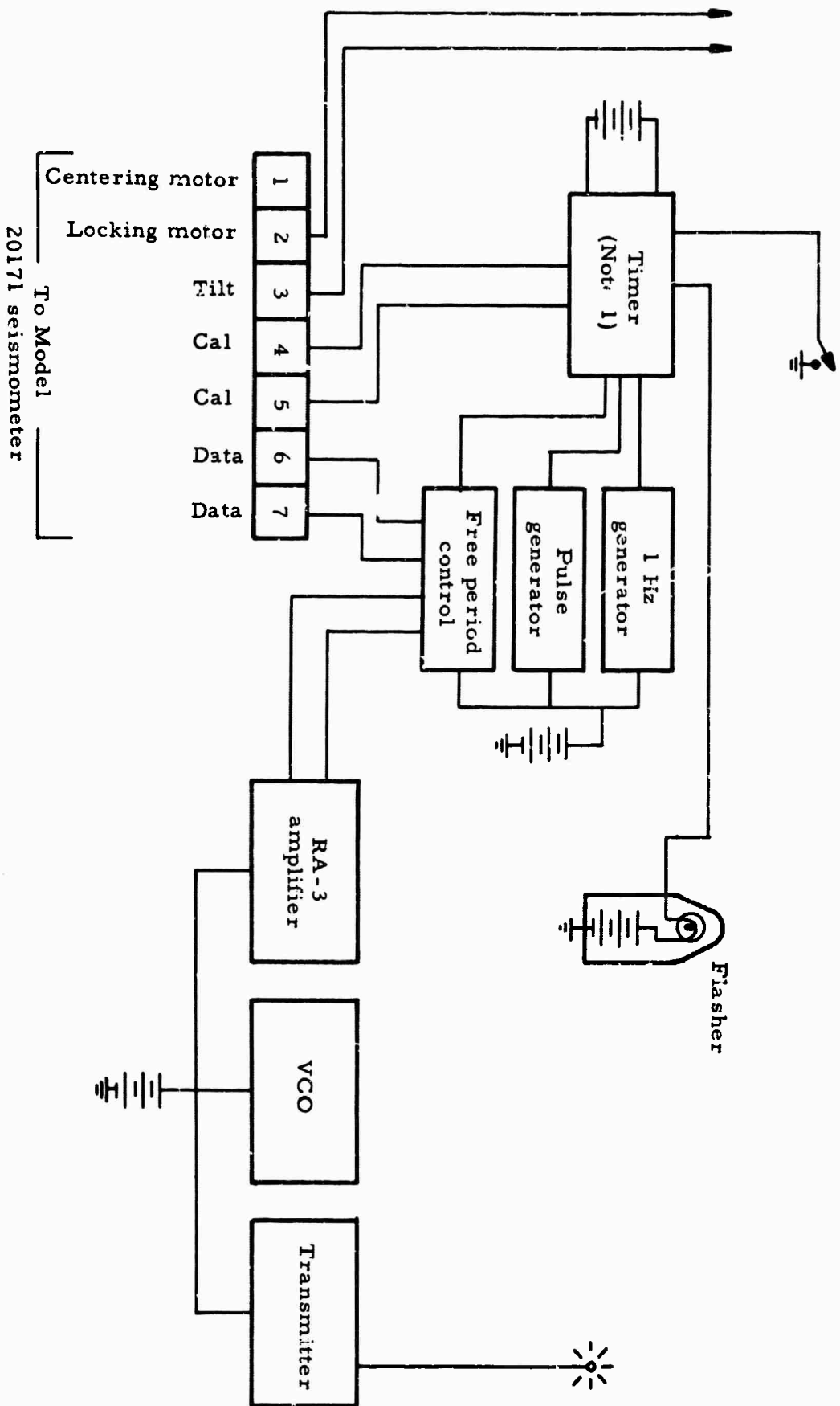
NOTE

1. Timer applies calibration signal, puts seismometer into free period and applies dc pulses once each day or when manually operated switch is actuated

24852

Research vessel

1/2-2 miles

Surface buoy with telemetry
and calibration equipment

Bridal

Cable

Mid buoys

150 Fathoms

Cable

Chain (for weight)

Danforth anchor
and weak link

500 ft-100 ft

<2200 fathoms

Weak link

Tetrahedron
and
seismometer

Figure 1. First system, off-shore measurements

Figure 4. Kinked cable, 9.5 mm diameter

8971
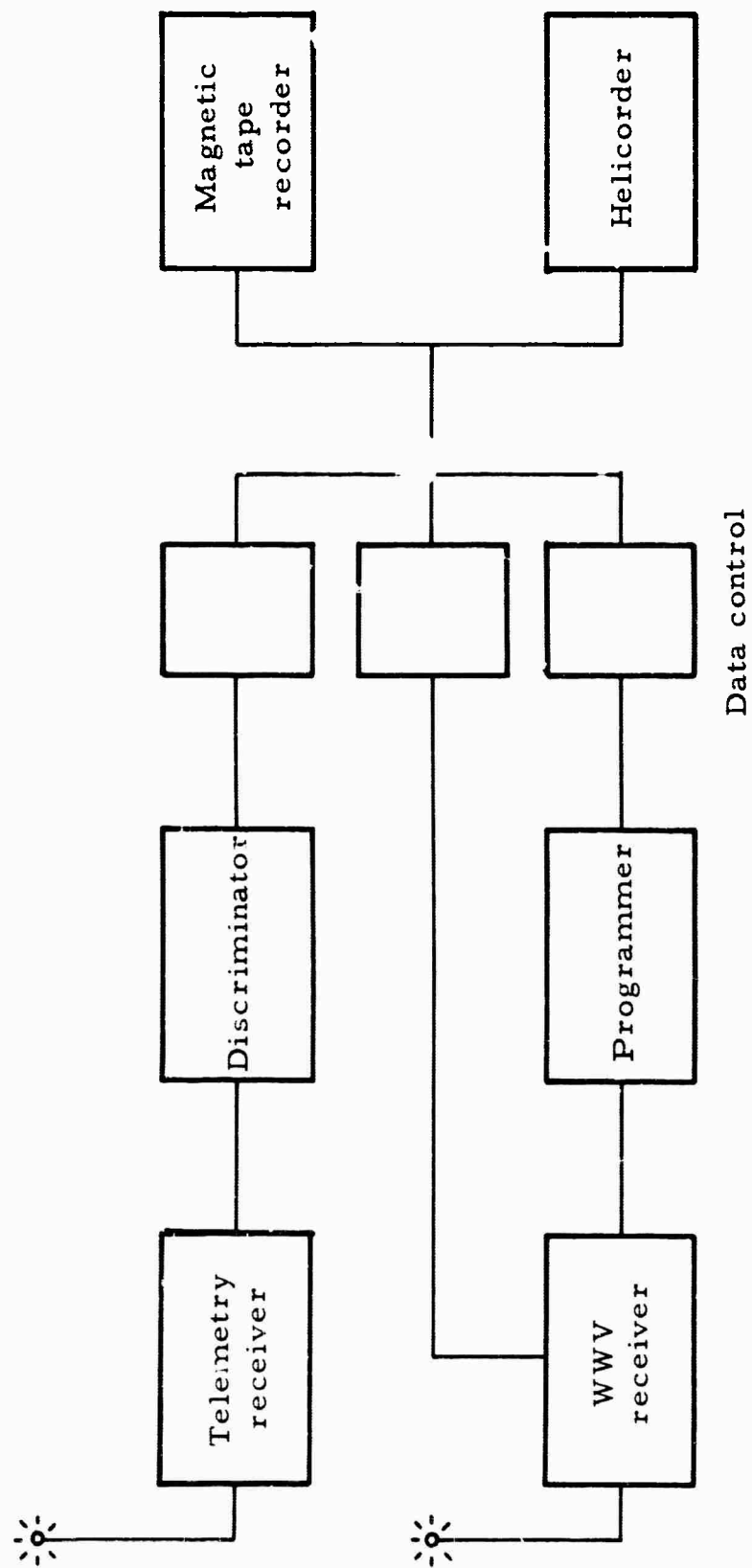
Figure 3. Receiving and recording

RESEARCH VESSEL

1/2-2 MILES

SURFACE BUOY WITH TELEMETRY AND CALIBRATION EQUIPMENT

DOUBLE BUOY

BRIDAL

T CLAMP

CABLE

CABLE CLAMP

FLOAT

POLYPROPYLENE LINE

CABLE

EXCESS CABLE

DANFORTH ANCHOR AND WEAK LINK

WEIGHTS

SLED, WEAK LINK, AND SEISMOMETER

< 2200 FATHOMS
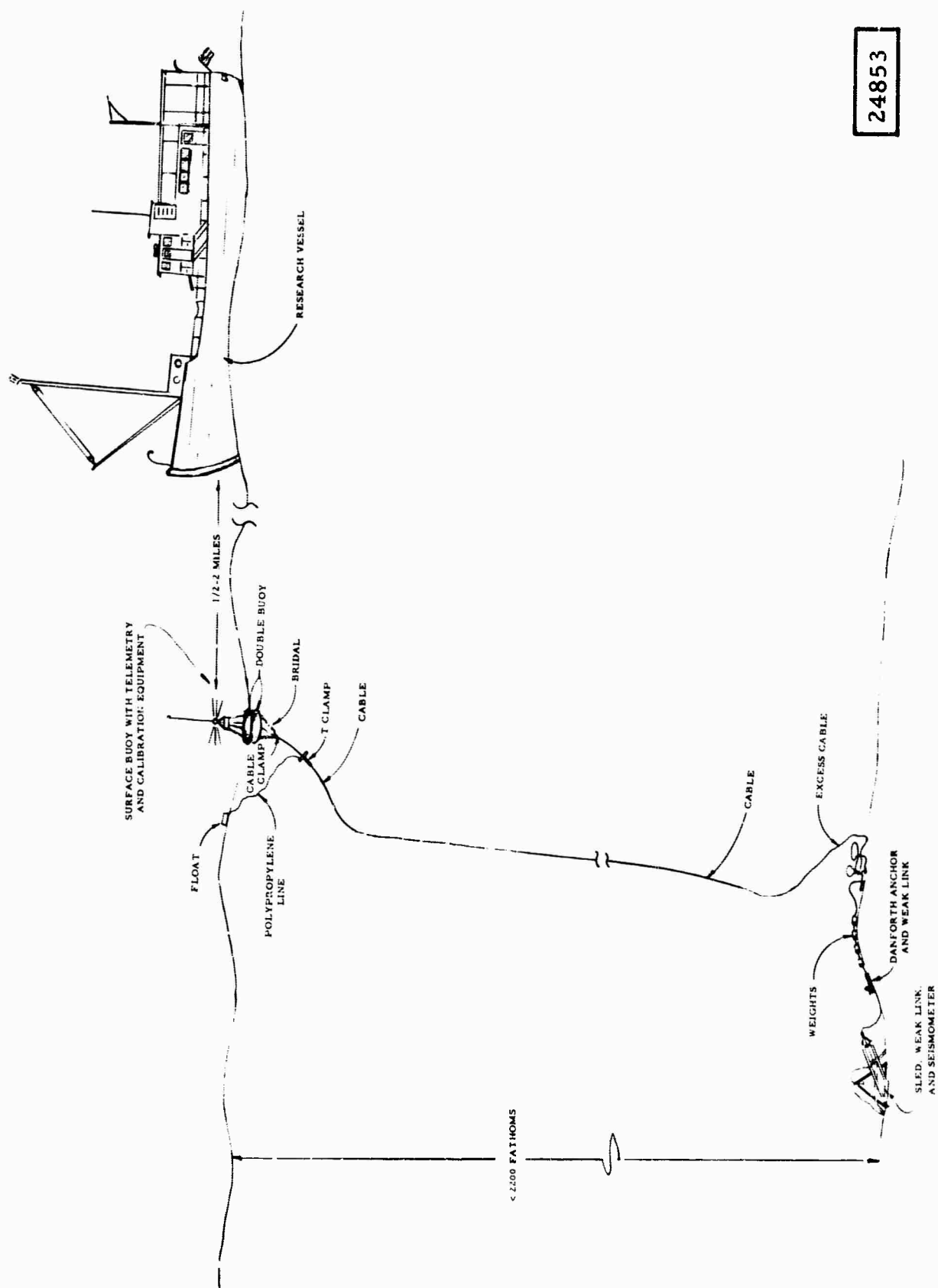
24853

Figure 6. Second system off-shore measurements

Figure 5. Sled being put over the side

8977
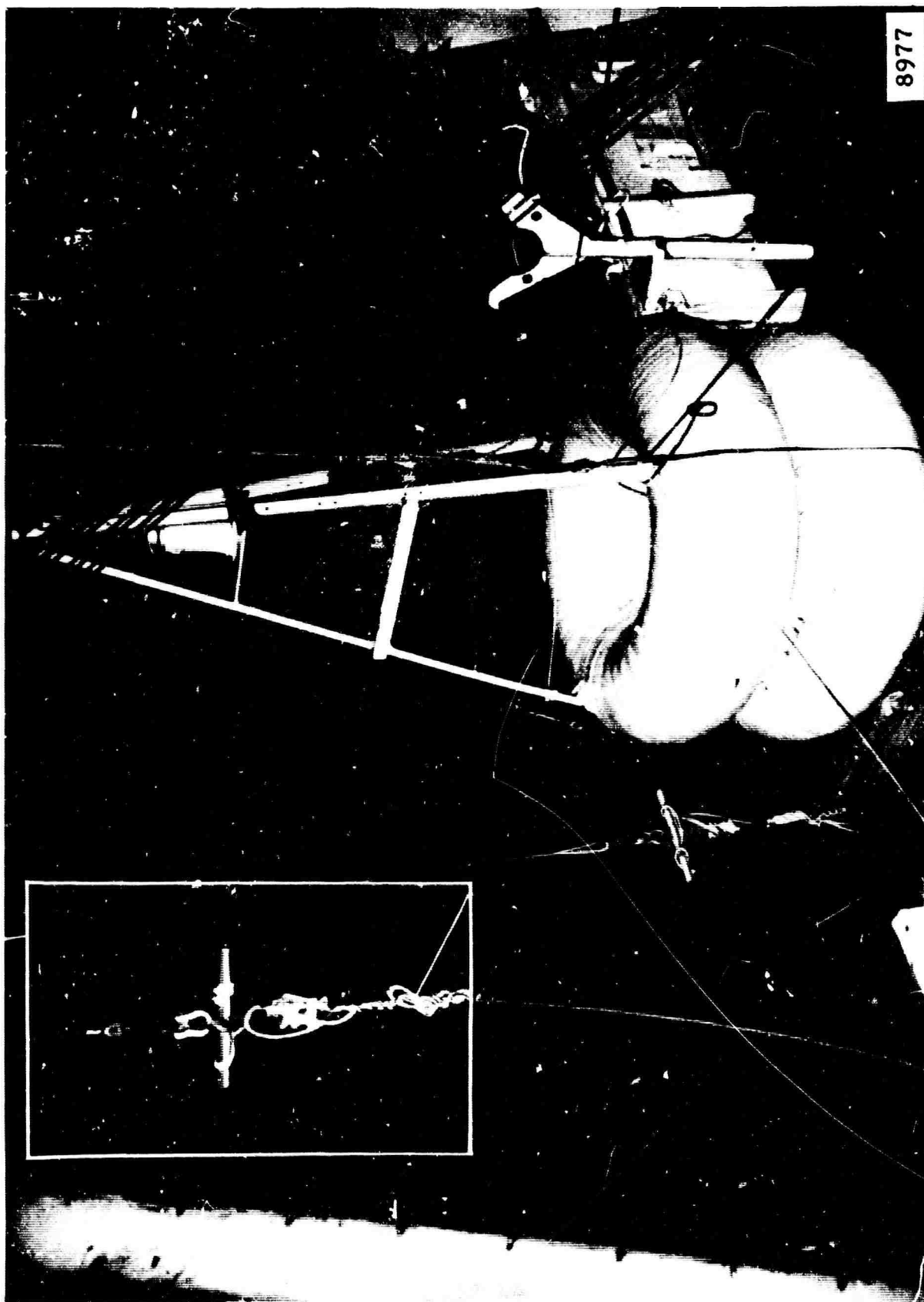
Figure 8. Cable twisted at T clamp

4.8 mm (3/16 in)
Wire Rope

INCHES

8973
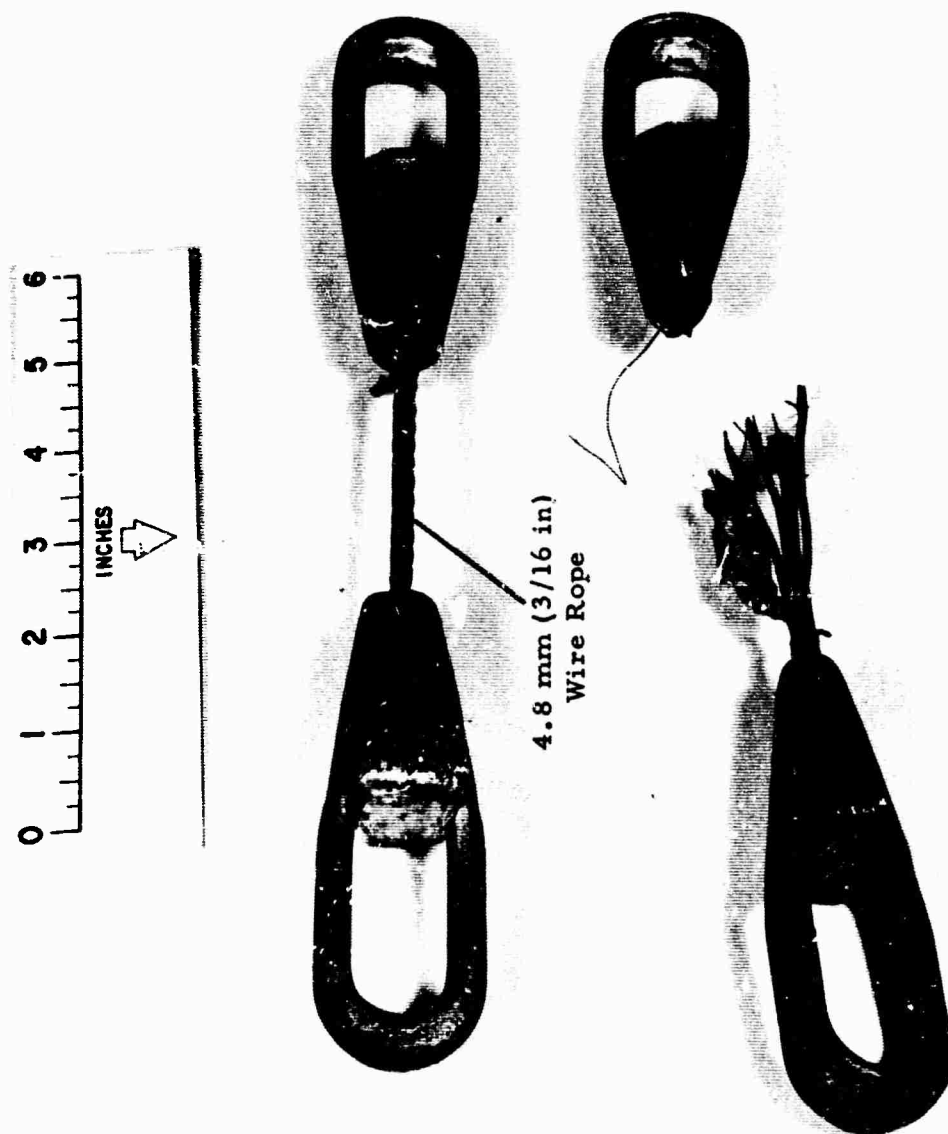
Figure 7. Weak Link (1590 kg Breaking Strength)

Figure 10. Noise recorded on 13 July 1965 on ocean bottom at 72°03'W, 36°11'N. Depth of water 3600m. Magnification 125K at 1 Hz

Figure 9. Buoy in the water
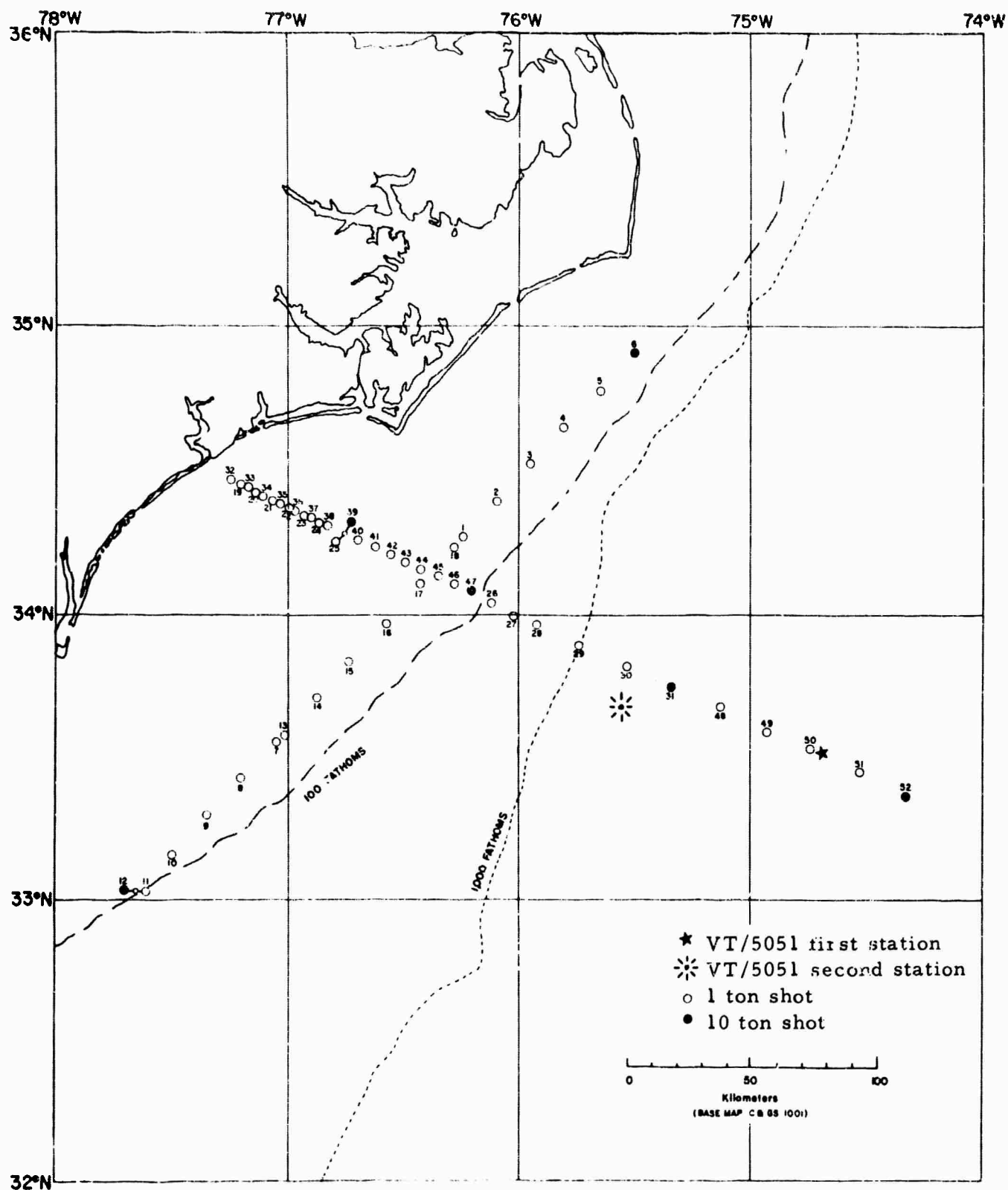
Figure 1.   ECOOE shot point locations, southern lines
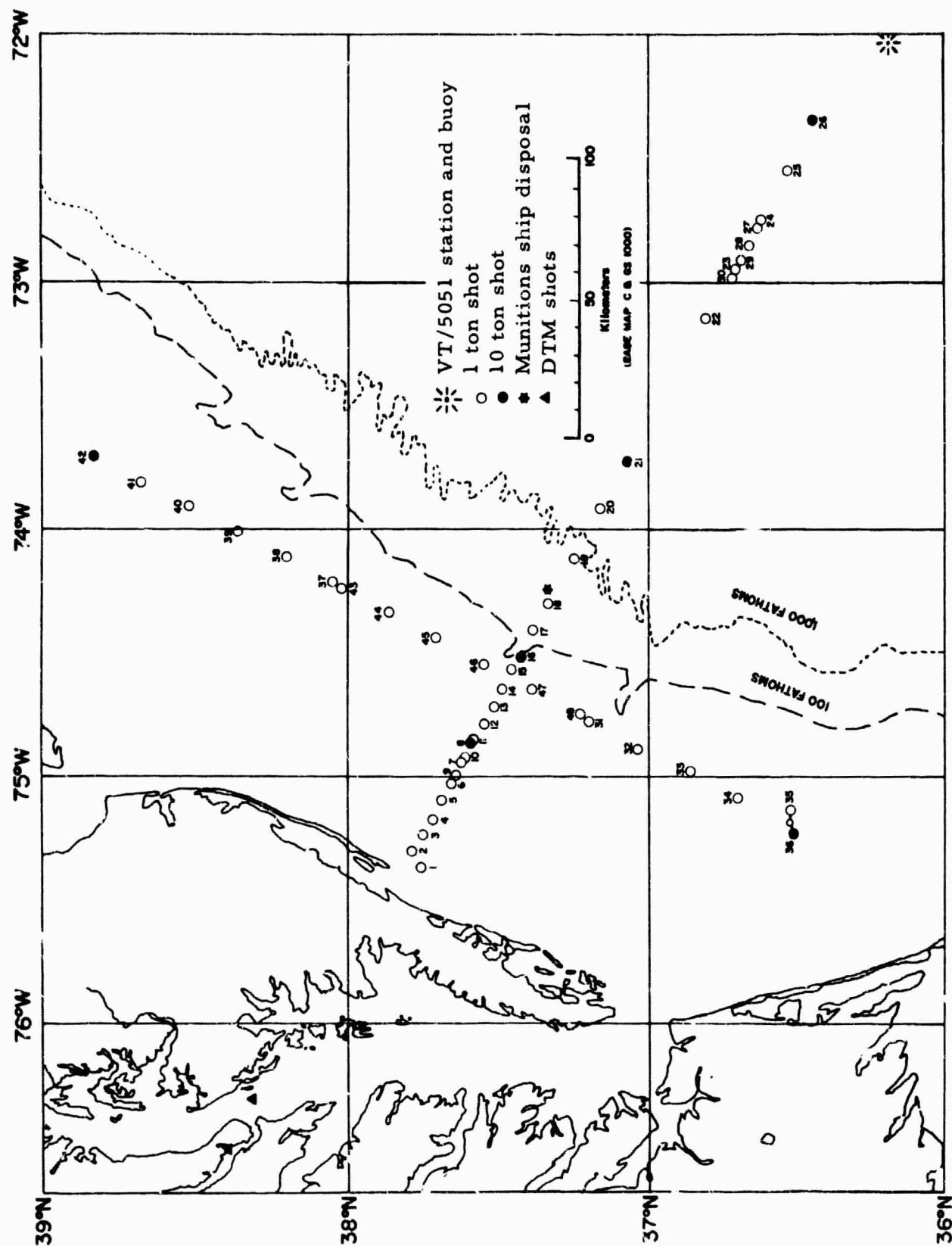
Figure 2. ECOOE shot point locations, northern lines

APPENDIX 4 to TECHNICAL REPORT NO. 65-112

PRELIMINARY EVALUATION OF
V_D x M VECTOR-CORRELATION PROCESS

TECHNICAL REPORT NO. 65-57

PRELIMINARY EVALUATION OF
$V_D \times M$ VECTOR-CORRELATION PROCESS

by

W. S. Mitcham

THE GEOTECHNICAL CORPORATION
3401 Shiloh Road
Garland, Texas

17 June 1965

BLANK PAGE

CONTENTS

CONTENTS, Continued

ILLUSTRATIONS

ILLUSTRATIONS, Continued

* * * * * * * * *

TABLES

ABSTRACT

A V_D x M vector-correlation process for a three-component set of orthogonal seismographs was examined. Preliminary theoretical considerations applicable to data interpretation under limiting assumptions were developed. One simple analog computer implementation of the process was developed and a limited amount of data was processed. Alternative approaches to the equipment and to the technique were considered. The result, based on a limited sample of data, indicate that the processor provided a trained analyst with information in a form suitable for discrimination between natural and manmade events on the basis of preliminary source location and depth from a single three-component set of seismographs.

TR 65-57

BLANK PAGE

PRELIMINARY EVALUATION OF
$V_D \times M$ VECTOR-CORRELATION PROCESS

1. INTRODUCTION

Th. report presents a preliminary evaluation of an experimental vector-cc .lation analog seismogram processor. Four earthquakes were analyzed having hypocentral depths 40 km, 115 km, 150 km, and 614 km. These earthquakes had been recorded by three-component seismographs. The processor picked si; 1als such as pP and sP that are essential for depth determinations. For the earthquakes at depths of 40 km and 614 km, pP could not have been detected without processing. The analog processor operated on a real-time continuous basis. Because of the encouraging results of this preliminary work using standard analog computers, various analog, digital, and hybrid approaches are presented for a real-time processor suitable for field or laboratory use.

The experimental processor used the cross-product term M to suppress vertical-seismograph data that does not exhibit linear correlation in the plane of the two instruments, since M is then small in amplitude, and to emphasize vertical-seismograph data (M approaches ± 1) that does exhibit linear correlation. According to Shimshoni and Smith (1964), the factor M is described ".... the cross-product M_j gives a measure of the rectilinearity and the total signal power. " It represents the time-averaged vector or cross-product between the measured vertical component of a signal and one of two horizontal components of the signal. Since the horizontal instruments discussed in this report are oriented north and east, respectively, the nomenclature M_{NZ} and M_{EZ} are used to specify which correlation orientation in space is being discussed. Shimshoni and Smith describe the measured vertical signal component by the symbol V. Since for analog implementation the processor time delay that must be introduced to recover first motion is less intimately introduced than is tru   a digital processor, this notation is modified to V_D, emphasizing its delayed character. If the oriented short-period instrument data are represented as SPZ (short-period vertical), SPN (short-period horizontal oriented toward north), and SPE (short-period horizontal oriented toward east), and the processor time delay is represented as T. D. , and the vector or cross-product is symbolized by "x" (sin 90° = 1), then:

$$V_D \times M_{NZ} \, \alpha \; SPZ(t - T.D.) \times \overline{[SPZ(t) \times SPN(t)]}$$

and

$$V_D \times M_{EZ} \, \alpha \; SPZ(t - T.D.) \times \overline{[SPZ(t) \times SPE(t)]}$$

These two orthogonal vector triple products represent the processor outputs. In practice they are utilized to detect individual seismic phases or signals in the presence of the somewhat randomly oriented coda or signal-generated noise. In particular, the recovery of the source-depth-determining signals, pP and sP, by the processor represents the most valuable processor output.

Section 2 of this report is devoted to developing some preliminary theory. The theory is developed for two purposes. First, the statistical concepts of measures are developed to bring out the similarities and the differences in the digital and analog approaches of implementing the processor. Some definitions are included which are developed into the statistical meaning of the processor. The second purpose of the theory is to develop the vector nature of the seismic data. Conceptually, this permits considering seismic signals as propagating vector fields rather than as linearly dependent time series. Although many of the assumptions required for a simple data interpretation must be considered tentative, this concept is developed far enough to provide some guides in determining the source location from the processor data.

Section 3, as well as the appendix, includes information on the simplest effective real-time continuo processor using analog implementation. In addition, this section shows experimental results from processing several events including four deep earthquakes. Depth-determining signals pP and sP, as well as others, were uncovered by the processor in all four examples. A trained analyst stated that two of the eight possible depth-determining signals were obvious without processing. One may or may not have been selected, and two would not have been selected without processing. The remaining three were not detected and may not have been present.

Section 4 develops possible approaches and considerations involved in the development of field or in-house processors. Various approaches are considered and some approximate equipment cost figures are included. Some of the techniques considered arise from the observed limitations of the experimental approach tested in section 3. A normalized analog processor is discussed along with some additional theory extending the theoretical concepts of section 2 to this more sophisticated processor. Hybrid and digital approaches of implementation are also considered.

Sections 5 and 6 present the conclusions and recommendations available at this time based on the theory and experimental results obtained so far.

This work was supported by the Advanced Research Projects Agency, Department of Defense, under the technical direction of the Air Force Technical Applications Center, Contract AF 33(657)-13668.

Work described in this report was performed for Project VT/5051, Contract AF 33(657)-13668.

2. THEORY

2.1 CROSS-CORRELATION OF DATA AVERAGES WITH "TIME SIGNIFICANCE" WEIGHTING

For purposes of the following discussion, cross-correlation is defined (see, for example, Y. W. Lee, 1960, p. 36, eq. 134, except for symbols) as $\varphi_{12}(t)$, where

$$\varphi_{12}(t) = \int_{-\infty}^{+\infty} f_1(\alpha)\, f_2(t+\alpha)\, d\alpha$$

In the special case where $f_2(t+\alpha)$ is an even function of α, cross-correlation as defined is identical to convolution. In the cases to be considered, however, $f_2(t+\alpha)$ is not generally an even function of α, and hence, the general designation, cross-correlation, rather than convolution must be used.

The mathematical expectation, stochastic average, ensemble average, or mean is defined for a piecewise continuous random variable $g'(x)$ with a piecewise continuous probability density function $p'_1(x)$ (see, for example, Davenport and Root, 1958, p. 46, eq. 4-3, except for symbols) as $E'[g'(x)]$, where

$$E'[g'(x)] = \int_{-\infty}^{+\infty} g'(x)\, p'_1(x)\, dx$$

The probability density function is assumed to be normalized, i.e.

$$\int_{-\infty}^{+\infty} p'_1(x)\,dx = 1$$

This definition makes it obvious that, in general, it is impossible to know the stochastic average of any infinite, random variable in finite time with only finite measures of the variable available.

Consequently, estimates of the average are the best that can be obtained in practice. A judgment situation exists in that a decision must be made as to how much of the data are required to ensure within reasonable confidence limits that the estimated average is sufficient for the problem considered. This requires an a priori decision that certain specific data are significant and that other data are not, or a decision must be made that certain data are more significant than other specific data by some weighting function.

One common method of estimating an average is to cross-correlate a data sample with a particular time significance weighting function $s(\alpha)$ that has unity weighting over an interval of length 2n and zero weighting elsewhere

$$s(\alpha) = 0, \quad -\infty \leq \alpha < t - n$$

$$s(\alpha) = 1, \quad t - n \leq \alpha \leq t + n$$

$$s(\alpha) = 0, \quad t + n < \alpha \leq +\infty$$

For this time significance weighting function, the estimate of the average, $E[g(t)]$, may be represented as follows

$$E[g(t)] = \frac{1}{2n} \int_{-\infty}^{+\infty} g(t + \alpha)\, s(\alpha)\, d\alpha$$

$$= 0 + \frac{1}{2n} \int_{t-n}^{t+n} 1 \times g(t + \alpha)\, d\alpha + 0$$

where

$$2n = \int_{t-n}^{t+n} 1\, d\alpha, \quad \text{the normalizing factor.}$$

This method of estimating an average has long been used. It is particularly easy to implement on digital computers either as a one-point estimate over an interval, or in more modern approaches, such as employed by Shimshoni and Smith (1964) as continuous estimates as seen through a moving rectangular time window (as t in the previous expression is allowed to vary instead of being considered fixed).

The meaning of an average for fixed t and fixed sample length 2n obtained by an analog processor is identical to that of the corresponding digital processor, and these techniques have been used interchangeably for many years. When the approach is modified by considering these estimates of the average as time varying functions (variable t), however, the approach most efficiently implemented by a digital processor is different from that most efficiently implemented by an analog processor.

The most efficient analog computer circuit for generating continuous time estimates of the average of a variable is the "leaky integrator," often erroneously referred to as a convolution averaging circuit. As has been shown by Joseph Otterman (1960), this technique involves the cross-correlation of the data with a time significance weighting function of exponential shape extending into the past of the data. This is the reason for the EMP (exponentially mapped past) nomenclature introduced by Otterman.

In terms of our present symbols, Otterman's definition of this type of estimate of an average involves the time significance weighting function $s(\alpha)$ where now

$$s(\alpha) = e^{\frac{\alpha}{\tau}} \quad -\infty \leq \alpha \leq t$$

$$= 0 \quad t < \alpha \leq +\infty$$

The symbol τ represents the time constant of the averaging circuit. As in the other approaches, the time significance weighting function is normalized by

$$\int_{-\infty}^{+\infty} s(\alpha) d\alpha = \int_{-\infty}^{0} e^{\frac{\alpha}{\tau}} d\alpha + 0 = \tau$$

Thus, for the typical analog processor, the continuous estimate, $E[g(t)]$, of the average of the variable $g(t)$ may be represented by

$$E[g(t)] = \frac{1}{T} \int_{-\infty}^{\infty} g(t+\alpha) \, s(\alpha) \, d\alpha$$

$$= \frac{1}{T} \int_{-\infty}^{0} g(t+\alpha) \, e^{\frac{\alpha}{T}} \, d\alpha + 0$$

in terms of this different time significance weighting function. Thus, the continuous analog processor may differ from the continuous digital processor in that the meaning of "average" represents the cross-correlation of a sample of the data with a different time significance weighting function.

This difference in the meaning of average represents one of the two differences between the analog processor discussed in this report and the digital processor introduced by Shimshoni and Smith (1964). The other difference, the method by which the processor obtains knowledge of future data, will be discussed in section 2.3, after section 2.2 introduces certain statistical interpretations (see Otterman, 1960) of EMP analog approach.

2.2 STATISTICAL PARAMETERS FOR ESTIMATING LINEAR CORRELATION

In section 2.1 it was shown that all averages were estimates, and that differing interpretations could be placed on the results depending on how the term average was defined in the processor. Since the meanings of the statistical parameters are common knowledge for the digital or unity-weighted, limited-sample approach, these will not be discussed. However, the meanings of these parameters for the case of the EMP time significance weighting functions are less common, so the definitions are presented in sections 2.2.1 through 2.2.7, below.

The definitions of the single population statistical variables which follow are paraphrased from Joseph Otterman (1960). The extensions of these concepts to multipopulation statistics are the authors', and although analogous to standard statistical practice, they may have slightly different interpretations from that of the usual approach.

The geometrical interpretation in section 2.2.8, below, is derived quite simply from the orthogonal vector nature of the specific class of measurements considered, and thus conceptually if not numerically, is relatively independent of the meaning attached to the method of estimation used.

2.2.1 Mean

$$\overline{g}(t) = \frac{1}{\tau} \int_{-\infty}^{0} g(t+\alpha)\, e^{\frac{\alpha}{\tau}}\, d\alpha$$

where $\int_{-\infty}^{0} e^{\frac{\alpha}{\tau}}\, d\alpha = \tau$ normalizes the definition.

2.2.2 Variance, σ^2

$$\sigma^2 [g(t)](t) = \frac{1}{\tau} \int_{-\infty}^{0} [g(t+\alpha) - \overline{g}(t+\alpha)]^2\, e^{\frac{\alpha}{\tau}}\, d\alpha$$

where $\int_{-\infty}^{0} e^{\frac{\alpha}{\tau}}\, d\alpha = \tau$ normalizes the definition.

2.2.3 Standard Deviation, σ

$$\sigma[g(t)](t) = + \sqrt{\sigma^2 [g(t)](t)}$$

2.2.4 Covariance, $\sigma^2[f, g](t)$ (Merritt, p. 352, art. 17-9)

$$\sigma^2 [f,g](t) = \frac{1}{\tau} \int_{-\infty}^{0} [f(t+\alpha) - \overline{f}(t+\alpha)][g(t+\alpha) - \overline{g}(t+\alpha)] e^{\frac{\alpha}{\tau}}\, d\alpha$$

where $\int_{-\infty}^{0} e^{\frac{\alpha}{\tau}}\, d\alpha = \tau$ normalizes the definition.

2 2.5 Pearson Moment Correlation, $r[f, g](t)$ (Merritt, p. 362, art. 17-21)

$$r[f, g](t) = \frac{\sigma^2 [f, g](t)}{\{\sigma[f](t)\}\{\sigma[g](t)\}}$$

2.2.6 Two-Dimensional Least Squares Regression (Merritt, art. 17-21)

$$[f(t) - \overline{f}(t)](t) = r[f, g](t) \frac{\sigma[f](t)}{\sigma[g](t)} [g(t) - \overline{g}(t)]$$

2.2.7 Standard Error of the Estimate of f from g, $S[f/g](t)$ (Merritt, art. 17-21)

$$S[f/g](t) = \sigma[f](t) \ \sqrt{1 - \overline{\overline{r^2[f, g]}(t)}}$$

2.2.8 Vector Interpretation

When t.e two data time series represent two orthogonal vector components, a geometrical interpretation of a vector in a plane can be attached to the expression of section 2.2.6 as follows
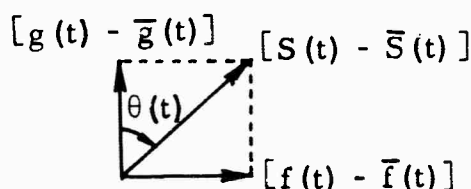
$$\frac{[f(t) - \overline{f}(t)](t)}{[g(t) - \overline{g}(t)](t)} = r[f, g](t) \frac{\sigma[f](t)}{\sigma[g](t)} = [\tan \theta](t)$$

Also the vector expressions

$$[S(t) - \overline{S}(t)](t) = \frac{[g(t) - \overline{g}(t)](t)}{[\cos \theta](t)}$$

$$= \frac{[f(t) - \overline{f}(t)](t)}{[\sin \theta](t)}$$

may be considered, because of the linear independence between the two components resulting from their spatial orthogonality.

2.3 INTRODUCTION OF TIME DELAYS

The digital moving rectangular time significance weighting function has no inherent knowledge of future data. However, by simply defining the average to be applicable at a delayed instant (t - n), a processor time delay is arbitrarily introduced into this approach. By selecting the median instant in the interval of definition, the time significance weighting function is made an

even function relative to the time-delayed processor output, and in addition, the p ocessor is capable of remembering data that are in the future relative to the delayed processor time.

The requirement of remembering future data is also a necessity for the analog EMP time significance weighting function. However, although time delays can be introduced for the EMP time significance weighting function, the weighting function is not thereby made even. A method using a modified weighting function $e^{-|\alpha|/\tau}$ that can be made even will discussed in a later report.

The necessity for time delays stems from the fact that the actual desired information content of the data resides in the transition probability between the decisions: (a) there is no signal and (b) there is a signal. It is possible that exponential weighting is desirable because of its lack of memory for the transition probabilities of the data (Poisson process).

Considering the cross-correlation of the data with the EMP time significance weighting function as defined in sections 2.1 and 2.2 as

$$E[g](t) = \frac{\int_{-\infty}^{0} g(t+\alpha) e^{\frac{\alpha}{\tau}} d\alpha}{\int_{-\infty}^{0} e^{\frac{\alpha}{\tau}} d\alpha} , \text{ and}$$

if we now consider an estimate delayed in time by an interval T.D. (also moving in time t), the normalizing factor can be broken into three parts

$$E[g](t) = \frac{\int_{-\infty}^{-T.D.} g(t+\alpha) e^{\frac{\alpha}{\tau}} d\alpha}{\int_{-\infty}^{-T.D.} e^{\frac{\alpha}{\tau}} d\alpha} + \frac{\int_{-T.D.}^{0} g(t+\alpha) e^{\frac{\alpha}{\tau}} d\alpha}{\int_{T.D.}^{0} e^{\frac{\alpha}{\tau}} d\alpha} + 0$$

Thus, evaluated at the instant (t - T.D), the average total significance for all past data is:

$$\int_{-\infty}^{-T.D.} e^{\frac{\alpha}{\tau}} d\alpha$$

and the average total significance for the future from (t - T.D.) to t is

$$\int_{-T.D.}^{0} e^{\frac{\alpha}{\tau}} d\alpha$$

and the average total significance for the future from t to $+\infty$ is

$$0$$

and the average total significance for all time is τ as has been shown. Then

$$\int_{-\infty}^{-T.D.} e^{\frac{\alpha}{\tau}} d\alpha + \int_{-T.D.}^{0} e^{\frac{\alpha}{\tau}} d\alpha + 0 = \tau$$

$$\tau \left[e^{\frac{\alpha}{\tau}} \right]_{\alpha = -\infty}^{-T.D.} + \tau \left[e^{\frac{\alpha}{\tau}} \right]_{\alpha = -T.D.}^{0} + 0 = \tau$$

$$\tau \left[e^{\frac{-T.D.}{\tau}} - 0 \right] + \tau \left[1 - e^{\frac{-T.D.}{\tau}} \right] = \tau$$

Thus in an average sense the ratio of $\left[1 - e^{\frac{-T.D.}{\tau}} \right]$ to $\left[e^{\frac{-T.D.}{\tau}} \right]$, which may be referred to as a significance ratio K, represents the fractional significance of the future T.D. (in seconds) to all past time evaluated at the instant t - T.D.

$$\frac{\left[1 - e^{\frac{-T.D.}{\tau}} \right]}{\left[e^{\frac{-T.D.}{\tau}} \right]} = K = e^{\frac{+T.D.}{\tau}} - 1$$

or

$$e^{\frac{+T.D.}{\tau}} = K + 1$$

Taking Naperian Logarithms

$$\ln \left[e^{\frac{T.D.}{\tau}} \right] = \ln \left[K + 1 \right]$$

or

$$\frac{T.D.}{\tau} = \ln \left[K + 1 \right]$$

One case of special interest occurs when K = 1, implying equal significance weighting

$$\frac{T.D.}{\tau} = \ln 2 = 0.69315$$

These average significance expressions can also be expressed as the two fractions of total (unity) significance in terms of the dimensionless ratio $(T.D./\tau)$ for past and future total significance. Figure 1 plots these two fractions against a logarithmic scale of $(T.D./\tau)$. The equal significance weighting is shown, as are the two significance weightings used in the experimental results discussed in section 3 of this report.

2.4 GEOMETRICAL INTERPRETATION OF RESULTS

2.4.1 Instruments

Consider three orthogonal seismographs: SPZ. oriented up; SPN, oriented toward north; and SPE, oriented toward east. Assume that a positive electrical signal represents earth motion upward, northward, and eastward, respectively, while a negative signal represents motion downward, southward, and westward, respectively.

2.4.2 Seismic Signals

For the remaining discussion, a seismic signal will be considered to be a vector field propagating in vector space. "Since any vector field can be separated into a part having zero curl (longitudinal or lamellar field) and another part having zero divergence (transverse or solenoidal field), ... " (Morse, 1958, p. 3-99) for an (assumed) isotropic region in the immediate vicinity of the instruments, "P" motion will be defined to be the component of motion in the direction of propagation, and "S" motion will be defined as the transverse component of motion in a plane perpendicular to the direction of propagation. It should be recognized that the homogeneous, isotropic assumptions are not valid for the earth even though they are utilized in all array processing approaches presently considered. Thus, as here defined, P motion is not necessarily in the direction of zero curl, although it is in the direction of propagation, and S motion does not necessarily have zero divergence although it is in a plane normal to the direction of propagation.
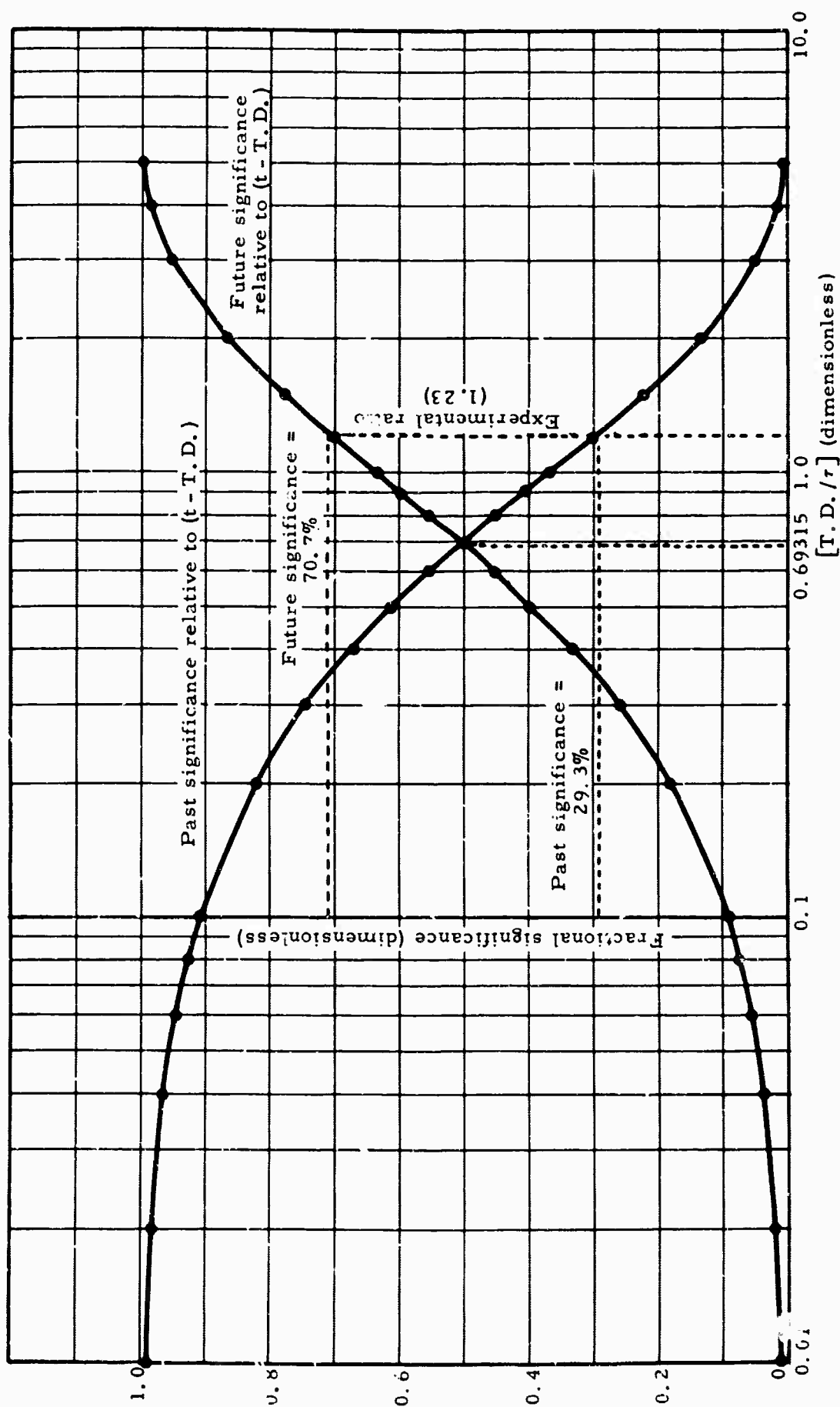
Figure 1. Relative time significance weighting versus (T.D. / τ)

2.4.2.1 Effect of P Motion on Instruments

First consider a signal P (φ, θ, t) at the point in space of the receiving instrument, where the signal is propagating toward θ and φ, and has a time varying pattern P(t) of compressions (earth motion toward θ and φ) and rarefactions (earth motion away from θ and φ). Then we have in the left-hand cartesian coordinate system of the instruments:
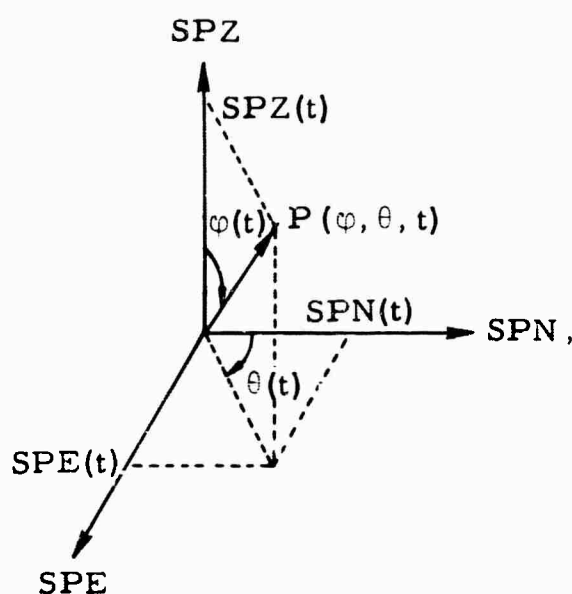
where

$$SPZ (t) = P(t) \cos \varphi (t),$$
$$SPN (t) = P(t) \sin \varphi (t) \cos \theta (t), \text{ and}$$
$$SPE (t) = P(t) \sin \varphi (t) \sin \theta (t).$$

2.4.2.2 Effect of S Motion on Instruments

Next consider an S-type signal propagating toward θ and φ at the time it strikes the receiving instruments with a time varying pattern of alternating positive and negative motions along a vector in the plane normal to the direction of propagation. In order to relate earth motions in this plane to our fixed instrumental left-hand cartesian coordinate system, one additional parameter must be specified. Since the receiving instrument coordinates are left hand, this parameter, which will be defined as the polarization angle ψ, will be defined in a left-hand manner for consistency. The reference line will be chosen to be the intersection of the plane of motion and a vertical plane including the propagation vector. The zero reference will originate at the point of the instruments and extend up and toward the source (back azimuth). For the undefined case of

exactly vertical incidence, the reference azimuth will be defined to be north. Positve S(t) represents compression toward ψ, negative S(t) represents rarefaction, or motion away from ψ.

The effect of this type of signal on the instruments is .
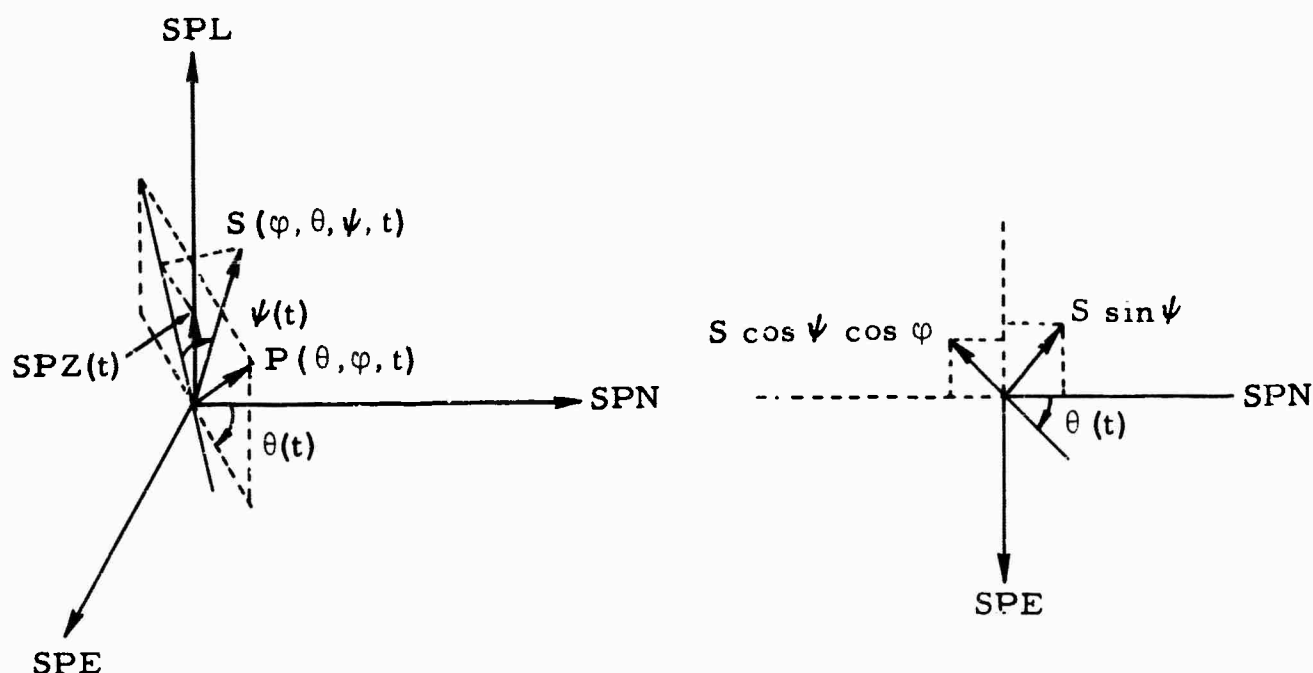
where $SPZ(t) = S(t) \cos \psi (t) \sin \varphi (t),$
$SPN(t) = S(t) [\sin \psi (t) \sin \theta (t) - \cos \psi (t) \cos \varphi (t) \cos \theta (t)]$
$SPE(t) = S(t) [-\sin \psi (t) \cos \theta (t) - \cos \psi (t) \cos \varphi (t) \sin \theta (t)]$

2.4.3 Effect of P and S Signals on M and $V_D \times M$

2.4.3.1 P Signals

2.4.3.1.1 Effect on M. As indicated by Shimshoni and Smith (1964), "M" represents a time average vector or cross product in a specific vertical plane. Although the meaning of M in the analog processor is strictly analogous to the meaning used in their digital approach, the meaning of "time averaged" has been changed by the mechanics of the analog approach (see section 2.1) from (Shimshoni and Smith, 1964, p. 665)

$$"M_j = \sum_{i=-n}^{n} H_{i+j} V_{i+j} "$$

to

$$M_{NZ}(t) = 2K'\left(\frac{1}{\tau}\right)\int_{-\infty}^{0} 30\left[\frac{SPN(t+\alpha) \times SPZ(t+\alpha)}{10}\right] e^{\frac{\alpha}{\tau}} d\alpha$$

$$= K\left(\frac{1}{\tau}\right)\int_{-\infty}^{0} [SPN(t+\alpha) \times SPZ(t+\alpha)] e^{\frac{\alpha}{\tau}} d\alpha, \quad -1 \leq M_{NZ} \leq +1$$

Also

$$M_{EZ}(t) = K\left(\frac{1}{\tau}\right)\int_{-\infty}^{0} [SPE(t+\alpha) \times SPZ(t+\alpha)] e^{\frac{\alpha}{\tau}} d\alpha, \quad -1 \leq M_{FZ} \leq +1$$

where K is an instrument gain factor which is made identical for both calcula-
tions.

Substituting in the signal parameters for the instrumental vector components
of the signal from section 2.4.2.1

$$M_{NZ}(t) = K\left(\frac{1}{\tau}\right)\int_{-\infty}^{0} P^2(t+\alpha)\left[\cos\varphi(t+\alpha)\sin\varphi(t+\alpha)\cos\theta(t+\alpha)\right] e^{\frac{\alpha}{\tau}} d\alpha$$

If we assume, in addition, that for the duration of this specific signal $\theta(t+\alpha)$
and $\varphi(t+\alpha)$ are approximately time stationary, $[\theta(t), \varphi(t)]$, this expression
reduces to

$$M_{NZ}(t) \approx K\left[\cos\varphi(t)\sin\varphi(t)\cos\theta(t)\right]\left(\frac{1}{\tau}\right)\int_{-\infty}^{0} P^2(t+\alpha) e^{\frac{\alpha}{\tau}} d\alpha, \quad -1 \leq M_{NZ} \leq +1$$

and, under the same assumptions

$$M_{EZ}(t) \approx K\left[\cos\varphi(t)\sin\varphi(t)\sin\theta(t)\right]\left(\frac{1}{\tau}\right)\int_{-\infty}^{0} P^2(t+\alpha) e^{\frac{\alpha}{\tau}} d\alpha, \quad -1 \leq M_{EZ} \leq +1$$

If for purposes of interpretation we further assume that no phases of interest
will have a downward component of propagation (i.e., ignore surface reflec-
tions temporarily), the term $[\cos\varphi(t)\sin\varphi(t)]$ is always positive $(0 \leq \varphi \leq 90^{\circ})$.

Similarly, $K \left(\frac{1}{T}\right) \int_{-\infty}^{0} P^2 (t + \alpha) \, e^{\frac{\alpha}{T}} \, d\alpha$, representing the EMP variance of the
signal's pattern of compressions and rarefactions is likewise always positive.
Thus, for incident P waves, the only parameter of the signal that affects the
polarity of M_{NZ} and M_{EZ} is the azimuth angle $\theta(t)$ toward which the P motion
is propagating. Figure 2 shows the $\sin \theta$ and $\cos \theta$ amplitude weighting func-
tions of signal propagation azimuth for P signals. The S signal weighting
functions under the assumptions of section 2.4.3.2 are also shown for com-
parison.

Since the instrumental directions N and E are noncollinear (in fact, orthogo-
nal) in a horizontal plane, together they provide adequate data for estimating
the horizontal component of the direction of propagation by quadrants,
depending only on the simultaneous polarities of M_{NZ} and M_{EZ}, as shown in
table 1.

Table 1. Azimuth determination from polarities of M_{NZ} and M_{EZ} for P signals

Azimuth of propagation	M_{NZ}	M_{EZ}	Back azimuth toward source
$0° - 90°$	+	+	$180° - 270°$
$90° - 180°$	-	+	$270° - 360°$
$180° - 270°$	-	-	$0° - 90°$
$270° - 360°$	+	-	$90° - 180°$

For purposes of quick location, the back azimuth is assumed to be directed
toward the source. For this to be strictly true would require that the travel
path of the particular signal lies wholly in the vertical plane including the
source and receiver, or alternately that any components of propagation
normal to this plane exactly cancel during the propagation of the signal.
Although the inhomogeneity and anisotropy of the earth prevent strict use of
this assumption, limited experience indicates that judicious interpretation of
the estimates for several signals from a single source provides a usable
estimate of the source azimuth.

In addition to the amplitude weighting introduced by the azimuth of signal
propagation, amplitude weighting due to the incidence angle of the signal
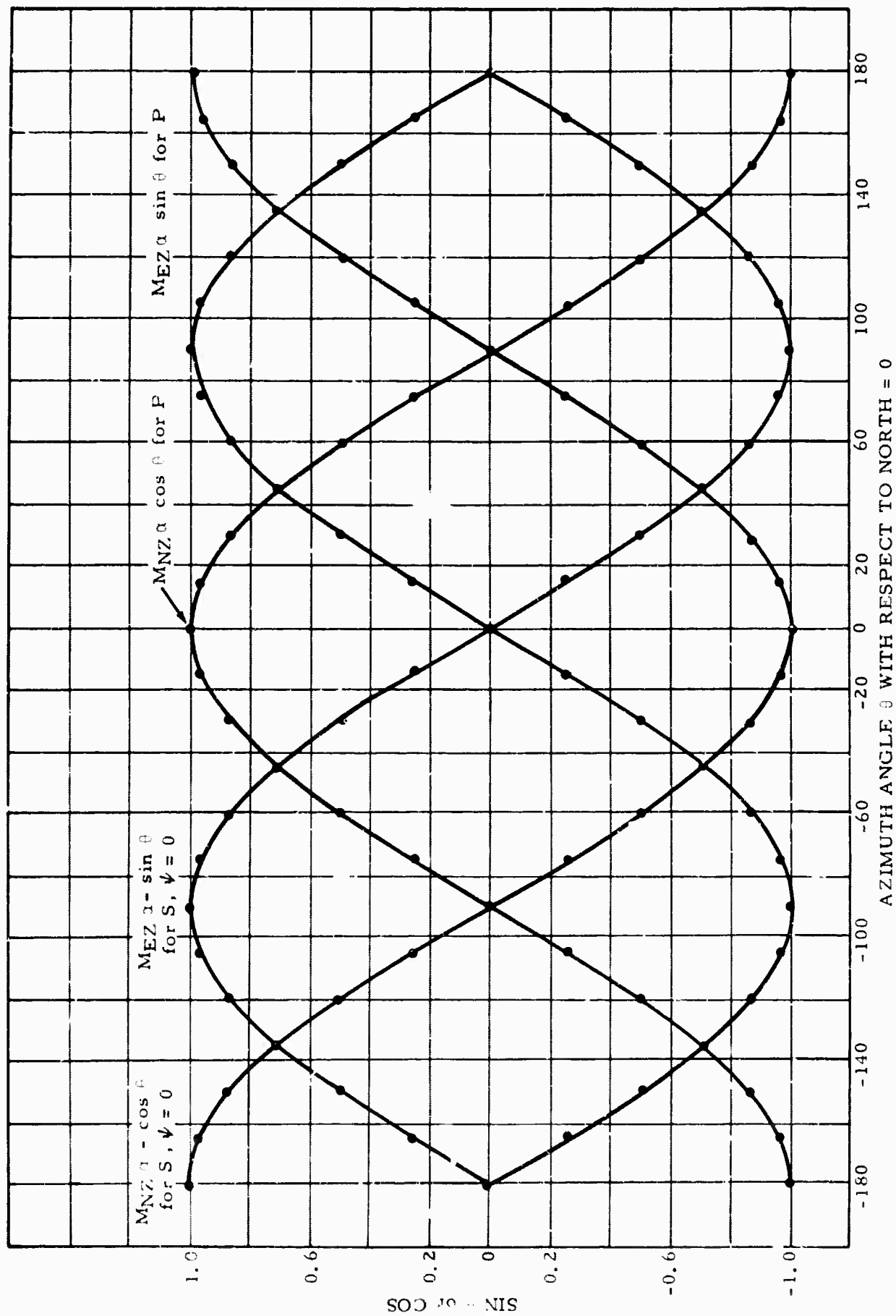
Figure 2. Relative amplitude weighting factor for M_{NZ} and M_{EZ} for P- and S-type signals propagating toward an azimuth θ

is also introduced. This amplitude weighting factor $[\sin \varphi(t) \cos \varphi(t)]$ is the same for both M_{NZ} and M_{EZ}. For surface instruments, $0 \leq \varphi \leq 90^{\circ}$, so the weighting factor is always positive in polarity for P signals. For deep-hole instruments, of course, a polarity inversion is introduced into both M_{NZ} and M_{EZ} for downward-propagating P-type signals. Such downward P-P reflections and S-P conversions at the local surface boundary, comprising part of the "signal generated noise," are thus treated differently from an incident P signal.

Figure 3 shows the inclination-angle amplitude weighting of M_{NZ} and M_{EZ} $(\sin \varphi \cos \varphi)$ for P motion. The S signals, under the assumptions of section 2.4.3.2, are identical in terms of inclination-angle amplitude weighting.

The last of the M factors to be considered, again identical for both M_{NZ} and M_{EZ}, is the term

$$K\left(\frac{1}{T}\right)\int_{-\infty}^{0} P^2\,(t+\alpha)\,e^{\frac{\alpha}{T}}\,d\alpha$$

If the expression $P^2\,(t+\alpha)$ were actually $[P(t+\alpha) - \bar{P}(t+\alpha)]^2$, this term would represent the EMP variance of the signal amplitude. If the size of the signal is considered to be represented by its standard deviation as defined in section 2.2.3, this factor will provide an amplitude weighting factor obeying the square law. In the experimental approach discussed in section 3 of this report, the term $P^2\,(t+\alpha)$ is used. However, for a field processor it is recommended that more equipment be utilized to permit this term to be $[P(t+\alpha) - \bar{P}(t+\alpha)]^2$ in accordance with the expressions derived under sections 2.2.4 and 2.2.8, so that this interpretation is more valid.

Figure 4 shows the variance versus the standard deviation as an approximation to the effects on the M terms of the rms "size" of the phase.

2.4.3.1.2 Effect on V_D x M. V_D, representing the delayed vertical component of the signal, is defined to be SPZ (t - T.D.), where T.D. is the time delay introduced in the processor. From section 2.4.2.1

$$V_D = SPZ\,(t - T.D.) = P\,(t - T.D.)\,\cos \varphi\,(t - T.D.)\,.$$
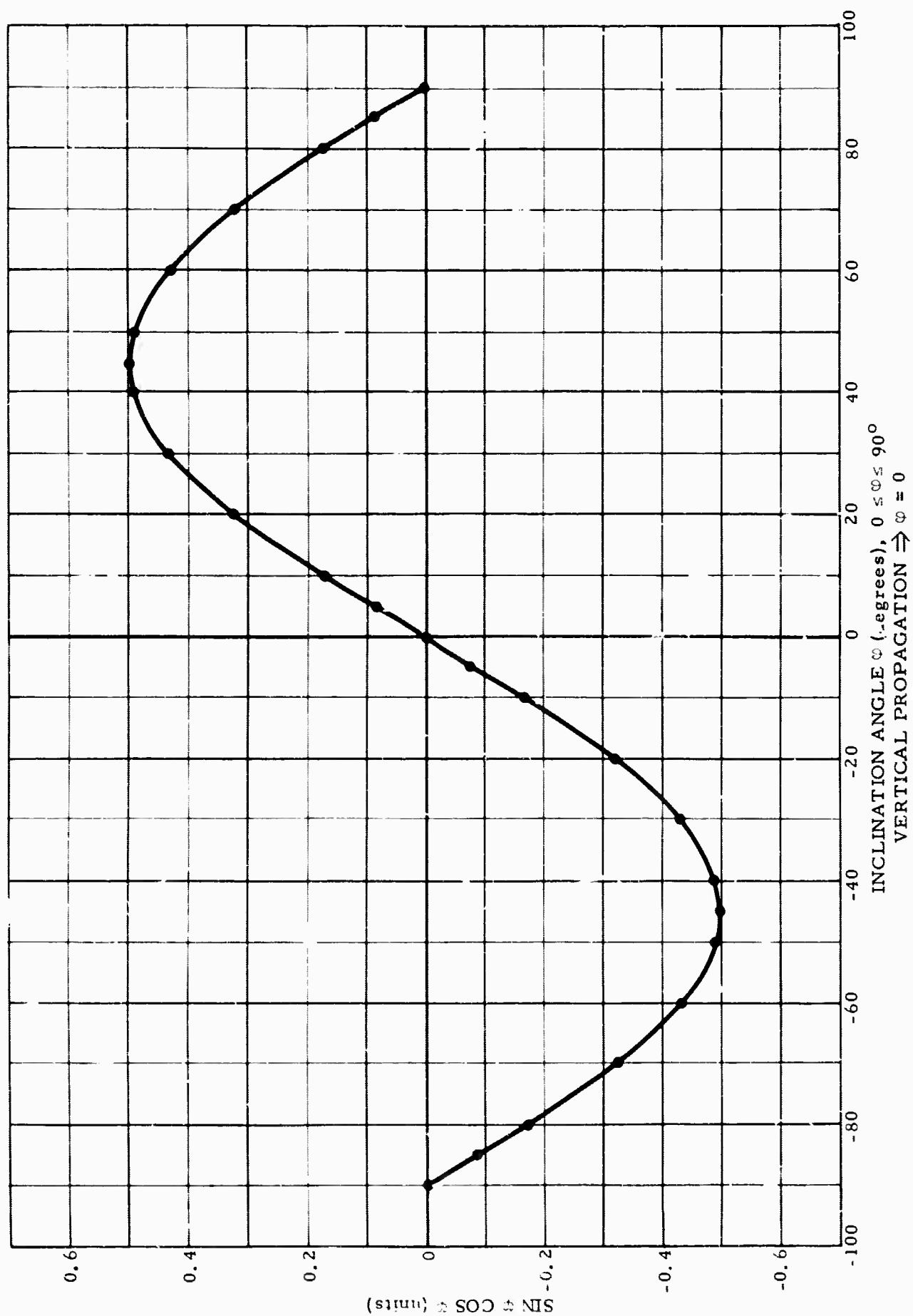
Figure 3. Relative amplitude weighting factor for M_{NZ} and M_{EZ} for P- and S-type signals propagating toward an inclination φ
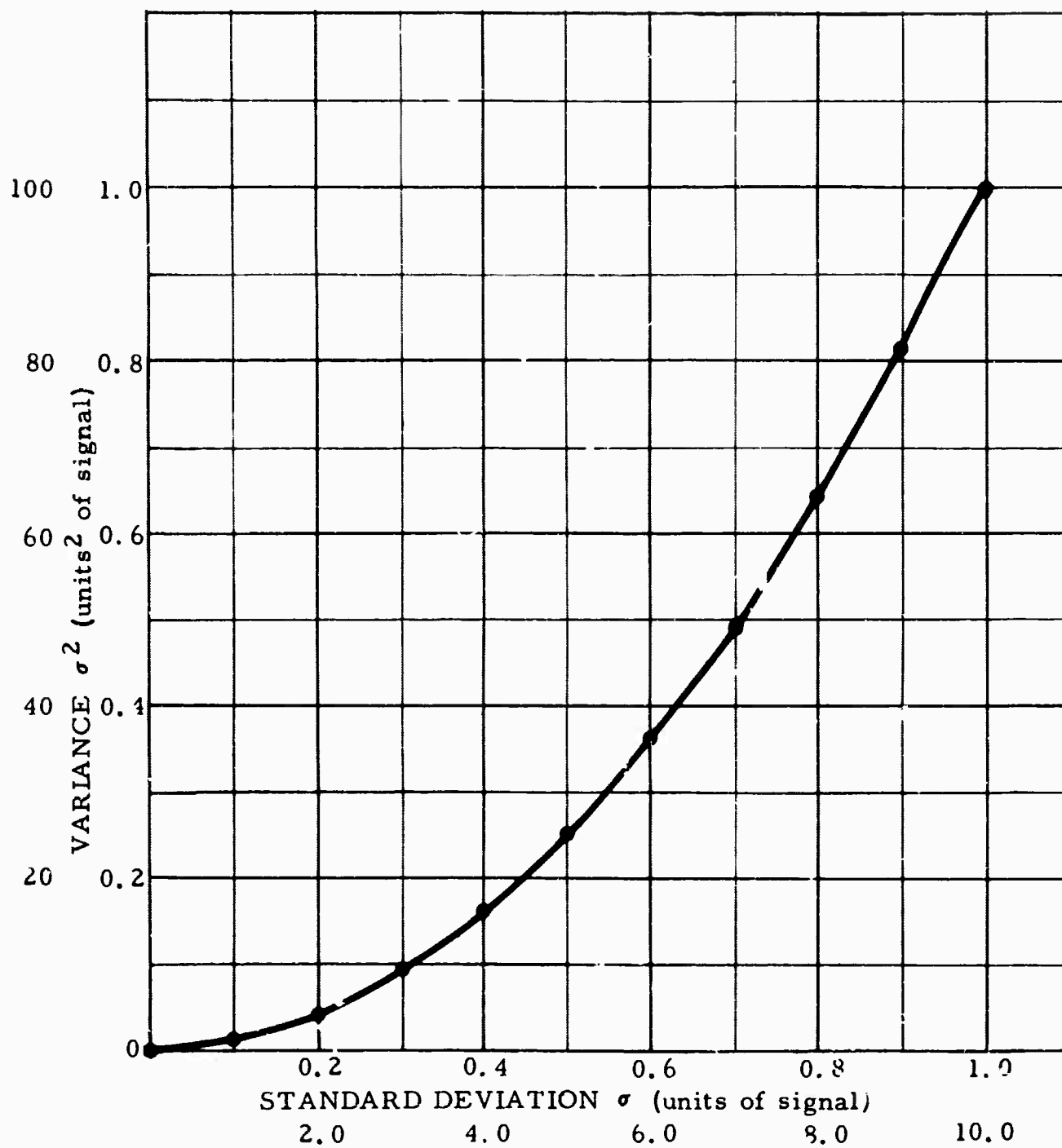
Figure 4. Square-law amplitude weighting

With the additional assumption that $\varphi(t)$ is approximately stationary for the delay time T.D. (i.e., the time delay is short with respect to the signal duration), $\cos\varphi(t - T.D.) \approx \cos\varphi(t)$ and

$$V_D \times M_{NZ} \approx P(t - T.D.)\,[\cos^2\varphi(t)\,\sin\varphi(t)]\,\cos\theta(t)\,(\frac{K}{T})\int_{-\infty}^{0} P^2(t+\alpha)\,e^{\frac{\alpha}{T}}\,d\alpha$$

and

$$V_D \times M_{EZ} \approx P(t - T.D.)\,[\cos^2\varphi(t)\,\sin\varphi(t)]\,\sin\theta(t)\,(\frac{K}{T})\int_{-\infty}^{0} P^2(t+\alpha)\,e^{\frac{\alpha}{T}}\,d\alpha$$

These expressions permit the same interpretation of signal azimuth angle as did the M terms discussed in 2.4.3.1.1. However, there is a modification of the incidence angle weighting for both M_{NZ} and M_{EZ} from $(\sin\varphi\cos\varphi)$ to $\cos^2\varphi\sin\varphi)$, which for P signals, places more emphasis on signals nearer vertical incidence than was true in the M terms above. In amplitude, the processor output will now approximately be proportional to the cube of the standard deviation (rms value) except for the smoothing introduced by averaging.

Figure 5 shows this modified amplitude weighting factor for P-type signals $(\cos^2\varphi\sin\varphi)$ as a function of inclination angle φ for both $V_D \times M_{NZ}$ and $V_D \times M_{EZ}$. For comparison the amplitude weighting factor $(\sin^2\varphi\cos\varphi)$ for S-type signals under the assumptions of section 2.4.3.2 for $\psi = 0^\circ$ are shown.

2.4.3.2 S Signals

2.4.3.2.1 **Effect on M.** As in the previous section

$$M_{NZ}(t) = K(\frac{1}{T})\int_{-\infty}^{0}[SPN(t+\alpha) \times SPZ(t+\alpha)]\,e^{\frac{\alpha}{T}}\,d\alpha,\ -1 \leq M_{NZ}(t) \leq +1$$

and

$$M_{EZ}(t) = K(\frac{1}{T})\int_{-\infty}^{0}[SPE(t+\alpha) \times SPZ(t+\alpha)]\,e^{\frac{\alpha}{T}}\,d\alpha,\ -1 \leq M_{EZ}(t) \leq +1$$
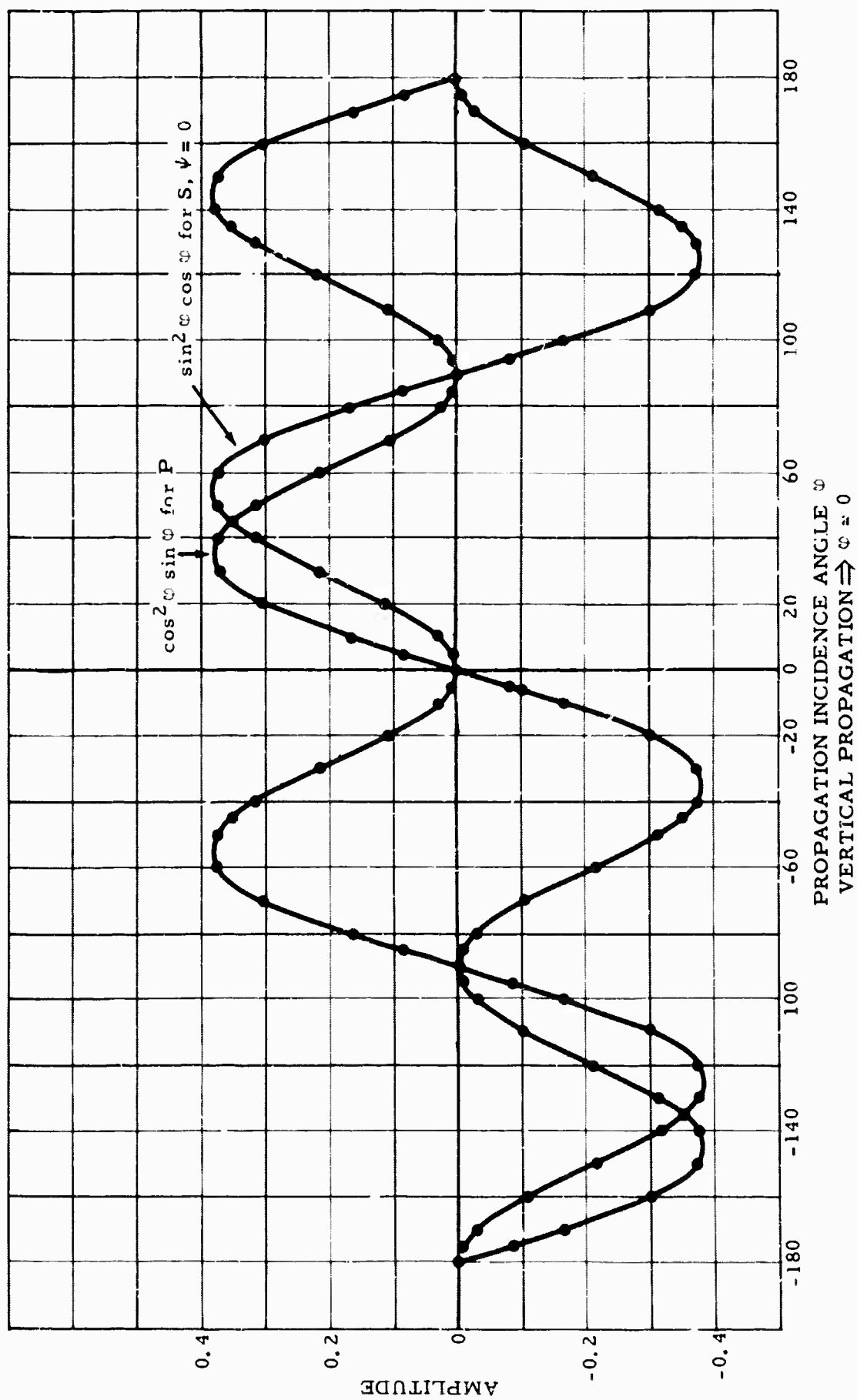
Figure 5. Relative amplitude weighting factor for $V_D \times M_{NZ}$ and $V_D \times M_{EZ}$ for P- and S-type signals propagating toward an inclination φ

Under the assumption that θ and φ are time-stationary for the duration of the phase, and substituting in the values of the instrument signal components from section 2.4.2.2 but not assuming that $\psi(t)$ is time-stationary for the phase

$$M_{NZ}(t) = K\left(\frac{1}{T}\right) \sin\varphi(t) \int_{-\infty}^{0} S^2(t+\alpha) \cos\psi(t+\alpha)\left[+\sin\psi(t+\alpha)\sin\theta(t) - \right.$$
$$\left. \cos\psi(t+\alpha)\cos\varphi(t)\cos\theta(t)\right] e^{\frac{\alpha}{T}} d\alpha$$

and

$$M_{EZ}(t) = K\left(\frac{1}{T}\right) \sin\varphi(t) \int_{-\infty}^{0} S^2(t+\alpha) \cos\psi(t+\alpha)\left[-\sin\psi(t+\alpha)\cos\theta(t) - \right.$$
$$\left. \cos\psi(t+\alpha)\cos\varphi(t)\sin\theta(t)\right] e^{\frac{\alpha}{T}} d\alpha$$

These forms are more difficult to interpret than was true for P-type motion. For purposes of illustration only, consider the two components of $\psi(t+\alpha)$ projected on unit vectors pointing toward $\psi = 0^{\circ}$ and $\psi = 90^{\circ}$, and assume (probably erroneously) that these components are time-stationary during the signal.

a. $\psi = 0^{\circ}$ Component

For this component $\cos\psi = 1$, $\sin\psi = 0$, then

$$M_{NZ}(t) = -\cos\theta(t)\left[\sin\varphi(t)\cos\varphi(t)\right] K\left(\frac{1}{T}\right) \int_{-\infty}^{0} S^2(t+\alpha)\, e^{\frac{\alpha}{T}}\, d\alpha$$

and

$$M_{EZ}(t) = -\sin\theta(t)\left[\sin\varphi(t)\cos\varphi(t)\right] K\left(\frac{1}{T}\right) \int_{-\infty}^{0} S^2(t+\alpha)\, e^{\frac{\alpha}{T}}\, d\alpha$$

Under these assumptions the amplitude weighting due to the signal amplitude $S(t+\alpha)$ is identical to the weighting of a similar amplitude P signal, as shown in figure 4. The amplitude weighting due to the signal incidence angle φ is of the form $(\sin\varphi\cos\varphi)$ identical to the weighting of a P signal of the same incidence angle, as shown in figure 3. However, the expressions for P and S signals differ in the interpretation of the azimuth weighting in that, in M_{NZ}, $(+\cos\theta)$ for P becomes $(-\cos\theta)$ for S, and that in M_{EZ}, $(+\sin\theta)$ for

P becomes $(-\sin \theta)$ for S. These weightings are shown in figure 2. Table 2 tabulates the comparison of polarities for S and P signals.

Table 2. Comparison of polarities of M_{NZ} and M_{EZ} for P and S signals

Azimuth of propagation	P signals		S signals, $\psi = 0^o$ or 180°		S signals, $\psi = 90^o$ or 270°		Back azimuth toward source
	M_{NZ}	M_{EZ}	M_{NZ}	M_{EZ}	M_{NZ}	M_{EZ}	
0° - 90°	+	+	-	-	0	0	180° - 270°
90° - 180°	-	+	+	-	0	0	270° - 360°
180° - 270°	-	-	+	+	0	0	0° - 90°
270° - 360^C	+	-	-	+	0	0	90° - 180°

As before, the back azimuth will exhibit considerable scatter (up to 30°) due to violations of the homogeneous isotropic assumptions about the medium. However, judicious weighting based on experience with several signals appears to offer hope that a weighted estimate of the back azimuth may be obtained that will be accurate to within $\pm 10^o$ for most events.

b. $\psi = 90^o$ Component

For this component, $\cos \psi = 0$, $\sin \psi = +1$ (-1 for 270°), then

$$M_{NZ}(t) = 0$$

and

$$M_{EZ}(t) = 0$$

These results are shown in table 2.

2.4.3.2.2 Effect on V_D x M. V_D is defined to be SPZ (t - T.D.) where T.D. is the time delay introduced for the processor (see 2.4.2.2).

Then

$$V_D = SPZ(t - T.D.) = S(t - T.D.) \cos \psi (t - T.D.) \sin \varphi (t - T.D.)$$

As before, the assumption is made that $\varphi(t)$ is approximately constant (stationary) over the time delay, as well as the signal duration, but initially $\psi(t - T.D.)$ will not be assumed constant.

With these assumptions, $V_D \times M$ reduces to

$$V_D \times M_{NZ} = S(t - T.D.) \cos \psi(t - T.D.) \sin^2 \varphi(t) K\left(\frac{1}{\tau}\right) \int_{-\infty}^{0} S^2(t+\alpha) \cos \psi(t+\alpha)$$

$$[\sin \psi(t+\alpha) \sin \theta(t) - \cos \psi(t+\alpha) \cos \varphi(t) \cos \theta(t)] e^{\frac{\alpha}{\tau}} d\alpha$$

and

$$V_D \times M_{EZ} = S(t - T.D.) \cos \psi(t - T.D.) \sin^2 \varphi(t) K\left(\frac{1}{\tau}\right) \int_{-\infty}^{0} S^2(t+\alpha) \cos \psi(t+\alpha)$$

$$[-\sin \psi(t+\alpha) \cos \theta(t) - \cos \psi(t+\alpha) \cos \varphi(t) \sin \theta(t)] e^{\frac{\alpha}{\tau}} d\alpha$$

Again for purposes of illustration only, consider the two components of $\psi(t+\alpha)$ projected on unit vectors toward $\psi = 0^O$, 180°, and toward 90°, 270°, and consider them (probably erroneously) to be constant during the signal duration.

      a. $\psi = 0^O$ Component

For $\psi = 0^O$, $\cos \psi = 1$, $\cos^3 \psi = 1$, $\sin \psi = 0$

Then

$$V_D \times M_{NZ} = -S(t - T.D.) [\sin^2 \varphi(t) \cos \varphi(t)][\cos \theta(t)] \ K\left(\frac{1}{\tau}\right) \int_{-\infty}^{0} S^2(t+\alpha) e^{\frac{\alpha}{\tau}} d\alpha$$

and

$$V_D \times M_{EZ} = -S(t - T.D.) [\sin^2 \varphi(t) \cos \varphi(t)][\sin \theta(t)] \ K\left(\frac{1}{\tau}\right) \int_{-\infty}^{0} S^2(t+\alpha) e^{\frac{\alpha}{\tau}} d\alpha$$

      b. $\psi = 180^O$ Component

For $\psi = 180^O$, $\cos \psi = -1$, $\cos^3 \psi = -$, $\sin \psi = 0$

Then

$$\bar{V}_D \times M_{NZ} = +S(t - T.D.)\,[\sin^2\varphi(t)\cos\varphi(t)]\,[\cos\theta(t)]\,K\left(\frac{1}{T}\right)\int_{-\infty}^{0} S^2(t+\alpha)\,e^{\frac{\alpha}{T}}\,d\alpha$$

and

$$V_D \times M_{EZ} = +S(t - T.D.)\,[\sin^2\varphi(t)\cos\varphi(t)]\,[\sin\theta(t)]\,K\left(\frac{1}{T}\right)\int_{-\infty}^{0} S^2(t+\alpha)\,e^{\frac{\alpha}{T}}\,d\alpha$$

     c. $\psi = 90^{\circ}$, 270° Component

For $\psi = 90^{\circ}$, 270°, $\cos\psi = 0$, $\sin\psi = \pm 1$
and

$$V_D \times M_{NZ} = 0$$

and

$$V_D \times M_{EZ} = 0.$$

The above expressions indicate that S-signal interpretation, even under the gross assumptions used, is more difficult than P-signal interpretation. The polarity reversal as a function of ψ merely indicates the fact that the processor cannot discriminate between compressive motion toward ψ and rarefaction motion toward $\psi \pm 180^{\circ}$. The amplitude weighting for azimuth is the same as for the M terms and is shown graphically on figure 2. The incidence angle weighting ($\sin^2\varphi\cos\varphi$) differs from the weighting for P signals and is shown in figure 5. The amplitude weighting is the same as for P-type signals, being represented very approximately by the estimated signal variance multiplied by the signal amplitude.

2.5 SUMMARY

It has been shown that the analog and digital $V_D \times M$ processors differ in two respects: (a) the meaning of time averaged (section 2.1) and (b) the method by which time delays are incorporated into the processor (section 2.3).

For reference purposes, a statistically oriented interpretation of data processed by analog processors is presented in section 2.2.

In section 2.4, the fact that processors utilizing three-component data permit interpretations based on a propagating vector field is presented. In addition, basic background for interpreting processor results is developed. The

assumptions involved are not proven, but preliminary results indicate that this vector point of view is helpful in data analysis.

3.   EXPERIMENTAL ANALOG REAL-TIME PROCESSOR

3.1 SYSTEM ORGANIZATION

The problem of developing a real-time analog $V_D \times M$ vector-correlation processor involves four steps.

a.   The first step involves signal buffering to adjust the seismograph outputs to the normalized and limited input requirements of the processor. This problem is easily handled using operational amplifiers.   The actual circuits required depend somewhat on specific details of the instrumentation, but a circuit that is capable of working either directly from the PTA or from an analog tape recorder was developed for these tests.   An improved model could easily be developed for either the in-house or field processor as desired.

b.   The second step of this particular approach requires a time delay for the time information and for the SPZ channel data.   In the in-house approach this was accomplished with a Honeywell Model 7400 tape recorder. An attempt to use a cheaper Tandberg tape recorder was unsuccessful.   Consideration was given to the use of passive delay lines, which are available at moderate cost, but this approach was not actually tried.   Consideration was also given to the use of analog Pade' approximation delay networks, but the cost was prohibitive for this approach.   Digital delays are also possible, but multiplexing, analog-to-digital conversion, and digital-to-analog conversion costs, in addition to computer costs, make this unattractive for an analog processor, although this is certainly the easiest approach for a digital processor.   The Honeywell recorder, including electronics, would be relatively expensive.

c.   The third step of this approach is the analog processor.   Various levels of complexity have been considered for this part of the processor.   For around \$18,000.00, the processor used experimentally could be duplicated for field use.   A processor substituting σ^2_{NZ} for M_{NZ} and σ^2_{EZ} for M_{EZ} can be developed at a comparable cost.   An unnormalized processor for three orthogonal pairs of azimuths instead of a single pair could be constructed at proportionally higher cost.

d.   The fourth step of this apporach is the data presentation. A 16-mm film readout can be incorporated using a Develocorder. An analog tape readout could be provided using recorders similar to those presently available in the observatories.

Figure 1 in the appendix shows the equipment actually used in the in-house experimental procedure, which is in accord with the above general equipment requirements.

3.2 EXPERIMENTAL RESULTS

Data processed for analysis by the V_D x M vector-correlation processor included 6 events: 4 deep earthquakes (40, 115, 150, and 614 km), 1 local event, and 1 near-regional event. Recordings of these events are shown in figures 6 through 14.

From each of the four deep earthquakes, the processor picked the depth signals pP or sP or both. In the 150-km earthquake (figure 13), both pP and sP were picked; neither of these signals would have been obvious without V_D x M vector processing. In figure 8 (the 614-km earthquake), pP may or may not, without the aid of processing, have been recognized by an analyst. Certainly processing made these signals more apparent. From the 40-km earthquake (figure 14) and the 614-km earthquake (figure 10), pP would have been seen by an analyst without processing.

In addition to its ability to make depth signals obvious or to "pull them out" of microseismic noise or signal codas entirely, the processor will pick signals such as PcP, PP, and PPP which may or may not have been obvious to the analyst. Of a total of 11 signals picked by V_D x M vector processing, 3 would have been evident without processing (figures 7 and 9), 3 may or may not have been (figures 8, 10, and 14), and 5 would not have been seen by an analyst (figures 11, 12, and 13). Several unidentifiable signals were noted at teleseismic distances (as in figure 6 at 00:33:15); however, these apparent signals can usually be eliminated because they fail to coincide with a normal sequence of other signals.

A feature of the processor which may be of considerable value is the "locator" (M_{NZ} and M_{EZ}) traces which will enable an analyst to determine within 10 to 15° the direction of origin of the earthquake. He can determine epicentral distance within 1 to 4° if two or more signals can be identified. Apparently

00:33:00   00:33:10   00:33:20

eP   00:33:00   00:33:10   00:33:20

Station WMSO, 22 December 1964
Δ = 51°
Azimuth to source = 144.41°
CGS location

Time 00:24:48.7
Lat 9.5°S, long. 71.3°W
H = 614 km
Mag = 5.29 CGS
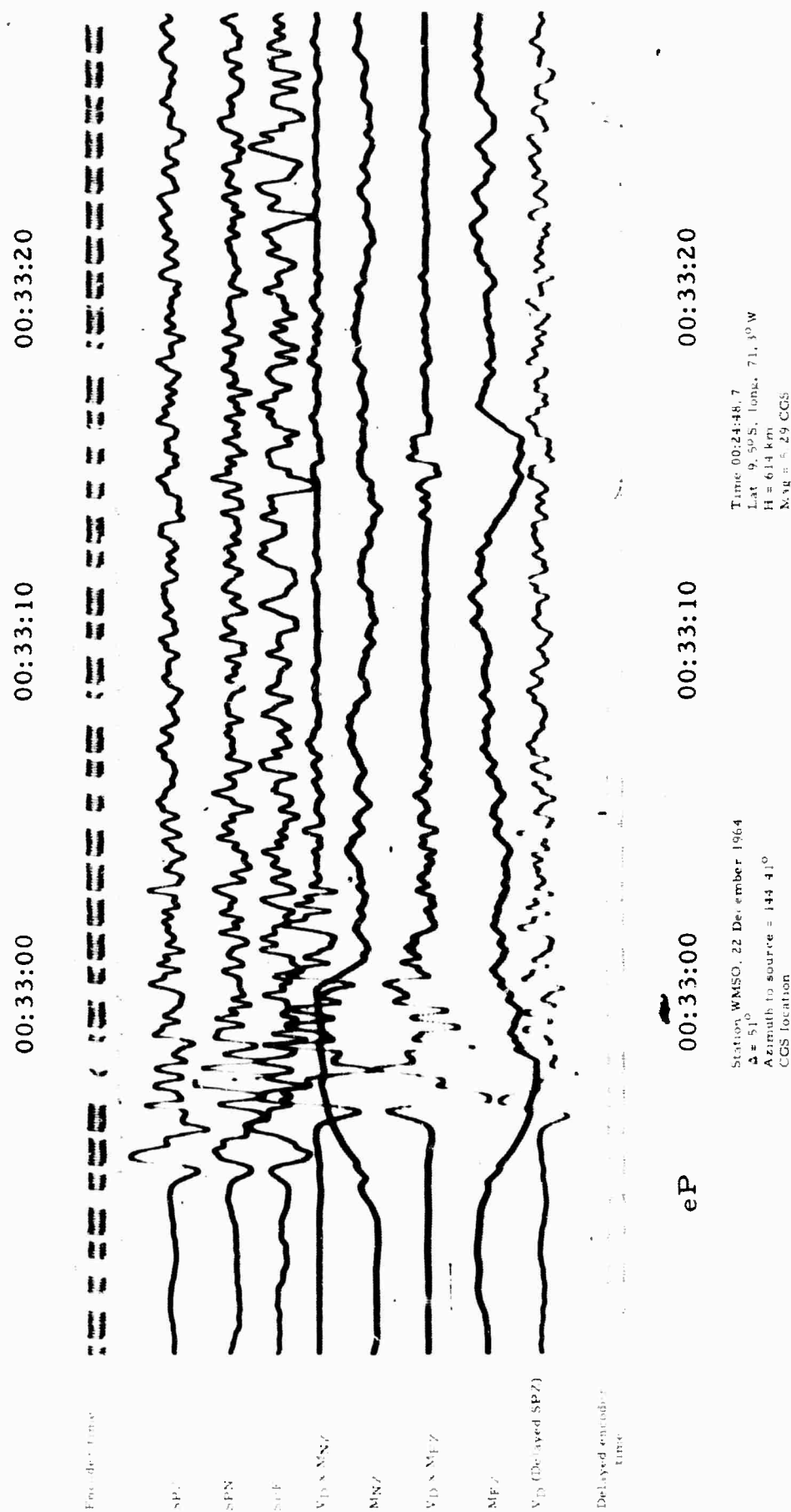
Figure 6. $V_D \times M$ data, WMSO, 22 December 1964, eP signal of 00:24:48.7 event
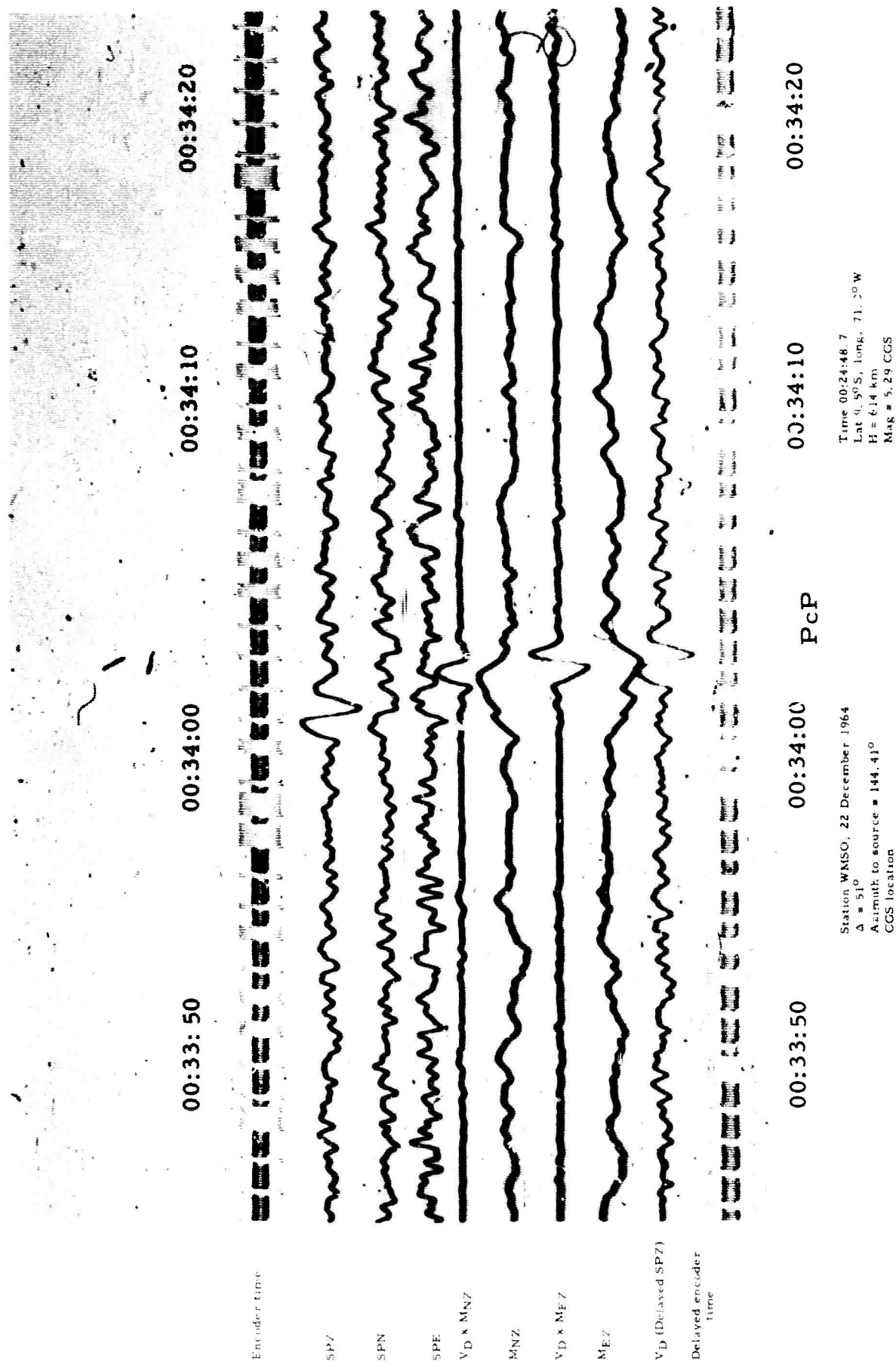
Figure 7. $V_D \times M$ data, WMSO, 22 December 1964, PcP signal of 00:24:48.7 event
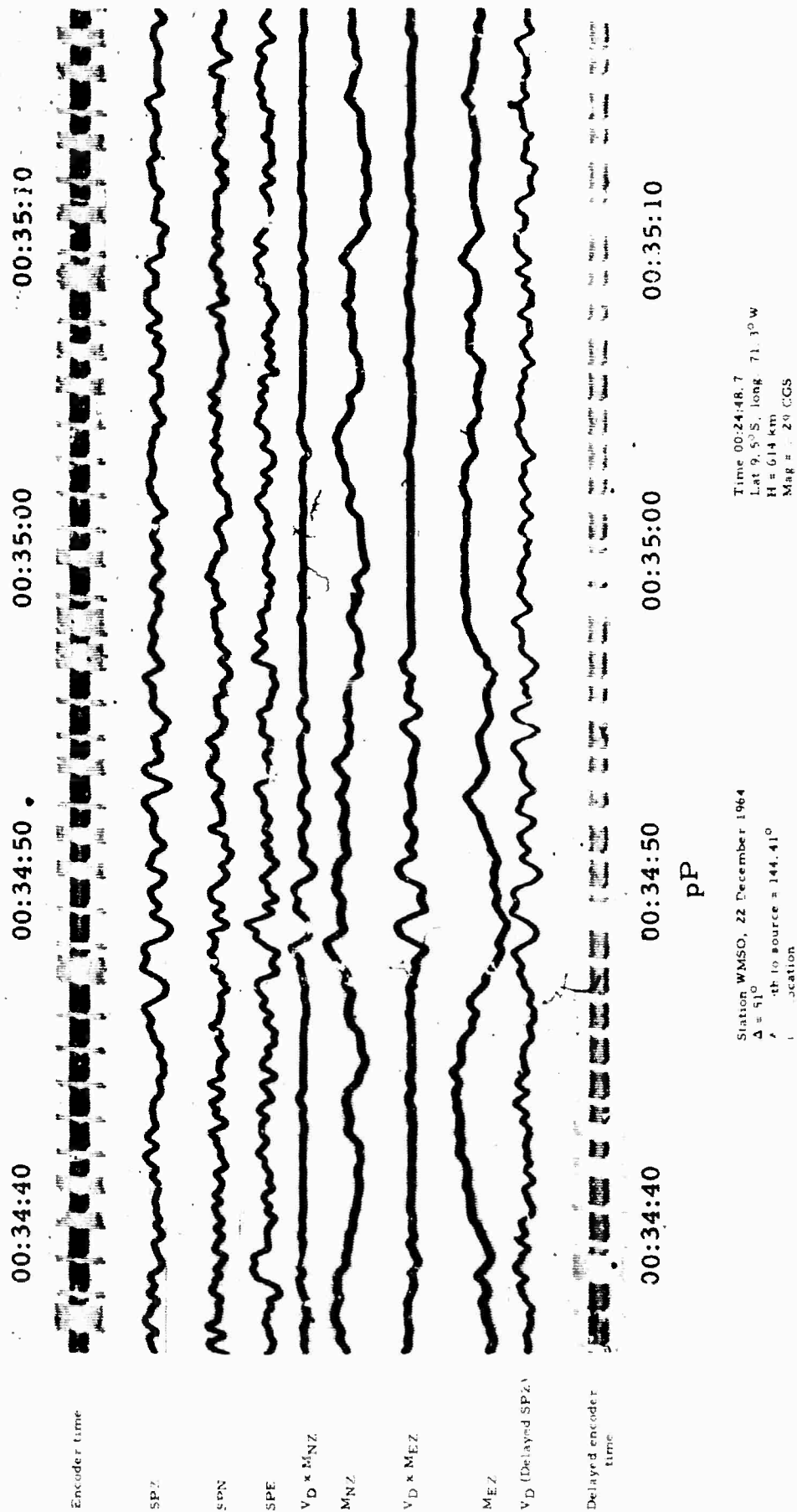
Figure 8. $V_D \times M$ data, WMSO, 22 December 1964, pP signal of 00:24:48.7 event

Station WMSO, 22 December 1964
$\Delta = 51°$
...th to source = 144.41°
...cation

Time 00:24:48.7
Lat 9.5°S, long 71.3°W
H = 614 km
Mag = .29 CGS
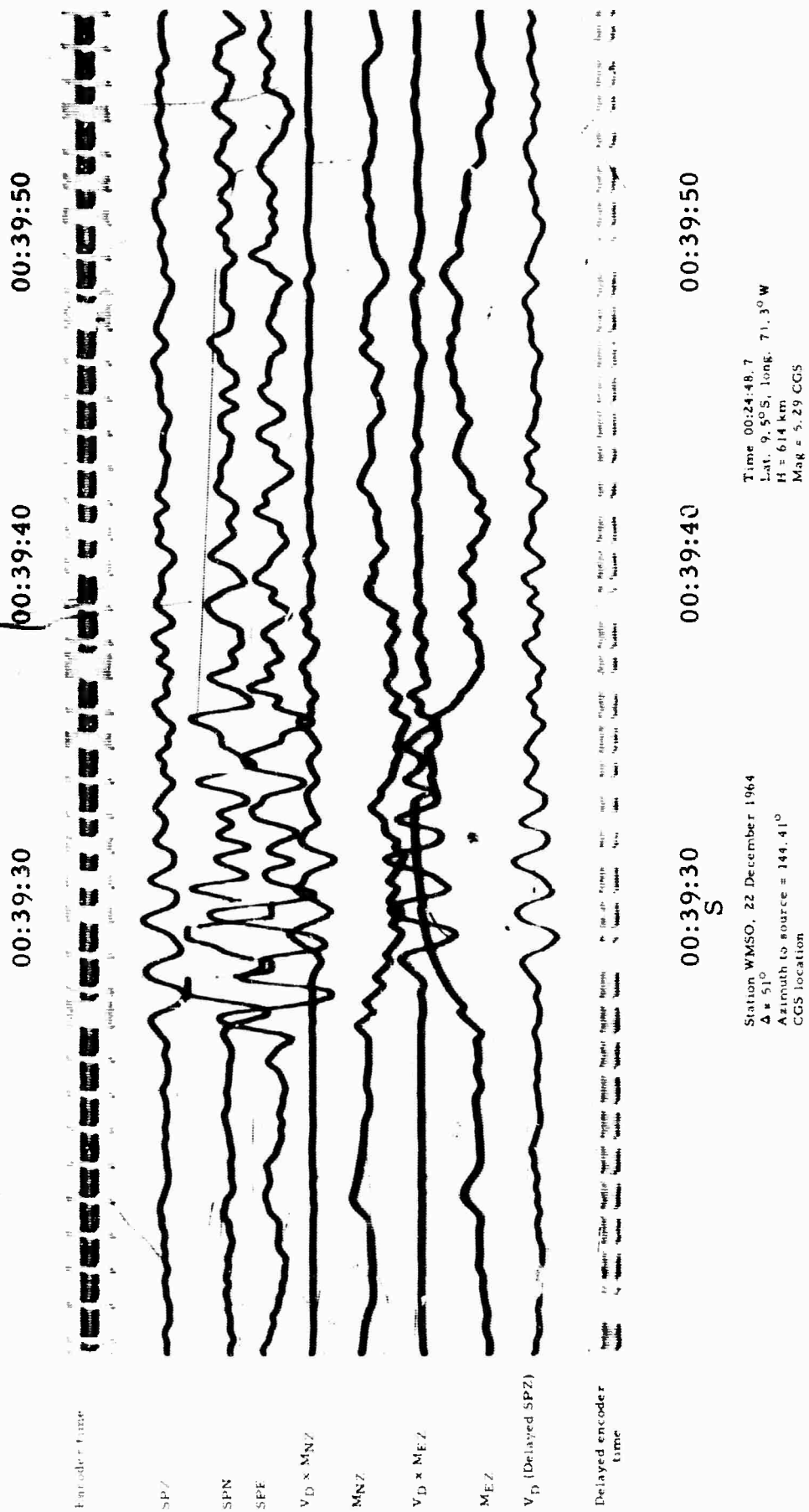
Figure 9. $V_D \times M$ data, WMSO, 22 December 1964, S signal of 00:24:48.7 event
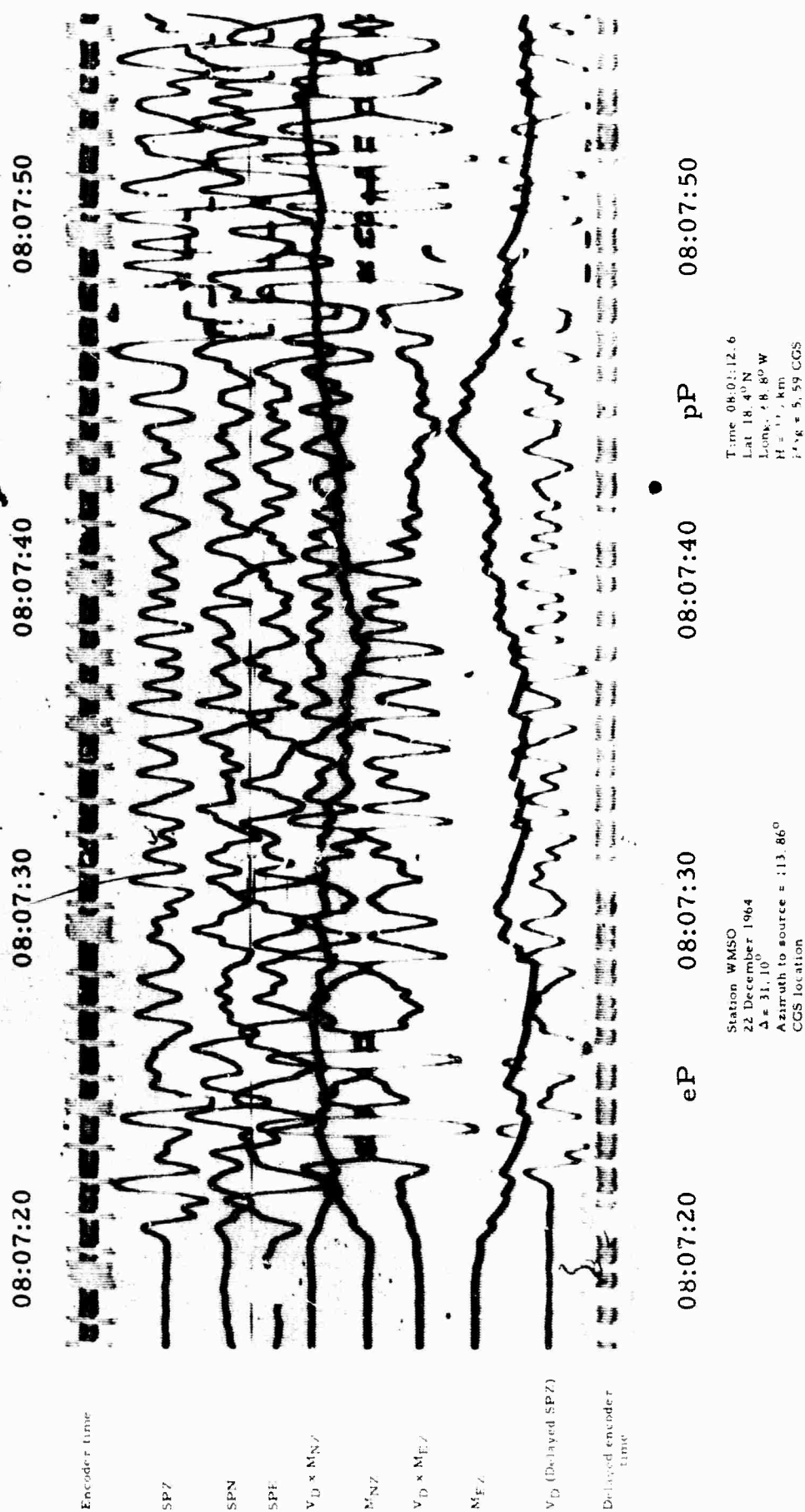
Figure 10. $V_D \times M$ data, WMSO, 22 December 1964, eP and pP signals of 08:01:12.6 event
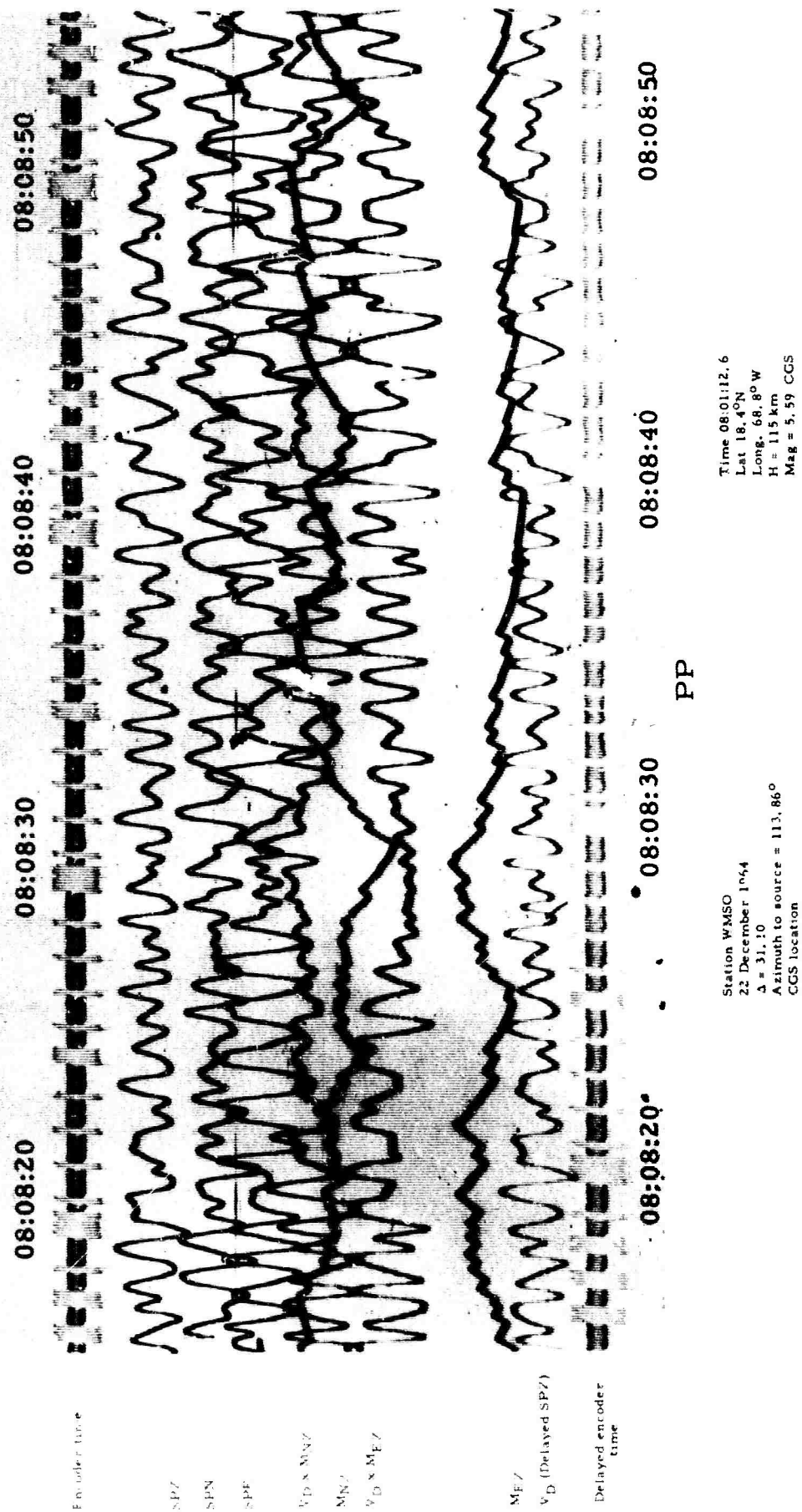
Figure 11. $V_D \times M$ data, WMSO, 22 December 1964, PP signal of 08:01:12.6 event
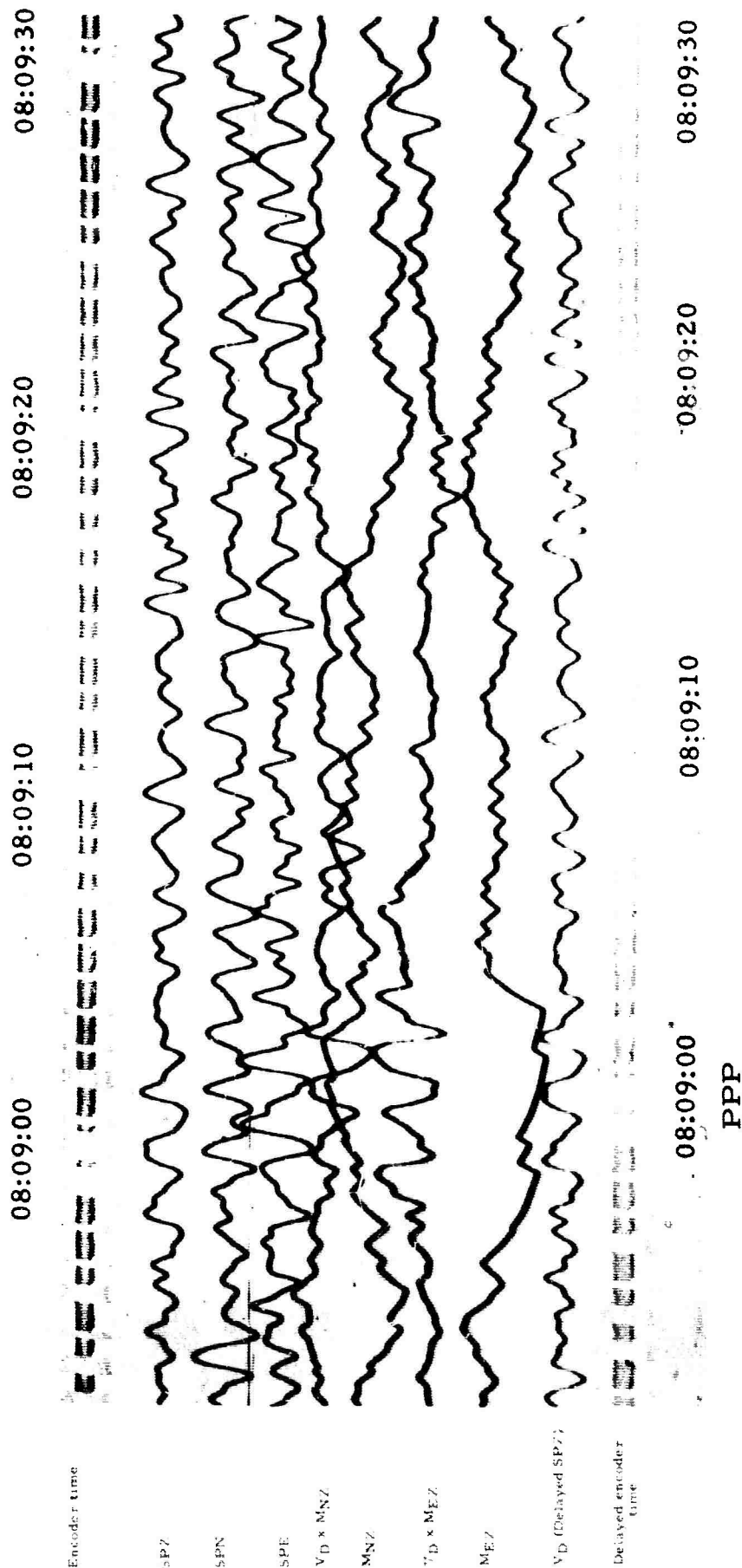
Figure 12. $V_D \times M$ data, WMSO, 22 December 1964, PPP signal of 08:01:12.6 event
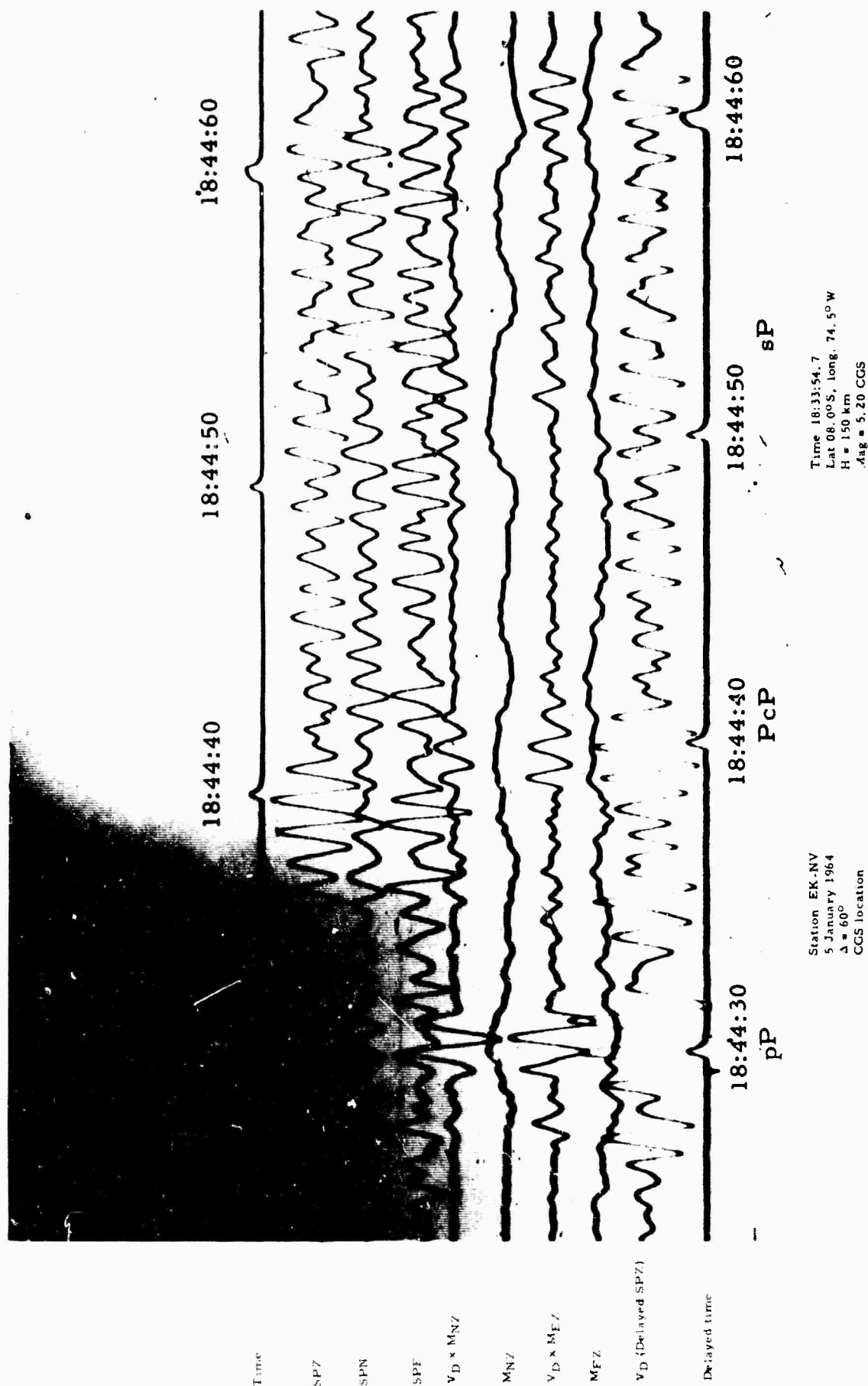
Figure 13. $V_D \times M$ data, EK-NV, 5 January 1964, pP, PcP, and sP signals of 18:33:54.7 event
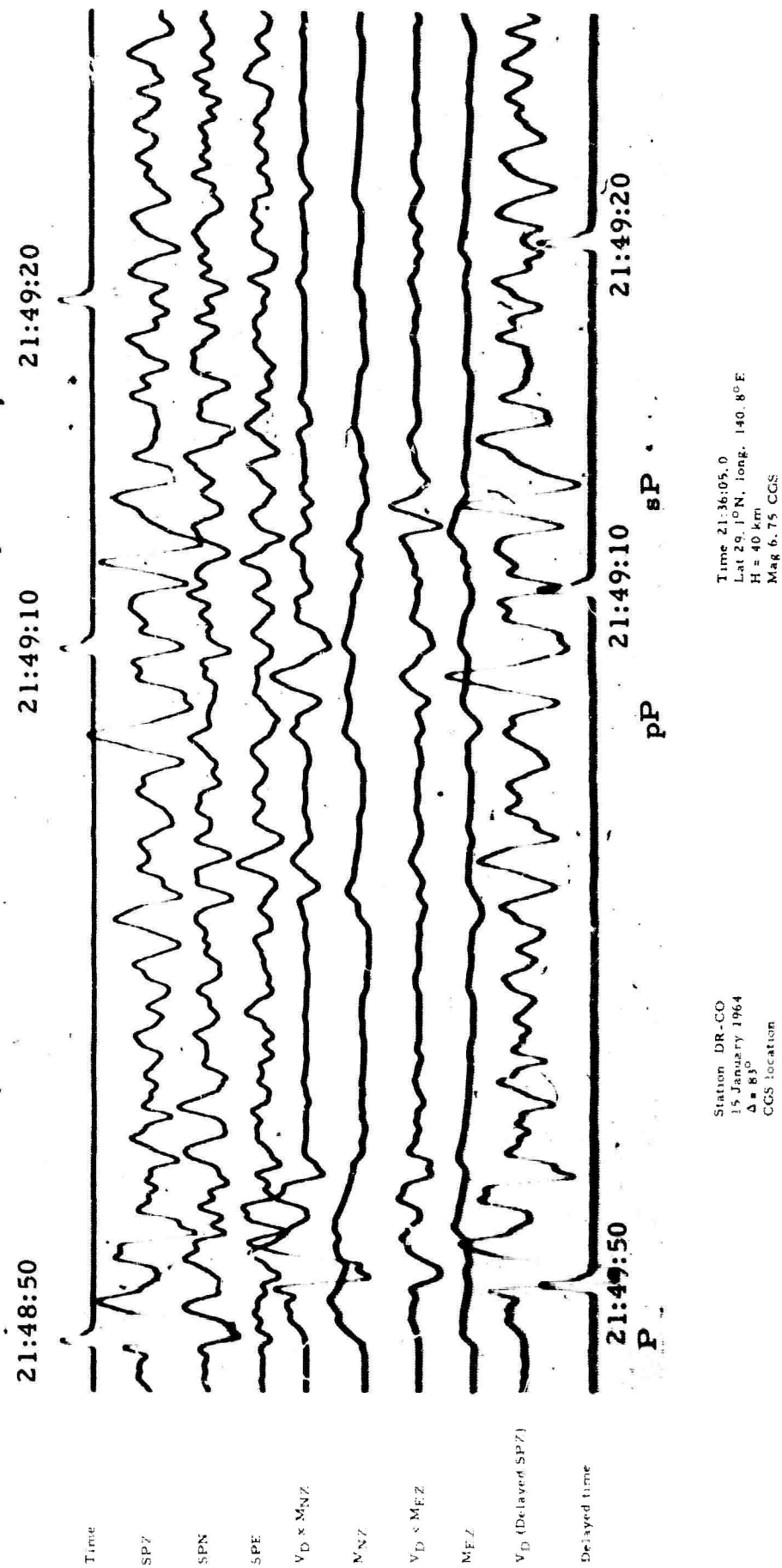
Figure 14. $V_D \times M$ data, DR-CO, 15 January 1964, P, pP, and sP signals of 21:36:05.0 event

(from data processed to date) the processor will provide these additional signals. The entire process of roughly locating an epicenter involves some 3 to 4 minutes. Knowing the general location, an analyst sufficiently familiar with seismic areas of the world can determine a more specific location by elimination of nonseismic areas within the area of the previously determined general location. Since areas in which nuclear testing occur are somewhat restricted, he could very quickly eliminate a large percentage of events as natural in origin.

Apparently one limitation on the usefulness of V_D x M processing for picking depth signals is its failure at near-regional distances. One such near-regional event was processed and the processor picked some seven or eight signals between P and S. It is assumed that these were multipath reflections since the travel path was predominately in the crust. Apparently, with a decrease in distance from epicenter to the seismometers, the number of multipath reflections picked by the processor increases and so establishes a lower limit of usefulness. Both the lower and upper distance limits remain to be established.

The main value of V_D x M vector processing, in the case of locals and near-regionals, is its locator traces, which enable the "geographically" trained analyst to quickly, though roughly, locate the event.

In summary, it would appear from data processed thus far that V_D x M processing will reveal depth signals from deep earthquakes. Additional data should be processed to determine the consistency of the process as well as the depth limitations, both upper and lower. In the case of near-surface and surface events, the processor's locator traces and its ability to reveal additional signals enable an analyst to locate an event accurately enough to place it within a known testing area.

4. FIELD AND IN-HOUSE PROCESSORS

In this section, approaches for implementing the V_D x M vector correlation process are considered. Certain possible alterations in the present processor have been considered in section 4. 1, which may or may not improve the results. In section 4. 2, an analog approach using the normalized Pearson moment-correlation function rather than M is considered. Some additional

theory is developed, extending previous theory to the normalized case. In section 4.3, concepts for realizing a processor using digital and hybrid computers are developed.

4.1 MINIMUM ANALOG PROCESSOR

The minimum analog processor for field or in-house processing consists of the $V_D \times M_{NZ}$ and $V_D \times M_{EZ}$ approach that was tried experimentally and discussed in section 3 of this report. During the course of the experiment, two modifications to the approach were suggested.

The first modification suggested was to perform data rotations in a horizontal plane, and calculate cross-correlation terms between the vertical and a set of three pairs of orthogonal data channels instead of the single pair actually processed. Doing this is, of course, quite feasible. However, for the following four reasons this approach is not recommended.

    a. As may be seen in figure 2, for a given incidence angle of any specific signal and for any azimuth angle, either M_{NZ} or M_{EZ} will be at least 70.7 percent as large as would be the equivalent term for instruments exactly in the horizontal azimuth of the signal. With data channels spaced 30° apart in azimuth, at least one of the terms would be 97 percent as large as would be a trace from the actual azimuth of the signal. However, an analyst would have to select the azimuth on which the phase appeared largest, and a discrimination between traces to 3 percent would be difficult in the presence of normal seismic noise.

    b. In some unpublished work in 1964, W. R. Clack of The Geotechnical Corporation performed analog analyses using horizontally rotated data signals (not including the $V_D \times M$ processor) at increments of 30° in azimuth for 23 events. His results indicate in part that, for known source locations, azimuthal variations of 5 to 30° from the true azimuth to the source were observed for individual signals from these azimuthal seismograms. In addition, the P and S azimuths are not even orthogonal in general for the events tested. Clack states in his conclusions from these data, "Azimuthal seismograms are of limited use in identification of phases subsequent to P for teleseismic events of large displacements." Approximately this same order of magnitude of error has been observed in efforts to estimate the source azimuth of individual signals from two events using $V_D \times M_{NZ}$ and $V_D \times M_{EZ}$ only.

c. The problem of data display becomes serious for rotated data. A film presentation would require 10 traces for the technique actually employed experimentally, but this increases to 18 traces for the proposed rotations. Although this is certainly possible, a net reduction in visual dynamic range per channel will be required, which might easily be greater than any improvements obtainable by the larger processor.

d. The c   ~f performing V_D x M will triple for the three-orthogonal-pair computati~   ~ith an additional cost for performing the rotations themselves. Prelin   ~y cost estimates indicate that the cost of horizontally rotated data processing as suggested would be as much as or more than the normalized correlation approach discussed in section 4.2, and this normalized processor should be an order of magnitude more amplitude-sensitive, compared to 30 percent greater sensitivity (at best) for the six-azimuth processor, and approximately equally sensitive in azimuth determination.

The second modification suggested was to perform an axis rotation in the vertical plane for purposes of calculating the cross-correlation M. In figure 3 this would have the effect of sliding the axes by the amount of the rotation performed. This would tend to make the processor more sensitive to vertically incident phases, at the cost of losing the azimuth polarity information now available in M. However, the inclined-axis geometry is inherent in the deep-hole inclined triaxial seismometer and will be investigated in conjunction with that instrument.

4.1.1 Analog Computer Requirements to Implement Processor

Figure 2 in the appendix shows the analog computer circuit used in the experimental tests discussed in section 3. This approach represents the maximum capability of a TR-10 or TR-20 analog computer, and has many shortcomings. A TR-20 computer to perform this function in a field processor could be purchased for about $12,500 at this time. The addition of circuits to calculate [Z - Z], as will be discussed in section 4.2, would be very desirable in reducing the processor sensitivity to microseisms, but this requires larger capability. A TR-48 capable of calculating the unnormalized, limited EMP covariance could be purchased for around $20,000, and would be capable of direct expansion to the normalized processor of section 4.2 at an additional expense of the same order of magnitude. Since the equipment elements for the TR-48 are more accurate than those for the TR-20, better results would be obtained for this additional initial equipment cost.

4.1.2 Capabilities and Limitations of the Processor

The processor appears capable of recovering one or both of the depth-determining signals pP or sP in the coda of large, deep, distant earthquakes. In the four deep events thus far examined, the processor has not failed to bring out at least one such signal. The possibility of failure does exist, and since the processor does accentuate signals for which no identification is presently possible, the possibility of misinterpretation does exist. In general, however, the processor appears to be effective in detecting the depth-determining signals in the high noise level of the coda.

Although this processor was not developed to be an epicenter-locating device, the form of its data presentation has been found by analysts to facilitate estimates of source azimuth. Of course, such estimates have been made without the aid of this processor. However, the form of the data presentation is such that azimuth estimates are both easier to make and faster to obtain (about 3 minutes) than when such estimates are made from the raw data alone.

The processor is obviously limited in dynamic range. All events large enough to merit USC&GS locations that have been processed appear to be well within the capabilities of the system, as are a few smaller local events. However, the processor is incapable of processing events of very low signal-to-noise ratio.

The processor was run for the experimental tests at the real-time rate to prove that continuous-duty field operation was feasible. However, for any extensive use of the processor off-line, time compression by a factor of five is desirable and entirely practical. Because of heavy utilization of the available equipment, only a very limited amount of data could be processed in this study without increasing the analog tape speed. The laboratory Develocorder is capable of this time compression, and reduction of the processor averaging time by a factor of five is a simple matter of readjusting four potentiometers. Times-five tape playback speed is already available and in normal use, and a times-five playback speed on the delay-tape recorder is available, although there may or may not be some additional expense involved for electronics depending on the number of channels to be delayed.

The overall equipment requirements are shown in figure 1 in the appendix.

4.2 NORMALIZED ANALOG PROCESSOR

The normalized analog processor calculates the Pearson moment-correlation function, which may be used to detect signals and gain-control the data by a multiplication process. The meaning of average in this processor is still the cross-correlation of all past data up to the instant t with the exponential time-significance weighting function. As in the unnormalized approach, a time delay is introduced to compensate in part for the lack of knowledge about the future of the data which would be taken care of automatically by an even time-significance weighting function.

4.2.1 Vector Interpretation of the Pearson Moment-Correlation Function

This processor works exclusively with terms of the form $(Z - \bar{Z})(t)$ where

$$\bar{Z} = \frac{1}{T} \int_{-\infty}^{0} Z(t + \alpha) \, e^{\frac{\alpha}{T}} \, d\alpha$$

as defined in section 2.2.

The variance $\sigma^2_{Z \cdot Z}$ is defined to be

$$\sigma^2_{Z \cdot Z}(t) = \frac{1}{T} \int_{-\infty}^{0} (Z - \bar{Z})^2 (t + \alpha) \, e^{\frac{\alpha}{T}} \, d\alpha$$

The notation $Z \cdot Z$ is used because numerically

$$(Z - \bar{Z})^2 = (Z - \bar{Z})(Z - \bar{Z}) \cos 0^{\circ}$$

and hence, this variance term for vector measures of the data can be interpreted as the variance of the dot or scalar product of the vector component in the direction of the measuring instrument.

The covariance $\sigma^2_{Z \times N}$ is defined to be

$$\sigma^2_{Z \times N} = \frac{1}{T} \int_{-\infty}^{0} [(Z - \bar{Z})(N - \bar{N})] (t + \alpha) \, e^{\frac{\alpha}{T}} \, d\alpha$$

The notation $\sigma^2_{Z \times N}$ is used because numerically

$$[(Z - \bar{Z})(N - \bar{N})] = [(Z - \bar{Z})(N - \bar{N})\sin 90^\circ]$$

and hence, this variance term for orthogonal vector measures of the data can be interpreted as the variance of the cross-product of two orthogonal components of the vector data in the plane of the measuring instruments.

The standard deviation $\sigma_{Z \cdot Z}$ is defined to be

$$\sigma_{Z \cdot Z} = + \sqrt{\sigma^2_{Z \cdot Z}}$$

The product of $\sigma_{Z \cdot Z}$ and $\sigma_{N \cdot N}$ may thus be thought of as

$$\sigma_{Z \cdot Z} \times \sigma_{N \cdot N} = \left[\sqrt{\sigma^2_{Z \cdot Z}}\right]\left[\sqrt{\sigma^2_{N \cdot N}}\right] \sin 90^\circ$$

or as the cross-product of the square roots of the dot products of the orthogonal vector components of the vector data field in the plane of the measuring instruments.

The Pearson moment-correlation function $P_{Z \times N}$ is defined to be

$$P_{Z \times N}(t) = \frac{\sigma^2_{Z \times N}}{\sqrt{\sigma^2_{Z \cdot Z}} \times \sqrt{\sigma^2_{N \cdot N}}}$$

It will be recognized that this function is independent of the function in time being measured at a point in space, but is determined by the temporary stationarity in time of the direction (in the plane of the two instruments) of this function being measured. The orthogonality of the measured Z and N implies that a high correlation itself implies linear temporal dependence between the vector measures.

The obvious extension of this technique to the three-dimensional case will be developed in a later report.

4.2.2 Analog Computer Requirements to Implement Processor

The normalized correlation function can be implemented in the analog processor shown in block diagram form as figure 15. An Electronic Associates, Inc., TR-48 can be purchased for approximately $40,000.00 with the complement of parts that will perform this function. Alternatively, a standard, fully expanded TR-48, if already available, could be modified to perform this function for approximately $15,000.00, depending on the exact equipment-complement initially available in the computer.

As may be seen in this figure, three orthogonal cross-correlation functions are computed, and in addition, the normalized equivalent of the V_D x M_{ZN} and V_D x M_{ZE} are computed. This processor could be substituted for the simpler unnormalized processor with only the addition of one additional readout channel for $P_{N \times E}$. The output is now seen to be:

$$[P_{Z \times N} \times V_D](t) = \left[\frac{\sigma^2_{Z \times N}}{\sqrt{\sigma^2_{Z \cdot Z}} \times \sqrt{\sigma^2_{N \cdot N}}}\right] (t) \times [SPZ(t - T.D.)]$$

for the normalized processor. This is the vector triple product $[A \times (A \times B)]$ except for the modification introduced by the averaging, normalization, and time-delay.

4.2.3 Advantages of the Normalized Processor

From a practical standpoint, the normalized vector correlator has several advantages over the unnormalized approach.

4.2.3.1 Dynamic Range

Theoretically, the normalized correlation function is independent of the amplitude or shape of the seismic signal detected. In a practical sense, it is still subject to the signal azimuth and incidence angle weighting illustrated in section 2.4. It is also limited in the practical sense by the dynamic range of the sensors, the delay circuit, and the analog computer. It is also subject to a reduction in the amplitude of the correlation function due to any noise present concurrently with the signal detected. However, the normalization might be expected to permit a 30-dB dynamic range of signal amplitude detection as compared to an expected 12-dB range for the unnormalized processor.

$+(E - \bar{E})$ $-(E - \bar{E})$

$+X$ $-X$ U

M

QSM   B $-\dfrac{(N - \bar{N}) \times (E - \bar{E})}{10}$ I.C. $+\dfrac{1}{10}\sigma^2_{N \times E}$

$+Y$ $-Y$

$+X$ $-X$ U

M
$(+X^2)$
QSM   B $+\dfrac{(N - \bar{N})^2}{10}$ +10   I.C. $-\dfrac{1}{10}\sigma^2_{N \cdot N}$ $+\sigma_N$

$+Y$ $-Y$ QSMI

$-SPN(t)$ $-N(t)$ $\frac{1}{\tau}$ I.C. $+\bar{N}(t)$ $+(N - \bar{N})(t)$

$\frac{1}{\tau}$

$+N(t)$ Output

$-X$ $-X$ U

M

QSM   B $-\dfrac{(Z - \bar{Z}) \times (N \times \bar{N})}{10}$ I.C. $+\dfrac{1}{10}\sigma^2_{Z \times N}$

$+Y$ $-Y$

$+X$ $-X$ U

M
$(-X^2)$
QSM   B $-\dfrac{(Z - \bar{Z})^2}{10}$ I.C. $+\dfrac{1}{10}\sigma^2_{Z \cdot Z}$ $-\sigma_Z$

$+Y$ $-Y$ QSMI

$-SPZ(t)$ $-Z(t)$ $\frac{1}{\tau}$ I.C. $+\bar{Z}(t)$ $+(Z - \bar{Z})(t)$

$\frac{1}{\tau}$

$+Z(t)$ Output

$+X$ $-X$ U

M

QSM   B $-\dfrac{(Z - \bar{Z}) \times (E - \bar{E})}{10}$ I.C. $+\dfrac{1}{10}\sigma^2_{Z \times E}$

$+Y$ $-Y$

$+X$ $-X$ U

M
$(+X^2)$
QSM   B $+\dfrac{(E - \bar{E})^2}{10}$ +10   I.C. $-\dfrac{1}{10}\sigma^2_{E \cdot E}$ $+\sigma_E$

$+Y$ $-Y$ QSMI

$-SPE(t)$ $-E(t)$ $\frac{1}{\tau}$ I.C. $+\bar{E}(t)$ $+[E - \bar{E}](t)$

$\frac{1}{\tau}$

To N x E Multiplier

$+E(t)$ Output

$+V_D$ Output

$-K\,SPZ$
$(t - T.D.)$ $-V_D$ To P x V_D Multipliers

A

Figure 15. Analog processor for signal discrimination using normalized vector correlation

⩘ 2.3.2 Frequency Response

This is essentially a transient processor, in contrast to most of the more sophisticated steady-state processing approaches so far proposed. However, the high-pass circuit generating the function $(Z - \bar{Z})$ is the dual of the low-pass circuit used for averaging the data to generate the variance terms. Thus, the processor is all-pass for the variance, standard deviation, and correlation functions. This fact was checked experimentally using a borrowed TR-48 computer, and it was shown that ergodic estimates of correlation were valid from frequencies of 0.2 $(1/\tau)$ to 10 $(1/\tau)$ to within 1 percent. The uncertainty or time variability of the estimate was greater for lower frequency signals.

However, total input energy is not conserved in the processor. The low-frequency energy lost in the high-pass circuit generating $[Z - \bar{Z}]$ is lost forever. Thus for nonsinusoidal wave-forms represented by Fourier components, there will be a net loss on a probability basis of long-period energy (relative to the processor time constant). This feature is, of course, desirable for data which are shorter in period than the interfering high-energy microseisms.

4.3 DIGITAL AND HYBRID METHODS

4.3.1 Introduction

The V_D x M process and similar nonlinear processes can be implemented using either a digital computer or a hybrid computer. To date, much digital processing of seismic data has been performed at various computation centers, but none has been performed in the field in a real-time environment. Consequently, the terminology may be unfamiliar to certain readers; therefore, several terms will be explained, and certain features of digital- and analog-processing techniques that must be considered when real-time, linear, or nonlinear data analysis is to be performed will be discussed.

The term digital computer is used in reference to a system capable of performing only digital arithmetic; whereas, the term hybrid computer will refer to a device capable of performing analog arithmetic, digital arithmetic, and for the true hybrid, combined analog-digital arithmetic. Digital computer techniques offer several distinct advantages over pure analog methods but at the same time introduce several new problems. By combining the best features of both

digital and analog computers, the hybrid computer is obtained, possessing (in theory at least) the desirable features of both analog and digital techniques while eliminating the weaknesses associated with each method.

Any combination of an analog computer and a digital computer, where the two are linked together, is generally termed a hybrid computer; however, most combinations of this type require that the two computers be programmed independently. The true hybrid computer is still in the development stage. For such a device, the analog and the digital computer sections are integrated and controlled by a central processor, which in turn is controlled by software programs. The Adage Ambilog 200 is perhaps the first true hybrid computer to be marketed, but others will undoubtedly appear soon since the computer manufacturers are interested in developing hybrid processors. The Seismological Laboratory at the California Institute of Technology has recently acquired an Ambilog 200 computer and has begun to accumulate operating experience with it.

4.3.2 General Evaluation of Analog and Digital Computer Techniques

There are several salient features of both analog and digital computer techniques that should be taken into consideration when implementing either a linear or a nonlinear data analysis process. Several of these are listed below.

4.3.2.1 Digital Computer Methods

Advantages are:

  a Large dynamic range is available.

  b. Highly accurate arithmetic is possible.

  c. Time delays are easily achieved.

  d. Two-sided window functions or transfer functions are readily implemented.

  e. Programs are flexible.

Disadvantages are:

  a. Only discretely spaced samples of the time series can be processed.

b. Arithmetic operations are fairly slow unless arithmetic hardware, which is expensive, is used.

c. Normally, only one operation at a time can be performed.

4.3.2.2 Analog Computer Methods

Advantages are:

a. Continuous data can be processed.

b. Many operations can be performed simultaneously.

c. Operations such as addition, integration, and multiplication by a constant can be handled inexpensively and quickly.

Disadvantages are:

a. The dynamic ranges of multipliers, dividers, squaring circuits, and function generators are poor.

b. Large time delays are extremely difficult to achieve.

c. Two-sided window or transfer functions are impractical.

4.3.3 V_D x M Process Considerations

Several features of the V_D x M process serve to more or less define the processing system requirements. These are discussed in the following sections, taking into consideration what would be desirable from the standpoint of implementing the operation on a digital or hybrid computer.

If the processing is to be performed on only selected data and off-line at a computation center, the problem is simplified and few restrictions hold. The data are collected in the field, digitized, and then processed whenever convenient. If on the other hand, real-time processing is to be performed in the field, certain process, hardware, software, and cost considerations become relevant.

It is doubtful that all V_D x M operations can be performed fast enough on a
small, inexpensive digital computer; consequently, some operations should
be performed with analog circuitry. This makes a hybrid computer or a
combination of a small digital computer and an analog computer the logical
system to use.

4.3.3.1 Window Functions

As yet it has not been determined whether or not there is an optimum window
function. Indications, however, are that it should be approximately 2 to
2-1/2 seconds long for short-period data. Furthermore, it should probably
be an even function, perhaps rectangular, exponential, or triangular in shape.

The processing system should possess enough flexibility to permit adjust-
ments of the window shape and length to be readily made while the optimum
window, if one exists, is being determined. The correlation function that is
used to control the gain of the input signal is produced by integrating the
window function times the product of two time series. If a rectangular win-
dow function is used, as the window function is moved along the time series,
only one product term is added and one product term is subtracted for each
step along the time series. If certain other window functions are used, up
to 75 product terms must be added or subtracted for each step along the
digitized signal, depending on the digitizing rate and window width.

4.3.3.2 Digitization Rate

The digitization rate will depend on the maximum frequency of interest. Two
factors concerning the digitization rate affect the digital processor. First,
if core storage is used to achieve time delays, extra sampling takes up
additional core storage that is expensive and badly needed for instruction
storage. Second, for on-line processing, all necessary computations and
data transfers must be made between individual sampling pulses. Conse-
quently, the effective computation time available is equal to the reciprocal of
the sampling rate; i.e., doubling the digitizing rate cuts the processing time
available in half.

4.3.3.3 Time Delays

To emphasize the first motion of rectilinear wave fronts, the signal should be
time-delayed with respect to the window function. This time delay can be

achieved by using one of several available methods. External, cyclic magnetic drums, disks, or tape loops can be used, or the core storage of the digital computer can be used. The last method should be the most reliable and inexpensive.

4.3.3.4 Coordinate Transformations

Coordinate transformations require approximately as much arithmetic as the overall $V_D \times M$ process using a rectangular window. These can be performed just as effectively outside of the digital computer using analog circuitry, because no nonlinear operations are involved, and thus cut down the number of digital arithmetic operations required.

4.3.3.5 Normalization

Since the $V_D \times M$ process involves a correlation operation, it may be desirable to normalize the window function, thus producing a measurable rectilinearity function that would facilitate the detection of an event and the determination of its direction of propagation.

Normalization can be performed very accurately within the digital computer, or it can be approximated fairly accurately using analog circuitry.

4.3.4 Possible System Configurations

The following is a list of general system functions required to perform the $V_D \times M$ process using digital or hybrid techniques. They are not necessarily listed in the order in which they would be performed.

    a. Coordinate transformations.

    b. Multiplex signal components.

    c. Digitize signals.

    d. Square signals, integrate squared signals, form products of integrals and square roots of products to obtain normalizing functions.

    e. Obtain products and additions necessary to form window functions.

    f. Normalize window functions.

g. Delay signals.

h Form products of window functions and delayed signals.

i. Decommutate output signals.

The process is fairly complex, and the processor might assume one of a number of possible configurations, depending on the division of processing steps between digital and analog sections and whether or not normalizing is required.

The basic system requirements are shown by figure 16. The system will be a variation of this scheme, depending on whether or not a completely digital, hybrid, or in-between approach is taken.

4.3.5 Recommendations

It is recommended that the following steps be taken in developing a digital or hybrid processing system to perform the $V_D \times M$ process.

a. Determine a set of preliminary specifications, i.e., dynamic range, digitizing rate, necessary programming flexibility, number of coordinate transformations, etc.

b. Examine various system configurations, ranging from an all-digital system to a strictly hybrid system. Determine the required digital computer, analog circuitry and interface equipment for each system configuration, and compare costs and expected performance of each system.

c. Selecting the digital processor will require that the word size, core storage, memory cycle time, instruction set, and data channels be specified. This will probably require that the process actually be programmed (at least partially) for each digital processor considered, so that timing and storage requirements can be accurately evaluated.

5. CONCLUSIONS

The preliminary results indicate that the $V_D \times M$ vector correlation processor provides a useful aid to a trained analyst in detecting the source-depth-determining signals pP and sP. In preliminary azimuthal determination, it
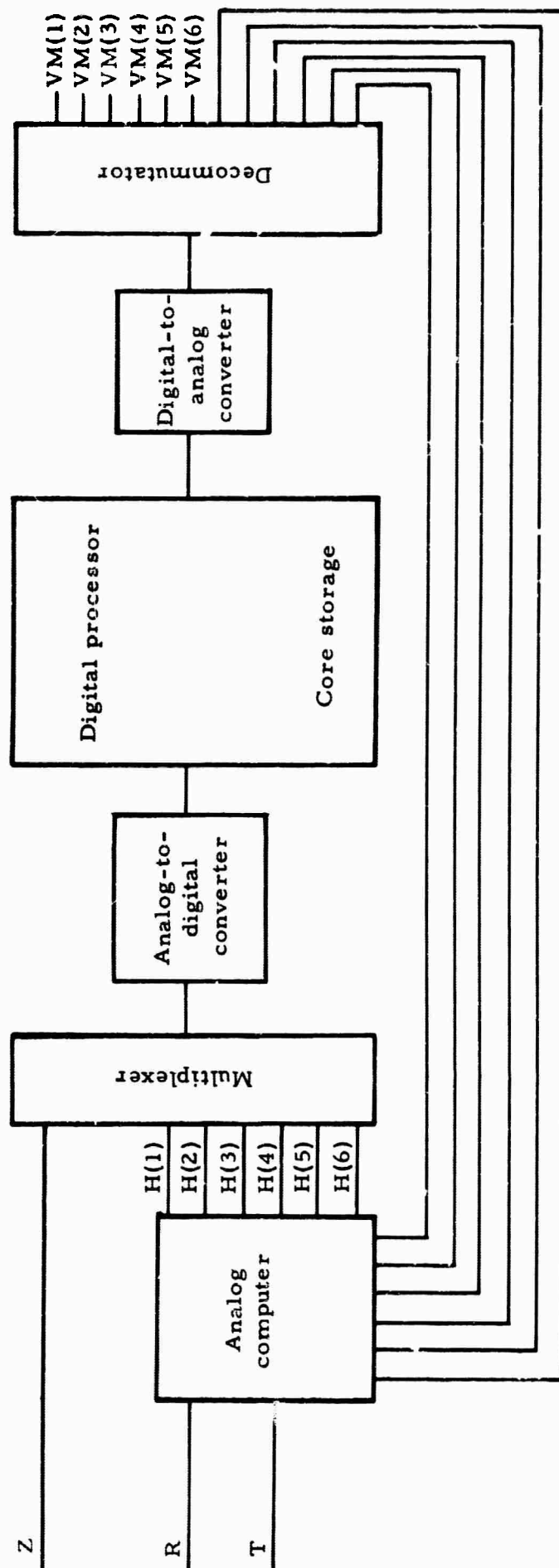
Figure 16. Digital processor

increases the speed of estimation. The data analyzed are too few in number to specify conclusively the limitations of the processor and the limitations of the theoretical interpretations of the data.

It has been shown that the analog processor can operate on a real-time, continuous basis. Insufficient data have been processed to specify completely the calibration requirements of the system and the processor down-time for maintenance purposes. However, since proven equipment has been utilized throughout, these requirements should be compatible with standard field operation experience.

The analog processor can be implemented on several levels of complexity and by numerous equipment approaches, depending on the utility of the approach and the funding available. The analog processor can be utilized as either a field or an off-line processor. Digital and hybrid approaches can probably also be used in both types of application, although an off-line developmental period would be required for a field proce sor.

6. RECOMMENDATIONS

On the basis of the preliminary work reported here, it appears that nonlinear vector correlation seismic data processing should be tested and developed further. We suggest a two-part program, as follows:

a. Develop and install an analog normalized or unnormalized $V_D \times M$ vector correlation processor at WMSO or other observatory as desired and operate the processor for a period of approximately 1 year. During this period, have a top analyst evaluate statistically the utility of the processor under normal field-operating conditions.

b. Continue theoretical and developmental work on the digital, analog, and hybrid approaches for the application of the vector correlation concept to array processing techniques.

7. REFERENCES

Davenport, Jr., W. B., and Root, W. L. 1958, An introduction to the theory of random signals and noise: New York, McGraw-Hill Book Company, Inc., p. 2.

Lee, Y W., 1960, Statistical theory of communication: New York, John Wiley & Sons, Inc., 509 p.

Merritt, Frederick S., 1962, Mathematics manual: New York, McGraw-Hill Book Company, Inc.

Morse, Phillips M., 1958, Vibrations of elastic bodies; wave propagation in elastic solid in Handbook of physics, Condon and Odishaw, eds.: New York, McGraw-Hill Book Company, Inc., p. 3-99.

Otterman, Joseph, 1960, The properties and methods for computation of exponentially-mapped-past statistical variables: IRE Transactions on Automatic Control, vol. AC-5, no. 1, p. 11-17.

Shimshoni, Michael, and Smith, Stewart W., 1964, Seismic signal enhancement with three component detectors: Geophysics, vol. XXIX, no. 5, p. 664-671.

8. ACKNOWLEDGMENT

APPENDIX to TECHNICAL REPORT NO. 65-57

SET-UP PROCEDURE: OFF-LINE ANALOG $V_D \times M$ VECTOR-
CORRELATION PROCESSOR

SET-UP PROCEDURE: OFF-LINE ANALOG V_D x M VECTOR-CORRELATION PROCESSOR

1. EQUIPMENT REQUIRED

The following equipment is required to implement this procedure:

a. 1 Honeywell Tape Recorder, Model 7400 (from VT/1124), with electronics for five channels (including compensation) at 0.3 inch per second (ips) to read data;

b. 1 Honeywell Tape Recorder, Model 7400, with electronics for three channels (including compensation) at 3.0 ips to delay data. A spliced tape loop is also required.

c. 1 TR-10 Analog Computer - in data processing area - plus:

    1 Multiplier, e.g., Model 7.045, from Fisher Processor
    4 100K Feedback resistors from Fisher Processor
    Patch panel boards for Multiplier;

d. 1 Develocorder, Model 4000, plus:

    Roll of 16-mm film
    Fix
    Developer;

e. 2 Data Control Frames, Model 5791, with 10 Model 5792B control modules;

f. 1 Data buffer (no model number), consisting of three inverting operational amplifiers, 100K input resistors, gain 3.32, ±10-V output range. This unit was constructed specifically for these tests, using three Philbrick P65A amplifiers and cne Philbrick PR-30C power supply.

g. 2 Oscilloscopes for equipment calibration;

h.   1 Frequency meter and 1 oscillator for FM frequency calibration of tape recorder electronics;

i.   1 Develocorder Switching Unit, Model 5970.

2.   SYSTEM BLOCK DIAGRAM

Figure 1 illustrates the required system patching to use the V_D x M processor. The functions performed include data read from magnetic tape, data scaling (data buffer and part of TR-10), time delay, computation of V_D x M, and data readout on Develocorder film.   The equipment setup and calibration requirements are indicated individually on this diagram and discussed individually in the following sections.

3.   HONEYWELL DATA READ TAPE RECORDER (VT/1124)

Adjust for 0. 3-ips operation on transport speed selector switch, and install appropriate electronics for this speed.

Calibrate discriminator outputs to 6 V peak-to-peak (p-p) for band-edge-to-band-edge inputs.

Check tape channel assignments to ensure that proper channels are specified.

Wire up compensation channel, and apply compensation to the four data channels required.

Patch outputs up to the remainder of the system.

Note that if the 6-V p-p amplitude cannot be obtained, a lesser voltage can be used provided the gain of the three data buffer amplifiers and pot. 17 in the TR-10 are adjusted to provide 20 V p-p for band-edge-to-band-edge frequency deviation on the analog tape.

Panel No. 3
Buss distribution

Data read

Honeywell
Model 7400
tape recorder
(VT/1124)

V.C.O. Inputs

Compensation
internally selected
for Ch. 7. Use
"Comp. on" for
doto channels

Discriminator outputs

Output panel

Input panel (trunks)

Pan. 5 Honeywell outputs

-SPZ

3.32

-SPN

3.32

-SPE

3.32

Data buffer

Pan. 7 computer in.

0.3 ips
6 V p-p Disc. output
Reads doto tape
Dubbed:
    SPZ – No. 2
    SPN – No. 4
    SPE – No. 6
    Comp.– No. 7
    Encoder time – No. 10

Honeywell
Model 7400
tape recorder
(VT/4051)

Compensation
internally generated
and selected.
Use "Comp on"
for data channels

Panel No. 1 Honeywell in

Panel No. 2 Honeywell out

SPZ/3.32

Encoder time

(SPZ/3.32) delayed

Delayed encoder time

3.0 ips
6.0 V p-p input/output
Continuous loop

A

Encoder time

TR - 10
Analog computer

4 mult.
20 amp.
16 pots.
4 diodes

Panel 5 computer out

Panel No. 2 Module inputs

Two Model 5791 data control frames with 16 5792B data control modules

Panel No. 2 module outputs

Pan. No. 3 Devel. SW. inputs

Develocorder Switching Unit, Model 5970. (Switch to Develocorder)

Develocorder, Model 4000

delayed 32) delayed $= V_D/3.32$

me

FILM PRESENTATION

1. Encoder time
2. SPZ
3. SPN
4. SPE
5. $V_D \times M_{NZ}$
6. M_{NZ}
7. $V_D \times M_{EZ}$
8. M_{EZ}
9. $V_D = SPZ$ (delayed)
10. Delayed encoder time

Figure 1. Equipment patching block diagram for in-house two-channel $V_D \times M$ analog data processor

4. HONEYWELL TIME-DELAY TAPE RECORDER (VT/4051)

Make and install a continuous spliced loop of 1-inch tape. Check patch wiring to ensure that the proper channels are being delayed.

Adjust for 3.0-ips operation on transport speed selector switch, and install appropriate read and playback electronics for this speed.

Calibrate VCO inputs and discriminator outputs to 6 V p-p for band-edge-to-band-edge frequency deviation of tape.

Note that if some other scaling level than 6 Vp-p were required for the read tape recorder, this new level must also be used on the time-delay unit.

5. DATA BUFFERS

Turn on ac power.

Set the three single-ended/double-ended switches to the single-ended position.

Set the three gain switches to 3.32.

Zero the outputs by:

    a. Short amplifier input;

    b. Read output voltage (to millivolts);

    c. Adjust dc balance control to zero output.

Patch the amplifiers as shown on figure 2.

6. TR-10 COMPUTER

First, remove the X^2 DFG from nonlinear position 7-8 in the chassis and in the patch panel.

Second, remove the multiplier chassis and patch panels from the Fisher processor computer.

Third, install the multiplier so borrowed into nonlinear position 7-8 of the data processing TR-10. Also borrow four 100K feedback resistors from the Fisher processor.

Patch the TR-10 in accordance with figure 2.

Install the patch board, temporarily grounding the four input signal leads to the computer ground buss.

Turn on and verify that all circuits are working.

Adjust the limiter amplifiers 3 and 4 for 9.5-V limiting.

Balance all amplifiers.

Examine the outputs of amplifiers 3 and 4, and adjust pots. 9 and 11 to get zero output. All other amplifiers should have zero outputs, except that the computer must be cycled through the reset mode to zero the outputs of integrator amplifiers 1 and 2.

Turn function switches off and patch the data inputs into the computer. Do not place these switches in the on position until after the read and time-delay recorders are both running. Turn them off before either tape recorder is stopped.

7. CONTROL MODULES

Calibrate the modules to give 2-cm deflections on film at X10 magnification when set at 20 dB for a 10-V calibration voltage (from computer output 10).

Set the module attenuators for proper data scaling. A setting of 26 dB on modules 1 and 10 (encoder time and encoder time delayed) has been found to be satisfactory. Film traces 2, 3, 4, 5, 7, and 9 should all be set at the same amplitude. A value of 26 dB has been found to work satisfactorily for the WMSO test. The M_{NZ} and M_{EZ} traces should be operated at the same amplitude. A value of 26 dB (± 1 cm maximum at X10 view) has been found to be satisfactory.

Input ground

Computer ground

-3.32 SPN(t)
(from computer input #3)

1   8   +3.32 SPN(t) (to computer output #3)

- X +
7-8 Mult.
X 7.045
- Y +

S S   7   0

0   10   5   0.300   13

+10 V

2 Exp.

S.J.

10
3
1

$\frac{1}{\tau} = 0.667$

I.C.

1
1   1

$\frac{1}{\tau} = 0.667$

3

4 Exp.

-10 V

9 Exp.

±10 V or gnd.

-3.32 SPZ(t)
(from computer input #2)

1   9   +3.32 SPZ(t) (to computer output #2)

+SPZ delayed (from computer i

1   20

- X +
11-12 Mult.
X 7.045
- Y +

S S   11   0

0   10   6   0.300   15

+10 V

6 Exp.

S.J.

10
4
5

$\frac{1}{\tau} = 0.667$

I.C.

1
1   2   2

$\frac{1}{\tau} = 0.667$

7

8 Exp.

-10 V

11 Exp.

±10 V or gnd.

-3.32 SPE(t)
(from computer input #4)

1   10   +3.32 SPE(t) (to computer output #4)

±10   19   #3 amp. in
or
#4 amp. in

Output Polarity		
	+	-
Amp. #3	Adj. pot #4	Adj. pot #2
Amp. #4	Adj. pot #8	Adj. pot #6

LIMITER ADJUSTMENT

1. Adjust output to limit at ≈ 9.5 V.

2. Adj. pots. 9 and 11 for zero output with grounded input (≈ 0.000 on pot.) may not be required.

A

Computer ground ⌐————o Output ground

0.200
(14)*
+M_NZ (to computer output #6)

13-14 Mult.
X 7.045

+M_NZ · V_D (to computer output #5)

+10 V ← Module calibration (to computer output #10)

0.332
(17)
+V_D

puter input #5)

+3.32 (V_D or SPZ-delayed) (to computer output #9)

15-16 Mult.
X 7.045

+M_EZ (to computer output #8)

+M_EZ · V_D (to computer output #7)

0.200
(16)*
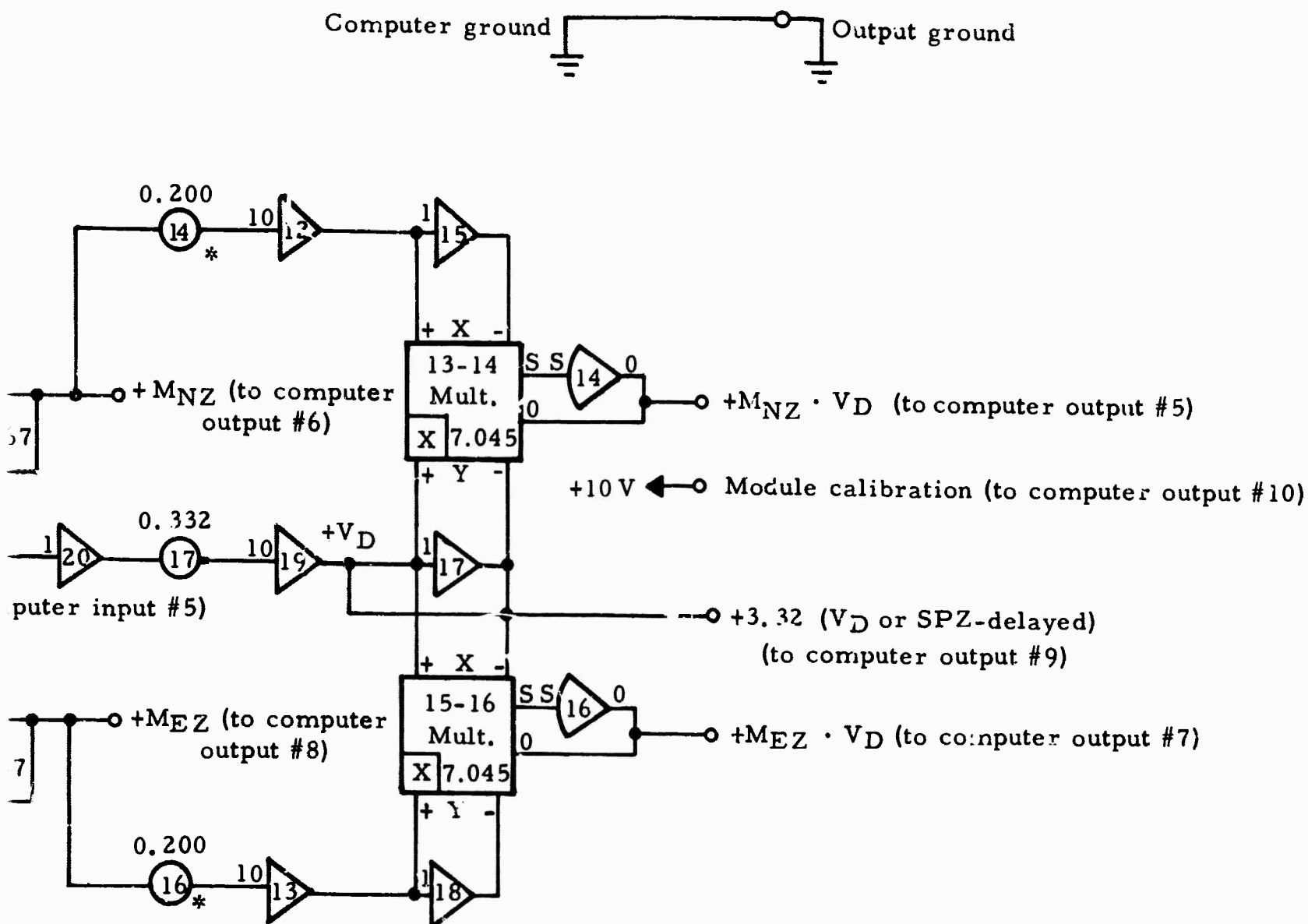
*Ground floating (bottom) end

Figure 2. Two-channel $V_D \times M$ analog computer circuit for in-house processor using TR-10 and borrowed multiplexer from Fisher Processor

8. DEVELOCORDER

Set switching unit to present data on the Develocorder.

Load the fix and developer tanks on the Develocorder.

Turn on the water.

The zero of the galvanometers should be adjusted to provide suitable spacings, and to verify that the film presentation order is correct.

Load on a new roll of 16-mm film.

9. SHUTDOWN

Open control module switches and computer inputs.

Turn off playback Honeywell, time delay Honeywell, and Develocorder power and water.

Replace all borrowed equipment; remove film, tape, tape loop, etc.; restore area.

APPENDIX 5 to TECHNICAL REPORT NO. 65-112

STATEMENT OF WORK TO BE DONE
AFTAC PROJECT AUTHORIZATION NO. VELA T/5051
AND
CONTRACT CHANGE NOTIFICATION NO. 1

STATEMENT OF WORK TO BE DONE
AFTAC PROJECT AUTHORIZATION No. VELA T/5051

1. Tasks.

   a. Conduct systems engineering on deep-well instrumentation to obtain a capability of operating up to 6 seismometers in a borehole simultaneously. Evaluate the applicability of multiconductor data cable with quick disconnect features between instruments in a vertical array. No major redesign of the deep-well seismometer is anticipated although mass size may be reduced to meet size and weight limitations. Following design approval by the government, assemble and conduct operational tests on the recommended deep-well seismographic system.

   b. Maintain and operate the deep-well test facility near Grapevine, Texas, for the purpose of testing equipment modifications, developing new handling and emplacement techniques, and qualifying calibration and operational procedures for the deep-well seismograph. In this regard, field evaluation of new or improved deep-well devices, such as the borehole triaxial SP seismometer under Project VELA T/072, will be conducted at Grapevine prior to use in field measurements tasks.

   c. Continue to measure signals and noise in deep and shallow boreholes where additional data are required. These field measurements do not antici-pate any preparation of new deep-well sites but provide for occupancy of several boreholes previously conditional and available. Data should be obtained for the purpose of supporting analysis of the behavior of seismic signals and noise with depth. A limited number of shallow boreholes may be required in support of this task.

   d. Provide for complete and detailed analysis of data resulting from field measurements and develop means of processing multiple signals from borehole arrays of 3 to 6 sensors. Major effort should be devoted to prediction of deep- and shallow-buried arrays under varying conditions of surface noise, environmental influences, geological structures, and geographic location. Large scale computer support of the CDC 1604 class is not author-ized but will be provided by separate arrangement with the AFTAC project officer.

2. Reports.

   a. A monthly letter-type management and progress report in 14 copies, summarizing work through the 25th of the month, will be dispatched to AFTAC by the end of each month. Specific topics will include technical and financial status, major accomplishments, problems encountered, future plans, and any action required by AFTAC. The financial status in each report should

include estimated expenditures and commitments to date, estimated funds
available to complete the work, and estimated excess or deficiency of funds.
Illustrations and photographs should be included as applicable. In
addition, the monthly report submitted for the reporting period occurring
6 months prior to the scheduled contract completion date shall contain
specific statements concerning recommendations or requirements and justifi-
cations for extensions, modifications, or expiration of work and any
changes in cost estimates which are anticipated by the contractor. The
heading of each report should contain the following information:

> AFTAC Project No. VELA T/5051
> Project Title
> ARPA Order No.
> ARPA Project Code No.
> Name of Contractor
> Date of Contract
> Amount of Contract
> Contract Number
> Contract Expiration Date
> Project Scientist's or Engineer's Name and Phone Number

b. A list of suggested milestones will be dispatched to AFTAC in
14 copies not later than 20 September 1964. Milestones are defined as
accomplishments which present significant progress when completed. Each
milestone should be briefly described and completion dates should be
estimated. Upon arrival of milestone information, copies of SD Form 350
will be furnished for reporting progress against the milestone schedule.
The SD Form 350 will be attached to the monthly report.

c. Special reports of major events will be forwarded by telephone,
telegraph, or separate letter as they occur and should be included in
the following monthly reports. Specific items are to include (but are
not restricted to) program delays, program breakthroughs, and changes in
funding requirements.

d. Special reports, as requested by the AFTAC project officer, may
be required upon completion of various portions of the work.

e. An initial technical summary report in 50 copies, covering work
performed through 30 January 1965, will be submitted to AFTAC within
15 days after the close of the reporting period. A semiannual technical
summary report in 50 copies, covering work performed through each
6-month period following the close of the initial reporting period, will
be submitted to AFTAC within 15 days following the close of the reporting

2

period. These reports will present a precise and factual discussion of the technical findings and accomplishments during the reporting period. The heading of the report will contain the heading information indicated in paragraph 2a.

3. Technical Documents. The contractor will be required to furnish the following technical documents:

a. All seismograms and operating logs, to include pertinent information concerning time, date, type of instruments, magnifications, etc., as requested by the AFTAC project officer.

b. Technical manuals on the installation and operation of all technical equipment installed during the duration of the contract for this project.

c. Two sets of reproducible engineering drawings and specifications for any changes or modifications in standard operational equipment and instruments, and for any new equipment designed, together with 2 sets of prints of these same drawings.

5. Miscellaneous. DD Form 1423, Contract Data Requirement List is attached. All technical reports and documents are to be forwarded to:

Hq USAF (AFTAC/VELA Seismological
Center/Maj Meek)
Wash DC 20333

3

Deam DCPS/2

CONTRACT CHANGE NOTIFICATION

1. MASTER SERIAL NO.	5N-2827
2. CCN NO.	1
3. PAGE 1 OF 1 PAGES	

4. TO:	5. FROM:
The Geotechnical Corporation 3401 Shiloh Road Garland, Texas	ASD (ASWKS) Special Projects Division Directorate of Specialized Subsystems & Equipment, Wright-Patterson AFB, Ohio

6. PURCHASE REQUEST NO.	7. CONTRACT NO. AND/OR PURCHASE ORDER NO.	8. PROPERTY CLASS
WK-5-RD-2103	AF 33(657)-13668	N/A

9. Pursuant to the clauses of the contract relating to changes, the above named Contractor is hereby authorized and directed to accomplish the changes listed below in respect to the articles called for under said contract as the same has heretofore and may hereafter be amended; subject, however, to the terms and provisions set forth on the reverse side hereof. Whenever both a purchase order number and a contract number are shown above, both numbers will be used in any shipping paper, packing sheet, invoice, correspondence, or related document, the purchase order number preceding the contract number.

I. The Statement of Work To Be Done, referred to in PART I is amended to include work under Project Authorization No. VELA T/5051/ASD/31 Amendment # 2 dated 26 May 1965, as follows:

" Task 1c of Project Authorization No. VELA T/5051 is amplified to include operational testing of the deep-well seismometer on the ocean bottom in approximately 15,000 feet of water at location designated by the AFTAC Project Officer.

" Four identical systems of deep-well seismometers, cables, transmitters, buoys and anchors will be provided, of which three (3) systems will serve as spares.

" This work shall be included in reports required by basic contract.

" Work shall begin 1 June 1965 and be completed by 1 August 1965"

II. It is anticipated that incorporation of the changes cited above will increase the contract price by an estimated amount of One Hundred and Twenty Thousand Dollars ($120,000.00). Funds in the amount of One Hundred and Twenty Thousand Dollars ($120,000.00) are hereby obligated to cover the estimated increase in price resulting from this CCN. This obligation is for administrative purposes only and will not affect the right of either party to negotiate an equitable adjustment according to the provisions of the clause pursuant to which this CCN is made.

MAILING DATE JUN 7 1965

FUND ALLOTMENT: 97X0400.1302 6124 P5810 920F VT/5051 S595600/591600

Effective Date: 26 May 1965

10. DATE	11. TYPED NAME, GRADE, AND SIGNATURE OF CONTRACTING OFFICER
26 May 1965	W. A. DALER

12. DISTRIBUTION
Dallas CAD, 500 Ervay Street, Dallas, Texas 75201

AFPI FORM 35
APR 59

PREVIOUS EDITIONS OF THIS FORM MAY BE USED.